



University of HUDDERSFIELD

University of Huddersfield Repository

Muo, Ugonnaya E.

Characterising Vibro-Acoustic Signals of a Reciprocating Compressor for Condition Monitoring

Original Citation

Muo, Ugonnaya E. (2018) Characterising Vibro-Acoustic Signals of a Reciprocating Compressor for Condition Monitoring. Doctoral thesis, University of Huddersfield.

This version is available at <http://eprints.hud.ac.uk/id/eprint/34964/>

The University Repository is a digital collection of the research output of the University, available on Open Access. Copyright and Moral Rights for the items on this site are retained by the individual author and/or other copyright owners. Users may access full items free of charge; copies of full text items generally can be reproduced, displayed or performed and given to third parties in any format or medium for personal research or study, educational or not-for-profit purposes without prior permission or charge, provided:

- The authors, title and full bibliographic details is credited in any copy;
- A hyperlink and/or URL is included for the original metadata page; and
- The content is not changed in any way.

For more information, including our policy and submission procedure, please contact the Repository Team at: E.mailbox@hud.ac.uk.

<http://eprints.hud.ac.uk/>

CHARACTERISING VIBRO- ACOUSTIC SIGNALS OF A RECIPROCATING COMPRESSOR FOR CONDITION MONITORING

Ugonnaya Enyinnaya Muo

A thesis submitted to the University of Huddersfield in partial fulfilment of the requirements
for the degree of

Doctor of Philosophy

Department of Mechanical Engineering

School of Computing and Engineering

The University of Huddersfield

September 2018

COPYRIGHT

- i. The author of this thesis (including any appendices and/or schedules to this thesis) owns any copyright in it (the “Copyright”) and she has given The University of Huddersfield the right to use such copyright for any administrative, promotional, educational and/or teaching purposes.
- ii. Copies of this thesis, either in full or in extracts, may be made only in accordance with the regulations of the University Library. Details of these regulations may be obtained from the Librarian. This page must form part of any such copies made.
- iii. The ownership of any patents, designs, trademarks and any and all other intellectual property rights except for the Copyright (the “Intellectual Property Rights”) and any reproductions of copyright works, for example graphs and tables (“Reproductions”), which may be described in this thesis, may not be owned by the author and may be owned by third parties. Such Intellectual Property Rights and Reproductions cannot and must not be made available for use without the prior written permission of the owner (s) of the relevant Intellectual Property Rights and/or Reproductions

ABSTRACT

Machine monitoring in industries such as chemical process plants, petroleum refineries and pulp and paper industries has significantly increased over the years, mainly because of the economic impact associated with the breakdown of a piece of equipment. With downtime sometimes costing up to 100,000 USD a day (Wachel, N.D), industrial organisations have made it mandatory to put in place systems for monitoring the condition of critical machines used for production purposes to prevent unforeseen machine breakdown. Reciprocating compressors are one of the widely used compressor types in diverse fields of application particularly in the oil and gas industry or chemical industry. In these industries, reciprocating compressors are mainly used to deliver high-pressure gas from one location to another. Due to the importance of these machines in delivering high-pressured air and sometimes toxic gases safely, their reliability has gained widespread interest over the years.

To improve reciprocating compressor operational performance and reliability, this research focuses on investigating the characteristics of vibro-acoustic signals from a reciprocating compressor based on a comprehensive analysis of non-intrusive vibration measurement and discharge gas oscillations (pulsations). This study will provide more knowledge on using two techniques (vibration and gas pulsations) for online monitoring and diagnosing of reciprocating compressor faults. Other monitoring techniques such as in-cylinder pressure, instantaneous angular speed (IAS), airborne acoustic as well as vibration are previously reported in literature, however, it is believed that no information for condition monitoring of discharge gas pulsation of a reciprocating compressor has been explored.

To fulfil this study, in-depth modelling and an extensive experimental evaluation for different and combined faults common to reciprocating compressor systems are explored for a wide discharge pressure range to better understand the vibro-acoustic sources. Three common faults including discharge valve leakage, intercooler leakage, discharge pipeline leakage and two combined faults: discharge valve leakage and intercooler leakage, discharge valve leakage and discharge pipeline leakage under various discharge pressures are studied in this thesis. The simulation of compressor performance with and without faults for several discharge pressures were in good agreements with the corresponding experimental evaluations, and was used to understand the compressor dynamics. Furthermore, a preliminary study on the effectiveness of conventional methods such as time-domain and frequency-domain analysis of both vibration and gas pulsation measurements were investigated. Results show that, these traditional

methods were insufficient in revealing fault characteristics in the vibration signal due to the usual noise contamination and nonstationary nature of the signal. Although, with the gas pulsation signal, waveform patterns and resonant frequencies varied with faults at several discharge pressures, nevertheless, effective band pass filtering needed to identify the best frequency band that can represent the characteristic behaviour of gas pulsation signals proved difficult and time consuming.

Amongst several advanced signal-processing approaches reviewed such as wavelet transform, time synchronous average, Hilbert transform, and empirical mode decomposition; wavelet packet transform is regarded as the most powerful tool to describe gas pulsation and vibration fault signals in different frequency bands. A combination of wavelet packet transform (WPT) and Hilbert transform (envelope analysis) is proposed to achieve optimal and effective band pass filtering for resonance band identification in gas pulsation signals, and WPTs de-noising property, which can effectively reduce excessive noise revealing key transient features in vibration signals.

Optimal band selection for vibration signal was achieved using entropy computation. The band with the highest entropy was used to reconstruct the signal and the envelope of the new vibration signal was used for classification. The fundamental frequency and its harmonics were used as a tool for fault classification. All fault conditions were clearly separated using the fundamental frequency and its third (3X) harmonic.

Regarding gas pulsation signals, the optimal band was selected by computing the root mean square (RMS) values of all eight enveloped band signals for several discharge pressures and faults. The band with the best RMS separation trend was selected for further classification using two main diagnostic features: the kurtosis and entropy of optimal band. The plot of kurtosis against entropy as a diagnostic tool showed good valve fault classification across a wide discharge pressure range.

Although the analysis of vibration signal using the proposed methods gave more reliable results for reciprocating compressor fault detection and diagnosis compared to the gas pulsation results, analysis of gas pulsation signals gave a better result on the optimal frequency band selection that can represent the behaviour of reciprocating compressor (RC) valve fault. Therefore, it can be deduced that analysis of the RC vibration signal together with the gas

CHARACTERISING VIBRO-ACOUSTIC SIGNALS OF A RECIPROCATING
COMPRESSOR FOR CONDITION MONITORING

pulsation signal has a promising potential to be used for condition monitoring and fault diagnostics of reciprocating compressors online.

DECLARATION

This dissertation is submitted for the degree of Doctor of Philosophy at the University of Huddersfield. I declare that the work in this dissertation was carried out in accordance with the Regulations of the University of Huddersfield. This work is original except where acknowledgement and references are made to the previous work. This dissertation has not been submitted for a degree, diploma or other qualification at any other university.

(UGONNAYA ENYINNAYA MUO)

DEDICATION

I dedicate this thesis to my parents Sir and Lady Enyinnaya Ogbulafor for their unconditional love and support particularly my father who has always encouraged me to work hard and chase my dreams.

ACKNOWLEDGEMENT

I would give all the praise and glory to the almighty God who has given me good health, wisdom, knowledge, and strength to carry on throughout this research period.

My propound gratitude goes to my supervisory team, which comprises the director of studies **Prof. Andrew David Ball** and **Dr Fengshou Gu**. For the excellent support, motivation, encouragement, advice, guidance and supervision from the beginning to the very end of my PhD studies. Their constant direction and generous contributions towards this research were of great help and was very much appreciated all through my four years of studies. I would also like to appreciate the **University of Huddersfield** for sponsoring my doctoral degree.

I would like to appreciate my parents Sir and Lady **Enyinnaya Ogbulafor** for their encouragement, prayers and support all through the period of my research.

Most of all I would like to appreciate my wonderful and handsome husband **Ifeanyichukwu Muo** for his patience, love, and his wholehearted support all through the years of my research. I cannot forget my princess **Daluchi Muo** and precious son **Jidechi Muo** whom is currently growing in me, mummy loves you both so much. Furthermore, my sincere gratitude goes to my sisters (**Onyinyechi Okpe and Dr. Ezinwa Uzukwu**), brother (**Odinakachi Ogbulafor**) and special aunty (**Ijeoma Oji**) for their unflagging love and prayers throughout my studies.

Finally, to my all my friends at **the Centre for Efficiency and Performance Engineering (CEPE)** research group **Dr. Misan, Osama, Naima, Zainab, Yuandong** and others I want to say a big thank you for their input and friendship.

PUBLICATIONS

- ❖ Zainab Mones, Guojin Feng, **Muo Ugonnaya**, Fengshou Gu, Andrew David Ball (2016) Performance evaluation of wireless MEMS accelerometer for reciprocating compressor condition monitoring. In: International Conference on Power Transmissions 2016 (ICPT 2016), Chongqing, P.R. China, 27–30 October 2016
- ❖ **Muo Ugonnaya**, Zainab Mones, Guojin Feng, Fengshou Gu, Andrew David Ball (2017) Application of Wavelet Packet Transform and Envelope Analysis to Non-stationary Vibration Signals For Fault Diagnosis of a Reciprocating Compressor. In: Conference: First World Congress on condition monitoring, London, 13-16 June, 2017 - BINDT
- ❖ **Muo Ugonnaya**, Madamedon Misan, Ball Andrew and Gu Fengshou (2017) Wavelet Packet Analysis and Empirical Mode Decomposition for the Fault Diagnosis of Reciprocating Compressors. In: 23rd International Conference on Automation & Computing, 7-8 September 2017 Huddersfield

TABLE OF CONTENTS

ABSTRACT.....	3
DECLARATION	6
DEDICATION	7
ACKNOWLEDGEMENT	8
PUBLICATIONS.....	9
TABLE OF CONTENTS.....	10
LIST OF FIGURES	17
LIST OF TABLES	23
LIST OF ABBREVIATIONS.....	25
LIST OF NOTATIONS	27
CHAPTER ONE.....	30
1 INTRODUCTION.....	30
1.1 Background and Research Motivation	31
1.2 Relevance of Monitoring Machinery	32
1.3 Problem Statements.....	35
1.4 Research Aim	35
1.5 Research Objectives	35
1.6 Thesis Outline	36
CHAPTER TWO	38
2 RECIPROCATING COMPRESSORS AND COMMON FAILURE MODES	38
2.1 Introduction	39
2.2 Compressor Types.....	39
2.2.1 Dynamic Compressors	40
2.2.2 Ejectors	42
2.2.3 Rotary Positive Displacement Compressors.....	42
2.2.4 Reciprocating Piston Compressors	45

CHARACTERISING VIBRO-ACOUSTIC SIGNALS OF A RECIPROCATING
COMPRESSOR FOR CONDITION MONITORING

2.2.4.1	Operating Principle of a Reciprocating Compressor	46
2.3	Typical Compressor Application	47
2.4	Compressor Problems	49
2.5	Reciprocating Compressor Components	50
2.5.1	Compressor Valves	50
2.5.2	Elements of a Compressor Valve.....	53
2.5.3	Compressor Cylinder	54
2.5.4	Compressor Cylinder Liner.....	54
2.5.5	Compressor Crankshaft.....	54
2.5.6	Compressor Piston	54
2.5.7	Compressor Bearings	55
CHAPTER THREE		56
3	REVIEW OF CONDITION-BASED MONITORING (CBM).....	56
3.1	Introduction	57
3.2	Visual Inspection.....	57
3.3	Cylinder Pressure Monitoring	57
3.4	Instantaneous Angular Speed	59
3.5	Airborne Acoustics.....	60
3.6	Vibration Monitoring	62
3.7	Signal Processing for Machine Monitoring	63
3.7.1	Time Domain	64
3.7.2	Frequency Domain Analysis.....	67
3.7.3	Time-Frequency Domain Analysis	68
3.8	Summary	70
CHAPTER FOUR.....		71
4	DESIGN AND CONSTRUCTION OF TEST-RIG FACILITY	71
4.1	Introduction	72

CHARACTERISING VIBRO-ACOUSTIC SIGNALS OF A RECIPROCATING
COMPRESSOR FOR CONDITION MONITORING

4.2	Test Rig Facility	72
4.2.1	The Broom Wade TS-9 Reciprocating Compressor	72
4.3	Measurement Instruments	74
4.3.1	Accelerometers	75
4.3.2	In-Cylinder Pressure Sensor	76
4.3.3	Airborne Acoustic Sensor	77
4.3.4	Static Pressure Sensor	78
4.3.5	Temperature Sensors.....	78
4.3.6	Shaft Encoder.....	79
4.4	Data Acquisition System (DAQ).....	80
4.4.1	Software: LabWindows TM/CVI Version 5.5.....	81
4.5	Data Measurement Practice.....	82
4.6	Fault Seeding.....	83
4.6.1	Valve Leakage Simulation	84
4.6.2	Intercooler Leakage Simulation.....	84
4.7	Repeatability of Measured Signals.....	85
4.7.1	Baseline.....	85
4.7.2	Discharge Valve Leakage	93
4.7.3	Intercooler Leakage	101
4.7.4	Summary.....	109
CHAPTER FIVE		110
5 DYNAMIC MODELLING OF A DOUBLE-STAGE, SINGLE-ACTING RECIPROCATING COMPRESSOR.....		110
5.1	Introduction	111
5.2	A Brief Review of Previous Reciprocating Compressor Modelling.....	112
5.3	Crankshaft Dynamic Model –Piston Kinematics.....	113
5.3.1	Mechanism of Crank shaft and Connecting Rod.....	113

CHARACTERISING VIBRO-ACOUSTIC SIGNALS OF A RECIPROCATING
COMPRESSOR FOR CONDITION MONITORING

5.4	Cylinder Volume	117
5.5	Equation of Motion	118
5.5.1	Calculating the Torques	118
5.6	Cylinder Pressure Models	120
5.7	Mass Flow Models	121
5.7.1	Suction Mass Flow Model	121
5.7.2	Discharge Mass Flow Model	122
5.8	Valve Dynamics	123
5.8.1	Suction Valve Motion	124
5.8.2	Discharge Valve Motion	125
5.9	Discharge Plenum Pressure	125
5.10	Fault Simulation	127
5.10.1	Second Stage Discharge Valve Leakage.....	127
5.10.2	Intercooler leakage.....	128
CHAPTER SIX.....		129
6	MODEL VALIDATION	129
6.1	Introduction	130
6.2	Model Analysis	130
6.2.1	Physical Parameters and Constants.....	130
6.3	Healthy Simulation Results.....	132
6.3.1	In-Cylinder Pressure Signal	132
6.3.2	Valve Displacement and Vibration Signals	134
6.3.3	Discharge Chamber Pressure	135
6.4	Discharge Valve Fault Simulation Results.....	136
6.4.1	In-Cylinder Pressure Fault Signal.....	136
6.4.2	Valve Displacement and Vibration Fault Signals.....	139
6.5	Intercooler Fault Simulation Results.....	142

CHARACTERISING VIBRO-ACOUSTIC SIGNALS OF A RECIPROCATING
COMPRESSOR FOR CONDITION MONITORING

6.5.1	In-Cylinder Pressure Fault Signal	142
6.5.2	Valve Displacement and Vibration Fault Signals	144
6.6	Discharge Chamber Fault Simulation Results	146
CHAPTER SEVEN		149
7 CHARACTERISTICS OF VIBRATION SIGNALS FROM A RECIPROCATING COMPRESSOR		149
7.1	Introduction	150
7.2	Time Domain Analysis of Vibration Signal.....	151
7.2.1	RMS	154
7.2.2	Kurtosis	155
7.3	Frequency Domain Analysis	157
7.4	Summary	161
CHAPTER EIGHT		163
8 CHARACTERISTICS OF DISCHARGE GAS PULSATION FROM A RECIPROCATING COMPRESSOR		163
8.1	Experimental Setup	164
8.1.1	Test Procedure	164
8.2	Time Domain Analysis.....	165
8.2.1	Gas Pulsation Time Domain Waveform for Fault Cases.....	167
8.3	Conventional Statistical Measures from Time Domain Signal.....	170
8.3.1	Probability Density Function	170
8.3.2	Root Mean Square and Kurtosis	172
8.4	Frequency Domain Analysis	173
CHAPTER NINE.....		179
9 ANALYSIS OF VIBRATION SIGNAL USING WAVELET PACKET TRANSFORM WITH ENVELOPE ANALYSIS.....		179
9.1	Theoretical Background of Wavelet Transform.....	180

CHARACTERISING VIBRO-ACOUSTIC SIGNALS OF A RECIPROCATING
COMPRESSOR FOR CONDITION MONITORING

9.1.1	Continuous Wavelet Transform (CWT)	180
9.1.2	Discrete Wavelet Transform (DWT)	180
9.1.3	Wavelet Packet Transform (WPT).....	181
9.2	Selecting Mother Wavelet.....	183
9.3	Envelope Analysis.....	184
9.4	Experimental Setup	185
9.5	Test Procedure.....	185
9.6	Results and Discussion.....	186
9.6.1	Traditional Time Domain and Frequency Domain Analysis.....	186
9.6.2	Wavelet Packet Transform and Wavelet Packet Energy	187
9.6.3	Fault Classification Using Harmonic Changes	191
9.7	Conclusions	191
CHAPTER TEN.....		193
10 ANALYSIS OF DISCHARGE GAS PULSATIONS USING WAVELET PACKET TRANSFORM WITH ENVELOPE ANALYSIS		193
10.1	Gas Pulsation Source and Resonance Assessment.....	194
10.1.1	Simplified Resonance Assessment of the System	195
10.1.2	Gas Pulsation Propagation Simulation.....	199
10.2	Application of Wavelet Packet Transform.....	200
10.2.1	Selection of Base Wavelet	201
10.3	Proposed Methodology	203
10.4	Experimental Results and Discussion	205
10.4.1	WPT Analysis of the Discharge Chamber Gas Pulsations	207
10.4.2	Envelope Analysis and Feature Extraction of Discharge Chamber Gas Pulsations 210	
10.4.3	Fault Classification using Statistical Features	212
10.5	Conclusion.....	214

CHARACTERISING VIBRO-ACOUSTIC SIGNALS OF A RECIPROCATING
COMPRESSOR FOR CONDITION MONITORING

CHAPTER ELEVEN.....215

11 CONCLUSIONS AND RECOMMENDATIONS FOR FURTHER WORK.....215

11.1 Review of Thesis Objectives and Achievement.....216

11.2 Conclusion on Condition Monitoring of Vibro-acoustic Signals from a Reciprocating
Compressor.....218

11.3 Contribution to Knowledge.....221

11.4 Recommendation for Future Work222

12 APPENDIX 1.....223

REFERENCES225

LIST OF FIGURES

Figure 1.1: Primary causes of unscheduled reciprocating compressor shutdown	31
Figure 1.2: Prognost compressor system failure mode survey 2009	32
Figure 1.3: Classification of Maintenance Strategies (Williams, Davies, & Drake, 1994).....	33
Figure 2.1: Compressor Classification.....	40
Figure 2.2: A Centrifugal Compressor (Boyce, 2009).....	41
Figure 2.3: An Axial Compressor (Giampaolo, 2010)	41
Figure 2.4: Typical Ejector (Brown, 2005).....	42
Figure 2.5: Schematics of a typical sliding vane compressor (Cipollone, 2016)	43
Figure 2.6: Helical Lobe compressor (Ormer, 2002).....	44
Figure 2.7: A typical Liquid Ring Compressor (Al-Qattan, 2007).....	44
Figure 2.8: Cross-section of a typical single-acting reciprocating compressor (Al-Qattan, 2007)	45
Figure 2.9: Single-acting compression steps of a compressor cylinder b) Actual P-V diagram of single stage compression cycle.....	47
Figure 2.10: Compressor types and their application range based on pressure and flow (Brown, 2005)	49
Figure 2.11: Channel Valve (Forsthoffer, 2017, p. 119)	52
Figure 2.12: Plate Valve (Forsthoffer, 2017, p. 120).....	52
Figure 2.13: Actual plate valve used for this research.....	53
Figure 3.1: Pressure measurement from a two stage reciprocating compressor.....	58
Figure 3.2: One cycle of IAS measurement from a reciprocating compressor.....	60
Figure 3.3: Simplified waveform parameters of airborne acoustic signal (Yan, et al., 2015).62	
Figure 3.4: Vibration signal from a two stage reciprocating compressor.....	63
Figure 3.5: Signal Processing Techniques	64
Figure 4.1: Pictorial representation of two- stage reciprocating compressor (Broom Wade TS9)	73
Figure 4.2: Schematic Diagram of the test rig system	74
Figure 4.3: Vibration measurement flow chat	75
Figure 4.4: Dynamic-pressure measurement flow chat	76
Figure 4.5: Acoustic Pressure measurement flow chat.....	77
Figure 4.6: Static tank-pressure flow chat	78
Figure 4.7: K type, Cr-Al thermocouple installation and temperature monitoring process	79

Figure 4.8: Optical Pulse Shaft Encoder and data collection flow chat.....	80
Figure 4.9a) Front and b) rear view panel of the CED Power1401 DAC.....	80
Figure 4.12: Second stage value plate a) with leakage and b) without leakage.....	84
Figure 4.13: intercooler leak simulation	84
Figure 4.14: Repeated in-cylinder waveforms at several discharge pressures	86
Figure 4.15: Interaction plot of RMS and several discharge pressures for pressure signals ...	87
Figure 4.16: repeated airborne acoustic wave signals at several discharge pressures	89
Figure 4.17: Interaction plots of RMS and several discharge pressure for airborne acoustic signals	90
Figure 4.18: Repeated vibration signals at several discharge pressures	92
Figure 4.19: Interaction plots of RMS and several discharge pressures for vibration signals.	93
Figure 4.20: Repeated in-cylinder pressure waveforms at several discharge pressure.....	94
Figure 4.21: Interaction plots of the RMS values for several discharge pressures and repeated pressure signals	95
Figure 4.22: Repeated airborne acoustic waveforms at several discharge pressures	97
Figure 4.23: Interaction plots of the RMS values for several discharge pressures and repeated airborne acoustic signals	98
Figure 4.24: repeated vibration signals at several discharge pressures	99
Figure 4.25: Interaction plots of the RMS values for several discharge pressures and repeated vibration signals	100
Figure 4.26: Repeated pressure signals at several discharge pressures	102
Figure 4.27: Interaction plots of RMS values for several discharge pressures and repeated pressure signals	103
Figure 4.28: Repeated airborne acoustic signals at several discharge pressures	104
Figure 4.29: Interaction plots of the RMS values for several discharge pressures and repeated airborne acoustic signals	105
Figure 4.30: Repeated vibration signals at several discharge pressures	107
Figure 4.31: Interaction plots of the RMS values for several discharge pressures and repeated vibration signals	108
Figure 5.1: Complete Reciprocating Compressor Model	112
Figure 5.2: Piston Mechanism of a Reciprocating Compressor with Acting Forces.....	115
Figure 5.3: Simplified Model of the V-shaped double-stage Reciprocating Compressor (Elhaj M. A., 2005).....	116

Figure 5.4: Torque applied to a Shaft	119
Figure 5.5: Single Degree of Motion of a Reciprocating Compressor Valve (Elhaj M. A., 2005)	123
Figure 5.6: Discharge plenum and piping system.....	127
Figure 6.1: Predicted healthy pressure signals at different tank pressures: a) first stage b) second stage	132
Figure 6.2: Experimental healthy pressure signals at different tank pressures: a) first stage b) second stage	133
Figure 6.3: Predicted and measured in-cylinder pressure signals at 0.827 MPa (120psi) first stage and second stage	133
Figure 6.4: Predicted suction and discharge valve motions for first stage cylinder at 0.827 MPa (120 psi)	134
Figure 6.5: Predicted suction and discharge valve motions for second stage cylinder at 0.827 MPa (120 psi).....	134
Figure 6.6: Measured vibration signals at 0.827 MPa (120psi) for a) first stage cylinder and b) second stage cylinder	135
Figure 6.7: Predicted plot of in-cylinder, cavity one, and cavity two pressure at discharge period	136
Figure 6.8: A) Cavity one B) Cavity two pressure predictions at different tank pressures ...	136
Figure 6.9: Predicted and experimental second stage discharge valve fault waveforms for first and second stage in-cylinder pressure at 0.823 MPa	137
Figure 6.10: Predicted and experimental first stage in-cylinder pressure waveforms for healthy and DVL-fault conditions	138
Figure 6.11: Predicted and experimental second stage in-cylinder pressure waveforms for healthy and DVL-fault conditions	138
Figure 6.12: First stage valve displacement comparison of healthy and valve leakage fault predictions.....	139
Figure 6.13: Measured first stage vibration signals for healthy and discharge valve fault conditions.....	140
Figure 6.14: Second stage valve displacement comparison of healthy and valve leakage fault predictions.....	141
Figure 6.15: Measured second stage vibration signals for healthy and discharge valve fault conditions.....	141

figure 6.16: Predicted and experimental intercooler leakage trends for first and second stage in-cylinder pressure at 0.823 MPa 142

figure 6.17: Predicted and experimental first stage in-cylinder pressure waveforms for healthy and ICL-fault conditions 143

figure 6.18: Predicted and experimental second stage in-cylinder pressure waveforms for healthy and ICL-fault conditions 143

figure 6.19: first stage valve displacement comparison of healthy and intercooler fault predictions..... 144

figure 6.20: Measured first stage vibration signals for healthy and intercooler fault conditions 144

figure 6.21: Second stage valve displacement comparison of healthy and intercooler fault predictions..... 145

Figure 6.22: Measured second stage vibration signals for healthy and intercooler fault conditions..... 146

Figure 7.1: Measured vibration signal at 0.82 MPa a) first cylinder, and b) second cylinder 150

Figure 7.2: First stage vibration signatures over a wide pressure range under normal (healthy) compressor condition 152

Figure 7.3: Second stage vibration signatures over a wide pressure range under normal (healthy) compressor condition..... 152

Figure 7.4: Healthy and faulty vibration signatures from first stage cylinder head at 0.82MPa 153

Figure 7.5: Healthy and faulty vibration signatures from second stage cylinder head at 0.82MPa 153

Figure 7.6: First and second stage vibration rms values for several tank pressures 154

Figure 7.7: Healthy and faulty first stage vibration RMS values at several tank pressures .. 155

Figure 7.8: Healthy and faulty second stage vibration RMS values for several tank pressures 155

Figure 7.9: Kurtosis values for first and second stage vibration signals at several tank pressures 156

Figure 7.10: Healthy and faulty kurtosis results for first stage vibration signals at several tank pressures..... 156

Figure 7.11: Healthy and faulty kurtosis results for second stage vibration signals at several tank pressures..... 157

Figure 7.12: One sided vibration spectra for healthy a) first stage and b) second stage vibration measurements at 0.82MPa 158

Figure 7.13 : Healthy first stag vibration spectra for several tank pressures 159

Figure 7.14: Healthy second stage vibration spectra for several tank pressures 159

Figure 7.15: Waterfall plots of first stage vibration spectrum for healthy and all fault cases 160

Figure 7.16: Waterfall plots of second stage vibration spectrum for healthy and all fault cases 161

Figure 8.1: a) Experimental test rig setup of the reciprocating compressor b) high-pressure cylinder with sensor installations, c) schematic of acoustic sensor installation 165

Figure 8.2: Healthy a) time domain of gas pulsation signal, b) gas pulsation and In-cylinder waveforms, identifying the four compressor processes. 166

Figure 8.3: One cycle waveform of gas pulsation signals at several tank pressures 167

figure 8.4: gas pulsation wave comparing normal and fault conditions at several discharge pressures..... 168

Figure 8.5: PDF curve of normal (BL) gas pulsation signal for different DPs..... 171

Figure 8.6: PDF fault comparison curves for gas pulsation signals at several DPs..... 171

Figure 8.7: Comparison of healthy and fault PDF peaks for several discharge pressures..... 172

Figure 8.8: RMS of gas pulsation signal against fault cases at several discharge pressures . 172

Figure 8.9: Kurtosis of gas pulsation signal against several discharge pressures for all cases 173

Figure 8.10: Sound pressure level of gas pulsation signals under normal condition (BL) for several discharge pressures 174

Figure 8.11: Waterfall plot of healthy and fault frequency spectrum at several discharge pressures..... 175

Figure 8.12: 1/3 octave band spectra of healthy and all fault cases at several discharge pressures 175

Figure 8.13: Healthy and fault comparison of octave band power of five resonances at several tank pressures..... 177

Figure 9.1: Three levels discrete wavelet decomposition tree 181

Figure 9.2: Illustration of three level wavelet packet transform decomposition tree 183

Figure 10.1: Gas pulsations waves from the discharge chamber of a healthy R.C at 0.827MPa194

Figure 10.2: Sources of reciprocating compressor gas pulsations 195

Figure 10.3: a) Mode shape of half wave response b) Mode shape of quarter wave response 196

Figure 10.4: Simplified model of the discharge chamber and storage tank pipe configuration with dimensions in [mm] 197

Figure 10.5: Speed of sound in gas for several discharge pressures of the RC 197

figure 10.6: Flow chart for fault diagnosis using gas pulsation signal205

Figure 10.7 a) Time domain and b) frequency domain analysis of gas pulsation signal at 0.827mpa.....206

Figure 10.8: Acoustic resonances for several tank pressures under normal conditions207

Figure 10.9: Spectrogram of healthy and faulty gas pulsation signals at 0.827MPa.....208

Figure 10.10: Reconstructed terminal node waveforms and corresponding spectrum for gas pulsation signal at 0.827mpa.....210

Figure 10.11: RMS of all terminal nodes for all conditions and tank pressures.....211

Figure 10.12: Envelope and B) Envelope Spectrum of terminal node 4 for all conditions at 0.827MPa211

Figure 10.13: envelope and b) envelope spectrum of terminal node 6 for all conditions at 0.827MPa212

Figure 10.14: Fault classification using entropy against kurtosis plot of terminal node 4 enveloped signal.....213

Figure 10.15: Fault classification using entropy against kurtosis plot of terminal node 6 enveloped signal.....214

Figure 11.1: Characteristics of vibro-acoustic signals from a reciprocating compressor221

LIST OF TABLES

Table 2.1: Compressor Applications.....	48
Table 2.2: Compressor Valves (Brown, 2005; O'Neill, 1993).....	50
Table 4.1: Accelerometer specifications.....	75
Table 4.2: In-cylinder Pressure Sensor Technical Specifications.....	76
Table 4.3: Analysis of variance for repeatability of pressure signals	86
Table 4.4: Analysis of variance for several discharge pressures	87
Table 4.5: Correlation coefficient and probability level of baseline test pressure signals	88
Table 4.6: Analysis of variance for repeatability of airborne acoustic signals	90
Table 4.7: Analysis of variance for several discharge pressures	90
Table 4.8: Correlation coefficient and probability level of baseline test airborne acoustic wave signals	91
Table 4.9: Analysis of variance for repeatability of vibration signals	92
Table 4.10: Analysis of variance for several discharge pressure.....	92
Table 4.11: Correlation coefficient and probability level of baseline test vibration signals ...	93
Table 4.12: Analysis of variance for repeatability of in-cylinder pressure signal under discharge valve fault condition	95
Table 4.13: Analysis of variance for several discharge pressures under discharge valve fault condition	95
Table 4.14: Correlation coefficient and probability level of baseline test pressure signals	96
Table 4.15: Analysis of variance for repeatability of airborne acoustic signals under discharge valve fault condition	97
Table 4.16: Analysis of variance for several discharge pressures under discharge valve fault condition	98
Table 4.17: Correlation coefficient and probability level of discharge valve leakage test airborne acoustic signals.....	98
Table 4.18: Analysis of variance for repeatability of vibration signals under discharge valve fault condition.....	100
Table 4.19: Analysis of variance for several discharge pressures under discharge valve fault condition	100
Table 4.20: Correlation coefficient and probability level of discharge valve leakage test vibration signals.....	101

Table 4.21: Analysis of variance for repeatability of in-cylinder pressure signals under intercooler fault condition.....	102
Table 4.22: Analysis of variance for several discharge pressures under intercooler fault condition	102
Table 4.23: Correlation coefficient and probability level of intercooler leakage test of pressure signals	103
Table 4.24: Analysis of variance for repeatability of airborne acoustic signals under intercooler fault condition	104
Table 4.25: Analysis of variance for several discharge pressures under intercooler fault condition	105
Table 4.26: Correlation coefficient and probability level of intercooler leakage test of airborne acoustic wave signals.....	106
Table 4.27: analysis of variance for repeatability of vibration signals under intercooler fault condition	107
Table 4.28: Analysis of variance for several discharge pressures under intercooler fault conditions.....	107
Table 4.29: Correlation coefficient and probability level of intercooler leakage test of vibration signals	108
Table 6.1: Physical parameters of the two-stage reciprocating compressor (Broom Wade, 1964; Comp Air UK Ltd, 2002).....	130
Table 10.1: Acoustic natural frequency and harmonics of the discharge pipe	198
Table 10.2: Helmholtz resonant frequencies of the RC at several tank pressures	199
Table 10.3: Real-valued quantitative measures for optimal base wavelet selection.....	203
Table 10.4: frequency range for each terminal node under 4092 Hz sampling frequency in gray code sequence	205
Table 10.5: Summarised differences between healthy and all faulty spectrograms	208
Table 12.1: Failure Modes of Positive Displacement Rotary Compressors	223
Table 12.2: Failure Modes of Reciprocating Positive Displacement Compressors.....	224

LIST OF ABBREVIATIONS

AC	Alternating Current	FD	Frequency Domain
ADC	Analogue to Digital Converter	FFT	Fast Fourier Transform
ANOVA	Analysis of Variance	FMEA	Failure Mode and Effects Analysis
BDC	Bottom Dead Centre	GUI	Graphical User Interface
BL	Baseline Leakage	Hp	Horse Power
B&K	Bruel & Kjaer	HT	Hilbert Transform
CBM	Condition Based Maintenance	IAS	Instantaneous Angular Speed
CED	Cambridge Electronic Design	ICL	Intercooler Leakage
CF	Crest Factor	IFFT	Inverse Fast Fourier Transform
CM	Condition Monitoring	LPG	Liquefied Petroleum Gas
CWT	Continuous Wavelet Transform	MATLAB	Matrix Laboratory
DAQ	Data Acquisition	PDF	Probability Density Function
dB	Decibel	PLL	Pipeline Leakage
DP	Discharge Pressure	PK	Peak Factor
DVC	Discharge Valve Closing	psi	Pounds per square inch
DVO	Discharge Valve Open	RMS	Root Mean Square
DVL	Discharge Valve Leakage	Rpm	Revolution per Minute
DWT	Discrete Wavelet Transform	SK	Skewness
EMD	Empirical Mode Decomposition	SVO	Suction Valve Open
ET	Elapsed Time	SVC	Suction Valve Closing

CHARACTERISING VIBRO-ACOUSTIC SIGNALS OF A RECIPROCATING
COMPRESSOR FOR CONDITION MONITORING

SNR Signal to Noise Ratio

USD United States Dollar

TDC Top Dead Centre

USSR Union of Soviet Socialist Republic

UK United Kingdom

WPT Wavelet Packet Transform

US United States

LIST OF NOTATIONS

A_{fd}	Max flow area of the discharge valve [mm ²]	C_d	Discharge valve damping coefficients [N/ms ⁻¹]
A_{fi}	Max flow area of the suction valve [mm ²]	C_{cd}	Discharge valve contact damping coefficients [N/ms ⁻¹]
A_l	Leakage valve size [mm ²]	D	Piston diameter [mm]
B_r	Transmission ratio [%]	d	Cylinder bore length [mm]
C	Damping constant of valve chamber [N/ms ⁻¹]	F	Cylinder air pressure force [N]
C_c	Speed of sound in the cylinder [ms ⁻¹]	f_{do}	Preset spring force of discharge valve [N. m]
C_i	Speed of sound in the inlet plenum [ms ⁻¹]	f_{hw}	Half wavelength Frequency [Hz]
C_{fd}	Force coefficient of discharge valve	f_{qw}	Quarter wavelength Frequency [Hz]
C_{fs}	Force coefficient of suction valve	F_s	Sampling frequency
$C_{di}(x)$	Variable suction coefficient	f_{so}	Preset spring force of suction valve [N. m]
$C_{dd}(x)$	Variable discharge coefficient	f_{vd}	Discharge pressure force [N. m]
C_s	Suction valve-damping coefficients [N/ms ⁻¹]	f_{vs}	Suction pressure force [N. m]
C_{cs}	Suction valve contact damping coefficients [N/ms ⁻¹]	f_{gs}	Gravitation force for suction valve [N. m]
		f_{gd}	Gravitation force for discharge valve [N. m]
		$f_{pL,H}$	Force produced by the air pressure [N. m]

CHARACTERISING VIBRO-ACOUSTIC SIGNALS OF A RECIPROCATING
COMPRESSOR FOR CONDITION MONITORING

$f_{mL,H}$	Force produced by the inertial force of reciprocating mass [N. m]	m	Mass of air inside cylinder [g]
g	Earth's gravitational field strength [9.8 N kg ⁻¹]	m_v	Mass of the valve plate plus one-third of the spring mass [g]
k	Valve spring stiffness [Nm ⁻¹]	p_w	Motor power [W]
J	Moment of inertia. [kg.m ²]	p_c	Cylinder air pressure [psi]
l	Connecting rod length [mm].	\dot{p}_c	Variable cylinder pressure [psi]
m_{rec}	Reciprocating inertial mass [g]	p_i	Suction pressure [psi]
m_{cr}	Connecting rod mass [g]	P_d	Discharge pressure [psi]
m_p	Piston mass [g]	r	Crank radius [m]
m_{plate}	Mass of valve plate [g]	S_c	Cylinder cross - sectional area [m ²]
m_{spring}	Mass of valve spring [g]	S_p	Piston area [m ²]
\dot{m}_{vi}	Mass flow rate through the inlet valve [kgs ⁻¹]	S_v	Valve slot area for a single channel [m ²]
\dot{m}_{vd}	Mass flow rate through the discharge valve [kgs ⁻¹]	Sp_c	Compressor speed [Hz]
\dot{m}_{ld}	Mass flow rate through the leakage discharge valve [kgs ⁻¹]	T_i	Atmosphere temperature [C ^o]
\dot{m}_{ls}	Mass flow rate through the leakage suction valve [kgs ⁻¹]	T_c	Cylinder absolute air temperature [K]
		$T(t)$	Temperature of air inside the cylinder [C ^o]
		T_m	Driving torque [N. m]

CHARACTERISING VIBRO-ACOUSTIC SIGNALS OF A RECIPROCATING
COMPRESSOR FOR CONDITION MONITORING

$T_{pm_{L,H}}$	Torque produced by cylinder air pressure and piston mass [N.m]	x_v	Valve plate displacement [mm]
$T_{f_{L,H}}$	Friction torque [N.m]	\dot{x}_v	Valve speed [ms^{-1}]
\dot{v}	Variable cylinders volume [m^3]	\ddot{x}_v	Valve acceleration [$\text{m}\cdot\text{sec}^{-2}$]
v_{co}	Cylinders clearance volume [m^3]	x_p	Piston displacement [mm]
v_c	Cylinder volume [m^3]	\dot{x}_p	Vertical piston speed [ms^{-1}]
ω	IAS of the crankshaft [rad/sec]	\ddot{x}_p	Vertical piston acceleration [$\text{m}\cdot\text{sec}^{-2}$]
ω_v	Valve unit frequency	θ	Crank angle [deg]
ω_n	Natural frequency of the valve unit [Hz]	ξ	Damping ratio of the valve unit.
ω_s	The motor speed in [rad/sec]	γ	Ratio of specific heats (1.4 for air)
x_{\max}	Max. valve plate displacement [mm]	ρ_c	Density of the air in the cylinder [kg/m^3]
x_{\max}^s	Suction valve max. lift [mm]	ρ_i	Density of the air in the plenum [kg/m^3]
x_{\max}^d	Discharge valve max. lift [mm]	λ	Wavelength

CHAPTER ONE

1 INTRODUCTION

This chapter presents a general introduction to condition monitoring of machines by outlining the relevance of monitoring machines, monitoring strategies available in industry. Finally, the aims and objectives of this research are given, and the chapter ends by describing the layout of the thesis.

1.1 Background and Research Motivation

Reciprocating piston compressors are one of the most common equipment that makes up process plants in several industries including oil and gas refineries, petrochemical industries, chemical plant industries, and many more (Grib & Zhukov, 2001). Compressed air or gases are used throughout production operations, and up to 90 percent of compressed air is lost either in the form of reusable heat, friction, misuse or noise (US Department of Energy, 2003). Also, research has shown that reciprocating compressors are not reliable enough because of the constant collision of mechanical parts, which increase noise levels, cause vibrations, and intensifying degradation of significant machine components (Grib & Zhukov, 2001), (Zheng, 2005). Therefore, it is vital that compressors are carefully monitored and maintained to improve its efficiency in industrial plants.

Monitoring is not restricted to only compressors; it has become exceedingly relevant to know the condition of all major machines, because machine components have reduced service life when subjected to process effects, defected, and are overused. Figure 1.1 highlights the percentage of maintenance costs for several compressor components according to results from a worldwide questionnaire by (Leonard, 1996).

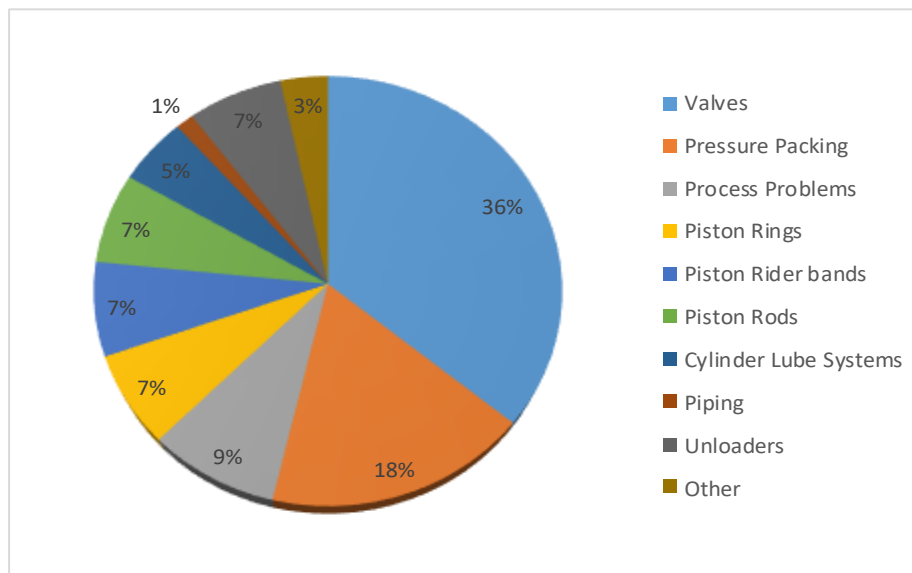


FIGURE 1.1: PRIMARY CAUSES OF UNSCHEDULED RECIPROCATING COMPRESSOR SHUTDOWN

Findings from the worldwide questionnaire, which involved ten countries including: United States, France, Germany, Canada, United Kingdom, China, Singapore, Belgium, Norway, Kuwait and the United Arab Emirates, revealed back in the 90s that compressor valves cost the

most in maintenance because they are actually the heart of the machine and are always subjected to high-pressured air.

A more recent survey carried out by Prognost in 2009 also showed that valve failures are one of the leading causes of unscheduled compressor shutdown (Daniel, 2014). The study was based on records of 524 compressor damages from 72 different plants (see Figure 1.2 below).

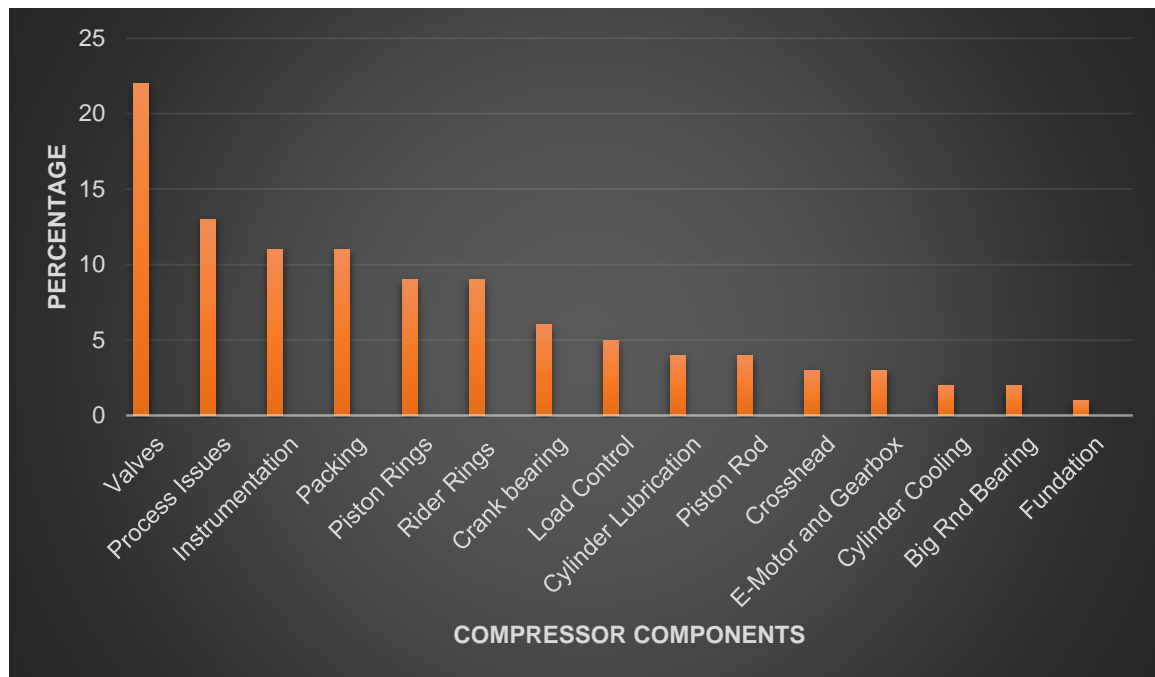


FIGURE 1.2: PROGNOST COMPRESSOR SYSTEM FAILURE MODE SURVEY 2009

Managers, engineers, maintenance personnel and even manufacturers are increasingly becoming interested in both the historical and present state of machinery in their industries because the condition of a machine has significant cost effect on the business with regards to maintenance and fault development. According to the investigation by Leonard, one of the factors, which increase reciprocating compressors' reliability, in hydrogen, services, for instance, is an unscheduled shutdown of reciprocating compressors. It was revealed that an unplanned shutdown of reciprocating compressors results in up to USD 100,000 per day in lost production revenue (Leonard, 1996). Therefore, there is a need to increase the reliability of reciprocating compressors to ensure continuous operation without unscheduled shutdown.

1.2 Relevance of Monitoring Machinery

Maintenance is a word closely associated with monitoring, and the reason is that machines can either fail early (shortly after installation) or later (within or after its lifespan expectancy).

Therefore, industrial professionals and maintenance specialists have realised from experience and years of research, that active monitoring of machines allow for the prediction of the inevitable maintenance requirement of a machine, which goes a long way in enabling its reliability (Williams, Davies, & Drake, 1994). The performance of any machine would deteriorate over time because of the effects on operating conditions (load, harsh environment, human errors, etc.), and the cost of maintenance is a major setback for managers in industry. However, studies have shown that the cost of machine failure or breakdown dramatically outweighs the cost of machine maintenance (Pascual, Meruane, & Rey, 2008); (Komonen, 2002); (Komonen, 1998).

To reduce the cost of unscheduled maintenance resulting from failed key machine components, an effective maintenance strategy is required, which ensures a satisfactory level of machine reliability is achieved throughout its service life. The primary focus of this study is to use vibration and gas pulsation measurements for condition monitoring of reciprocating compressors; however, a brief discussion on maintenance strategies is presented to introduce condition based monitoring/maintenance (CBM).

Corrective maintenance, emergency maintenance, preventive maintenance scheduled maintenance, and condition-based maintenance are some of the widely implemented maintenance practices used in industries (Williams, Davies, & Drake, 1994). These maintenance strategies are classified into two main categories: planned maintenance and unplanned maintenance. Figure 1.3 gives a detailed outline of the two main classes of maintenance strategies.

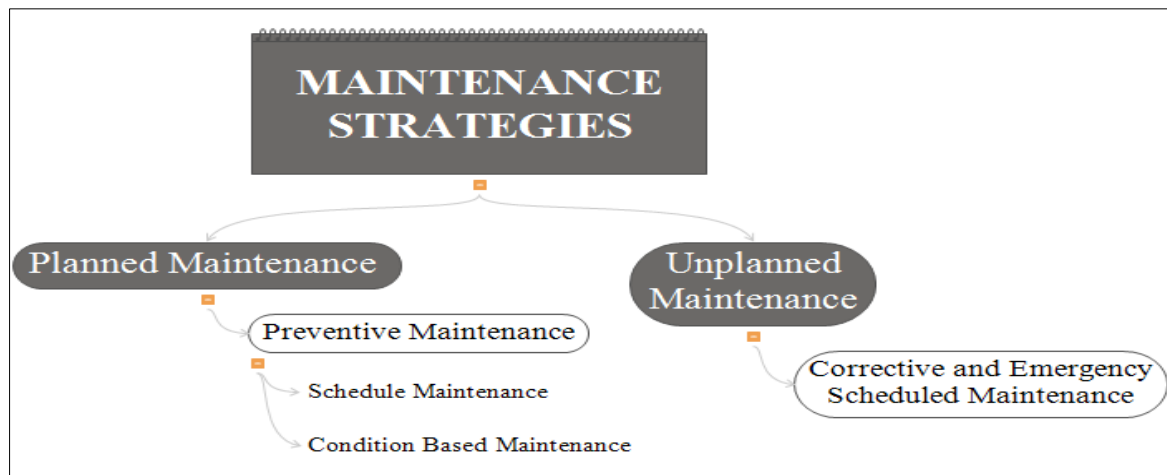


FIGURE 1.3: CLASSIFICATION OF MAINTENANCE STRATEGIES (WILLIAMS, DAVIES, & DRAKE, 1994)

These are all good maintenance practices; however, one or two of these strategies have proven to be more effective and have greater economic advantage over the others. Preferences can be made depending on the size of the equipment being maintained. Unplanned maintenance strategy, which is applied when a failure has already occurred, would be most suitable if the equipment in question is significantly small and the cost of replacement is frugal, with the exception of this, it would be economically unwise to adopt this strategy for large and expensive equipment. Preventive and conditioned based maintenance under planned maintenance strategies are most commonly adopted in industries that use large and very expensive hi-tech equipment. This is because the cost of replacing the entire unit in the event of a problem or even the cost of shutting down the system to detect and diagnose a problem that has no monitoring history would have a great effect on the productivity of the business as a whole (Bentley, 1993). Already business owners and machine manufacturers have taken to condition based monitoring as a viable technique for early detection and diagnosis of machine faults. Early detection of faults and potential problems have proven to result in the following:

- Improved plant performance
- Machine reliability
- Prevents unpredicted shutdown
- Improves Operating efficiency of the machine, and
- Reduced maintenance cost

(Bentley, 1993)

Condition-based maintenance (CBM) also known as on-condition maintenance involves regular or continuous monitoring of the machine to detect particular components within the system that develop faults for appropriate actions to be taken immediately (depending on the degree of effect the problem could cause) to prevent failure or total process shutdown. Condition-based monitoring ensures maintenance action is taken only when the normal operating state of monitored machines change due to a developing fault. Some of the widely adopted condition based monitoring techniques for machine monitoring are:

- Wear debris analysis
- Visual inspection
- Lubrication analysis
- Vibration based monitoring

- Airborne acoustic monitoring
- Gas Pulsation monitoring
- Current monitoring

(Rao, 1998; Williams, Davies, & Drake, 1994)

This study focuses particularly on the employment of vibration and gas pulsation monitoring to determine the condition of a reciprocating compressor. Detailed discussion on key condition monitoring techniques are presented in Chapter three of this thesis.

1.3 Problem Statements

Although several monitoring techniques are available, there are still gaps in the efficiency and effectiveness of some of these available techniques to accurately detect faults, and lead to the prevention of an unplanned shutdown of the reciprocating compressors. These gaps are extant because of the harsh and inevitable operating conditions these machines are subjected to in industrial settings. Therefore, there is a call for researchers to investigate and source new and improved ways of monitoring to improve the efficiency of these industrial machines exposed to ineluctable harsh working conditions.

1.4 Research Aim

To determine the characteristics of faults detected using vibro-acoustic signals from a two-stage single acting reciprocating compressor. This would lead to the discovery of the characteristics and effectiveness of gas pulsation signals and vibration signals for condition monitoring purposes.

1.5 Research Objectives

One: To set up a comprehensive reciprocating compressor test rig, and to develop experimental procedures for condition monitoring of the two-stage reciprocating compressor. This will allow condition monitoring using gas pulsation and vibration sensors, and will allow specific compressor faults to be seeded into the compressor: valve leakage, intercooler leakage, and pipeline discharge leakage.

Two: To review various condition based monitoring techniques presently adopted in industry, and to assess the performance of crucial monitoring techniques suitable for early fault detection.

Three: To develop a mathematical model of the two-stage reciprocating compressor, which includes the gas pulsation behaviour to aid in understanding the physical properties of the reciprocating compressor.

Four: To validate the mathematical model developed by correlating measured and simulated results.

Five: To determine the characteristics of gas pulsation and vibration measurements from the reciprocating compressor using traditional signal processing methods.

Six: To analyse and examine the nonstationary vibration and gas pulsation signatures by the application of advanced signal processing techniques, such as Hilbert transform based convolution and wavelet packet transform.

Seven: To provide guidelines for future research in this field based on the investigations conducted.

1.6 Thesis Outline

Chapter 1: The motivation and background of this research work are presented in this chapter. Also, a brief discussion on maintenance strategies, which leads to the introduction of machinery condition monitoring, is given, and finally the aims, objectives and thesis outline are presented.

Chapter 2: This chapter reviews several compressor types and their typical applications. Then the failure mode and effects analysis (FMEA) of the compressor types discussed is presented following some detailed discussion on crucial reciprocating compressor components.

Chapter 3: This chapter surveys the literature on signal processing techniques used for condition monitoring of machines such as reciprocating compressors. Relevant methods are discussed briefly to help understand the results presented in Chapters 7 to 10.

Chapter 4: This chapter describes the test rig and supporting facilities, which includes all transducers used for the experiment, the hardware (data acquisition system) and software (MATLAB) used for data processing. Finally, common reciprocating compressor faults seeded on the machine are described.

Chapter 5: The mathematical model of the reciprocating compressor developed and modified is presented in this chapter. The model gives the In-cylinder pressure, valve dynamics and

discharge chamber waves of the reciprocating compressor. The experimental signatures are used to validate the model predictions.

Chapter 6: This chapter verifies the accuracy of the developed model by comparing in-cylinder pressure, valve displacement and gas pulsations (at the discharge chamber) predictions with trends from the experimental study under normal conditions. More so, the prediction trends for the fault simulations are also compared with experimental fault measurements.

Chapter 7: To investigate the characteristics of vibration signals from the reciprocating compressor cylinder heads, traditional signal processing techniques such as time domain and frequency domain methods are explored in this chapter.

Chapter 8: This chapter investigates the characteristics of second-stage gas pulsation signals from the discharge chamber of the reciprocating compressor by applying traditional signal processing techniques such as time domain and frequency domain methods. In addition, the effectiveness of these techniques are investigated when three common reciprocating compressor faults are present (valve leakage, intercooler leakage and discharge pipeline leakage).

Chapter 9: This chapter presents the analysis of vibration signal using advanced signal processing technique wavelet packet transform for detecting two common reciprocating compressor faults (valve leakage and intercooler leakage) including the effects of the two faults combined.

Chapter 10: This chapter presents the analysis of gas pulsation signal using advanced signal processing technique wavelet packet transform for detecting common reciprocating compressor faults (valve leakage, intercooler leakage, and discharge pipeline leakage) including the effects of valve leakage and discharge leakage simultaneously.

Chapter 11: In this chapter, the research objectives and achievements are reviewed. Furthermore, a summary of the novel features and contribution to knowledge regarding this research are detailed, and finally, recommendations for future work are presented.

CHAPTER TWO

2 RECIPROCATING COMPRESSORS AND COMMON FAILURE MODES

This chapter briefly reviews different types of compressors and their applications. Then the operating principles of reciprocating compressors are presented for single-stage and double-stage compressors. Failure mode and effects analysis (FMEA) of the positive displacement type compressors are carried out, and finally, key components of the reciprocating piston compressors are reviewed.

2.1 Introduction

Compressors are used to move gases or other fluids with pressures as low as 35psi (pound per square inch) from one location to a different location at an increased pressure of about 65000 psi in extreme cases (Heinz & John, 1996). These machines are one of the oldest and most popular devices widely used in refineries, chemical plants, and oil production facilities. Compressor history dates as far back as the 1850s and was very popular for its design simplicity and ability to provide very high pressures under variable loading.

The following sections give a brief overview of several compressor types (see Figure 2.1) to provide an elementary understanding of all compressor concepts and their functions. The ability to identify and understand several compressor types and their application can significantly reduce the extra cost accrued from unplanned maintenance, or compressor failure (Robison & Beaty, N.d).

2.2 Compressor Types

Compressors vary in sizes, operation mechanism and application range (power requirement, stage requirement, pressure ratios etc.). Based on the compression mode, compressors can be subdivided into two primary modes or types namely:

- Intermittent – Meaning that compression takes place in cycles or phases and compression can only continue after a cycle is completed.
- Continuous – This means that compression of the gas is not interrupted at any time until the whole process is completed.

These two modes of compression, intermittent and continuous are further grouped into positive displacement and dynamic compressors. The positive displacement compressor types have the needed volume of gas enclosed in a space and displaced at a higher pressure, mechanically changing the volume of the enclosed gas. On the other hand, the dynamic compressors make use of a rotating element to continuously move gas in and out of the device (Brown, 2005). Figure 2.1 presents a brief listing of different types of compressors classified according to the compression modes discussed.

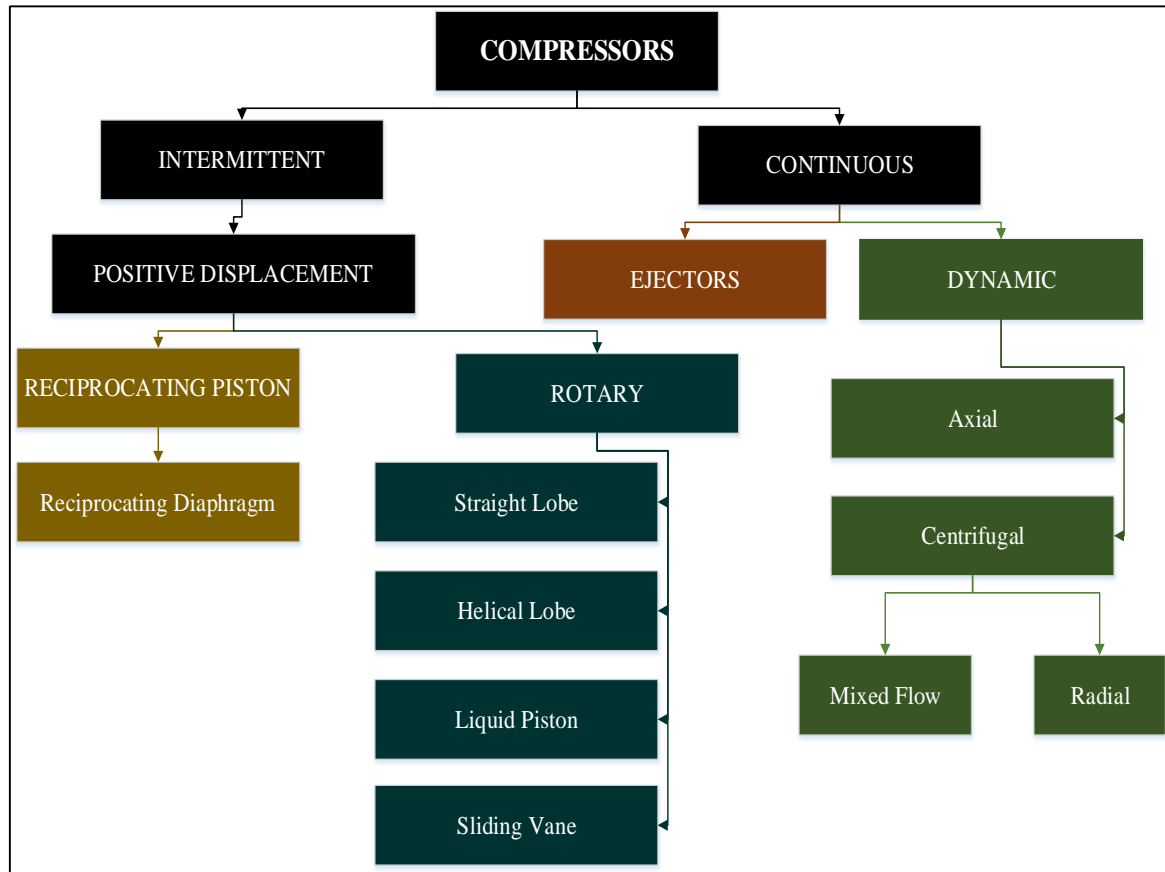


FIGURE 2.1: COMPRESSOR CLASSIFICATION

2.2.1 Dynamic Compressors

Dynamic compressors are of the continuous flow class; they mainly transport suction fluid into a diffuser through a high-velocity steam jet (Boyce, 2009). The two main types of dynamic compressors are briefly described in the following subsections (2.2.1.1 and 2.2.1.2).

2.2.1.1 Centrifugal Compressors

A centrifugal compressor is a dynamic machine that typically functions using impellers continuously accelerating gas through a diffuser and out of the compressor chamber. As seen in Figure 2.2, the diffuser consists mainly of vanes, which are tangential to the impeller. These type of compressors use three acting forces – centrifugal, aerodynamic, and change in velocity to produce an increased discharge pressure higher than the initial suction gas pressure. Centrifugal compressors are mainly used in petrochemical industries because of their smooth operation process and high reliability compared to other compressor types (Boyce, 2009).

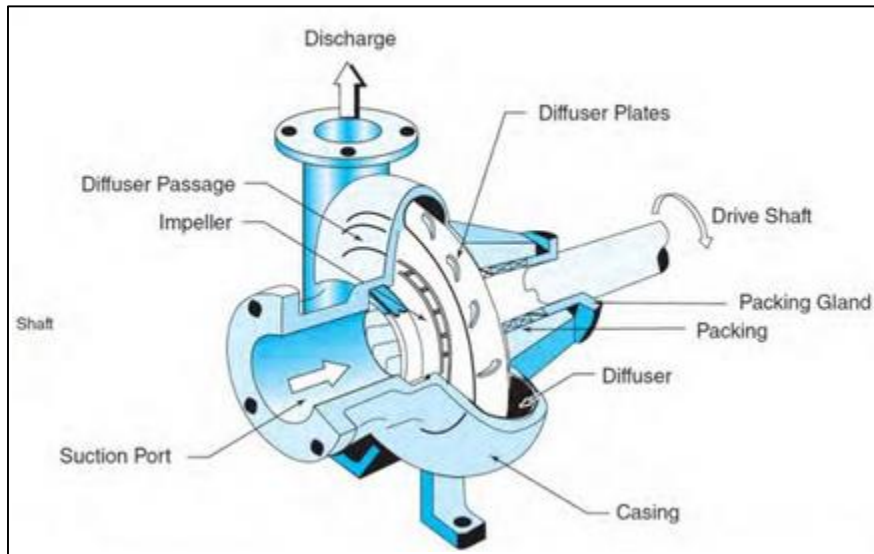


FIGURE 2.2: A CENTRIFUGAL COMPRESSOR (BOYCE, 2009)

2.2.1.2 Axial Compressors

The axial compressor, like the centrifugal counterpart, is a dynamic machine mostly used in large gas turbines. Compression is achieved by applying inertia forces through rotors to increase the speed of the fluid. The fluid is diffused by another row of stationary blades called stator, to increase fluid pressure (Boyce, 2009); (Giampaolo, 2010). Figure 2.3 shows a typical schematic of the axial compressor. The axial compressors are usually of higher efficiency, but when it comes to large operating region and cost, the centrifugal type is preferred.

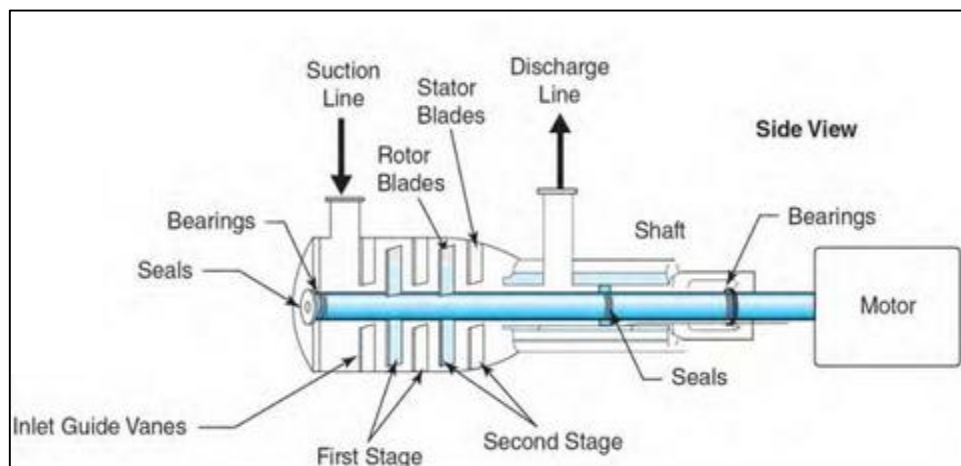


FIGURE 2.3: AN AXIAL COMPRESSOR (GIAMPAOLO, 2010)

2.2.2 Ejectors

Ejectors are continuous compression flow machines; however, unlike the dynamic compressors, which also exhibit the same flow mechanism, they have no moving parts as seen from the schematics in Figure 2.4 (Brown, 2005).

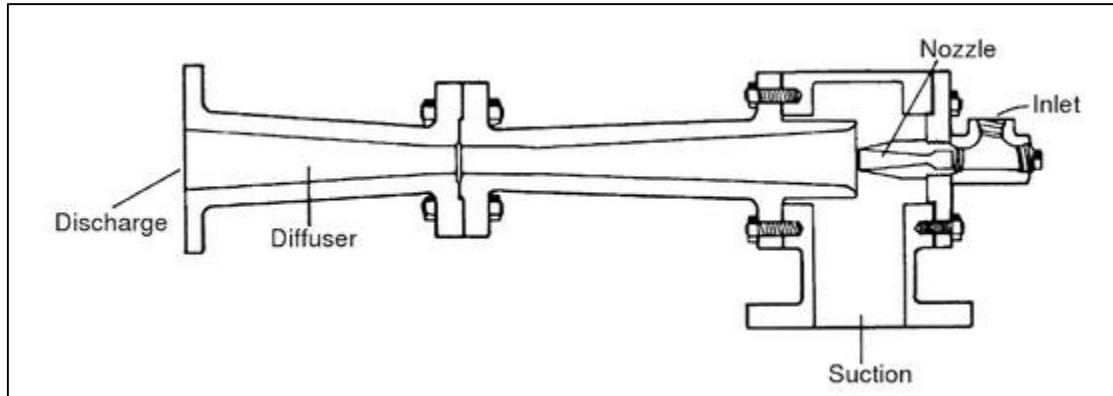


FIGURE 2.4: TYPICAL EJECTOR (BROWN, 2005)

2.2.3 Rotary Positive Displacement Compressors

Rotary positive displacement compressors are compressors that function by using a rotary device - blade or impeller to push the fluid (gas or liquid) from one place to another increasing its pressure as it moves. This group of compressors are compact, relatively low-priced, and require very little maintenance (Mobley, Root Cause Failure Analysis: Plant Engineering Maintenance Series, 1999). They can be categorised into three main types.

2.2.3.1 Sliding Vane Compressors

The essential elements of the sliding vane are the cylindrical housing and the rotor assembly. Sliding vane compressors have blades embedded within an eccentrically fitted cylinder located in a tube that rotates. The major difference between a reciprocating compressor and the sliding vane is the absence of spring-loaded valves, which are present in reciprocating compressors and not in sliding vane compressors (Mobley, 1999).

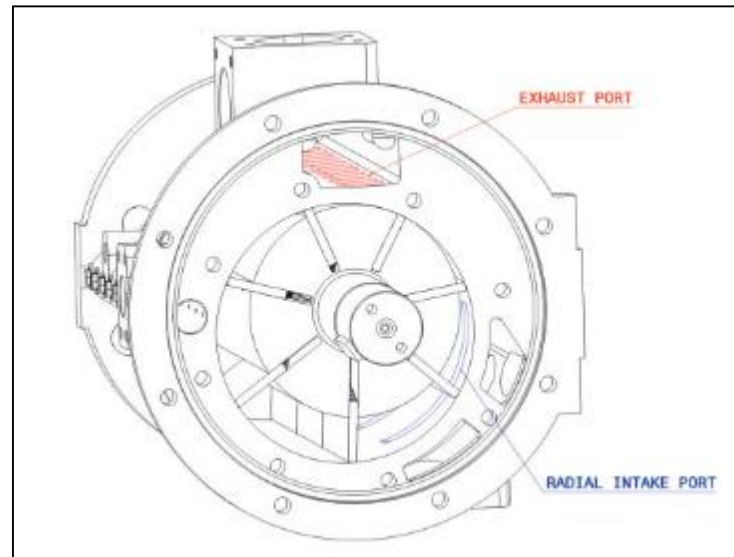


FIGURE 2.5: SCHEMATICS OF A TYPICAL SLIDING VANE COMPRESSOR (CIPOLLONE, 2016)

2.2.3.2 Helical Lobe Compressors

The Helical lobe compressor is also known as a rotary screw compressor. It works by using two inter-meshing screws (one male and the other female) rotating towards each other causing the gas to be trapped in the centre cavity and finally discharging the gas through the outlet, creating a higher gas pressure (Mobley, 1999). Two primary characteristics of the helical lobe are:

1. Variable pressure,
2. Constant volume.

Failure of these machines is prevented via control measures, which entail setting the relief valves and safety valves within 10 percent of absolute discharge pressure (Mobley, 1999). These compressors can handle moderate amount of liquid, dirty gases, and do not encounter pulsating flow.

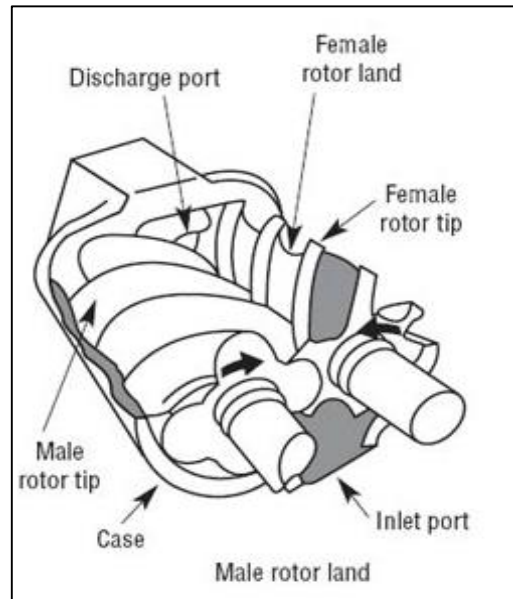


FIGURE 2.6: HELICAL LOBE COMPRESSOR (ORMER, 2002)

2.2.3.3 Liquid-Seal Ring Compressors

The liquid ring is also called liquid-piston and consist of a rotor with several forward-turned blades, rotating about the middle cone, which has suction and discharge ports as seen in Figure 2.7. The liquid ring though similar to sliding vane type differs from the sliding vane compressor as both liquid and gas are introduced to the chamber for compression; the liquid is separated from the compressed gas with the aid of a conventional baffle or a centrifugal separator (Mobley, 1999).

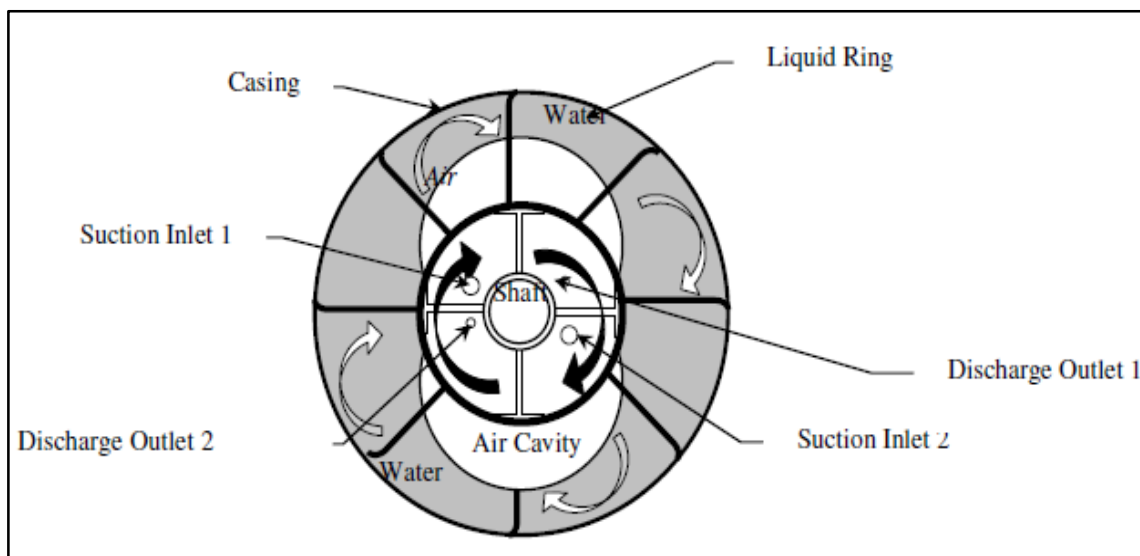


FIGURE 2.7: A TYPICAL LIQUID RING COMPRESSOR (AL-QATTAN, 2007)

2.2.4 Reciprocating Piston Compressors

The reciprocating compressor is an intermittent flow, positive displacement machine that functions by the forward and backwards (reciprocating) movement of a piston in a cylinder to deliver fixed volume gas at a higher pressure. They are one of the most efficient compressor types according to Mobley (1999) and can be used for applications that require high-pressure at a low flow rate. However, because of the high number of components within the reciprocating machine which require maintenance, these compressor types are considered unreliable (Brown, 2005). The primary components of this compressor type are labelled in Figure 2.8.

Depending on the compression ratio required for a particular application, the reciprocating piston compressors can be single-stage or multi-stage; Also, for refrigeration services and smaller air compressors, single-acting cylinders are employed. However, for process services and larger air compressors, double-acting configuration is usually used (Brown, 2005). Double-acting construction uses both sides of the piston for compression, and two piston strokes are present in one revolution, while with the single-acting configuration, only one side of the piston is used for air compression.

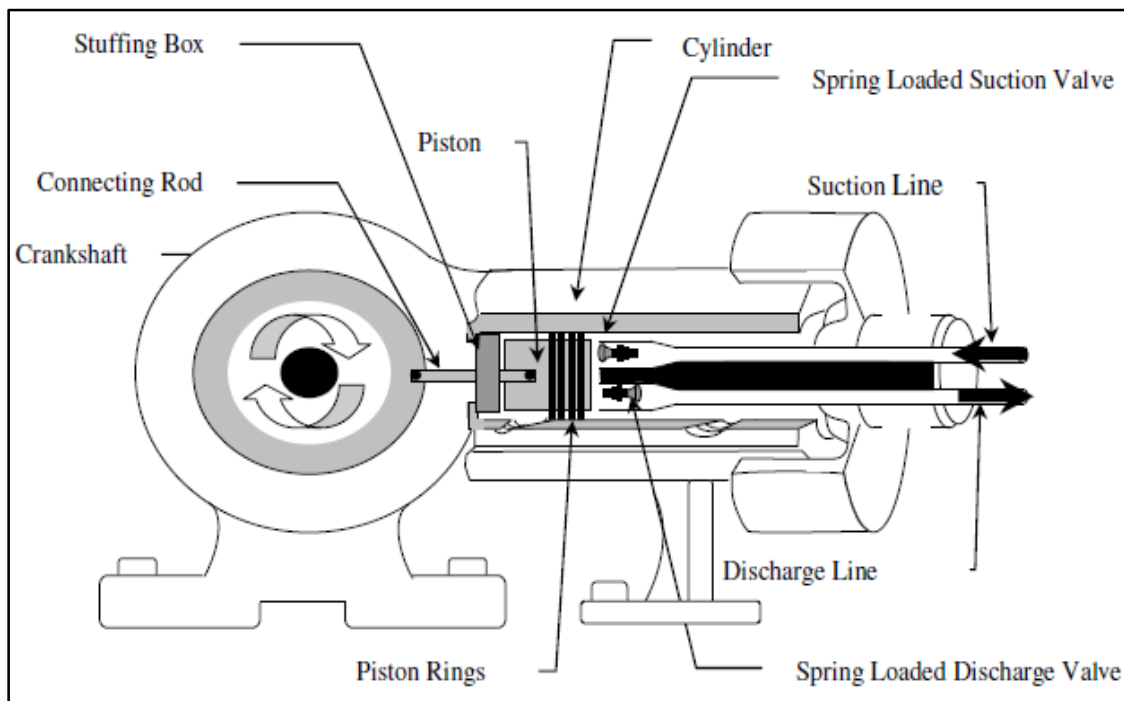


FIGURE 2.8: CROSS-SECTION OF A TYPICAL SINGLE-ACTING RECIPROCATING COMPRESSOR (AL-QATTAN, 2007)

2.2.4.1 Operating Principle of a Reciprocating Compressor

Figure 2.9a illustrates the piston movement and valve behaviour of a reciprocating compressor, and Figure 2.9b shows an actual pressure-volume diagram for one compression cycle for a single-acting reciprocating compressor. The typical operating principle of a single-acting, single-stage reciprocating compressor often begins with both suction and discharge valves closed, then the piston travelling in the opposite direction from the cylinder head causing a pressure drop in the cylinder, which opens the suction valve allowing gas to enter into the cylinder. This process is illustrated in Figure 2.9a POSITION A. Once the pressure in the cylinder is equal to the suction-line pressure, the suction valve closes, and by this time or crank angle, the piston is at bottom dead centre (BDC) as seen in POSITION B. The crankshaft rotation causes the piston to move in the reverse direction travelling back towards the cylinder head at top dead centre (TDC), compressing the suctioned gas and increasing the cylinder pressure (POSITION C). The discharge valve opens as soon as the valve spring force is overcome and the cylinder pressure is higher than the discharge-line pressure; this takes place in POSITION D of Figure 2.9a. The discharge valve closes when the gas is equal to volumetric clearance, which is when the piston reaches TDC. This process is repeated as the piston moves back towards the BDC of the cylinder because of crankshaft movement (Arnold & Stewart, 1999); (Brown, 2005). These compression steps are illustrated in the p-v diagram (see Figure 2.9b), which helps to identify the condition of the reciprocating compressor at each process of the compressor cycle.

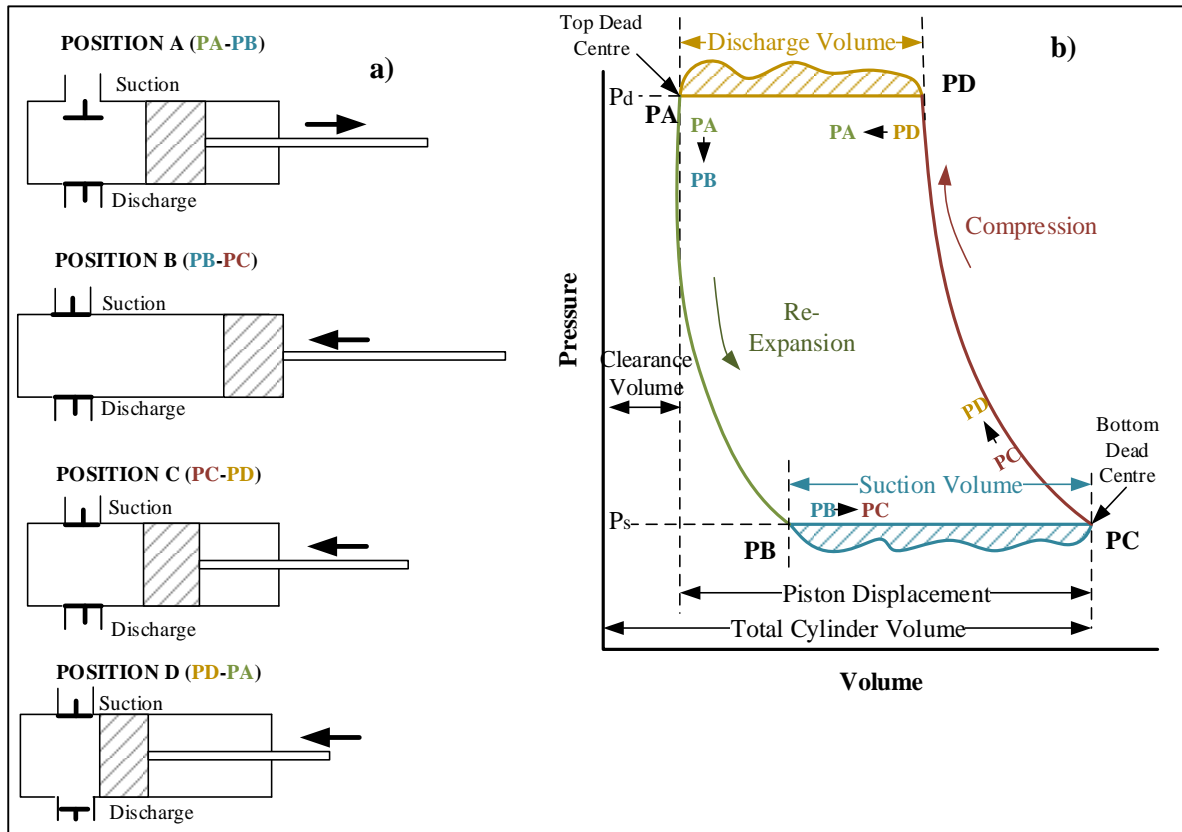


FIGURE 2.9: SINGLE-ACTING COMPRESSION STEPS OF A COMPRESSOR CYLINDER B) ACTUAL P-V DIAGRAM OF SINGLE STAGE COMPRESSION CYCLE

2.3 Typical Compressor Application

This section reviews some typical compressor applications. The choice of what compressor to use for any particular application depends on three main factors: the flow rate, pressure required and characteristics of the fluid to be compressed. Table 2.2 gives a list of some applications and several compressor types used in industries; also, Figure 2.10 shows a graphical illustration of flow ranges for various compressor types used in refineries, chemical and gas processing industries.

Centrifugal compressors have the broadest application range; while the reciprocating compressors can compress lower volumes compared to the centrifugal type and are most suitable for very high-pressure applications. Axial compressors are best for applications requiring high capacity, whereas, the rotary types (including sliding vane, helical lobe, and liquid ring) are chosen for reasons not relating to pressure and capacity range.

TABLE 2.1: COMPRESSOR APPLICATIONS

INDUSTRY	APPLICATION/SERVICES	COMPRESSORS USED
Oil and Gas	Booster	Centrifugal and/or Reciprocating compressors
	Gas Lift	Centrifugal Compressors
	Flash Gas	Centrifugal, Screw Compressors
	Vapour Recovery	Sliding Vane/ or Screw Compressors
	Overhead or flare Gas compression	Reciprocating compressors
	Gas transmission applications	Reciprocating compressors
Refineries	Fluid Catalytic Cracking air blower	Axial Compressors,
	In chemical processes that require high capacity air compression	Axial and Reciprocating Compressors
	Combustion Gas turbines	Axial Compressors
	Processing unit hydrogen make-up	Reciprocating Compressors
Petrochemical Industry	Flammable and hazardous gas services	Reciprocating Compressors
	Freon and Ammonia refrigeration	

CHARACTERISING VIBRO-ACOUSTIC SIGNALS OF A RECIPROCATING
COMPRESSOR FOR CONDITION MONITORING

LPG	Plant air, some wet services, and services with vacuum suction conditions	Rotary Compressor types
Other Services	Smaller Air Compression Services	Reciprocating Compressors

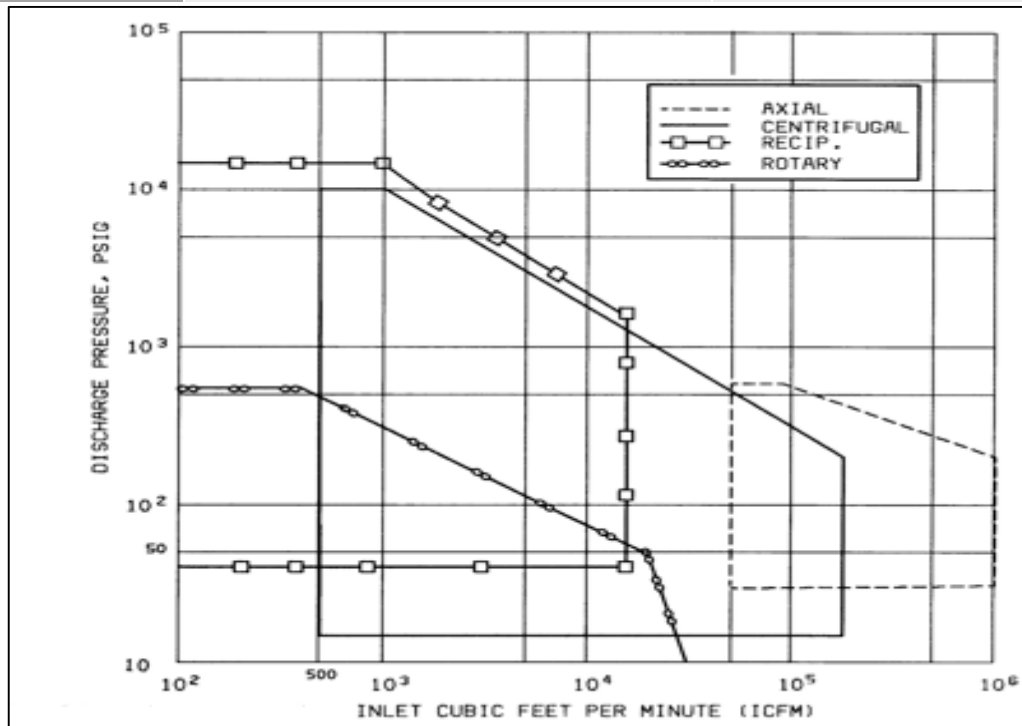


FIGURE 2.10: COMPRESSOR TYPES AND THEIR APPLICATION RANGE BASED ON PRESSURE AND FLOW (BROWN, 2005)

2.4 Compressor Problems

No proper operating process can remain in the same condition without appropriate maintenance and checks being carried out from time to time or at a scheduled time. This is because, on constant or continuous use, components within any system would deteriorate over time and eventually lead to unwanted failure. Appendix I presents some common problems and their causes often associated with positive displacement compressors according to Mobley, (2004). Valve failure, pulsations and imbalance are the most common problems that occur with the positive displacement compressors. These problems are heavily associated with the inherent nature and vibrations from the system. Extensive variations in molecular weight and specific heat of gas, temperature, and pressure results in the following problems:

- The available driver power could be exceeded

- Failure to meet the required throughput.
- The required discharge pressure will not be achieved and the inability to achieve the desired discharge pressure would cause the operation to shut down

(Giampaolo, 2010)

2.5 Reciprocating Compressor Components

2.5.1 Compressor Valves

The compressor valves also known as check valves, are used to control the inlet (suction) flow and discharge flow of gas within the compressor cylinder. They are known to be the key component in a reciprocating compressor because valve fault would directly affect the efficiency (capacity and horsepower) and reliability of the compressor (Hanlon, 2001).

The opening and closing of check valves are due to the differential pressure of the substance being compressed; however, in certain conditions, the springs could be used in addition to the differential pressure of the gas to aid opening and closing. The valve displacement must be large enough to allow the required amount of gas into the system for every revolution of the crankshaft. Compressor efficiency would increase with smaller valve displacement because less energy will be needed to open the valve. Furthermore, a lower valve displacement would result in smaller impact velocities of the valve body on its seat, reducing fatigue, noise, and failure of valves. Table 2.5 outlines common valve types used in compressors.

TABLE 2.2: COMPRESSOR VALVES (BROWN, 2005; O'NEILL, 1993)

VALVES	DESCRIPTION	ADVANTAGES
Poppet valves	These valves are commonly used for low compression ratio and low speed compressors.	They are sturdy and have a high resistance level.
	Poppet valves made of polymer is used for systems with higher compression ratios	They are tolerant to rust, dirt etc.

CHARACTERISING VIBRO-ACOUSTIC SIGNALS OF A RECIPROCATING
COMPRESSOR FOR CONDITION MONITORING

Mini-poppet Valves	They are common poppet valves with a much smaller poppet and valve seat hole, used mostly for high compression ratio compressors.	
Reed valves	<p>Sufficient pressure from the gas in the appropriate direction overcomes the spring force of the reed and causes it to bend allowing gas flow.</p> <p>They are used in high-performance two-stroke engines.</p>	These valve types are very flexible, allowing both suction, and discharge valves to be incorporated into one valve plate.
Channel valve	These valves have a series of straight slots in the valve body for gas to pass through. They are generally applied to industrial air machines	They are durable
Concentric Ring Valves	These valves are made up of one or more relatively narrow rings arranged concentrically about the centreline of the valves	They are commonly used valves in air and gas compressors.
		It has a high tolerance for impacts.
Ported Plate valves	They are similar to concentric ring valves, but the rings of the ported plate valves are joined into a single element	Easy to control flow because the valve has a single element; impact on the valve is reduced due to the single element
Feather Valve	These valves are mostly applied to industrial air machines and are made up of rectangular elements	

Poppet valves, ring valves, and plate valves, rectangular element (feather, channel and reed valves) are four common valve configurations used in reciprocating compressors (Arnold &

Stewart, 1999; Brown 2005). Some of the valves described above are seen in Figures 2.11 and 2.12.

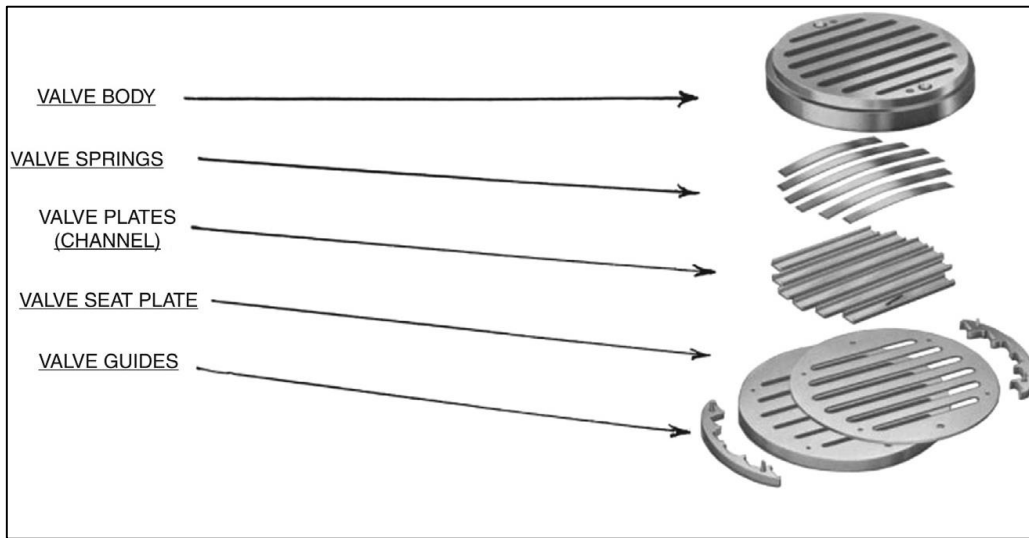


FIGURE 2.11: CHANNEL VALVE (FORSTHOFFER, 2017, p. 119)

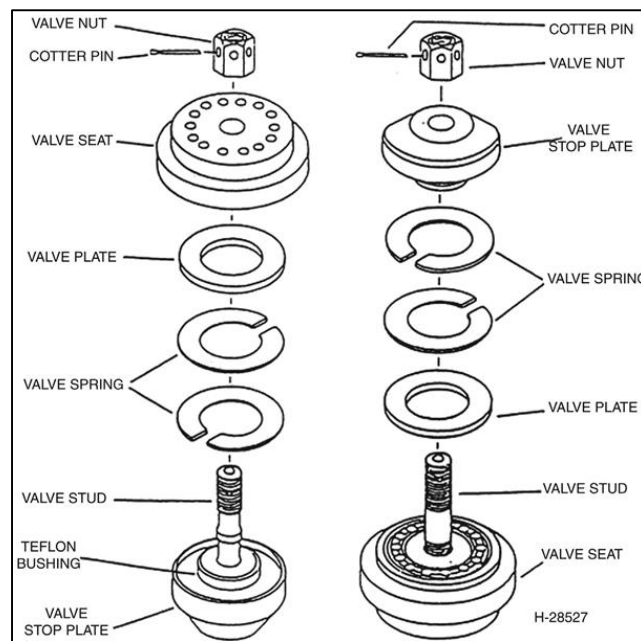


FIGURE 2.12: PLATE VALVE (FORSTHOFFER, 2017, p. 120)

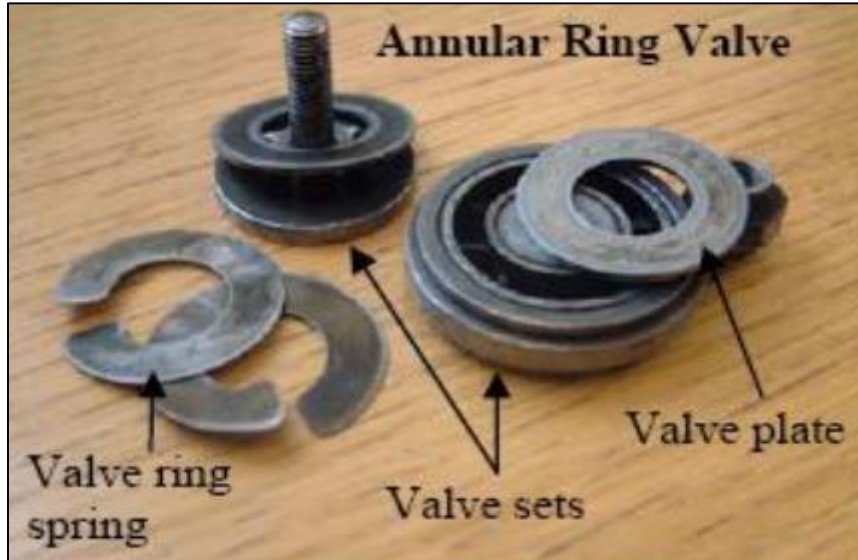


FIGURE 2.13: ACTUAL PLATE VALVE USED FOR THIS RESEARCH

2.5.2 Elements of a Compressor Valve

Four essential components of a compressor valve are: valve seat, sealing element(s), lift constraint (guard), and spring(s). To calculate the dynamics of a valve, the difference in pressure across the force area of the valve plate A_v ; the springing of the valve and the contribution made by the viscous forces during the initial stages of the valve opening are three factors to be considered together with the resulting force in the equation (2.1) below:

$$m_v \ddot{x}_v = (p_1 - p_2) A_v - k(x_v + l_1) - F_{adh} \quad (0.1)$$

Where:

m_v = Mass of Valve plates

k and l_1 = the stiffness of springing and initial deflection of the springs

p_1 and p_2 = pressure in front of the valve and pressure behind the valve respectively

F_{adh} = adhesion force and is determined by the equation

$$F_{adh} = f_1 \frac{\dot{x}_v}{x_v^3} \quad (0.2)$$

The type of compressor valve used in this study is the annular ring valve See Figure 2.13. This valve consist of concentric rings held against ring springs. These annular ring valves are

suitable for corrosive environments, also, its design allows for easy fitting and removal of valve components for maintenance purposes.

2.5.3 Compressor Cylinder

The compressor cylinder is a vessel used to keep the gas during compression (SPE International, 2013; Arnold & Stewart, 1999). As mentioned above, the cylinder can be either single or double acting type.

It is also worth mentioning that according to the reports from SPE International (2013), the maximum allowable working pressure (MAWP) for any cylinder should be at least 10% higher than the design discharge pressure or a minimum of 25 psi.

2.5.4 Compressor Cylinder Liner

These are usually included in the cylinder composition to make the cylinders last longer, and these liners can be easily replaced if damaged as a result of heat or piston action.

However, one disadvantage of having these liners is that they increase the clearance between the valve and piston thereby lowering the capacity and efficiency of the cylinder.

2.5.5 Compressor Crankshaft

The crankshaft revolves around the centre of the frame, causing the crosshead connected to the rod to rotate. The piston rod and piston is driven by the linear reciprocating motion of the crankshaft (Arnold & Stewart, 1999; SPE International, 2013). (Arnold & Stewart, 1999)

Material specification for compressor crankshafts:

- For large compressors (above 150 to 200 horsepower) – forged steel crankshafts
- For medium size compressors – cast crankshafts

2.5.6 Compressor Piston

The piston prevents the gas from spreading through to unwanted areas within the cylinder, and is situated at the end of the piston rod. Aluminium and cast iron are two common lightweight materials that the piston is made of and damages to the piston are prevented by using wear bands and piston rings (SPE International, 2013; Arnold & Stewart, 1999).

2.5.7 Compressor Bearings

Bearings are located in several areas within the reciprocating compressor system. For instance, the main bearing is located between the crankshaft and frame (Arnold & Stewart, 1999). Bearings are mainly used to tightly secure the crankshaft, connecting rod, and crosshead within the compressor frame to ensure proper positioning.

CHAPTER THREE

3 REVIEW OF CONDITION-BASED MONITORING (CBM)

This chapter presents a critical review of common machine monitoring methods and techniques applicable to reciprocating compressors and their limitations. The second part of this chapter reviews possible statistical parameters and features for fault detection of industrial machinery.

3.1 Introduction

Condition monitoring is a practice that has been in existence since the late 70s; In a general sense of understanding, condition based monitoring or maintenance (CBM) can be seen as practices that enable long term reliability and sustainability of assets (Scott, 2011). Various components within a machinery have limited lifespans, and frequent use may cause these components to wear before reaching its service life. There is a need to assess the condition of process machinery to prevent unexpected failures, which can disrupt industrial operations. By consistent monitoring of measurable parameters, changes that result from the continuous use of machines are detected and 10 to 20% catastrophic failures in unmonitored reciprocating compressors can be prevented according to finding by Schultheis, Lickteig, and Parchewsky (2007).

Machine monitoring and diagnostics allow for early detection of faults, and these faults can develop into severe problems if not managed in time. Monitoring also allows for effective analysis of information retrieved from measuring instruments to give an appropriate diagnosis of system-generated issues. Furthermore, production capacity, product quality, and the effectiveness of production plants can be massively improved by implementing an effective monitoring system (Rao B. K., 1998). Some of the most popular techniques suitable for condition monitoring of reciprocating compressors include visual inspection, cylinder pressure monitoring, instantaneous angular speed, air-borne acoustic (gas pulsation) monitoring, and vibration monitoring are briefly discussed.

3.2 Visual Inspection

Visual inspection is one of the simplest and oldest traditional condition monitoring techniques; it requires the human senses such as sight, touch, and sound to detect abnormalities on the reciprocating compressor. It is cost effective but requires the assessor to have basic knowledge or some experience on condition monitoring of the machine for an accurate assessment. Visual inspection is often used for detection of cracks, corrosion, excessive noise, excess leakage and heavy vibrations. However, this technique is usually supported by other monitoring techniques for a reliable and valid assessment.

3.3 Cylinder Pressure Monitoring

Cylinder pressure monitoring is an effective way to determine the overall condition of a reciprocating compressor. Valuable information on the compressor capacity and power, piston

rings, suction and discharge valves can be obtained from the dynamic cylinder pressure measurement. Figure 3.1 shows a typical one revolution pressure measurement from a two-stage reciprocating compressor.

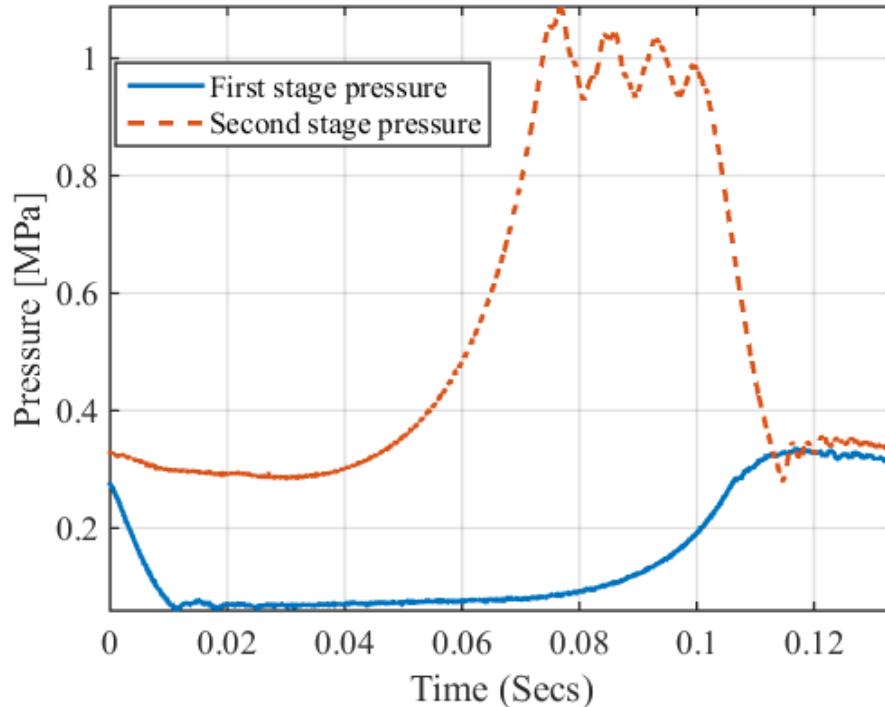


FIGURE 3.1: PRESSURE MEASUREMENT FROM A TWO STAGE RECIPROCATING COMPRESSOR

The dynamic cylinder pressure profile is of great value because it provides the ability to correlate events from noisy vibration measurements with events in the pressure plots (Caie & Bickmann, 2017). However, the pressure-volume diagram which was a popular visualisation indicator used for monitoring the condition of reciprocating compressors with slow speeds is no longer practical when used on machinery with increased speed according to (Goldman, 1984). Also, it might not always be feasible to physically mount a pressure sensor directly inside the cylinder of a reciprocating compressor due to mechanical and sensor safety reasons. This is why non-destructive means are often preferred for condition monitoring of reciprocating compressors.

Several approaches have been explored using pressure signals to detect faults on the reciprocating compressor. Pichler and his colleagues used the pressure-volume diagram (PV diagram) to detect leaks from the reciprocating compressor valves. Their study revealed that the shape of the P-V diagram is distorted when there are leaks on the valves especially when the valves are closed (Pichler, et al., 2013). Whereas, Wang, et al., used pressure-volume

diagram together with a support vector machine (SVM) for fault diagnosis of reciprocating compressor valves (Wang, Song, Zhang, & Li, 2010). Elhaj, et al. developed the numerical simulation of a two-stage reciprocating compressor to show the effects of several operating conditions and fault conditions on the pressure and instantaneous angular speed (IAS) waveform. The simulation study showed that the two techniques used can show waveform fluctuations, which can be used to identify different valve faults on the suction and discharge valve plates. Although the pressure measurements presented clear detection features, it was acknowledged that this technique was difficult to implement due to its intrusive installation means (Elhaj, et al., 2008).

3.4 Instantaneous Angular Speed

The instantaneous angular speed (IAS) measurement is also an effective method for condition monitoring of reciprocating compressors, mostly because the speed contains relevant information about the cylinder pressure and has been successfully employed in fault detection of valve leakage and worn valve spring on the reciprocating compressor (Elhaj, et al., 2008); (Al-Qattan, Al-Juwayhel, Elhaj, Ball, & Gu, 2009). To apply this method, an encoder fitted to the crankshaft of the flywheel is required to measure the angular speed at any instant in radians per second or revolution per second. Processing of the encoder signal is done by counting the number of pulses in a given period and measuring the elapsed time for one cycle of the encoder signal (Li, et al., 2005).

Machine monitoring via IAS measurement has been studied widely in recent years because IAS signals have less noise contamination and are closely related to the machine dynamics compared to other traditional methods such as vibration and airborne acoustics, and it is less intrusive than monitoring using pressure measurement. Figure 3.2 shows a typical one revolution IAS signal from a reciprocating compressor under normal operating condition.

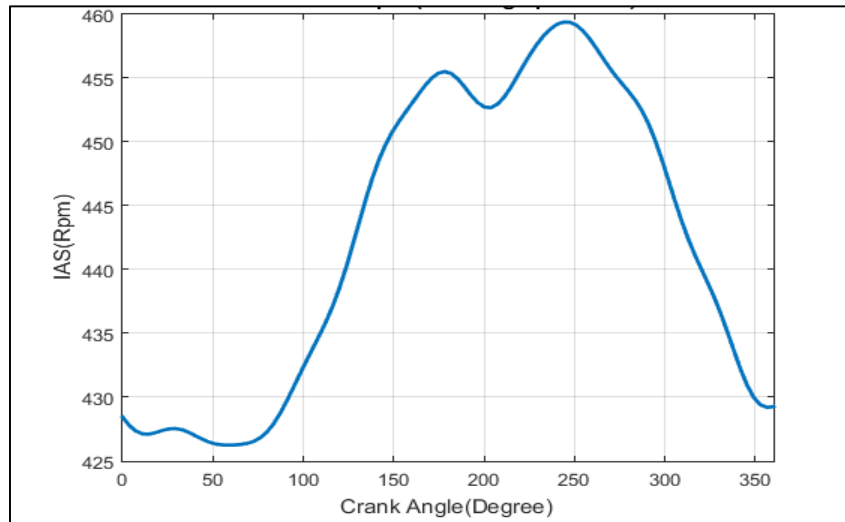


FIGURE 3.2: ONE CYCLE OF IAS MEASUREMENT FROM A RECIPROCATING COMPRESSOR

3.5 Airborne Acoustics

Structure-borne and air-borne analyses are two main approaches used for sound monitoring. The air-borne approach captures radiated sound waves above the human hearing range (above 20kHz) using contactless microphones or sound transducers whereas the structure-borne approach captures structural vibration through sensors mounted on the surface of the system. Compared to the structural vibration approach, airborne acoustic transducers are easier to install; can detect low and high frequency range; allow more sensitive detection and the signals are easier to analyse (Scruby, 1987); (Liebetau & Grollnisch, 2017). However, one major drawback of this technique is in its susceptibility to environmental acoustics and intrusive background noise.

The effectiveness of acoustic sensors in condition monitoring of machines, particularly diesel engines have been the widely studied by scholars, and from literature it has been established that an appropriate filter technique is required to extract useful information from the contaminated acoustic signals. For instance, due to high environmental influences on acoustic data, Gu, Ball, & Li, highlighted the need to extract foreign noise generated together with wanted sound signals before the exact characteristics of sound signals could be used to diagnose faults (Ball, Gu, & Li, 2000). Another study carried out by Albarbar, Gu, Ball, & Starr, used adaptive filtering techniques to remove unwanted noise from the signal generated from acoustic monitoring of diesel fuel injection needle (Albarbar, Gu, Ball, & Starr, 2010). Furthermore, Jiang, et al., introduced the use of acoustic one-port source theory and the use of

exhaust acoustic measurements to effectively monitor diesel engine combustion. Their research showed that despite the harsh operating conditions these machines function under, a two-load acoustic method could accurately detect and diagnose abnormalities caused by faults (Jiang, et al., 2008). The acoustic condition monitoring of diesel has gained massive attraction over the years; however little work has been performed on RC noise characteristics or the use of gas pulsation from the reciprocating compressor for early fault detection.

Several studies by (Brablik J. , 1972), (Stiaccini, Galoppi, Ferrari, & Ferrara, 2016), (Zhou, Kim, & Soedel, 2001), and (Zhan, Cheng, & Quanke, 2015) exist on modelling philosophies to accurately predict pulsations on reciprocating compressors. Furthermore, Pan and Jones investigated airborne sound transmission in a spherically shaped reciprocating compressor, using simulation predictions and experimental results to understand the relationship between gas pulsations inside the cavity and noise radiation from the compressor (Pan & Jones, 1999). Glen and Eugen focused on the use of acoustic signals to predict pressure and mass fluctuations from a reciprocating compressor (Glen & Eugene, 1989). As a result of Glen and Eugen’s investigations, they concluded that vibration analysis is not very sensitive to high –frequency noise emitted by fluid mechanical motion. Salah et al. proposed an automatic diagnosis of reciprocating valve condition by adopting support vector machine based on acoustic emission (AE) parameters. Their generated model could accurately diagnose valve condition in a single-stage reciprocating compressor (Salah, Hui, Hee, & Salman, 2018). The AE signal together with simulated valve motion was used by Wang and his colleagues to diagnose reciprocating compressor valve faults including valve leakage, valve flutter, delayed closing, and improper valve lift (Wang, Gao, Zheng, & Peng, 2015). Their technique has an advantage of distinctly extracting valve fault features without applying complex signal processing techniques.

The amplitude of a sound wave is expressed as sound intensity or sound pressure level. The total acoustic power emitted by the sound source is given by the Sound power, which is defined as the power per unit area per unit time of the sound wave (Watt / m^2). The sound pressure level (SPL) is calculated as per Equation (3.1) and expressed in decibels (dB).

$$SPL = 20 \log_{10} \left(\frac{p}{p_{ref}} \right) \quad (3.1)$$

Where p is the root mean square amplitude of the pressure wave and p_{ref} is the reference sound pressure (Mohanty, 2015).

Analysing emitted sound waves from the reciprocating compressor allows for the detection of system defects such as leak detection, crack detection, and provides access to the general condition of the machine. Under normal operating conditions, most machines emit consistent sound patterns, but with the development of component defects, regular patterns are distorted. Figure 3.3 gives a typical airborne acoustic waveform with key characteristic features according to Yan, et al., 2015.

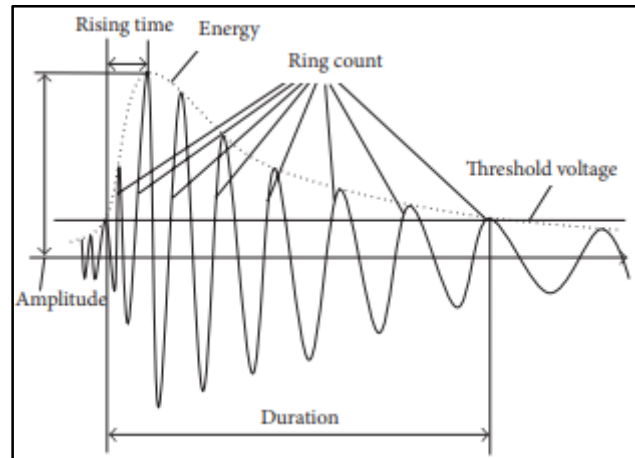


FIGURE 3.3: SIMPLIFIED WAVEFORM PARAMETERS OF AIRBORNE ACOUSTIC SIGNAL (YAN, ET AL., 2015)

3.6 Vibration Monitoring

Vibration signals from a machine contains vital information needed to determine and predict the condition of the machine. Vibration-based techniques are the most common and widely established monitoring technique used in industries (Gu, Li, Ball, & Leung, 2000). This is because almost all machines vibrate, and these vibrations can be measured easily and interpreted to determine the state of a machine. Imbalances in forces acting in the upwards, downwards, or side to side direction of the mechanical system prevent a smooth flow of energy thereby causing the system to vibrate. Factors such as overload due to stress on a machine, little or no maintenance of mechanical components, and lifespan exhaustion of mechanical parts can cause mechanical systems to vibrate excessively. The vibration levels can be monitored using appropriate sensors and microphones can be used to detect noise levels resulting from excessive machine vibration.

The characteristic features of vibrations from a reciprocating compressor are very complicated because they include excitations from valve impacts, time-varying properties, and non-stationary responses, which make it difficult to adequately analyse the vibration signal and

diagnose faults (Geng, Jin, & Hull, 2003). A typical vibration signal from a two-stage reciprocating compressor is presented in Figure 3.4.

The interpretation of vibration data from the reciprocating compressor is one area that has attracted lots of research attention. For instance, Gu & Ball experts in machine condition monitoring conducted a study using smooth pseudo-Wigner–Ville distribution to interpret vibration data from reciprocating compressors (Gu & Ball, 1995). Naid, Gu, & Ball more recently, carried out a study introducing the use of kurtosis to develop a diagnostic method for differentiating valve leakage, intercooler leakage and loose drive belt on a reciprocating compressor after proofing that the conventional bispectrum is not so effective in analysing amplitude modulation current signals (Naid, Gu, & Ball, 2007). Some studies suggest that vibration monitoring together with other monitoring techniques should be used to give a full monitoring condition of reciprocating machinery (Rao B. K., 1998); (Dong, 2012).

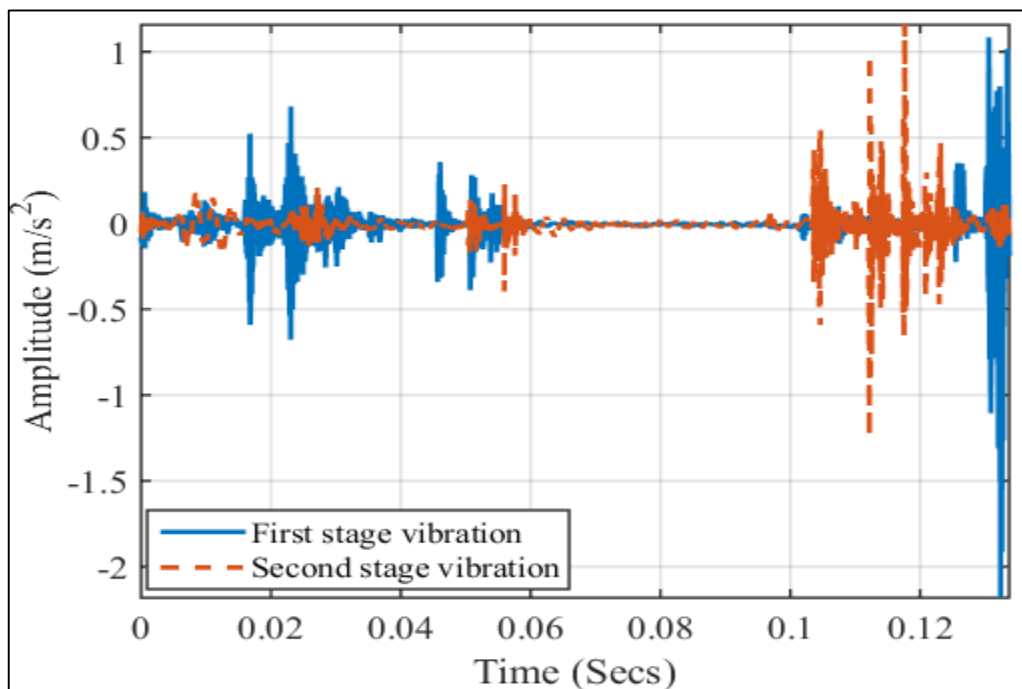


FIGURE 3.4: VIBRATION SIGNAL FROM A TWO STAGE RECIPROCATING COMPRESSOR

Several approaches have been implemented by analysing vibration signals for fault diagnosis. However, fault diagnosis of compressor valves based on the vibration and acoustic emission signals is considered more efficient because it can be accomplished non-intrusively (Wang, Xue, Jia, & Peng, 2015).

3.7 Signal Processing for Machine Monitoring

Data collected from measuring instruments used for condition monitoring needs to be analysed and interpreted to reveal critical information and machine characteristics (Smith, 1999). Effective condition monitoring of machines often depends on the use of an appropriate signal processing method or a combination of two or more methods. There are three most popular methods used for signal processing, and they include:

- Time domain analysis
- Frequency domain analysis
- Time-frequency analysis

(Norton & Karczub, 2003).

Figure 3.5 shows a list of some common signal processing methods used for condition monitoring.

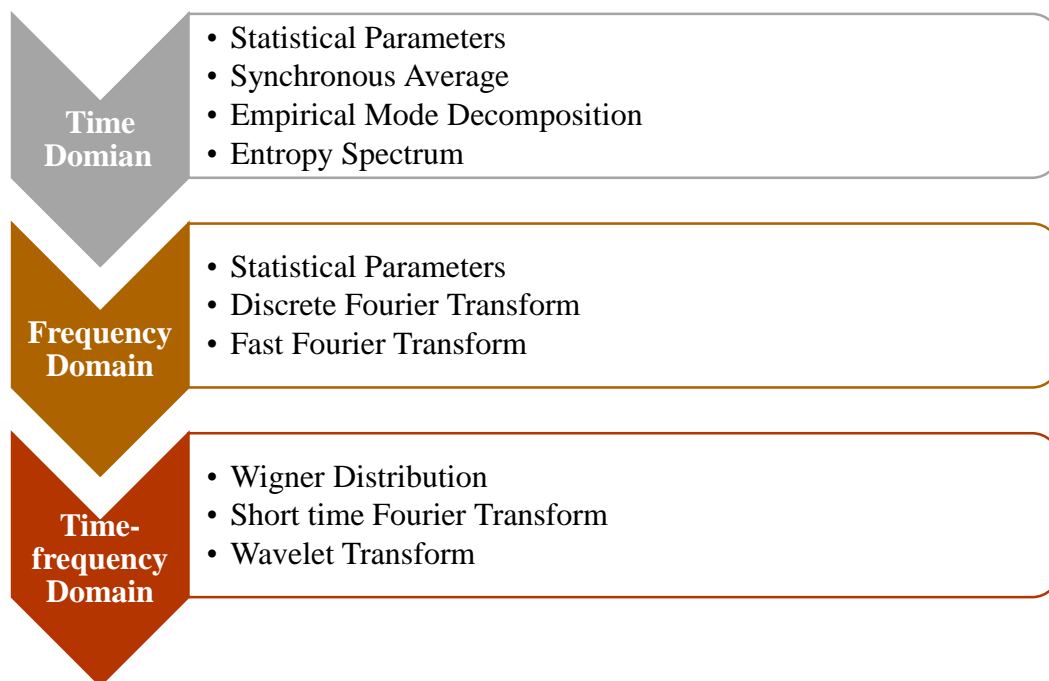


FIGURE 3.5: SIGNAL PROCESSING TECHNIQUES

3.7.1 Time Domain

Time domain signal representation contains useful information for understanding machine condition, and the signal is represented as a function of time, which is a plot of the amplitude against time. Characteristic features of a signal in the form of statistical methods such as root mean square (RMS), the peak value (PK), crest factor (CF), kurtosis (KT), skewness (SK), probability density, and variances are used to summarise the data obtained and to draw suitable

conclusions. Some of these techniques would be used when analysing the vibration and gas pulsation signals collected from the Broom Wade TS9 reciprocating compressor in chapters seven and eight.

The two most widely used statistical parameters are the root mean square (RMS), which is a measure of the signals strength or power. The peak value describes the maximum absolute value of a signal.

3.7.1.1 RMS

RMS is used to evaluate the overall condition of the machine and to track general fault progression rather than early incipient fault (Zhu, Nostrand, Spiegel, & Morton, 2014). For a set of data, $X_1, X_2, X_3, \dots, X_N, X_{rms}$ is defined as (Zhu, Nostrand, Spiegel, & Morton, 2014):

$$X_{rms} = \sqrt{\frac{1}{N} \sum_{i=1}^N X_i^2} \quad (3.2)$$

Where, X_{rms} is the root mean square value of the data set X at every instant i , and N is the number of data points.

3.7.1.2 Peak Value

For a set of data, $X_1, X_2, X_3, \dots, X_N$, the peak value (PK) is expressed as (Zhu, Nostrand, Spiegel, & Morton, 2014):

$$X_{PK} = \max(|X|) \quad (3.3)$$

where, $|X|$ is the absolute value.

3.7.1.3 Crest Factor (CF)

Creak factor (CF) is another common statistical feature used in time domain analysis to determine the repeated impulses of a signal; it is the measure of the number and sharpness of the peaks of a signal. CF is expressed as the ratio of the peak value (X_{PK}) to the RMS value (X_{rms}) of the time domain waveform (Zhu, Nostrand, Spiegel, & Morton, 2014):

$$CF = \frac{X_{PK}}{X_{rms}} \quad (3.4)$$

The crest factor is used in condition monitoring to detect changes in signal pattern due to impulsive vibration sources. A high crest factor value is an indication of possible component deterioration.

3.7.1.4 Skewness

Skewness (SK) is a measure of the lack of symmetry in the data distribution, and this is expressed in the following equation:

$$S_K = \frac{\sum_{i=1}^N (X_i - \bar{X})^3}{(N-1)S^3} \quad (3.5)$$

Where, \bar{X} is the mean of the data set $X_1, X_2, X_3, \dots, X_N$, and S is the standard deviation of the distribution given as:

$$S = \sqrt{\frac{\sum_{i=1}^N (X_i - \bar{X})^2}{N}} \quad (3.6)$$

A time series is positively skewed (right tail) with a positive SK value, if it has many small values and a few large values, while a negative SK value signifying a negatively skewed (left tail) time series is obtained when a lot of large values and a few small values are present (Zhu, Nostrand, Spiegel, & Morton, 2014).

3.7.1.5 Kurtosis

Kurtosis describes how sharp (peaked) or flat the distribution is. Kurtosis value is given by the following equation (Raharjo, 2013):

$$K_T = \frac{\sum_{i=1}^N (X_i - \bar{X})^4}{(N-1)S^4} \quad (3.7)$$

A negative kurtosis value indicates that the distribution is flatter than the Gaussian, while a positive value means its distribution is more peaked than a Gaussian (Raharjo, 2013).

3.7.1.6 Probability Density Function

Sharma and Parey used the improved RMS probability density function and entropy measurement to detect gear faults with initial and advanced cracks for different speed profiles.

They found that initial cracks were detectable using percentage increase in entropy values for RMS PDF compared to advanced cracks (Sharma & Parey, 2016). Experiments by Zhuang and his colleagues revealed that the probability density method based on Parzen window was able to detect motor air gap eccentricity and ball cage broken bearing faults on vibration signals (Zhuanga, Li, & Wei, 2012). Toyota, Niho, Chen, & Komura proposed a new method based on rotating angle density function of vibration signal and its normalised power density function because of the drawbacks of PDF analysis in time-domain and frequency-domain, which are insensitivity of signal pulse phase shifting and small local change in amplitude (Toyota, Niho, Chen, & Komura, 2001)

A study conducted by Yang, Hwang, Kim, and Chit tan suggests that not all features extracted from time domain are useful for effective detection and diagnosis of reciprocating compressor faults (Yang, Hwang, Kim, & Chit Tan, 2005). Some advanced time domain signal processing techniques using dynamic time warping (Zhen, Alibarbar, Zhou, Gu, & Ball, 2011), empirical mode decomposition (EMD) (Muo, Madamedon, Gu, & Ball, 2017), (Yongbo, Xu, Wei, & Huang, 2014), and entropy spectrum (Ogbulafor, Guojin, Mones, Gu, & Ball, 2017) amongst others have been proposed because they are suitable for processing nonlinear and non-stationary time series of reciprocating compressor signals.

3.7.2 Frequency Domain Analysis

Frequency domain analysis is another technique for signal processing; it represents signal data in the form of a spectrum. Spectrum analysis is a measure of signal amplitude as a function of frequency. In many machineries, especially rotating types, components within the system have a specific operating frequency, which is related to the dynamics of its operation and can be used for condition monitoring purposes (Rao S. S., 2004); (Thobiani, 2011); (Robinson, 1990). This technique is prevalent in analysing vibration response. The most basic frequency domain tool is the Fast Fourier Transform (FFT), which enables the conversion of the time domain signal to frequency domain or spectrum. The central concept of frequency domain analysis is either to look at the entire spectrum, or to closely analyse specific frequency components (Jardine, Lin, & Banjevic, 2005), (Dong, 2012).

Frequency domain analysis has several advantages in machine condition monitoring and decades of practical applications have confirmed the effectiveness of this technique in identifying frequency components, which indicate the development of certain faults (Albarbar,

Elhaji, Gu, & Ball, 2004); (Elhaji, Gu, Shi, & Ball, 2001); (Bradley, Ball, & Gu, 2000); (Staszewski W. , 1994); (Yesilyurt, 1997); (Braun, 1986); (Collacott, 1977).

However, some limitations such as aliasing, spectral leakage and picket-fence affect its practical application and lead to errors in spectrum estimation (Dong, 2012). Moreover, in reality, signals from rotating machinery are often non-stationary, that is, the spectra vary with time and the FFT cannot depict the changes in signals that have time-varying features (Goyal & Pabla, 2016).

3.7.3 Time-Frequency Domain Analysis

The limitations of time domain and frequency domain analysis has caused the application of time-frequency analysis. Frequency spectrum analysis is unable to diagnose faults from non-stationary waveform signals accurately and can only represent the signals' energy in one-dimensional function (frequency), whilst time domain waveform only presents the signals time information. Therefore, the time-frequency domain analysis, which shows signal information in two-dimensional functions (time and frequency) has been exploited and found useful for fault diagnosing. Particularly, with non-stationary signals. There are several time-frequency techniques used in analysing non-stationary signals for condition monitoring purposes. However, three of the most popular methods according to Jardine, Lin, & Banjevic (2005) are the short-time Fourier transform (STFT) also known as spectrograms, Wigner-Ville distribution (WVD) and wavelet transform (WT).

3.7.3.1 Short-Time Fourier Transform (STFT)

STFT works by dividing the whole waveform signal into segments with short-time window and applying Fourier transform to each segment. The problem with this technique come about when acquiring a more accurate frequency resolution because the window size used along the time axis of the signal does not always coincide with the stationary timescales for non-stationary signals with fast changes in dynamics (Jardine, Lin, & Banjevic, 2005). In other words, to get an accurate time representation, the frequency resolution would have to be less precise, and for an accurate frequency representation the reverse is the case, this is known as the uncertainty principle.

3.7.3.2 Wigner-Ville Distribution (WVD)

WVD was created to solve the uncertainty principle problem associated with the short-time Fourier transform by giving excellent resolutions in both domains. This technique has proven

successful in many studies, for instance, it was applied by (Wu & Chiang, 2009), to analyse non-stationary sound emission signals combined with the probability neural network for fault diagnosis of an internal combustion engine. They concluded that their proposed approach could improve the cost of the fault diagnosis system and reduce mistaken recognition. Then Staszewski and Worden investigated the characteristics of gearbox vibration signals and found that the Wigner-Ville distribution is capable of detecting local tooth faults in spur gears (Staszewski & Worden, 1997). A more recent study carried out by Albarbar et al., successfully extracted non-stationary air-borne acoustic features from a diesel engine by using the Wigner-Ville distribution technique (Albarbar, Gu, Ball, & Starr, 2010). However, the drawback of Wigner-Ville distribution according to Jardine, Lin, & Banjevic (2005), is in the interference terms (generation of spurious frequency not contained in the initial signal) formed by the transformation itself, although, improved transforms such as Choi-Williams distribution can be applied to counter these interference terms.

3.7.3.3 Wavelet Transform (WT)

Jean Morlet introduced wavelets in 1982 to achieve the best balance between time resolution and frequency resolution. However, wavelet transform only became very popular in condition monitoring of non-stationary signals in the last fifteen years (Loutas & Kostopoulos, 2017). Unlike other time-frequency techniques that use complex cosines and sine functions to graph the signal into a two-dimensional function, wavelet transform consists of a family of simple time functions that are dilated and shifted independently to represent the signal in both time and frequency domain (Goyal & Pabla, 2016).

There are several ways of calculating the wavelet transform of a signal, but the three common methods are the continuous wavelet transform (CWT), the discrete wavelet transform (DWT) and the wavelet packet transform (WPT). Wavelet transform has been used extensively in several fields such as biomedical engineering (Manea, Mihaela, & Mutihac, 2018), transportation engineering, mechanical engineering (Ogbulafor, Guojin, Mones, Gu, & Ball, 2017), (Kumar, Srinivasa, Sriram, & Vijay, 2014), (Peng & Chu, 2004), power engineering (Gursoy, Yilmaz, & Ustun, 2018), image processing (Khan, 2018) and many more. It has the advantages of noise elimination, data compression and it is computationally very efficient.

Irrespective of some of the problems associated with the wavelet transform, it is currently one of the best available technique for analysing non-stationary signals. In this research work,

wavelet packet transform is employed to determine the characteristics of vibration and gas pulsation signals for condition monitoring of the reciprocating compressor.

3.8 Summary

The increasing demand for quality products, machine sustainability, and improved human safety have created a requirement for more revealing diagnostic information from machines through condition monitoring and signal processing techniques. A wide range of novel monitoring techniques has been investigated by several scholars, with some proving more successful than others. Analysis of vibration signals from mechanical systems has proven to be the most widely used and most promising due to its non-intrusive nature and the rich signal information.

Therefore, a combination of two or more signal processing techniques have been strongly encouraged to accurately determine the characteristics of vibro-acoustic signals generated from a two-stage reciprocating compressor for condition monitoring purposes.

CHAPTER FOUR

4 DESIGN AND CONSTRUCTION OF TEST-RIG FACILITY

This chapter presents the design and construction of the test rig used to carry out all experiments including measurement parameters associated with condition monitoring of the double-stage, single-acting reciprocating compressor. Details of relevant transducers and data acquisition system used to carry out this study is also described within this chapter. First a detailed setup description of the two-stage reciprocating compressor is presented, followed by brief descriptions and specifications of the measurement instruments and data acquisition system used for the entire study. Also, the manner in which data is collected and processed is described, and finally fault simulation strategies are described and repeatability analysis of signals for healthy and fault conditions are presented.

4.1 Introduction

This chapter is aimed at developing a reciprocating compressor test rig suitable for the investigation of condition monitoring signatures such as pressure, vibration, instantaneous speed and the newly investigated pressure pulsation waves in the discharge chamber, which will be used to ascertain the working condition and investigated fault conditions on the two-stage reciprocating compressor. Furthermore, relevant experimental signatures are used to verify the improved mathematical model presented in chapter five of this study. A reciprocating compressor was chosen as the test machine because of its long-standing relevance in several industries, particularly in the oil and gas sector and chemical production industries. Advances in condition monitoring of such machines would help in maintenance cost reduction and further prolong the life of the machine.

First, a detailed description of the test rig and specifications are given. Secondly, each measurement instrumentation used to collect relevant data is described; the data acquisition system and measurement practice are explained. Finally, the common reciprocating compressor faults investigated are described, and the repeatability of signals used for this research study are analysed.

4.2 Test Rig Facility

4.2.1 The Broom Wade TS-9 Reciprocating Compressor

The experiment is carried out on a previously existing two-stage single acting reciprocating compressor identified as the Broom Wade TS9 in Figure 4.1 below. This machine was used to provide compressed air for the School of Computing and Engineering at the University of Huddersfield. It has proven suitable for condition monitoring purposes over the years as it allows for practical investigations and measurement of real-life working conditions and faults applicable to many industrial fields to be effectively implemented.

The V-shaped reciprocating compressor is made up of two cylinders positioned at an angle of 90° to each other giving it the V-shape (see Figure 4.1 and 4.2). These cylinders are tailored to deliver compressed air between 1 bar (0.1 MPa) to 8.3 bar (0.83 MPa) to a 13.8 bar (1.38MPa) capacity storage tank. An intercooler coil connecting the first-stage cylinder (after discharge) to the second-stage cylinder (before suction) is used to cool down the temperature of the gas from the first stage for improved compressor efficiency. The compressor is powered by a

CHARACTERISING VIBRO-ACOUSTIC SIGNALS OF A RECIPROCATING COMPRESSOR FOR CONDITION MONITORING

2.5KW squirrel cage, three-phase induction motor, which transfers electrical current to the compressor pulley to mechanical move the crankshaft causing the pistons to move up and down within the cylinders.

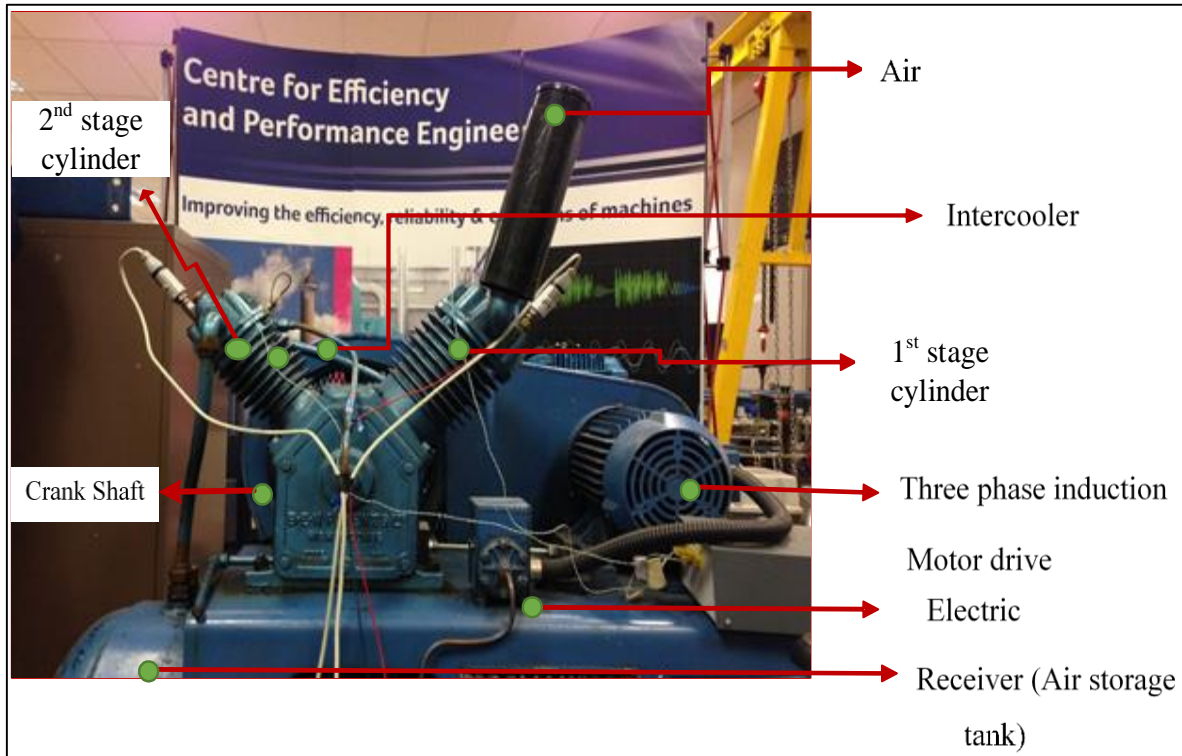


FIGURE 4.1: PICTORIAL REPRESENTATION OF TWO- STAGE RECIPROCATING COMPRESSOR (BROOM WADE TS9)

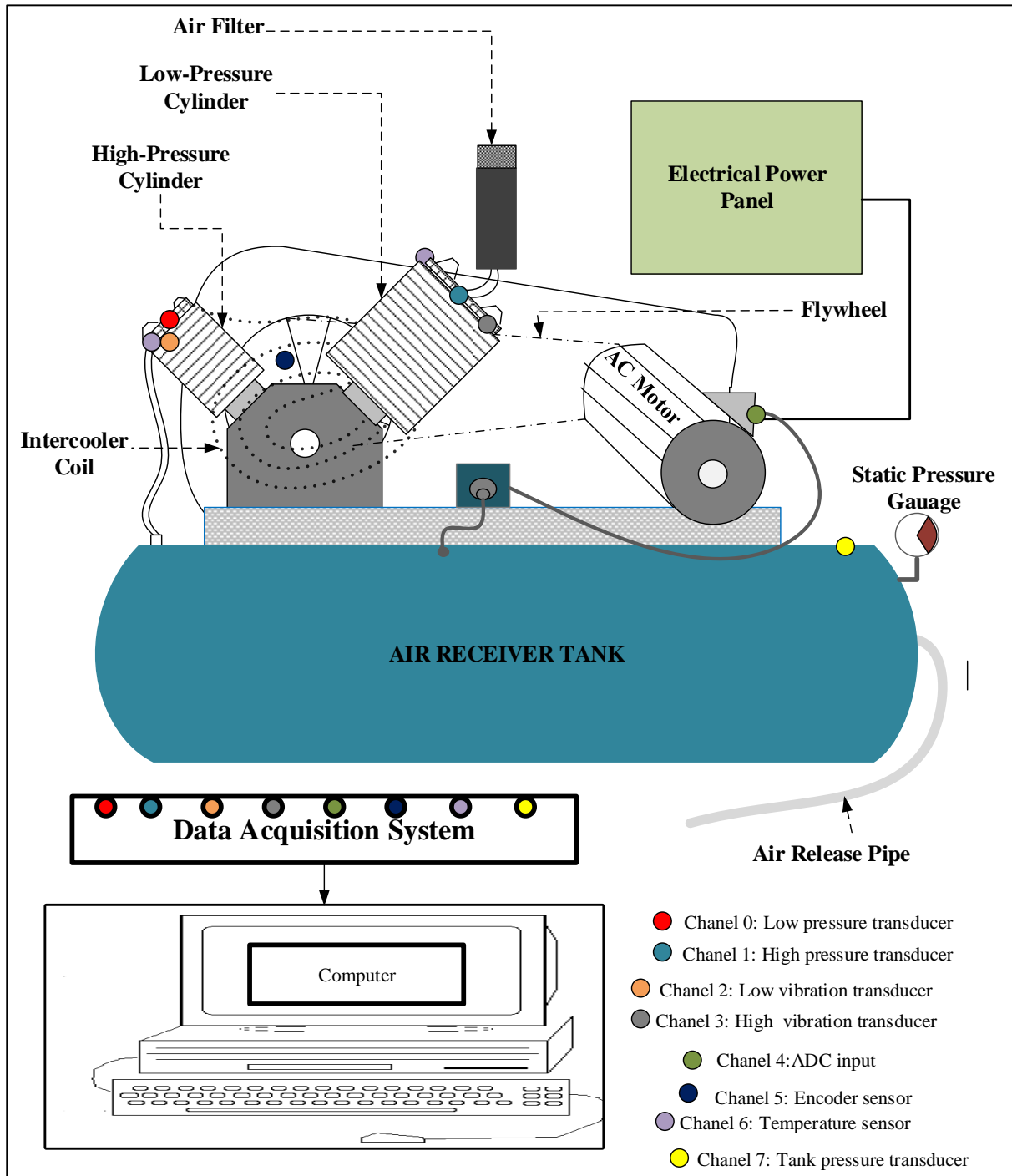


FIGURE 4.2: SCHEMATIC DIAGRAM OF THE TEST RIG SYSTEM

4.3 Measurement Instruments

A variety of sensors including accelerometers, pressure transducers, thermocouples and an angular speed encoder were fitted on specific areas of the reciprocating compressor system to enable data collection for experimental purposes. The main parameters to be investigated for this study are vibration and airborne acoustics (acoustic wave propagation), however, other

parameters such as temperature, pressure and shaft speed are obtained to support the vibration and airborne acoustic measurements; and also gives an added understanding of the dynamic system of the reciprocating compressor.

4.3.1 Accelerometers

Two accelerometers, Bruel & Kjaer type 4384 mounted on the surface of each cylinder head of the reciprocating compressor are used to detect surface vibrations. These piezoelectric transducers are robust and suitable for most applications including rough industrial field conditions. The specifications for the accelerometers used are listed in Table 4.1.

The accelerometer is attached by bonding a screw-threaded brass stud with ceramic cement to the compressor casing; Figure 4.3 shows the configuration and data processing flow diagram for obtaining raw vibration signals from the reciprocating compressor. Piezoelectric accelerometers are known for their high output impedance and weak signals (Barber, 1992), therefore, a charge amplifier is used to reduce the impedance value and amplify the signal.

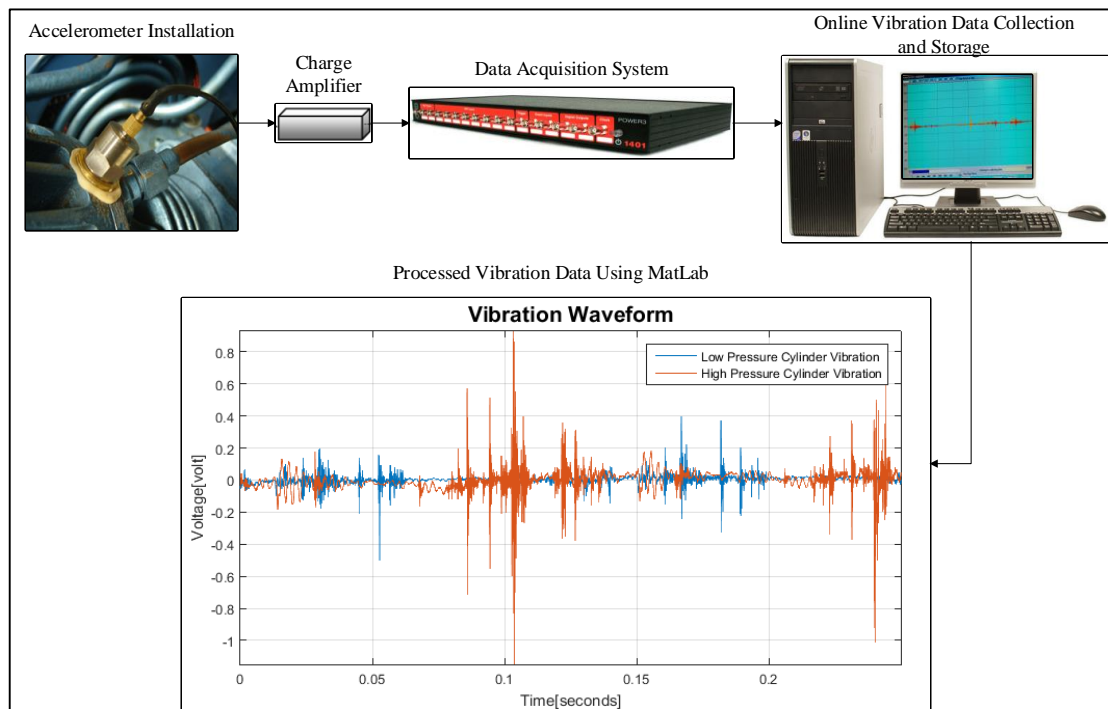


FIGURE 4.3: VIBRATION MEASUREMENT FLOW CHAT

TABLE 4.1: ACCELEROMETER SPECIFICATIONS

Features	Specifications
Type	TD-5-2

Frequency range	15kHz
Acceleration	2000 ms ⁻²
Temperature range	Up to 150°C
Sensitivity	45mv/ms ²

4.3.2 In-Cylinder Pressure Sensor

For In-cylinder pressure measurement, a pressure transducer is installed on the head of each cylinder by drilling a small duct for the sensor to be fitted as seen in Figure 4.4. The GEMS type 2200 strain gauge pressure transducers with an output of 100mV for full pressure range were chosen because of their low cost, and temperature compatibility features. Furthermore, no amplification of the collected pressure signal was required, so the sensors are directly connected to the data acquisition system for signal processing as seen in the flow diagram below. Other specifications of the pressure transducer are listed in Table 4.2.

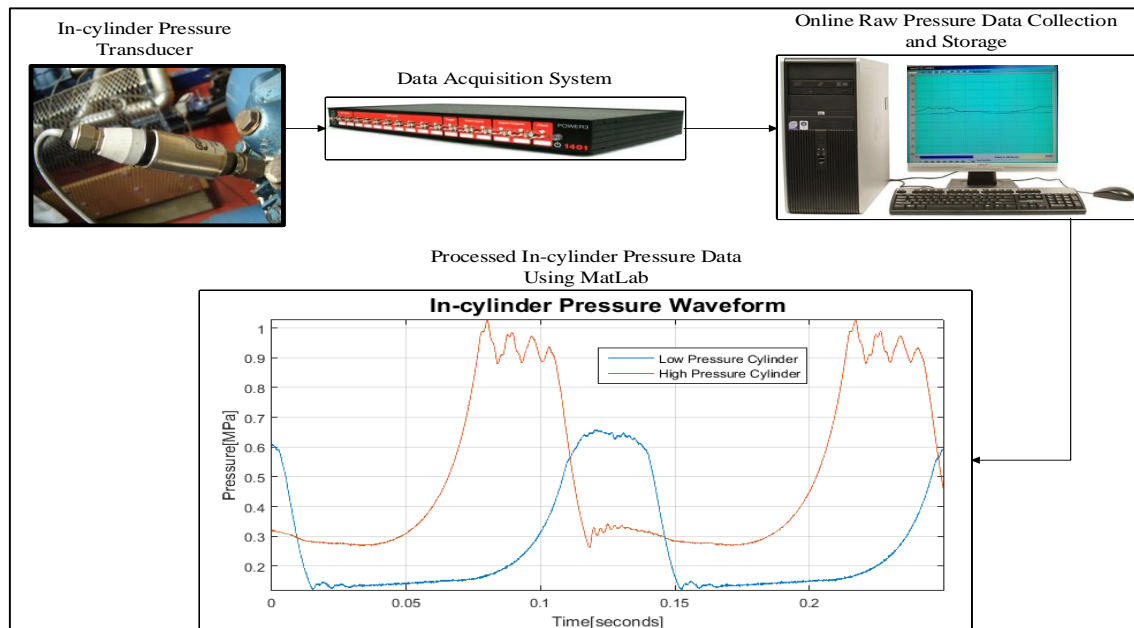


FIGURE 4.4: DYNAMIC-PRESSURE MEASUREMENT FLOW CHAT

TABLE 4.2: IN-CYLINDER PRESSURE SENSOR TECHNICAL SPECIFICATIONS

Features	Specifications
Type	GEMS type 2200 strain gauge

Output	100mV
Power supply	10Vdc
Pressure range	4Mpa (600psi)
Frequency limit	4kHz

4.3.3 Airborne Acoustic Sensor

Acoustic Pressure waves at the discharge chamber of the second stage cylinder are obtained by means of a CY-YD-212 piezoelectric pressure transducer. This sensor is placed within an adaptor with a small duct fitted on the head of the valve chamber allowing air to travel from the chamber just after the valve to the sensor. The CY-YD-212 piezoelectric pressure transducer is small-sized, lightweight and particularly suitable for testing cylinder pipeline pressure & explosion pressure and has a wide frequency response range of over 100 kHz. Figure 4.5 shows the flow diagram for acoustic discharge pressure-wave signal collection and sensor installation on the compressor.

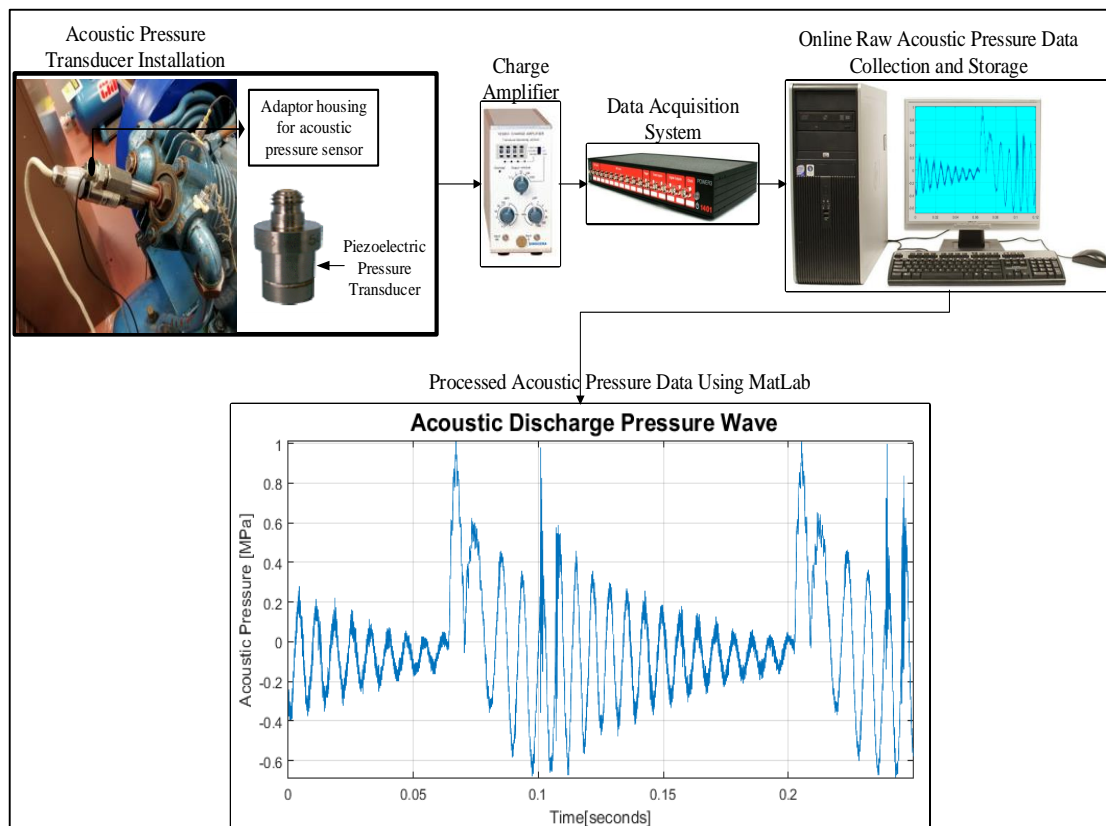


FIGURE 4.5: ACOUSTIC PRESSURE MEASUREMENT FLOW CHAT

4.3.4 Static Pressure Sensor

A Gem type PS20000 static pressure sensor used to trigger data collection at pre-set pressures and to automatically switch the motor off at cut-off pressure is installed on the air storage tank (see Figure 4.6). Its operating range is from 0 to 1.35MPa (200Psi), with a maximum output of 100mV when the supply voltage is 15V; operating temperature range is between -20°C to $+105^{\circ}\text{C}$. Knowing the pressure delivered to the storage tank allows the efficiency of the compressor to be calculated.

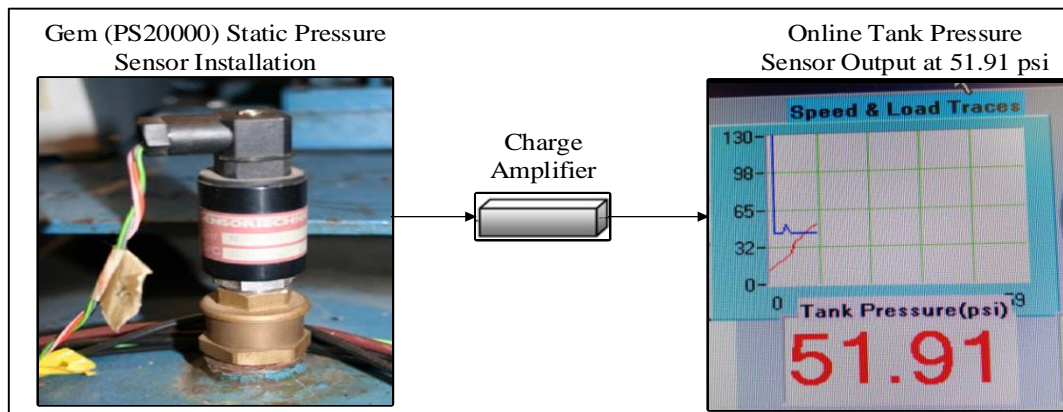


FIGURE 4.6: STATIC TANK-PRESSURE FLOW CHAT

4.3.5 Temperature Sensors

The K-type thermocouples with a linear response of -20°C to 220°C are used to measure the temperature readings of the discharge pressure for both cylinders. These thermocouples have the following advantages: fast response time, affordable cost, wide industry application range, relative accuracy and durability. The thermocouple is made up of two metal wires connected in one end known as the measurement junction, and the other end of each of the wires is connected to the reference junction, which has the same wire type on a PCB (Printed Circuit Board) and is connected to the DAQ. Figure 4.7 shows the thermocouple installation on the cylinder and the data monitoring processes to ensure safe machine condition.

CHARACTERISING VIBRO-ACOUSTIC SIGNALS OF A RECIPROCATING COMPRESSOR FOR CONDITION MONITORING

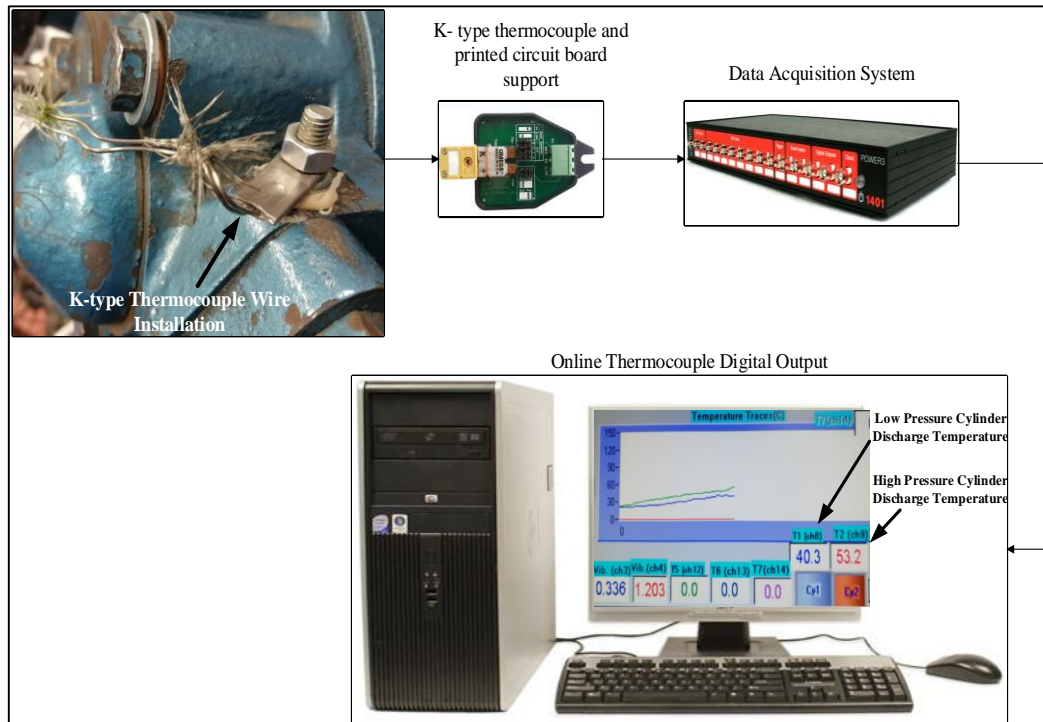


FIGURE 4.7: K TYPE, CR-AL THERMOCOUPLE INSTALLATION AND TEMPERATURE MONITORING PROCESS

4.3.6 Shaft Encoder

Encoders are sensors used to measure the angular speed of a rotating device; for the purpose of this study, the optical pulse high-resolution shaft encoder, which produces a pulse for a unit of angular distance when the crankshaft rotates is fitted as seen in Figure 4.9 through a spindle adapter attached to the compressor crankshaft end. The encoder converts the rotary displacement of the crankshaft into 360 equally spaced pulse signals per revolution. The TDC trigger marker in Figure 4.8 represents the start of every revolution. The encoder is directly connected to the computer via the data acquisition system hence; no amplification of the measured instantaneous speed signal (IAS) is needed.

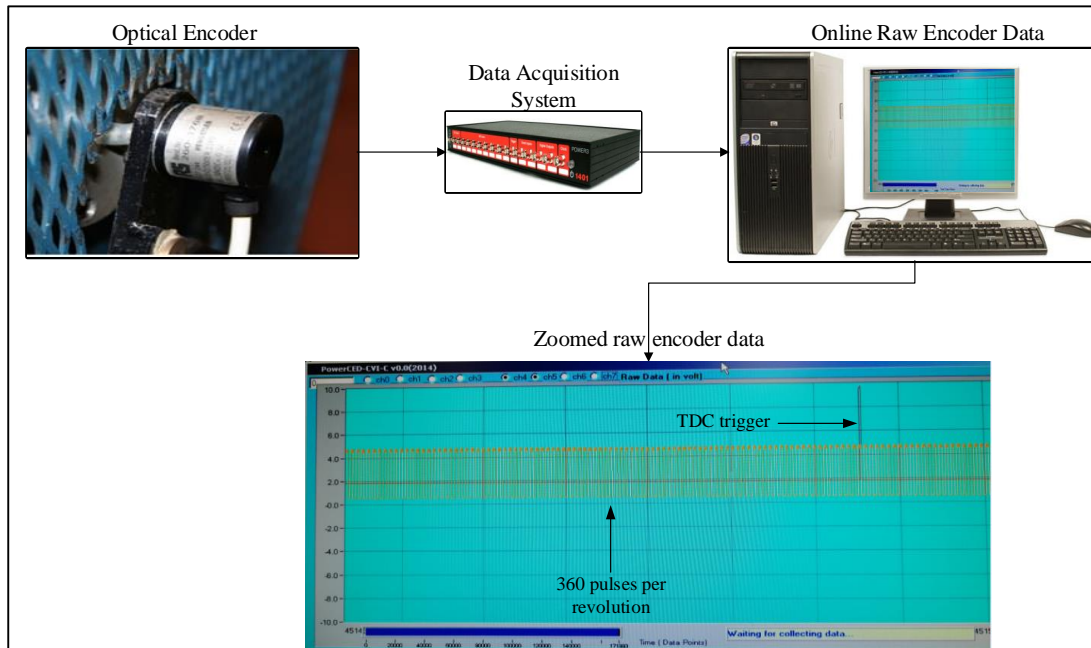


FIGURE 4.8: OPTICAL PULSE SHAFT ENCODER AND DATA COLLECTION FLOW CHAT

4.4 Data Acquisition System (DAQ)

The Cambridge Electronic Design CED Power1401 high-performance data acquisition system is used to capture experimental data from installed sensors on the reciprocating compressor. It records waveform data, digital event and marker information for real-time data processing and data storage through a 1 GHz Marvell processor with up to 2GB on board memory (Cambridge Electronic Design Limited, 1991). There are eight channels of 16-bit waveform input on the front panel of the hardware labelled ADC Inputs as seen in Figure 4.9a), and another eight through the rear panel (Analogue Expansion) D-socket as seen in Figure 4.9b).

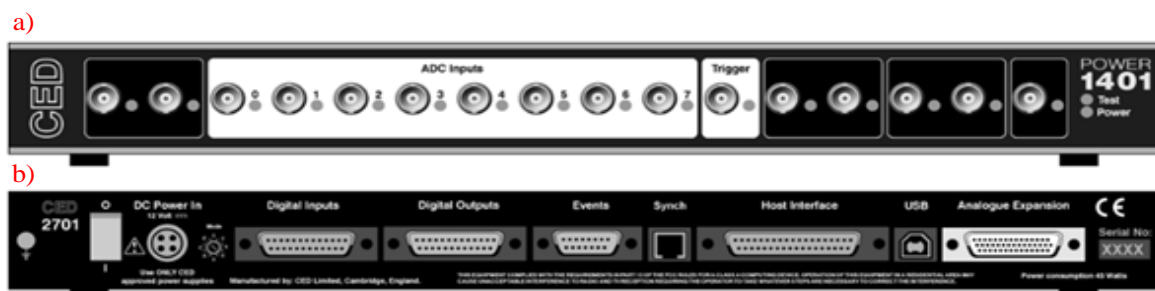


FIGURE 4.9A) FRONT AND B) REAR VIEW PANEL OF THE CED POWER1401 DAC

4.4.1 Software: LabWindows TM/CVI Version 5.5

The data acquisition software is a National Instruments Lab Windows TM/CVI Version 5.5. It is an interactive development environment written in the programming language C (National Instrument Company, 2003). This program includes data acquisition, analysis, user interface and a large set of run-time libraries for instrument control. Compared to other programming software's, the Lab Windows TM/CVI provides an inbuilt graphical user interface (GUI) editor which contains many measurement specific features that allow easy C based programming.

The Data Acquisition software enables multiple channels of dynamic data (e.g. IAS, vibration, dynamic, pressure, motor current, sound and temperature) to be acquired simultaneously at different rates and data lengths. Also, the sampling frequency and sample data length are manually adjusted to ensure an optimal dataset is collected for subsequent off-line analysis.

Figure 4.10 below presents the configuration-setting panel of the software and Figure 4.11 displays the data acquisition process.

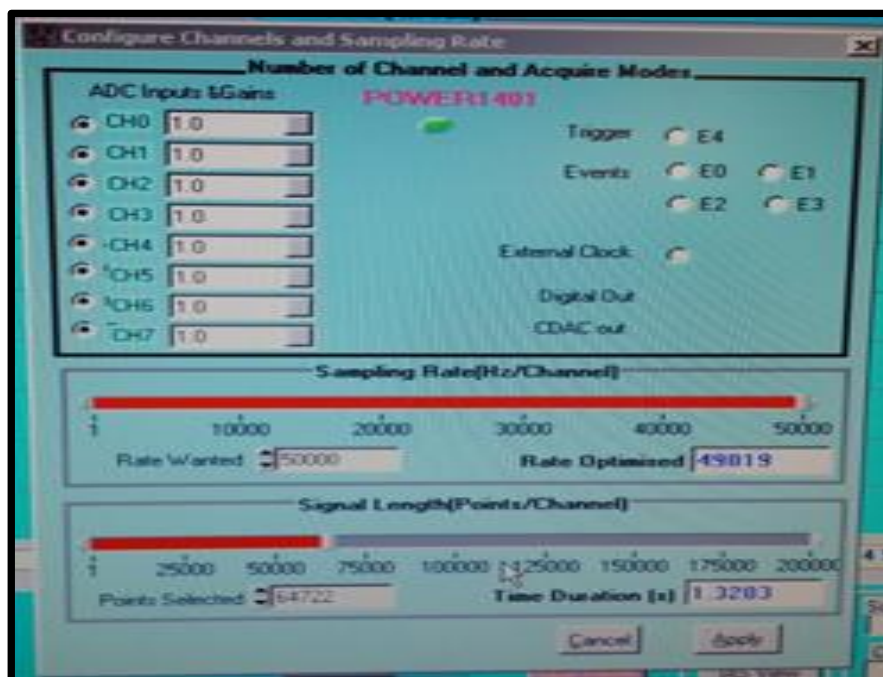


FIGURE 4.10: LAB WINDOWS TM/CVI CONFIGURATION SETTING PANEL SCREEN

The maximum sampling frequency is set at 49019Hz to obtain high frequencies associated with transient events such as valve impacts; the data length is set at 64,722 samples per 1.3203 seconds. The following equation calculates the time duration:

$$t(\text{seconds}) = N_{\text{samples}}(\text{number of samples}) \div F_s(\text{sampling frequency}) \quad (4.1)$$



FIGURE 4.11: DATA ACQUISITION PROCESS

Numerical values of monitored parameters including temperature, compressor speed, tank pressure etc. are displayed in the data acquisition panel for compressor monitoring. A trigger signal is used to automatically set the start time of data collection when the piston is at top dead centre (TDC), this ensures that data is collected at the same crank position every time for accurate time domain averaging of data segment during analysis. Data files were saved in binary format and analysed offline using MATLAB, which provides an easy platform for data analysis.

4.5 Data Measurement Practice

A standard test procedure was developed and followed to ensure proper and safe measurement practice. The procedures are as follows:

- First, the machine is checked to determine its safety status
- Then all wires and connections are traced to ensure proper connections
- The drain valve connected to the receiver is closed after the compressed air has been released.
- The monitor and central processing unit are switched on together with the data acquisition unit.
- The data acquisition software application is opened on the monitor
- The CED setup tab/icon is clicked taking the user to the configuration channel and sampling rate page where the user checks that all channels are checked/on; and also ensures that the Trigger E4, if off is clicked on.

- The ‘apply’ button is clicked for the system to effect the instruction given by the user.
- Click on the data file tab to check that the correct settings are set; then the ACQ mode, which takes the user to the measurement task page, is changed to automatic and the data file head name is changed to the users’ preference name.
- The operating button/tab is clicked-on to display the operating conditions of the sensors installed on the reciprocating compressor.
- Finally, the acquire tab is selected as the compressor power is turned on to begin data collection.

The diaphragm pressure switch automatically stops the electric motor from powering the reciprocating compressor when the maximum working pressure (1.38MPa) is reached. After the experiment is completed and sufficient data are collected, the drainage valves are opened until the pressure switch goes back on or until all the compressed air in the storage tank is released. Then the compressor and all the monitoring systems are switched off.

4.6 Fault Seeding

Two common faults; discharge valve leakage and intercooler leakage (see Figures 4.12 and 4.13) were seeded on the reciprocating compressor. These two faults were investigated separately, and then together presenting a combined fault condition. For convenience, the simulations of stated defects were done under controlled conditions in the laboratory, unlike practical industrial situations where faults would have to be sort. The experimental investigations were carried out as follows:

- a healthy compressor operating under normal conditions,
- a leaky discharge valve on the second stage valve discharge system,
- a non-intrusive leak on the intercooler coil.

The reciprocating compressor is examined by a qualified technician to ensure the compressor is operating normally. On this note, the baseline signature is recorded, then each fault is seeded onto the compressor, and their signatures are recorded. The healthy and faulty signals from specific transducers are compared, and deviations from normal operations are recorded for condition monitoring purposes.

4.6.1 Valve Leakage Simulation

The discharge valve leakage is simulated by drilling a hole of 2mm diameter on the valve plate increasing the cross-sectional area by 2 percent. As stated in section 1.1, the reciprocating compressor valves are the most common components to fail. The leakage allows air in and out of the cylinder irrespective of whether the valve is closed or open; this leads to reduced compressor efficiency.

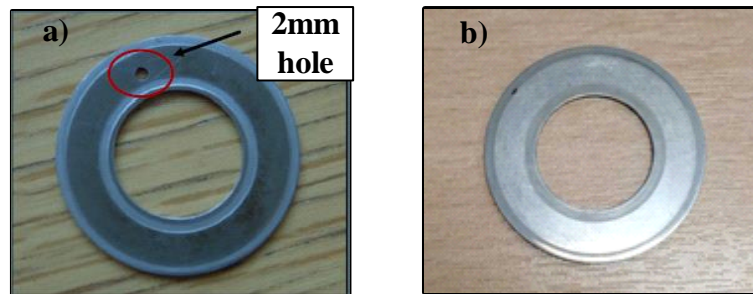


FIGURE 4.12: SECOND STAGE VALVE PLATE A) WITH LEAKAGE AND B) WITHOUT LEAKAGE

4.6.2 Intercooler Leakage Simulation

It is common to have leakages at the joints of pipelines carrying process gas from the first stage to the second stage or from the second stage to the storage tank. For the intercooler leakage simulation, a loose intercooler joint is seeded by untightening the pipeline screw nut pictured in Figure 4.13. This simulation is considered realistic; however, it was difficult to quantify the leak as a proportion of the cross-sectional flow area.

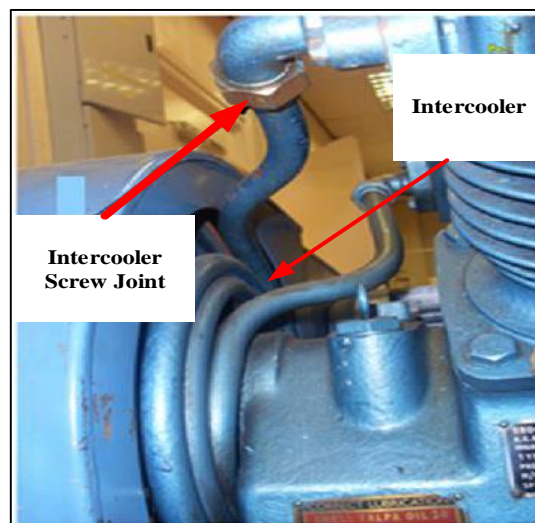


FIGURE 4.13: INTERCOOLER LEAK SIMULATION

4.7 Repeatability of Measured Signals

The repeatability of the experimental results is an important analysis to assess the reliability of the measurement data collected; repeatability evaluation ensures signal reliability. This section investigates the reliability of second stage pressure signals, airborne acoustic wave signals, and second stage vibration signals collected from the two-stage reciprocating compressor. Each experiment is run three times under four different discharge pressures (0.0069 MPa, 0.276 MPa, 0.552 MPa, and 0.827 MPa) and three operating conditions (baseline, discharge valve leakage and intercooler leakage).

The repeatability evaluation is divided into three subsections based on the results from each operating condition listed above. In each subsection, the waveform of the three repeated tests for each parameter (cylinder pressure, airborne acoustic waves, and vibration) are presented. Also, results from the one-way analysis of variance (ANOVA) of the root mean square values and the correlation coefficient results of the repeated signals for all conditions and discharge pressures investigated are used to determine the relationship between the repeated test signals.

4.7.1 Baseline

The experiments are carried out when the two-stage reciprocating compressor is working under normal conditions, that is, no faults seeded. The data is collected for three measurements including In-cylinder pressure, airborne acoustics (pressure pulsations), and vibration.

4.7.1.1 Second Stage In-Cylinder Pressure

Figure 4.14 presents the time domain In-cylinder pressure waveform for several discharge pressures repeated three times (Test1, Test2 and Test3). It can be observed that for each discharge pressure investigated there are no visible significant difference between repeated measurements (Test1, Test2 and Test3). The root mean squared values for each of the repeated experiments are computed and used for ANOVA investigation.

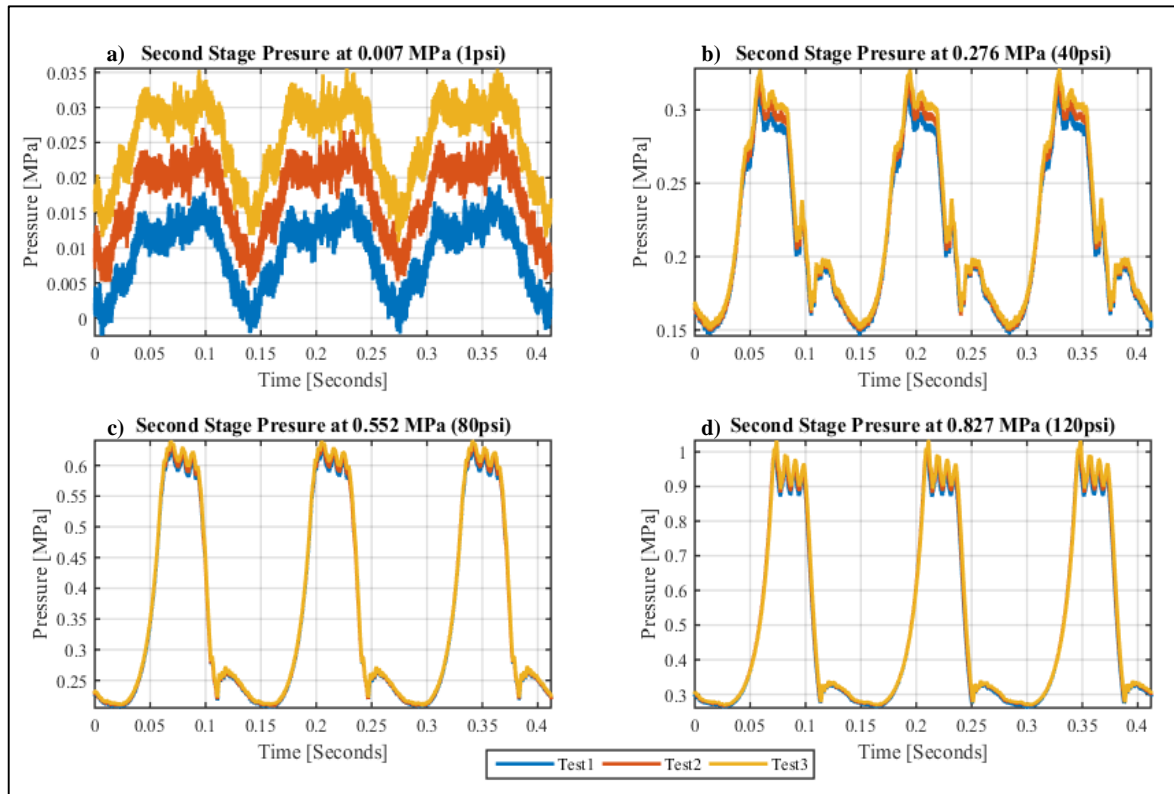


FIGURE 4.14: REPEATED IN-CYLINDER WAVEFORMS AT SEVERAL DISCHARGE PRESSURES

The One-way ANOVA null hypothesis states that all means are equal and analysis was done specifying 95 per cent level of confidence, which is 5 per cent level of significance. From Table 4.3, the P-value of the ANOVA of repeated pressure tests is higher than 0.05, so the null hypothesis is accepted. However, the ANOVA table for several discharge pressures in Table 4.4 shows that the P-value is less than 0.05; therefore, we reject the null hypothesis because at least one of the group is different. Figure 4.15 presents the interaction plots for repeated tests and several discharge pressures. An increasing linear trend is observed with increasing discharge pressures; also, it can be seen that the differences between means of several discharge pressures are significantly different with ph_BL4 (0.83 MPa) having the highest means value. On the other hand, the differences in mean values of the repeated pressure tests are not so different for each discharge pressure case.

TABLE 4.3: ANALYSIS OF VARIANCE FOR REPEATABILITY OF PRESSURE SIGNALS

Source	Degrees of Freedom(DF)	Adjusted (Adj) Sum Squares	Adjusted (Adj) Mean Squares	F-Value	P-Value
--------	------------------------	----------------------------	-----------------------------	---------	---------

CHARACTERISING VIBRO-ACOUSTIC SIGNALS OF A RECIPROCATING
COMPRESSOR FOR CONDITION MONITORING

Repeated Pressure Tests	2	0.000291	0.000145	0.00	0.997
Error	9	0.500024	0.055558		
Total	11	0.500315			

TABLE 4.4: ANALYSIS OF VARIANCE FOR SEVERAL DISCHARGE PRESSURES

Source	DF	Adj Sum Squares	Adj Mean Squares	F-Value	P-Value
Discharge Pressure	3	0.499992	0.166664	4134.90	0.000
Error	8	0.000322	0.000040		
Total	11	0.500315			

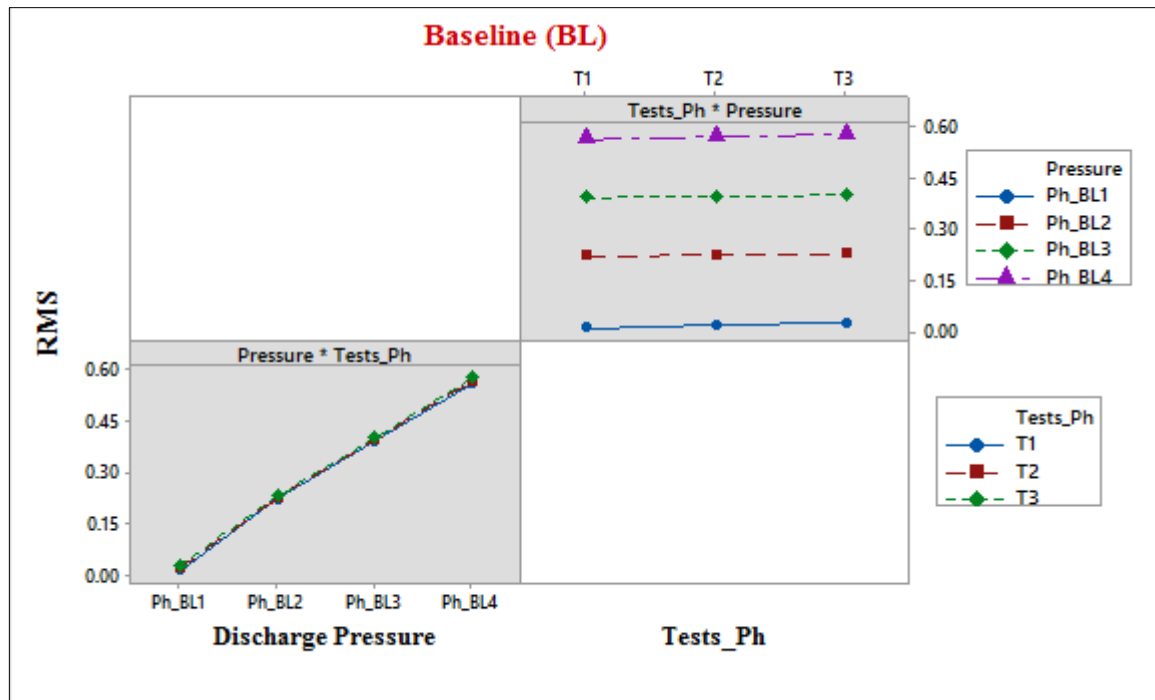


FIGURE 4.15: INTERACTION PLOT OF RMS AND SEVERAL DISCHARGE PRESSURES FOR PRESSURE SIGNALS

The Pearson correlation coefficient is computed as an additional statistical analysis to determine the strength of the similarity between the three test signals (Test1, Test2, and Test3) within several discharge pressures. The strength of the correlation coefficient is given by r , which ranges from -1 to +1. Large r values means there is a strong relationship between the signals while small r values indicates little to no relationship between signals. The significance of the relationship is expressed in probability levels p . A small p level usually less than 5%

means the relationship is statistically significant while a large p level (greater than 5%) means the correlation r is not statistically significant.

The Pearson correlation coefficient r is given as (Maurice, Kendall, & Alan, 1961):

$$\rho(A, B) = \frac{1}{N_r - 1} \sum_{i=1}^{N_r} \left(\frac{A_i - \mu_A}{\sigma_A} \right) \left(\frac{B_i - \mu_B}{\sigma_B} \right) \quad (4.2)$$

$$r = \begin{pmatrix} \rho(A, A) & \rho(A, B) \\ \rho(B, A) & \rho(B, B) \end{pmatrix} \quad (4.3)$$

where $\mu_{A,B}$ and $\sigma_{A,B}$ are the mean and standard deviation of A & B , respectively, N_r is the number of pairs of the variables A and B .

TABLE 4.5: CORRELATION COEFFICIENT AND PROBABILITY LEVEL OF BASELINE TEST PRESSURE SIGNALS

Correlation Coefficients r				
Baseline				
	0.007MPa	0.276MPa	0.552MPa	0.83MPa
Test 1	1	1	1	1
Test 2	0.9489	0.9988	0.9999	0.9996
Test 3	0.9443	0.9983	0.9999	0.9973
Probability Level p				
Test 1	1	1	1	1
Test 2	0	0	0	0
Test 3	0	0	0	0

Table 4.5 shows the correlation coefficients and the probability level of the baseline second-stage pressure test signals (Test1, Test2, and Test3) for several discharge pressures. For a particular discharge pressure say 0.007MPa, the r and p values are computed to establish the relationship between the repeated test signals (Test1, Test2, and Test3). It can be concluded that the test signals within each discharge pressure condition are very similar since the correlation coefficient values r are close to 1 and the p values are less than 0.05. This tells us that there is a strong linear relationship between the repeated test signals.

4.7.1.2 Airborne Acoustic (pressure pulsation) Waves

Figure 4.16 presents the time domain airborne acoustic waves in the cavity of the second-stage cylinder at discharge pressures mentioned earlier. The experiment is repeated three times

(Test1, Test2, and Test3), and no significant statistical differences can be seen between repeated tests for each discharge pressure investigated.

Table 4.6 presents the ANOVA summary for repeatability of airborne acoustic signals. The P-value is higher than 0.05, so the null hypothesis is accepted, and the P-value for variances between discharge pressures less than 0.05, therefore, the null hypothesis is rejected because at least one of the group is different. The interaction plot is presented in Figure 4.17, and it can be seen clearly from the top right subplot that means of the higher discharge pressures AA_BL3 and AA_BL4 (0.552 MPa and 0.827 MPa) are different. The variances between the lower discharge pressures AA_BL1 and AA_BL2 (0.0069 MPa and 0.276 MPa) are not statistically significant enough.

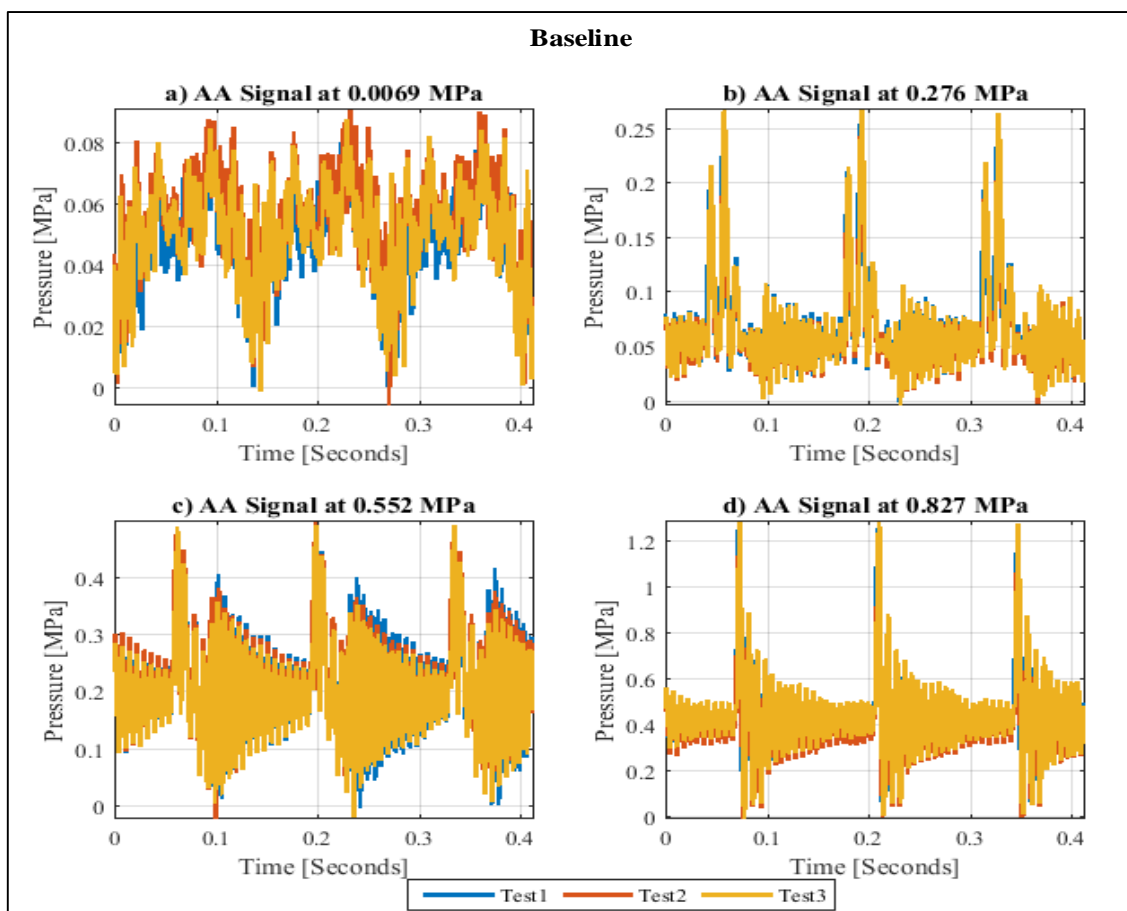


FIGURE 4.16: REPEATED AIRBORNE ACOUSTIC WAVE SIGNALS AT SEVERAL DISCHARGE PRESSURES

TABLE 4.6: ANALYSIS OF VARIANCE FOR REPEATABILITY OF AIRBORNE ACOUSTIC SIGNALS

Source	DF	Adj Sum Squares	Adj Mean Squares	F-Value	P-Value
Repeated Airborne Acoustic Tests	2	0.000059	0.000030	0.00	0.999
Error	9	0.304548	0.033839		
Total	11	0.304608			

TABLE 4.7: ANALYSIS OF VARIANCE FOR SEVERAL DISCHARGE PRESSURES

Source	DF	Adj Sum Squares	Adj Mean Squares	F-Value	P-Value
Discharge Pressure	3	0.303821	0.101274	1029.47	0.000
Error	8	0.000787	0.000098		
Total	11	0.304608			

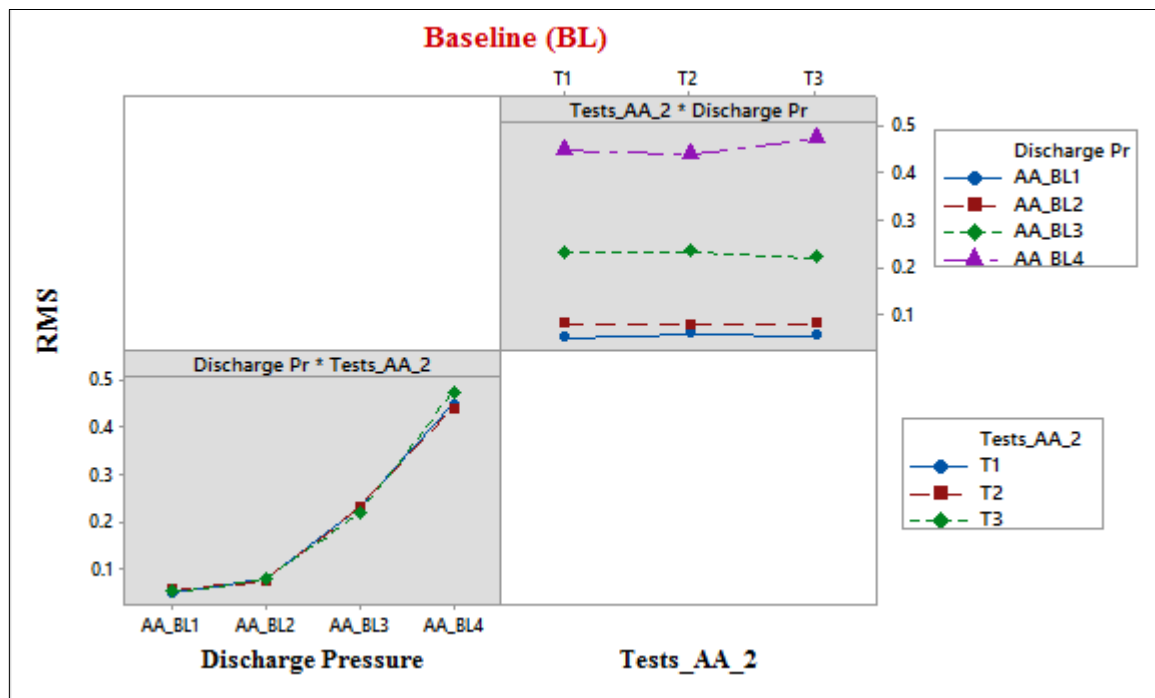


FIGURE 4.17: INTERACTION PLOTS OF RMS AND SEVERAL DISCHARGE PRESSURE FOR AIRBORNE ACOUSTIC SIGNALS

Table 4.8 shows the correlation coefficients and the probability level of the baseline airborne acoustic wave test signals (Test1, Test2, and Test3) at several discharge pressures. It can be concluded that the test signals are very similar since the correlation coefficient values r are close to 1 and the P values are less than 0.05.

TABLE 4.8: CORRELATION COEFFICIENT AND PROBABILITY LEVEL OF BASELINE TEST AIRBORNE ACOUSTIC WAVE SIGNALS

Correlation Coefficients r				
Baseline				
	0.007MPa	0.276MPa	0.552MPa	0.83MPa
Test 1	1	1	1	1
Test 2	0.7825	0.9666	0.9866	0.9614
Test 3	0.7569	0.9325	0.9771	0.7903
Probability Level p				
Test 1	1	1	1	1
Test 2	0	0	0	0
Test 3	0	0	0	0

4.7.1.3 Second Stage Vibration

Figure 4.18 presents the time-domain vibration signals from the second-stage cylinder at discharge pressures 0.0069 MPa, 0.276 MPa, 0.552 MPa, and 0.827 MPa. The baseline experiment is repeated three times (Test1, Test2 and Test3) to determine the reliability of the vibration signal. It can be observed that, for each discharge pressure investigated, there are no significant statistical differences between repeated measurements (Test1, Test2 and Test3); however, reliable analysis of the signal is required to prove this.

The one-way ANOVA is used to verify findings. Table 4.9 presents the ANOVA summary for repeatability of vibration signals. The P-value is higher than 0.05, so the null hypothesis is accepted, and the P-value for variances between discharge-pressures is less than 0.05 (see Table 4.8); therefore, the null hypothesis is rejected because at least one of the discharge pressure RMS value is different. The interaction plot is presented in Figure 4.19, and a random trend can be seen in the RMS values at several discharge pressures, and although there is a slight difference in the RMS values of repeated signals at Vh-BL4 (0.827 MPa), the variances are not statistically significant enough as seen in the top right subplot.

The correlation coefficients and the probability level of the baseline vibration test signals (Test1, Test2, and Test3) at several discharge pressures are presented in Table 4.11. From the results, there is inconclusive evidence about the significance of the relationship between the vibration test signals at certain discharge pressures (0.007MPa and 0.552MPa) as their p values are greater than the significance level of 0.05.

CHARACTERISING VIBRO-ACOUSTIC SIGNALS OF A RECIPROCATING COMPRESSOR FOR CONDITION MONITORING

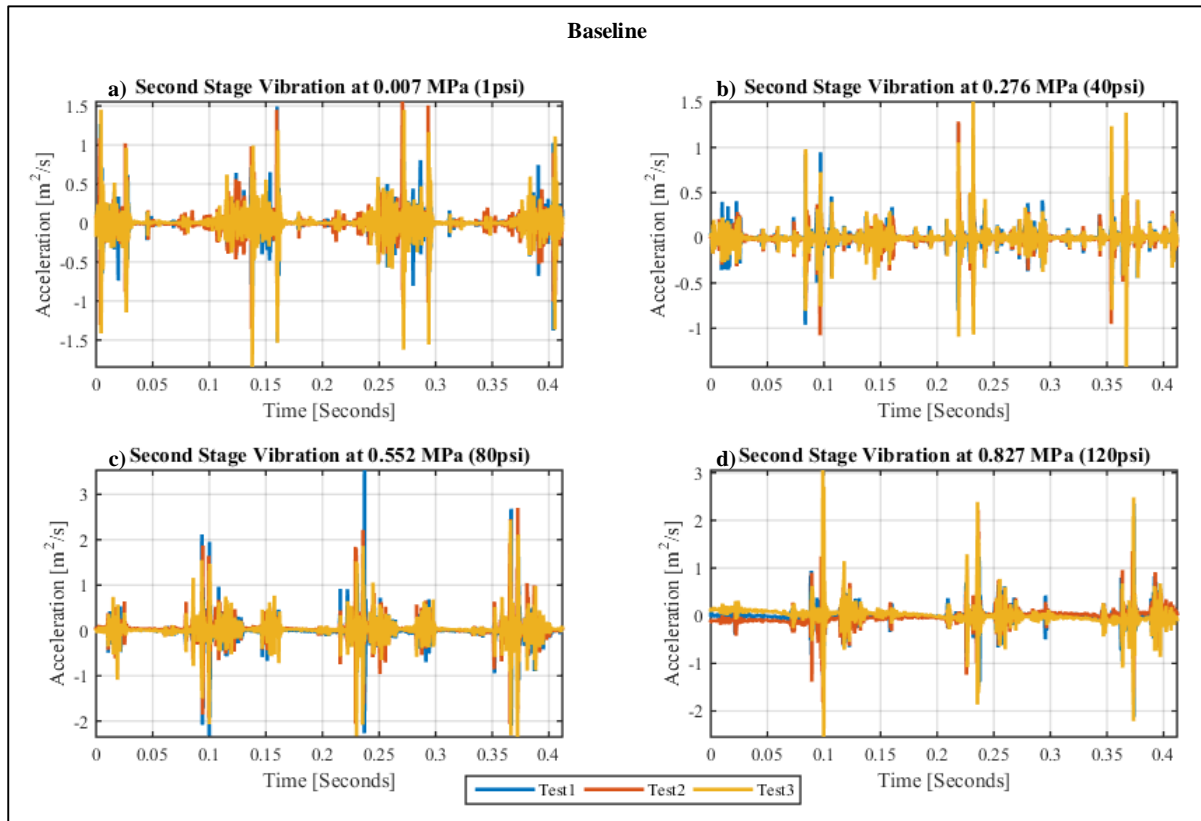


FIGURE 4.18: REPEATED VIBRATION SIGNALS AT SEVERAL DISCHARGE PRESSURES

TABLE 4.9: ANALYSIS OF VARIANCE FOR REPEATABILITY OF VIBRATION SIGNALS

Source	DF	Adj Sum Squares	Adj Mean Squares	F-Value	P-Value
Repeated Tests	2	0.000167	0.000083	0.06	0.946
Error	9	0.013463	0.001496		
Total	11	0.013630			

TABLE 4.10: ANALYSIS OF VARIANCE FOR SEVERAL DISCHARGE PRESSURE

Source	DF	Adj Sum Squares	Adj Mean Squares	F-Value	P-Value
Discharge pressure	3	0.013060	0.004353	61.06	0.000
Error	8	0.000570	0.000071		
Total	11	0.013630			

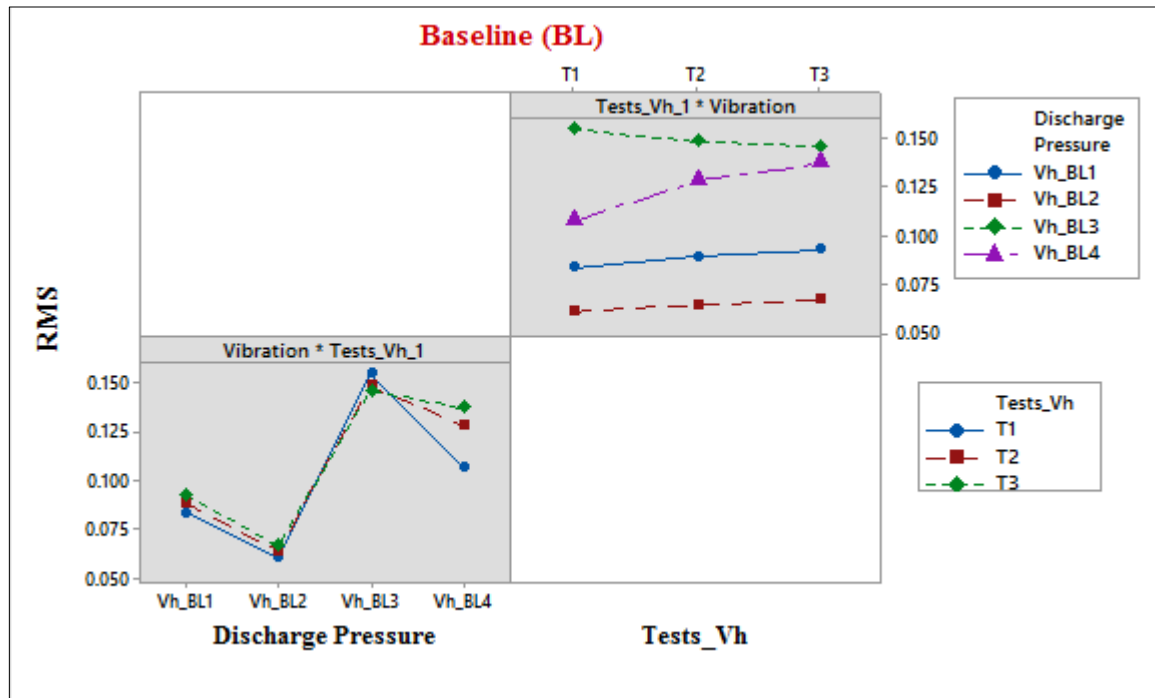


FIGURE 4.19: INTERACTION PLOTS OF RMS AND SEVERAL DISCHARGE PRESSURES FOR VIBRATION SIGNALS

TABLE 4.11: CORRELATION COEFFICIENT AND PROBABILITY LEVEL OF BASELINE TEST VIBRATION SIGNALS

Correlation Coefficients r				
Baseline				
	0.007MPa	0.276MPa	0.552MPa	0.83MPa
Test 1	1	1	1	1
Test 2	-0.0036	0.0595	0.0064	0.00463
Test 3	-0.0039	-0.0098	-0.0118	0.00547
Probability Level p				
Test 1	1	1	1	1
Test 2	0.4649	0	0.2007	0
Test 3	0.4356	0.0486	0.0179	0

4.7.2 Discharge Valve Leakage

The experiments are carried out when there is a discharge valve leakage seeded on the two-stage reciprocating compressor. The data is collected for three measurements including In-cylinder pressure, airborne acoustics, and vibration.

4.7.2.1 Second Stage In-Cylinder Pressure

Figure 4.20 presents the time domain In-cylinder pressure waveform for several discharge pressures under the discharge valve fault condition. The experiment is repeated three times

(Test1, Test2 and Test3) to analyse the repeatability of the signal. Some slight variations are observed in the waveform representation during the discharge process. However, an analysis of variance (ANOVA) of the repeated tests for each discharge pressure is computed for robust conclusions.

Table 4.12 presents the ANOVA summary for repeatability of In-cylinder pressure signals. The P-value is higher than 0.05, which means there is no significant statistical difference in the repeated tests, so the null hypothesis is accepted. The P-value for variances between discharge pressures is less than 0.05, which implies that the RMS values of the discharge pressures are significantly different (see Figure 4.21).

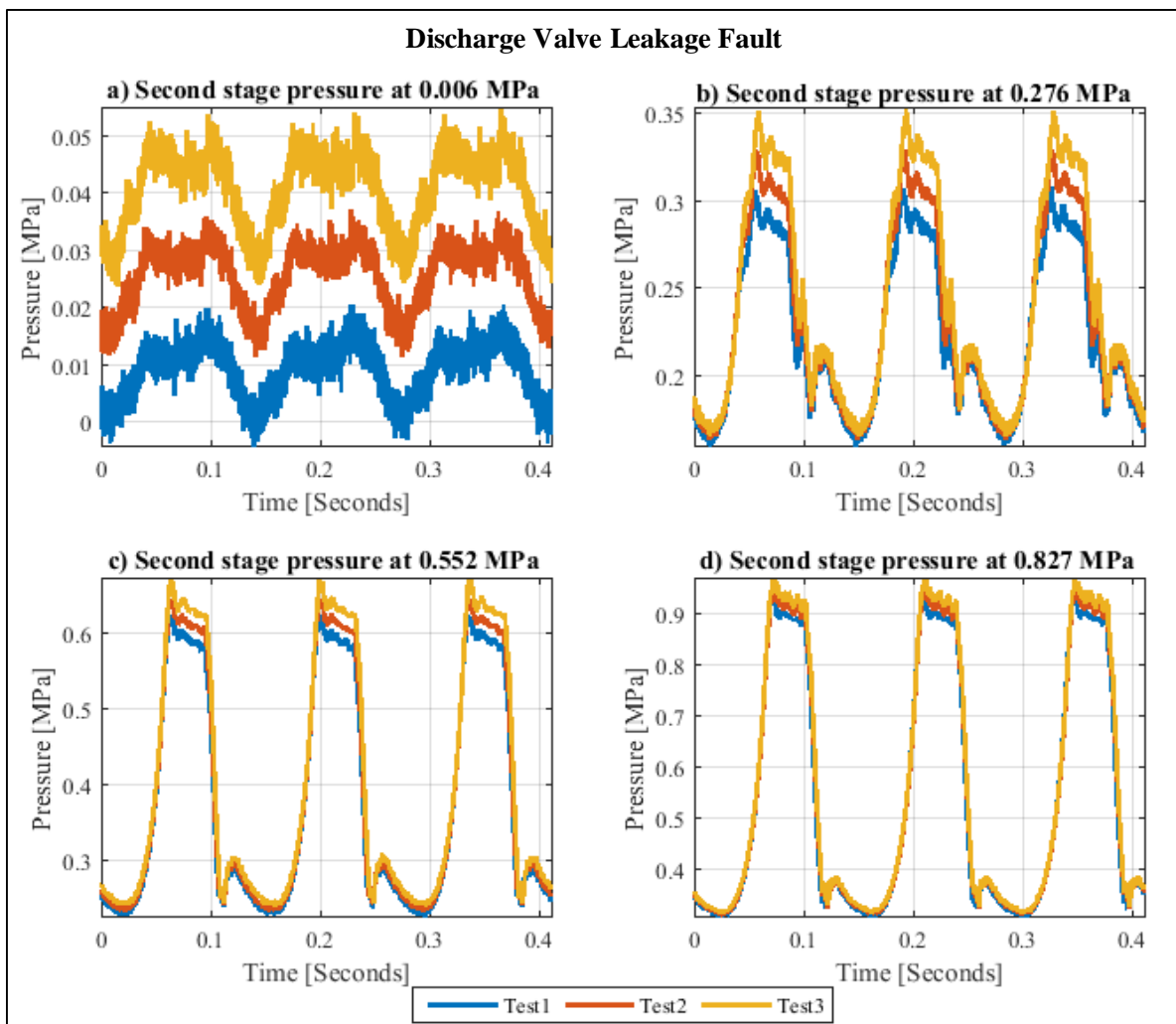


FIGURE 4.20: REPEATED IN-CYLINDER PRESSURE WAVEFORMS AT SEVERAL DISCHARGE PRESSURE

TABLE 4.12: ANALYSIS OF VARIANCE FOR REPEATABILITY OF IN-CYLINDER PRESSURE SIGNAL UNDER DISCHARGE VALVE FAULT CONDITION

Source	DF	Adj Sum Squares	Adj Mean Squares	F-Value	P-Value
Repeated Pressure Tests (DVL)	2	0.000291	0.000145	0.00	0.997
Error	9	0.500024	0.055558		
Total	11	0.500315			

TABLE 4.13: ANALYSIS OF VARIANCE FOR SEVERAL DISCHARGE PRESSURES UNDER DISCHARGE VALVE FAULT CONDITION

Source	DF	Adj Sum Squares	Adj Mean Squares	F-Value	P-Value
Discharge Pressure	3	0.556493	0.185498	1181.82	0.000
Error	8	0.001256	0.000157		
Total	11	0.557749			

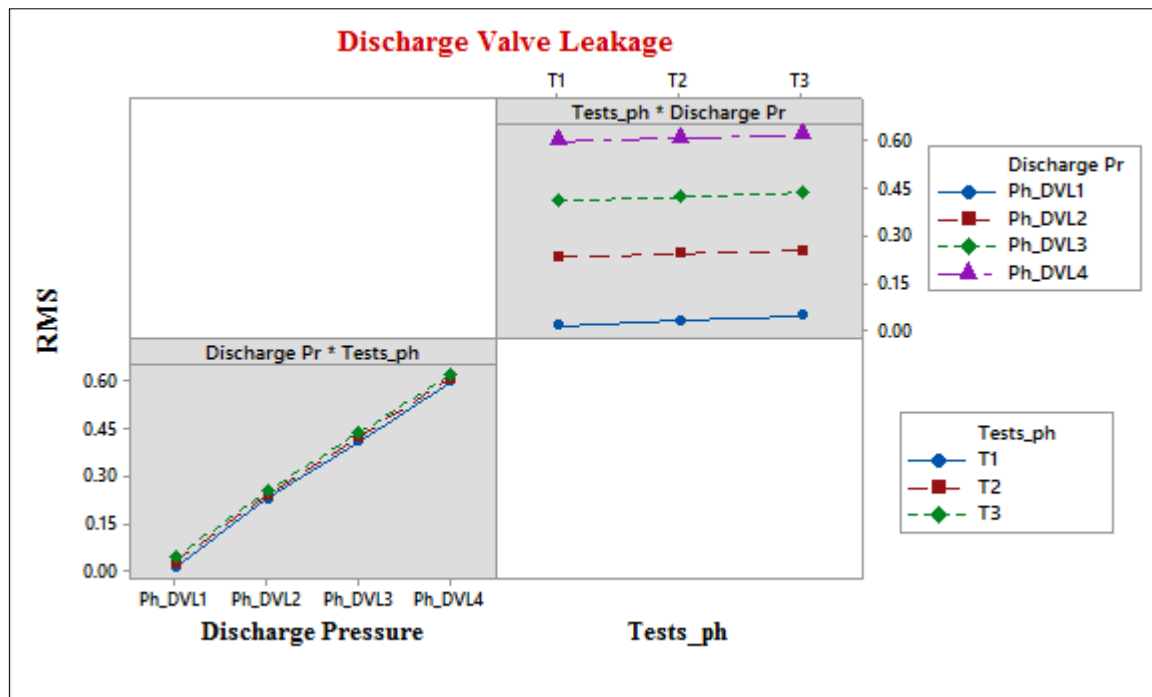


FIGURE 4.21: INTERACTION PLOTS OF THE RMS VALUES FOR SEVERAL DISCHARGE PRESSURES AND REPEATED PRESSURE SIGNALS

Table 4.14 shows the correlation coefficients and the probability level of the discharge valve leakage fault test signals (Test1, Test2, and Test3) at several discharge pressures. It can be

concluded from the results that the test signals are very similar since the correlation coefficient values of Test 2 and 3 are close to 1 and the P values are less than 0.05.

TABLE 4.14: CORRELATION COEFFICIENT AND PROBABILITY LEVEL OF BASELINE TEST PRESSURE SIGNALS

Correlation Coefficients r				
Discharge Valve Leakage (DVL)				
	0.007MPa	0.276MPa	0.552MPa	0.83MPa
Test 1	1	1	1	1
Test 2	0.8959	0.9957	0.9991	0.9978
Test 3	0.8647	0.9807	0.9955	0.9975
Probability Level p				
Test 1	1	1	1	1
Test 2	0	0	0	0
Test 3	0	0	0	0

4.7.2.2 Airborne Acoustic Waves

Figure 4.22 presents the time domain airborne acoustic waves in the cavity of the second-stage cylinder for several discharge pressures under leaking discharge valve condition. The experiment is repeated three times (Test1, Test2, and Test3), and from the subplots, it is quite difficult to see the differences between the three repeated tests for all discharge pressure cases. Again, the ANOVA test is computed and the summary of the investigations are presented in Tables 4.15 and 4.16.

Table 4.15 shows a P-value higher than 0.05, which means there are no significant differences in the repeated tests, so the null hypothesis is accepted. The P-value for variances between discharge pressures is less than 0.05, which implies that the RMS values of the discharge pressures are significantly different (see Table 4.16).

The RMS interaction plots between several discharge pressures and the repeated airborne acoustic signals are presented in Figure 4.23. The RMS values of the discharge pressure subplot show an increasing linear trend as the discharge pressure increases (AA_DVL1, AA_DVL2, AA_DVL3, and AA_DVL4, which represents 0.0069 MPa, 0.276 MPa, 0.552 MPa and 0.827 MPa respectively). The variances between the RMS values of the repeated signals show no significant statistical difference (see the top right subplot).

Table 4.17 shows the correlation coefficients and the probability level of the discharge valve leakage airborne acoustic wave test signals (Test1, Test2, and Test3) at several discharge

pressures. It can be concluded that the test signals are very similar since the correlation coefficient values r are close to 1 and the P values are less than 0.05.

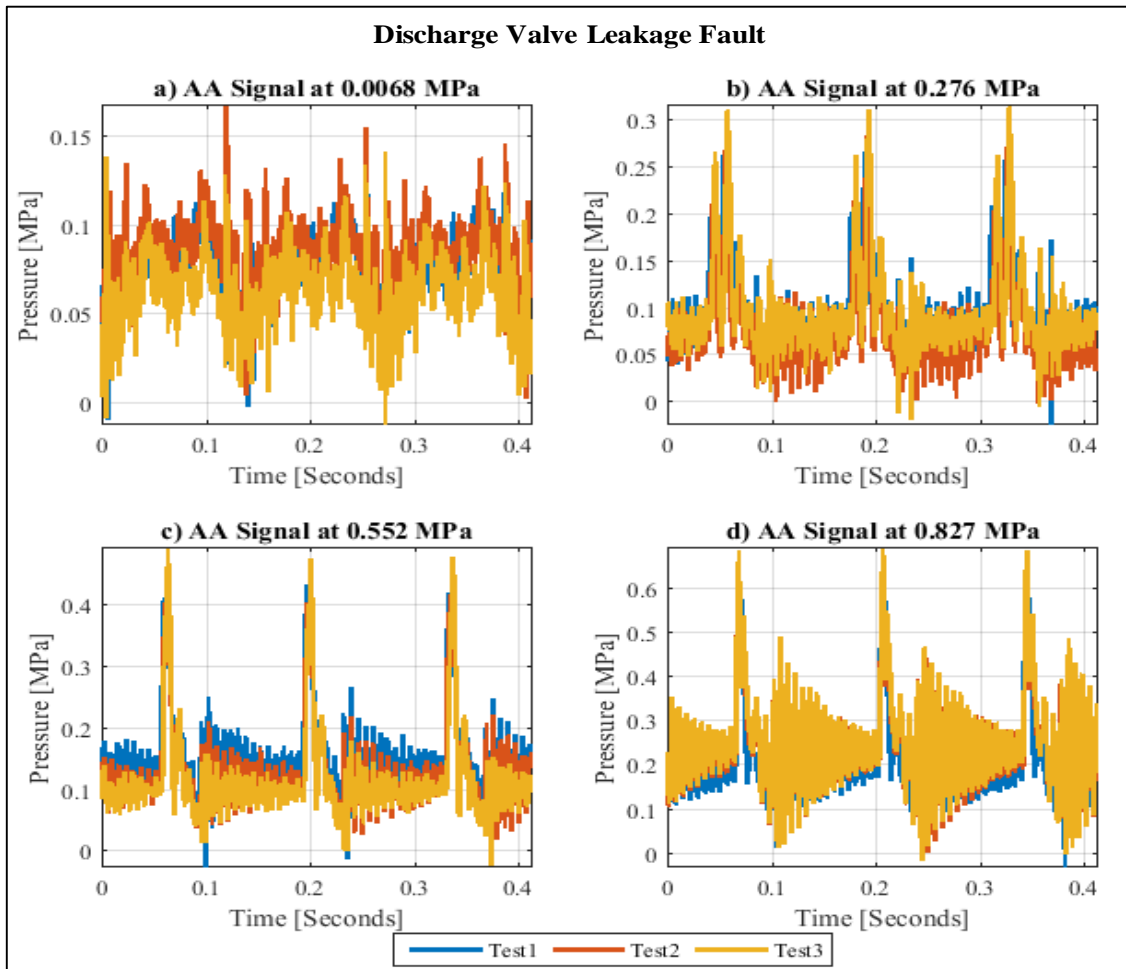


FIGURE 4.22: REPEATED AIRBORNE ACOUSTIC WAVEFORMS AT SEVERAL DISCHARGE PRESSURES

TABLE 4.15: ANALYSIS OF VARIANCE FOR REPEATABILITY OF AIRBORNE ACOUSTIC SIGNALS UNDER DISCHARGE VALVE FAULT CONDITION

Source	DF	Adj Sum Squares	Adj Mean Squares	F-Value	P-Value
Repeated (DVL) Airborne Acoustic Tests	2	0.000127	0.000064	0.01	0.990
Error	9	0.057223	0.006358		
Total	11	0.057350			

TABLE 4.16: ANALYSIS OF VARIANCE FOR SEVERAL DISCHARGE PRESSURES UNDER DISCHARGE VALVE FAULT CONDITION

Source	DF	Adj Sum Squares	Adj Mean Squares	F-Value	P-Value
Discharge Pressure	3	0.054272	0.018091	47.02	0.000
Error	8	0.003078	0.000385		
Total	11	0.057350			

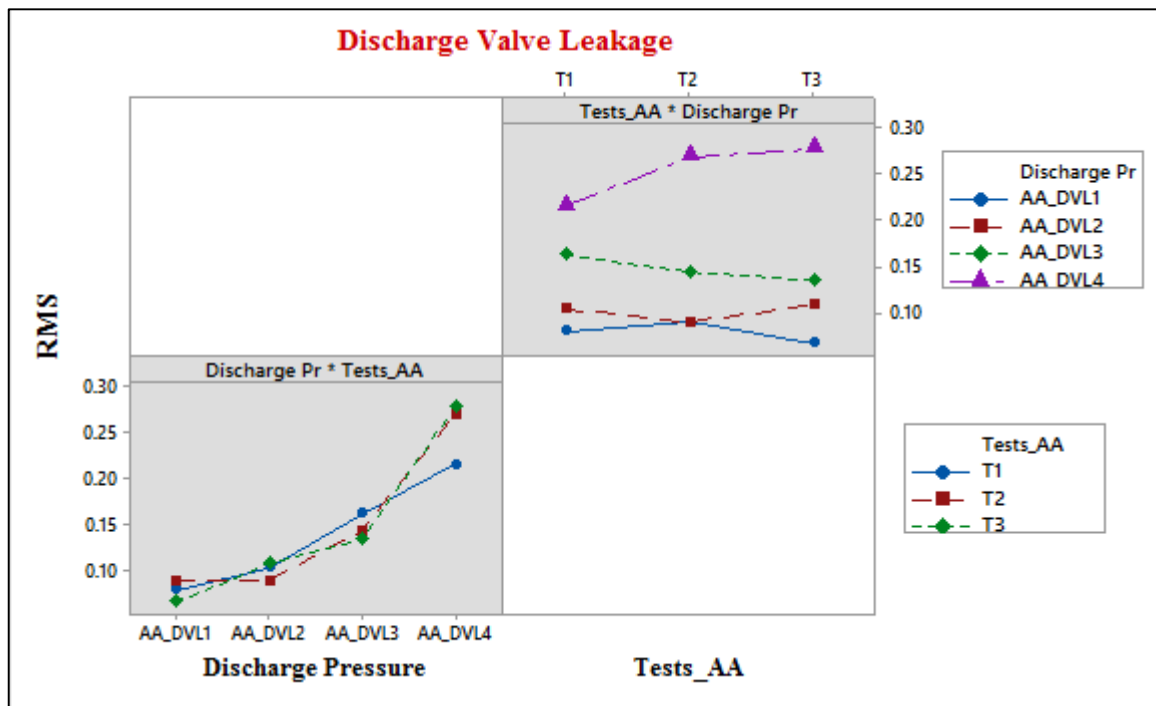


FIGURE 4.23: INTERACTION PLOTS OF THE RMS VALUES FOR SEVERAL DISCHARGE PRESSURES AND REPEATED AIRBORNE ACOUSTIC SIGNALS

TABLE 4.17: CORRELATION COEFFICIENT AND PROBABILITY LEVEL OF DISCHARGE VALVE LEAKAGE TEST AIRBORNE ACOUSTIC SIGNALS

Correlation Coefficients r				
Discharge Valve Leakage (DVL)				
	0.007MPa	0.276MPa	0.552MPa	0.83MPa
Test 1	1	1	1	1
Test 2	0.6669	0.8145	0.9394	0.7875
Test 3	0.5179	0.4776	0.7708	0.7861
Probability Level p				
Test 1	1	1	1	1
Test 2	0	0	0	0
Test 3	0	0	0	0

4.7.2.3 Second Stage Vibration

Figure 4.24 presents the time-domain vibration signals from the second-stage cylinder for several discharge pressures under the leaking discharge valve condition. From the subplots, it is impossible to see the differences between the three repeated tests for all discharge pressure cases. Therefore, the ANOVA test is computed, and the summary of the investigations are presented in Tables 4.18 and 4.19.

Table 4.18 shows a P-value higher than 0.05, which means there is no significant differences in the repeated tests, so the null hypothesis is accepted. The P-value for variances between discharge pressures is 0.046, which is very close (due to the randomness of vibration signals) but still less than the significance level (0.05). Therefore, it can be concluded that the RMS values of the discharge pressures are significantly different (see Table 4.19).

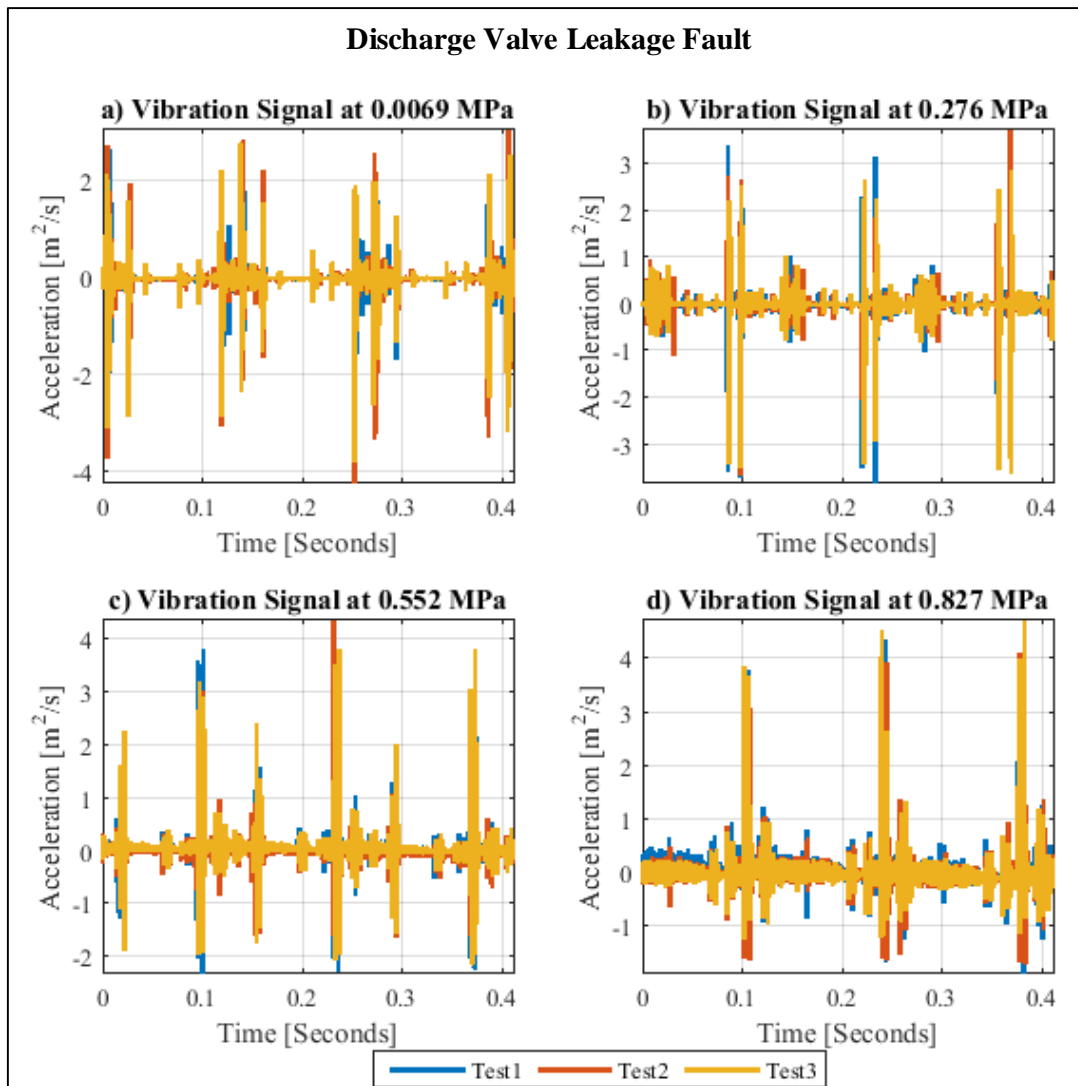


FIGURE 4.24: REPEATED VIBRATION SIGNALS AT SEVERAL DISCHARGE PRESSURES

TABLE 4.18: ANALYSIS OF VARIANCE FOR REPEATABILITY OF VIBRATION SIGNALS UNDER DISCHARGE VALVE FAULT CONDITION

Source	DF	Adj Sum Squares	Adj Mean Squares	F-Value	P-Value
Repeated (DVL) Vibration Tests	2	0.000173	0.000087	0.17	0.843
Error	9	0.004485	0.000498		
Total	11	0.004658			

TABLE 4.19: ANALYSIS OF VARIANCE FOR SEVERAL DISCHARGE PRESSURES UNDER DISCHARGE VALVE FAULT CONDITION

Source	DF	Adj Sum Squares	Adj Mean Squares	F-Value	P-Value
Discharge Pressure	3	0.002852	0.000951	4.21	0.046
Error	8	0.001806	0.000226		
Total	11	0.004658			

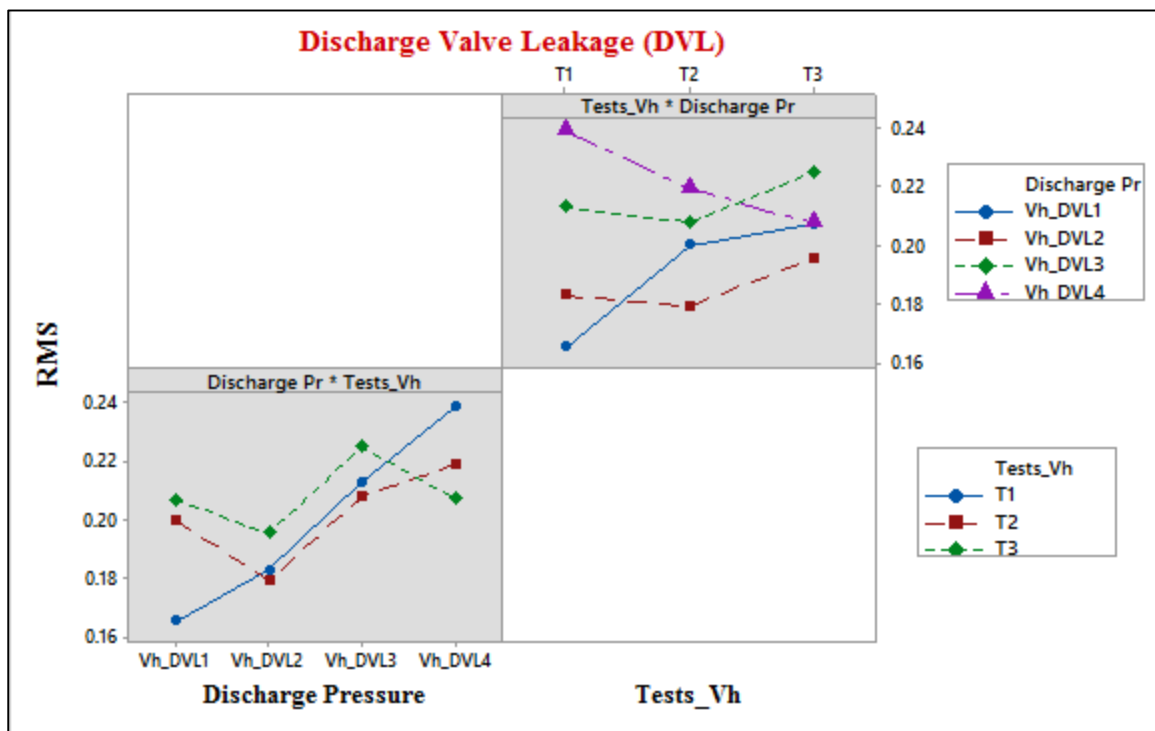


FIGURE 4.25: INTERACTION PLOTS OF THE RMS VALUES FOR SEVERAL DISCHARGE PRESSURES AND REPEATED VIBRATION SIGNALS

The correlation coefficients and the probability level of the discharge valve leakage fault test signals (Test1, Test2, and Test3) at several discharge pressures are presented in Table 4.20.

From the results, there are inconclusive evidence about the significance of the relationship between the vibration test signals at certain discharge pressures (0.007MPa, 0.276MPa and 0.83MPa) as their p values are greater than the significance level of 0.05. The results for test signals at 0.552MPa, show that the signals (Test 2 and 3) have a positive but significantly weak relationship between Test 1.

TABLE 4.20: CORRELATION COEFFICIENT AND PROBABILITY LEVEL OF DISCHARGE VALVE LEAKAGE TEST VIBRATION SIGNALS

Correlation Coefficients r				
Discharge Valve Leakage (DVL)				
	0.007MPa	0.276MPa	0.552MPa	0.83MPa
Test 1	1	1	1	1
Test 2	-0.0055	0.0234	0.0472	0.0216
Test 3	-0.0021	-0.0086	0.0379	0.0019
Probability Level p				
Test 1	1	1	1	1
Test 2	0.2703	0	0	0
Test 3	0.6789	0.0845	0	0.7042

4.7.3 Intercooler Leakage

The experiments are carried out when there is an intercooler leakage seeded on the two-stage reciprocating compressor. The data is collected for three measurements including In-cylinder pressure, airborne acoustics, and vibration.

4.7.3.1 Cylinder Pressure

Figure 4.26 presents the time domain In-cylinder pressure waveform for several discharge pressures under a leaking intercooler condition. The experiment is repeated three times (Test1, Test2 and Test3) to analyse the repeatability of the signal. Some slight variations are observed in the waveform representation during the discharge process. However, an analysis of variance (ANOVA) of the repeated tests for each discharge pressure is computed.

Table 4.21 presents the ANOVA summary for repeatability of In-cylinder pressure signals. The P-value is higher than 0.05, which means there is no significant difference in the repeated tests, so the null hypothesis is accepted. The P-value for variances between discharge pressures is less than 0.05, which implies that the RMS values of the discharge pressures are significantly different (see Table 4.22 and Figure 4.27).

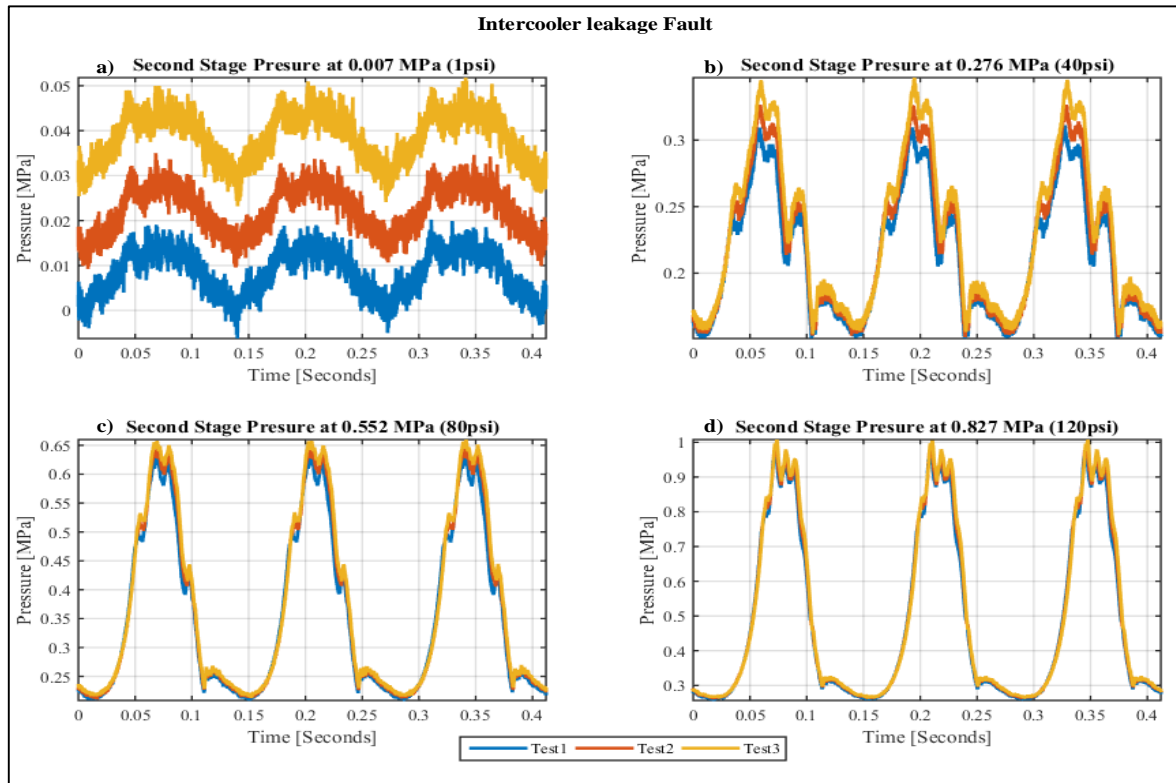


FIGURE 4.26: REPEATED PRESSURE SIGNALS AT SEVERAL DISCHARGE PRESSURES

TABLE 4.21: ANALYSIS OF VARIANCE FOR REPEATABILITY OF IN-CYLINDER PRESSURE SIGNALS UNDER INTERCOOLER FAULT CONDITION

Source	DF	Adj Sum Squares	Adj Mean Squares	F-Value	P-Value
Repeated (ICL) Pressure Tests	2	0.000554	0.000277	0.00	0.995
Error	9	0.498331	0.055370		
Total	11	0.498885			

TABLE 4.22: ANALYSIS OF VARIANCE FOR SEVERAL DISCHARGE PRESURES UNDER INTERCOOLER FAULT CONDITION

Source	DF	Adj Sum Squares	Adj Mean Squares	F-Value	P-Value
Discharge Pressure	3	0.498327	0.166109	2382.41	0.000
Error	8	0.000558	0.000070		
Total	11	0.498885			

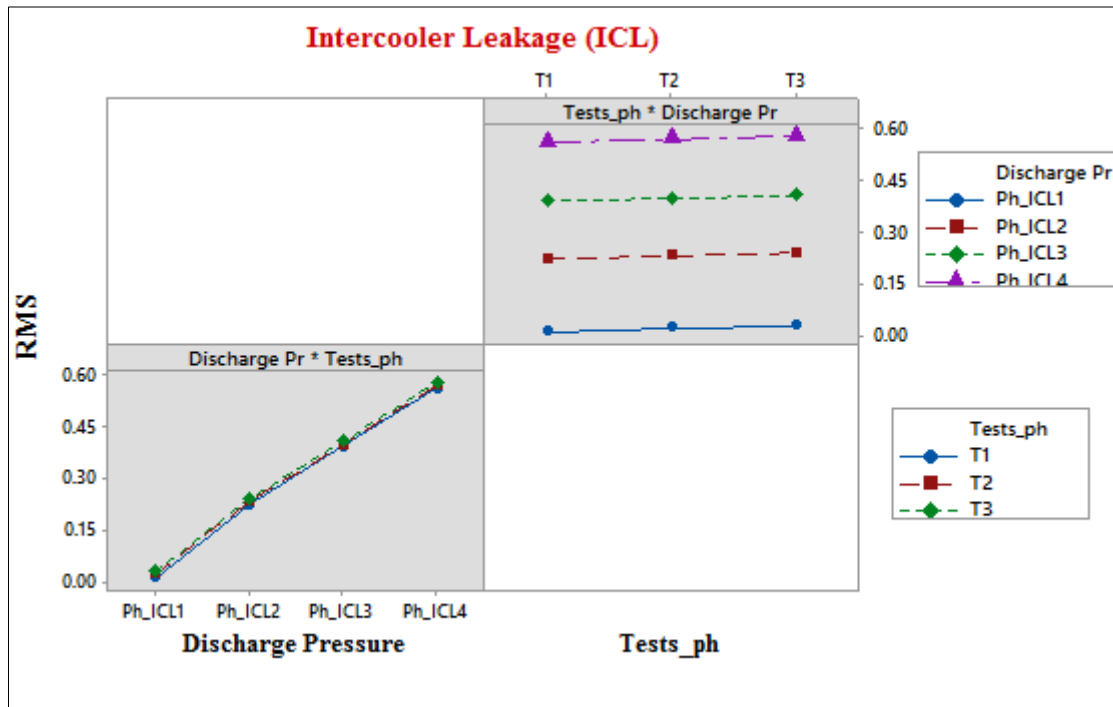


FIGURE 4.27: INTERACTION PLOTS OF RMS VALUES FOR SEVERAL DISCHARGE PRESSURES AND REPEATED PRESSURE SIGNALS

Table 4.23 shows the correlation coefficients and the probability level of the baseline second-stage pressure test signals (Test1, Test2, and Test3) at several discharge pressures. It can be concluded that the test signals are very similar since the correlation coefficient values r are close to 1 and the P values are less than 0.05.

TABLE 4.23: CORRELATION COEFFICIENT AND PROBABILITY LEVEL OF INTERCOOLER LEAKAGE TEST OF PRESSURE SIGNALS

Correlation Coefficients r				
Intercooler Leakage (ICL)				
	0.007MPa	0.276MPa	0.552MPa	0.83MPa
Test 1	1	1	1	1
Test 2	0.9413	0.9923	0.9992	0.999
Test 3	0.9091	0.9841	0.9977	0.997
Probability Level p				
Test 1	1	1	1	1
Test 2	0	0	0	0
Test 3	0	0	0	0

4.7.3.2 Airborne Acoustic Waves

Figure 4.28 presents the time domain airborne acoustic waves in the cavity of the second-stage cylinder for several discharge pressures under a leaking intercooler condition. The experiment

is repeated three times (Test1, Test2, and Test3). From the subplots, it is difficult to see the differences between the repeated tests in all discharge pressure cases. Again, the ANOVA test is computed, and the summary of the investigations are presented in Tables 4.24 and 4.25.

From the two tables it can be concluded that there are no significant statistical differences in the repeated tests, and the RMS values of the discharge pressures are significantly different. The interaction plots in Figure 4.29 show the differences.

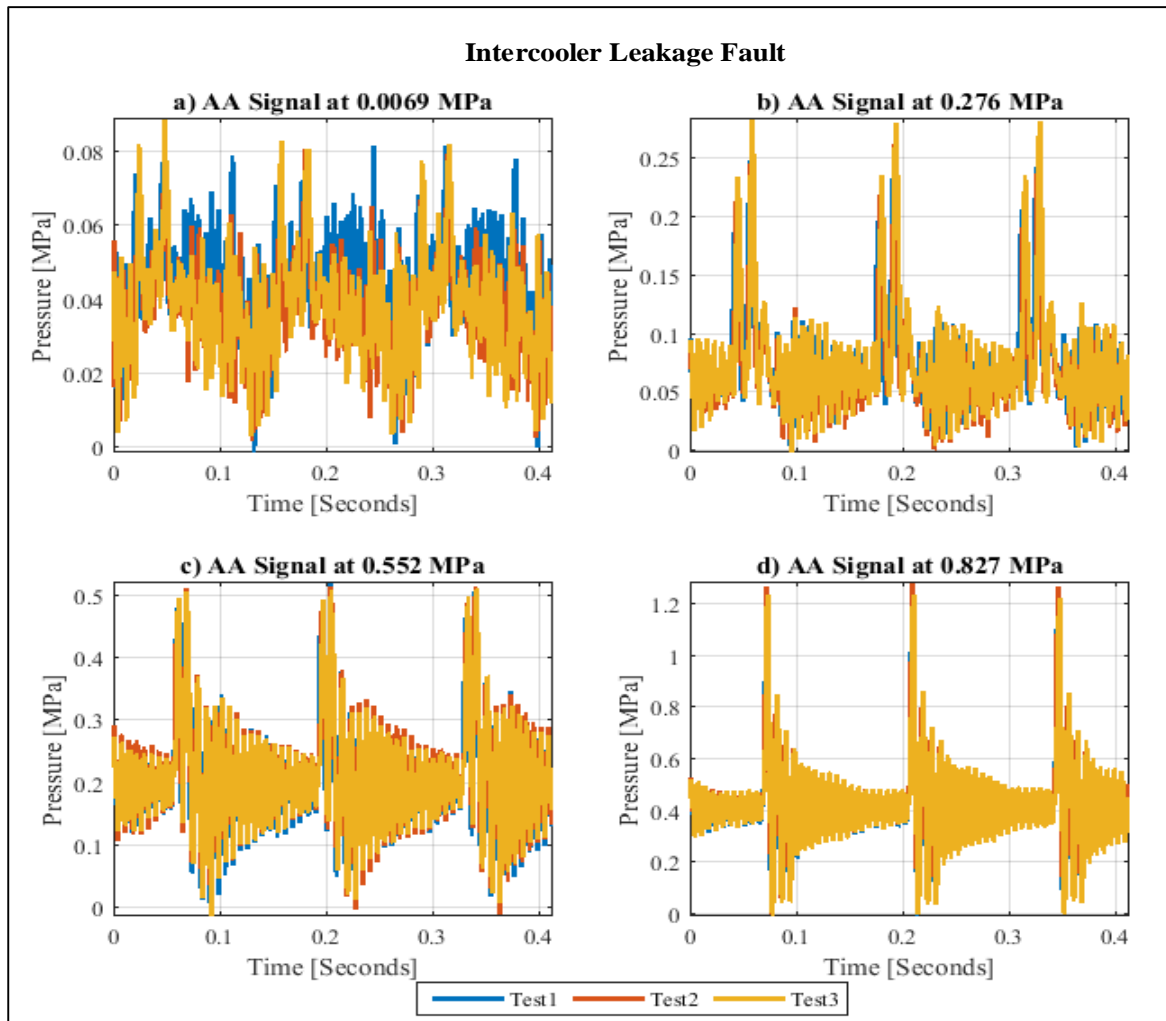


FIGURE 4.28: REPEATED AIRBORNE ACOUSTIC SIGNALS AT SEVERAL DISCHARGE PRESSURES

TABLE 4.24: ANALYSIS OF VARIANCE FOR REPEATABILITY OF AIRBORNE ACOUSTIC SIGNALS UNDER INTERCOOLER FAULT CONDITION

Source	DF	Adj Sum Squares	Adj Mean Squares	F-Value	P-Value
Repeated (ICL) Airborne Acoustic Tests	2	0.000030	0.000015	0.00	1.000

CHARACTERISING VIBRO-ACOUSTIC SIGNALS OF A RECIPROCATING
COMPRESSOR FOR CONDITION MONITORING

Error	9	0.307923	0.034214		
Total	11	0.307953			

TABLE 4.25: ANALYSIS OF VARIANCE FOR SEVERAL DISCHARGE PRESSURES UNDER INTERCOOLER FAULT CONDITION

Source	DF	Adj Sum Squares	Adj Mean Squares	F-Value	P-Value
Discharge Pressure	3	0.307776	0.102592	4652.85	0.000
Error	8	0.000176	0.000022		
Total	11	0.307953			

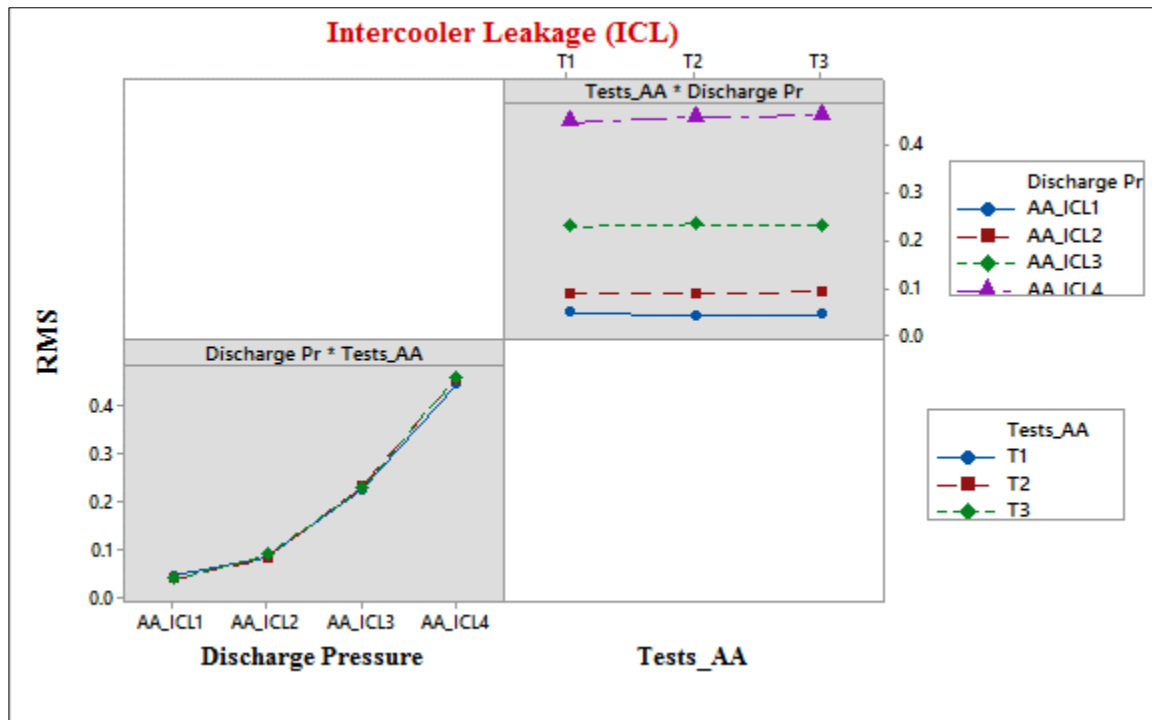


FIGURE 4.29: INTERACTION PLOTS OF THE RMS VALUES FOR SEVERAL DISCHARGE PRESSURES AND REPEATED AIRBORNE ACOUSTIC SIGNALS

Table 4.26 shows the correlation coefficients and the probability level of the ICL fault test signals (Test1, Test2, and Test3) at several discharge pressures. It can be concluded that the test signals are very similar since the correlation coefficient values r are close to 1 and the P values are less than 0.05. However, the r values for 0.007MPa and 0.276MPa Test 3 signals show that there is a weak but weak and moderate linear relationship respectively.

TABLE 4.26: CORRELATION COEFFICIENT AND PROBABILITY LEVEL OF INTERCOOLER LEAKAGE TEST OF AIRBORNE ACOUSTIC WAVE SIGNALS

Correlation Coefficients r				
Intercooler Leakage (ICL)				
	0.007MPa	0.276MPa	0.552MPa	0.83MPa
Test 1	1	1	1	1
Test 2	0.6113	0.7705	0.9452	0.9933
Test 3	0.1846	0.5009	0.8156	0.7886
Probability Level p				
Test 1	1	1	1	1
Test 2	0	0	0	0
Test 3	0	0	0	0

4.7.3.3 Surface Vibration

Figure 4.30 presents the time-domain vibration signals from the second-stage cylinder for several discharge pressures under a leaking intercooler condition. Again, it is difficult to assess the repeatability of the signal by merely observing the signatures. Therefore, the ANOVA test is computed, and the summary of the investigations are presented in Tables 4.26 and 4.27.

From the two tables, it can be concluded that there are no significant differences in the repeated tests since the P-value is higher than 0.05 and the RMS values of the discharge pressures are significantly different as the P-value is zero. The interaction plot in Figure 4.31 shows the relationship between the RMS values of the repeated tests and all discharge pressures investigated.

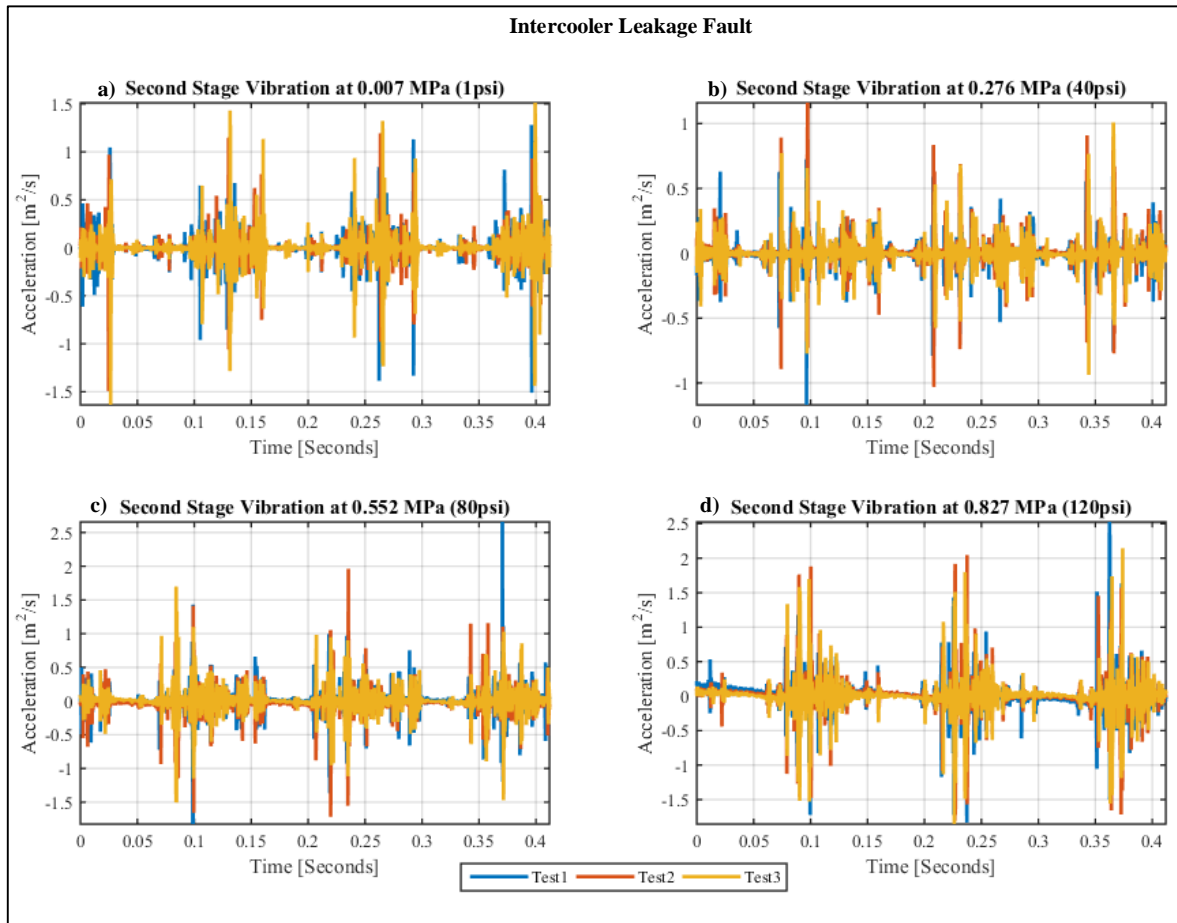


FIGURE 4.30: REPEATED VIBRATION SIGNALS AT SEVERAL DISCHARGE PRESSURES

TABLE 4.27: ANALYSIS OF VARIANCE FOR REPEATABILITY OF VIBRATION SIGNALS UNDER INTERCOOLER FAULT CONDITION

Source	DF	Adj Sum Squares	Adj Mean Squares	F-Value	P-Value
Repeated (ICL) Vibration Tests	2	0.000147	0.000073	0.10	0.907
Error	9	0.006685	0.000743		
Total	11	0.006832			

TABLE 4.28: ANALYSIS OF VARIANCE FOR SEVERAL DISCHARGE PRESSURES UNDER INTERCOOLER FAULT CONDITIONS

Source	DF	Adj Sum Squares	Adj Mean Squares	F-Value	P-Value
Discharge Pressure	3	0.006301	0.002100	31.63	0.000
Error	8	0.000531	0.000066		
Total	11	0.006832			

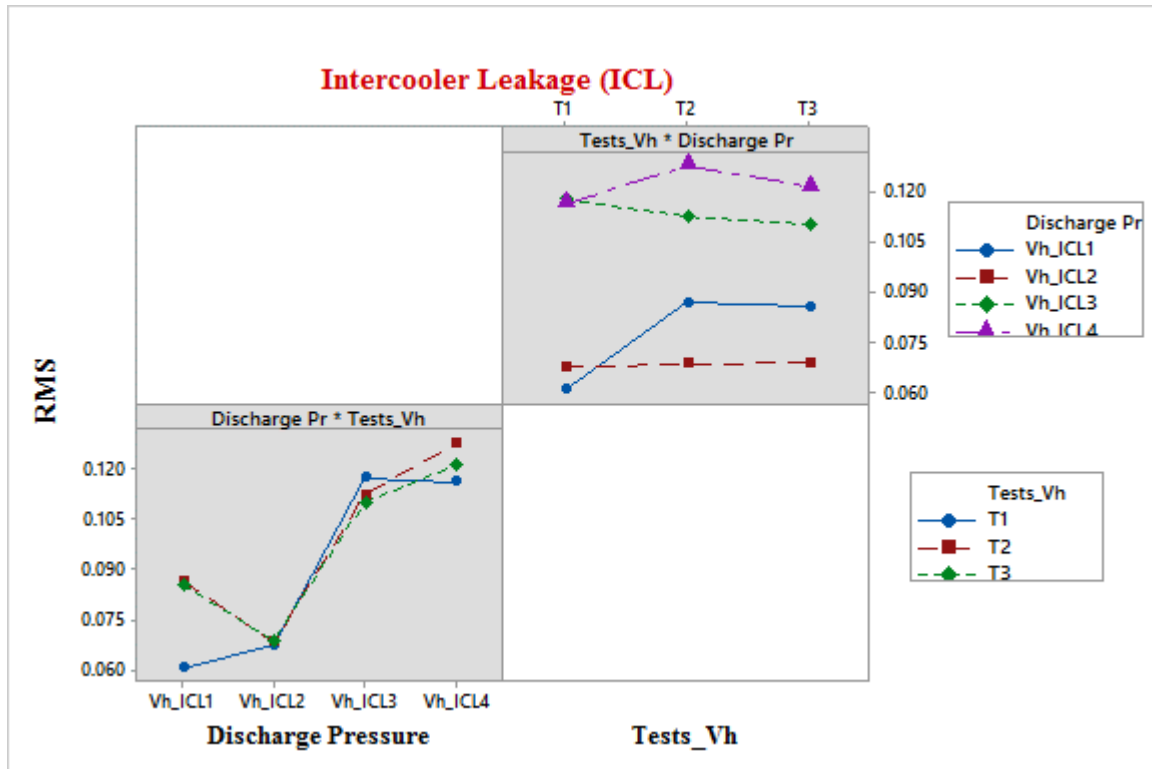


FIGURE 4.31: INTERACTION PLOTS OF THE RMS VALUES FOR SEVERAL DISCHARGE PRESSURES AND REPEATED VIBRATION SIGNALS

Table 4.29 shows the correlation coefficients and the probability level of the ICL fault vibration test signals (Test1, Test2, and Test3) at several discharge pressures. It can be concluded from the results that there are inconclusive evidence about the significance of the relationship between the vibration test signals at all discharge pressures except those whose r values are written in red.

TABLE 4.29: CORRELATION COEFFICIENT AND PROBABILITY LEVEL OF INTERCOOLER LEAKAGE TEST OF VIBRATION SIGNALS

Correlation Coefficients r				
Intercooler Leakage (ICL)				
	0.007MPa	0.276MPa	0.552MPa	0.83MPa
Test 1	1	1	1	1
Test 2	-0.0074	0.0041	-0.0195	0.0236
Test 3	0.0031	-0.0029	0.0033	0.0215
Probability Level p				
Test 1	1	1	1	1
Test 2	0.1354	0.4047	0.0001	0
Test 3	0.538	0.563	0.5012	0

4.7.4 Summary

To ensure that correct results are obtained every time an experiment is run, the repeatability of the signals for the three measurement signals including In-cylinder pressure, airborne acoustics (pressure pulsations), and surface vibration under healthy and fault conditions for several discharge pressures are analysed.

One-way analysis of variance (ANOVA) is used to check if the differences in RMS values of repeated signals and several discharge pressures are significantly substantial. Findings showed that there were no significant changes in the RMS values of the repeated signals for all measurements and conditions. In addition, the differences in RMS values of several discharge pressures were investigated for all measurements and conditions. The P-values were zero, strongly indicating that there is at least one or two discharge pressure signals are different as expected.

CHAPTER FIVE

5 DYNAMIC MODELLING OF A DOUBLE-STAGE, SINGLE-ACTING RECIPROCATING COMPRESSOR

The chapter presents various mathematical models developed for the simulation of the double-stage, single-acting reciprocating compressor used for this research. A number of physical processes including: mechanical, thermal, flow and electric-magnetic processes involved with the compressor have been redeveloped to fully understand the dynamics of the machine and corresponding fault models are developed simultaneously. The model developed based on the first principles consists of three main equations: crankshaft motion, two cylinder pressure equations and, four valve motion equations. In addition, the second-stage discharge chamber pressure is incorporated into the model.

5.1 Introduction

The main principle of the reciprocating compressors' operation is the conversion of mechanical rotational motion of the crankshaft into linear motion. The crankshaft is powered by an electrical motor, which translates this motion by means of the connection rod to linear motion as illustrated in Figure 5.1. The connecting rod moves the piston linearly within the cylinder bore to deliver the desired high-pressure air. The piston proceeds downwards from top dead centre (TDC) to bottom dead centre (BDC), pressure decreases, and the suction valve opens by means of pressure difference over the valve head. Furthermore, just as the piston reaches BDC and starts to return to TDC, air in the cylinder is compressed. Once the in-cylinder pressure is greater than the plenum pressure (pressure after the valve), the valve is forced open allowing high-pressure air out of the cylinder. The process described above forms the foundation for the model simulation of in-cylinder pressure, discharge chamber pressure and vibration of the cylinders.

Reciprocating compressors are high priced and complicated machines, and understanding the dynamic process is paramount for design modification, and fault prediction. Modelling of the reciprocating compressor has received a great deal of research attention over the years. Much of this fame is attributed to the prospects of numerical models being used for real time applications such as machine condition and fault diagnostics. In addition, some underlying benefits include improved machine efficiency, reduced maintenance cost and improved machine reliability.

This chapter describes the developed mathematical model of several distinct but interactive components of the reciprocating compressor such as the crank mechanism, the cylinder, and the valve and discharge systems of double-stage single-acting reciprocating compressor and effects of specific faults on the compressor. This model has previously been developed by fellow scholar Elhaj Mohamed in 2005 (Elhaj M. A., 2005), however, as an addition, the discharge chamber (plenum) is incorporated into the already existing model to simulate the effects of gas pulsations on the system.

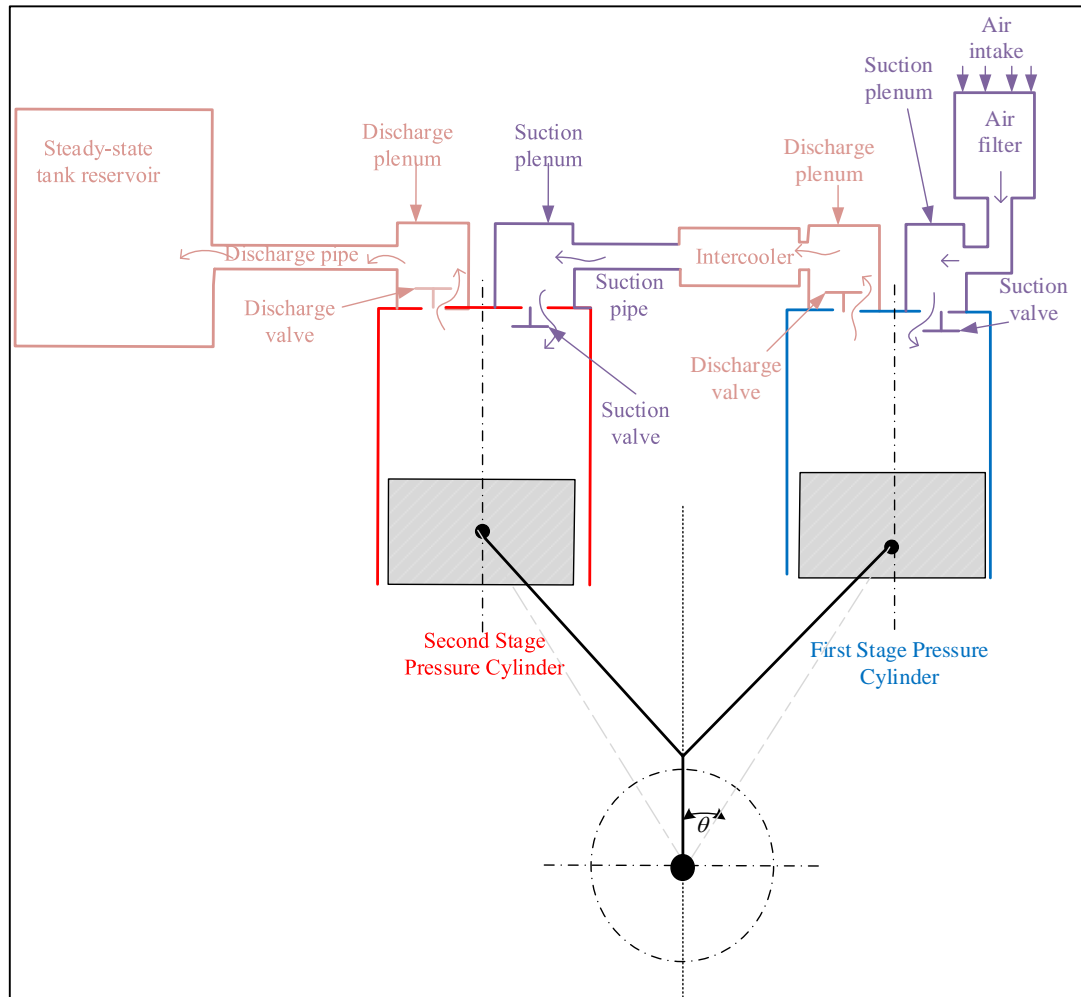


FIGURE 5.1: COMPLETE RECIPROCATING COMPRESSOR MODEL

The key modelling assumptions are:

- One-dimensional incompressible flow
- Isentropic process (reversible adiabatic)
- Valves with one degree of freedom

5.2 A Brief Review of Previous Reciprocating Compressor Modelling

The first mathematical model for a reciprocating compressor was developed based on a one degree-of-freedom reed valve dynamics (Costagliola, 1950). A couple of years later in 1966, Wasmbasgans modelled a high-speed hermetically sealed compressor similar to that of Costagliolas' but focused of modelling more than one degree of freedom of the reed valve dynamics (Wasmbasgans, 1966). Advances in the use of digital computers to simulate valve dynamics were later achieved by several scholars (McLaren & Kerr, 1968); (Padilla, 1971); (Schwerzler, 1971). Hamilton went a step further by accounting for friction, heat transfer and

real gas properties to obtain a better representation of the model (Hamilton, 1974). The main objectives of these studies were to develop a mathematical model, which would help in understanding the working principles of the compressor for appropriate design changes to be implemented for improved machine performance.

Various faults were incorporated into the compressor model by Manepatil, Yadava, and Nakra to determine their effects on parameters such as pressure signals for performance monitoring (Manepatil, Yadava, & Nakra, 2000). Furthermore, Liang, Gu and Ball developed a procedure for detecting and diagnosing valve faults by analysing the analytically modelled valve impacts (Liang, Gu, & Ball, 1996).

For a while, the modelling trend for reciprocating compressors was based on simulating the cylinder processes without accounting for discharge/suction system and line oscillations. Singh suggests that both cylinder process and discharge or suction systems of the reciprocating compressor should be modelled together to account for the strong interaction mechanisms between them (Singh, 1975). He also strongly suggests that for an accurate prediction of pressure distribution, mass flow rate and valve responses, the line pulsations should be included in the computer simulation. This is because the valves interact strongly with the suction and discharge flows, and the valve dynamics and mass flow rates are heavily dependent on the pressure differentials across the cylinder and the discharge chamber (Singh, 1975); (Maclaren , Kerr, Tramschek, & Sanjines, 1974).

Brablik was one of the first to couple compressor and piping models; based on his findings, he advised that the cylinder thermodynamics, valve flow and fluid motion in the lines should be simulated concurrently for precise and realistic pulsation predications (Brablik J. , 1969); (Brablik J. , 1972).

A complete model of the reciprocating compressor as seen in Figure 6.1, which includes the discharge chamber and piping system are incorporated into the compressor model to determine their influence on the valve system.

5.3 Crankshaft Dynamic Model –Piston Kinematics

5.3.1 Mechanism of Crank shaft and Connecting Rod

The schematic diagram of a typical piston-cylinder mechanism of a reciprocating compressor with indications of forces acting on it is given in Figure 5.2. The piston inside the cylinder

moves in a reciprocating motion by means of the crankshaft, which is driven by the induction motor. The interaction between the crankshaft and the connecting rod changes the direction of the normal force between the piston and the cylinder (Soedel, 2007). The entire simulation is based as a function of the crankshaft angle represented as (θ), therefore, the conversion of time to crankshaft angle is given by the following equation:

$$\theta(t) = \frac{N}{60} 2\pi * t \quad (5.1)$$

Where;

N = revolutions per minute (RPM),

t = time.

The cycle starts at TDC where $\theta = 0^\circ$ and ends at the same point with $\theta = 360^\circ$ after one revolution of the crankshaft. The gas pressure exerts a force F against the piston when the suction valve opens. In Figure 5.2 the action of the force F can be countered by the magnitude $F/\cos \phi$ induced by the torque M_t , and the magnitude $F \tan \phi$ acting in the ZY direction (Ball A. D., 2000).

Because the crankshaft has no translational movement, the bearings of the crankshaft exerts forces F in the vertical (ZX) and $F \tan \phi$ in the horizontal (ZY) directions.

The displacement x_{dp} of the piston is calculated in terms of the crank angle θ as;

$$x_{dp} = r \left[\left(\frac{l}{r} + 1 \right) - \left(\frac{l}{r} \cos \phi + \cos \theta \right) \right] \quad (5.2)$$

Where;

x_{dp} = downward displacement of the piston from TDC,

θ = the crank angle from TDC,

l = length of the connecting rod

r = radius of the crank (= stroke/2).

Considering the geometry and connecting rod,

$$l \sin \phi = r \sin \theta \quad (5.3)$$

$$\sin \phi = \frac{r}{l} \sin \theta \quad (5.4)$$

Let $n = \frac{l}{r}$,

$$\cos \phi = \sqrt{1 - (\sin \phi)^2} = \sqrt{1 - \frac{\sin^2 \theta}{n^2}} \quad (5.5)$$

$$\cos \phi = \frac{1}{n} \sqrt{n^2 - \sin^2 \theta} \quad (5.6)$$

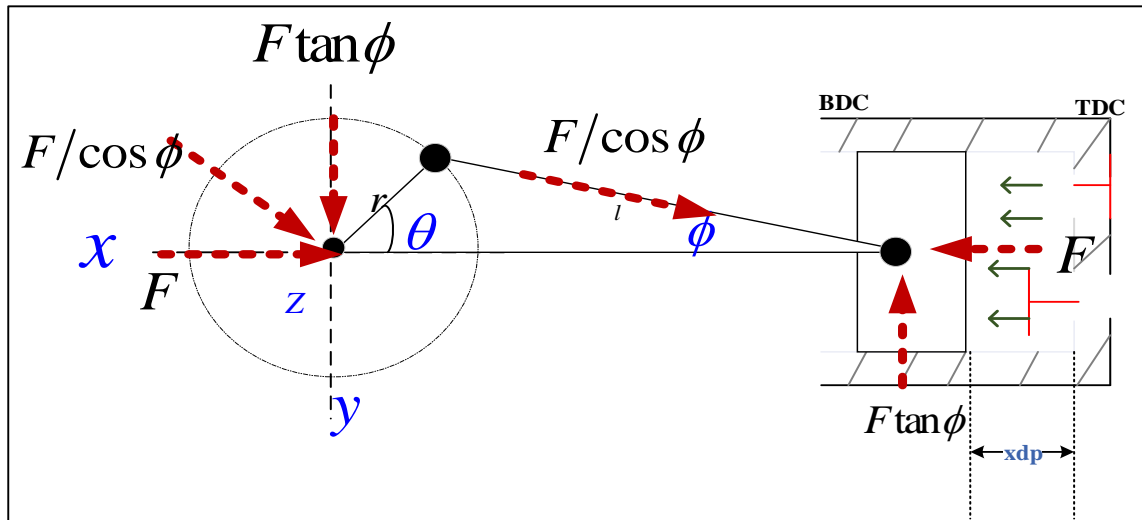


FIGURE 5.2: PISTON MECHANISM OF A RECIPROCATING COMPRESSOR WITH ACTING FORCES

Substituting Equation. (5.6) into Equation. (5.2), gives

$$x_{dp} = r \left[(n+1) - \left(\sqrt{n^2 - \sin^2 \theta} + \cos \theta \right) \right] \quad (5.7)$$

Equation (5.7) is then differentiated to obtain the expressions for velocity and the acceleration of the piston in Equation (5.8 and 5.9).

$$\dot{x}_{dp} = \omega r \left[\sin \theta + \frac{\sin 2\theta}{2n} \right] \quad (5.8)$$

Assuming $\left(\frac{r^2}{l^2}\right) \sin^2\theta \ll 1$ then the expression for the acceleration may be written as:

$$\ddot{x}_{dp} = \omega^2 r \left(\cos\theta + \frac{\cos 2\theta}{n} \right) \quad (5.9)$$

The model equations given above is for a single-stage reciprocating compressor, however, this experimental study is based on a two-stage single acting reciprocating compressor and the mathematical model for this is given as:

$$x_{dpL} = r(1 - \cos\theta) + \left(\frac{l}{r} - \sqrt{\frac{l^2}{r^2} - \sin^2\theta} \right) \quad (5.10)$$

$$x_{dpH} = r \left(1 - \cos\left(\theta + \frac{\pi}{2}\right) \right) + \left(\frac{l}{r} - \sqrt{\frac{l^2}{r^2} - \sin^2\left(\theta + \frac{\pi}{2}\right)} \right) \quad (5.11)$$

Where;

x_{dpL} is the piston displacement for the first cylinder (stage) and x_{dpH} represents piston displacement for the second cylinder (stage).

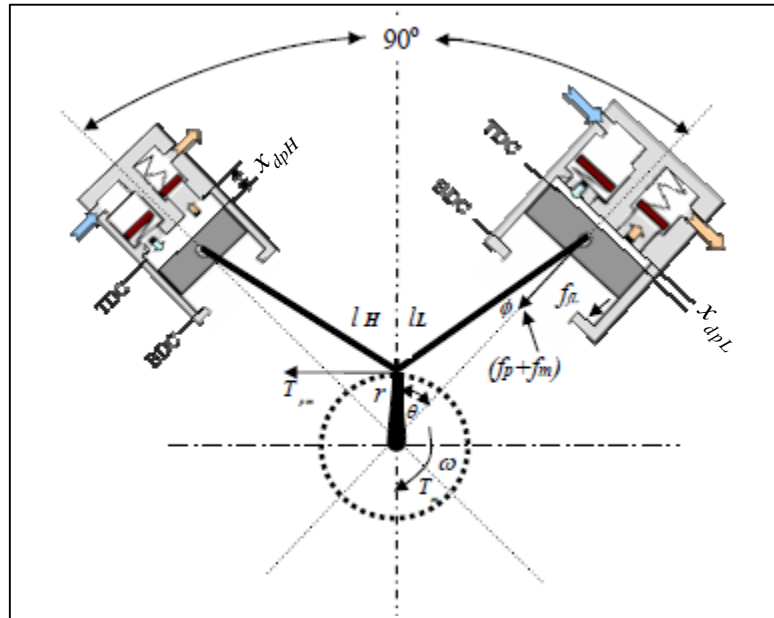


FIGURE 5.3: SIMPLIFIED MODEL OF THE V-SHAPED DOUBLE-STAGE RECIPROCATING COMPRESSOR (ELHAJ M. A., 2005)

The velocity $\dot{x}_{dpL,H}$ and acceleration $\ddot{x}_{dpL,H}$ of the first and second stage pressure cylinders are given after differentiation as: -

$$\dot{x}_{dpL} = \omega r \left[\sin\theta + \frac{\sin 2\theta}{2n} \right] \quad (5.12)$$

$$\dot{x}_{dpH} = \omega r \left[\sin\left(\theta + \frac{\pi}{2}\right) + \frac{\sin 2\left(\theta + \frac{\pi}{2}\right)}{2n} \right] \quad (5.13)$$

$$\ddot{x}_{dpL} = \omega^2 r \left(\cos\theta + \frac{r}{l} \cos 2\theta \right) \quad (5.14)$$

$$\ddot{x}_{dpH} = \omega^2 r \left(\cos\left(\theta + \frac{\pi}{2}\right) + \frac{r}{l} \cos 2\left(\theta + \frac{\pi}{2}\right) \right) \quad (5.15)$$

The configuration of the Broom Wade TS-9 compressor is such that, the displacement of the piston in the second stage leads the displacement of the first stage by $\pi/2$. Which is why $\pi/2$ is added in all the equations concerning second stage pressure cylinder.

The systems of equations given above allows for the evaluation of the piston displacement, crank angle acceleration, angular velocity and crank angle position. The cylinder volume is then calculated based on the crank angle position and the piston displacement.

5.4 Cylinder Volume

The volume of a cylinder is the area of one side of the cylinder multiplied by its height. This is expressed mathematically by the equation below:

$$V_{cyl} = \pi r^2 h \quad (5.16)$$

Where r is the radius and h is the height of the cylinder.

The volume of the first and second cylinders is determined using the equation below:

$$v_{cL,H}(t) = V_{coL,H} + s_{pL,H} \dot{x}_{dpL,H} \quad (5.17)$$

Where;

$v_{coL,H}$ is the clearance volume for both first and second stage respectively in m^3 , $s_{pL,H} = \frac{\pi}{4} D_{L,H}^2$ is the cross sectional area of the piston in $[m^2]$, $\dot{x}_{dpL,H}$ is the piston displacement in $[m]$, and $D_{L,H}$ is the piston diameter for first and second stages also in $[m]$ (Jiangming & Weirong, 2012); (Elhaj M. A., 2005).

Substituting the equation for displacement given in equation 5.10 and 5.11, the total volume of the cylinder for first and second stage becomes:

$$v_{cL}(t) = v_{coL} + s_{pL} r (1 - \cos\theta) + \left(\frac{l}{r} - \sqrt{\frac{l^2}{r^2} - \sin^2\theta} \right) \quad (5.18)$$

$$v_{cH}(t) = v_{coH} + s_{pH} r \left(1 - \cos\left(\theta + \frac{\pi}{2}\right) \right) + \left(\frac{l}{r} - \sqrt{\frac{l^2}{r^2} - \sin^2\left(\theta + \frac{\pi}{2}\right)} \right) \quad (5.19)$$

5.5 Equation of Motion

According to the model given above, the equation of crank motion is derived from Newton's second law as:

$$J \ddot{\theta} = T_m - T_{pmL,H} - T_{fL,H} \quad (5.20)$$

The crankshaft angle θ is a function of time t , J is the equivalent inertial moment of the compressor system. T_m is the driving torque from the electric motor and would be described further shortly; $T_{pmL,H}$ is the resultant torque due to air pressure inside the cylinder and the unbalanced inertial force of the piston and the connecting rod of both first and second stage (Elhaj M. A., 2005). $T_{fL,H}$ is the friction torque of the two pressure cylinders.

5.5.1 Calculating the Torques

Torque is a force applied to the shaft of a compressor system causing it to rotate about the axis of the arm length. The torque is mathematically defined as the cross product of the force vector F and the position vector r (Danielson, 2003).

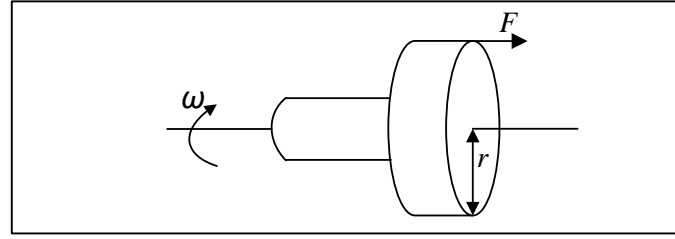


FIGURE 5.4: TORQUE APPLIED TO A SHAFT

The torque generated by the gas pressure in both cylinders is a result of the vertical unbalanced inertial force on the two-stage compressor and the driving load torque of the power unit device. The driving torque from the torque, which is used to calculate the equation of motion, is given as:

$$T_m = \frac{P_w}{\omega_s} B_r \quad (5.21)$$

Where P_w is the motor power in watts, B_r is the transmission ratio = 3, and ω_s is the motor speed in rad/sec. The resultant torque due to air pressure inside the cylinder $T_{pm_{L,H}}(t)$ is expressed as the effective radius of the crankshaft Re_L & Re_H for first and second stage respectively, multiplied by the force produced by the air pressure in both cylinders f_{pL} and f_{pH} , plus inertial force of the reciprocating mass f_{mL} and f_{mH} . This expression is presented in equation (5.22) below (Elhaj M. A., 2005):

$$T_{pm_{L,H}} = (f_{pL,H} + f_{mL,H}) Re_{L,H} \quad (5.22)$$

$$\begin{aligned} Re_L &= r \frac{\sin(\theta + \phi)}{\cos\phi} \\ &= r \frac{\sin\theta \cos\phi + \cos\theta \sin\phi}{\cos\phi} \\ &= r \sin\theta + r \frac{\cos\theta \sin\phi}{\cos\phi} \end{aligned} \quad (5.23)$$

$$\sin\phi = \frac{r \sin\theta}{l} \quad (5.24)$$

Therefore, substituting $\sin\phi$ into equation (5.23) gives:

$$Re_L = r \sin\theta + \frac{r^2}{l} \frac{\cos\theta \sin\theta}{\cos\phi} \quad (5.25)$$

$$Re_L = r \sin\theta + \frac{r^2}{2l} \sin 2\theta / \sqrt{1 - \frac{r^2}{l^2} \sin^2(\theta)} \quad (5.26)$$

The effective crankshaft radius for the second stage pressure cylinder is given as:

$$Re_H = r \sin\left(\theta + \frac{\pi}{2}\right) + \frac{r^2}{2l} \sin 2\left(\theta + \frac{\pi}{2}\right) / \sqrt{1 - \frac{r^2}{l^2} \sin^2\left(\theta + \frac{\pi}{2}\right)} \quad (5.27)$$

Also, the forces produced by the air pressure in both cylinders can be expressed as equation (5.28)

$$f_{pL,H} = p_{cL,H} s_{cL,H} \quad (5.28)$$

Where $s_{cL,H} = 0.25\pi d_{L,H}^2$ is the cross-sectional area for the first and second stage cylinders and $d_{L,H}$ is the bore diameter for both cylinders. Then finally, the force produced by the vertical inertial force for both cylinders becomes:

$$f_{mL,H} = -m_{recL,H} x_{dpL,H} \quad (5.29)$$

The reciprocating inertial mass of both stages m_{recL} and m_{recH} are calculated from the equation below:

$$m_{recL,H} = m_{pL,H} + 0.5m_{crL,H} \quad (5.30)$$

Where m_{pL} and m_{pH} are the piston mass of both first and second stage cylinders; m_{crL} and m_{crH} are the connecting rod mass for both cylinders.

5.6 Cylinder Pressure Models

Filtered gas (in this case air), enters the first stage (low) cylinder through the suction port and into the suction chamber as seen in the complete model description in Figure 5.1. As the piston moves back up to TDC, it starts to compress the collected air until the pressure of the air is greater than the intercooler pressure just outside the discharge valve causing the air to discharge into the intercooler pipe/coil. As the air passes through the intercooler, heat is lost. The cooled air enters the second stage (high) cylinder and the process is repeated for the second stage cylinder, but the compressed air is discharged at a higher pressure into the air receiver tank.

The first law of thermodynamics is used to derive the equation of instantaneous cylinder pressure in both cylinders as.

$$\dot{P}_{cL,H} = \frac{1}{V_{cL,H}} \left[c_{iL,H}^2 \dot{m}_{viL,H} - c_{dL,H}^2 \dot{m}_{vdL,H} - \gamma P_{cL,H} \dot{V}_{cL,H} \right] \quad (5.31)$$

Where;

$\dot{m}_{viL,H}$ and $\dot{m}_{vdL,H}$ are the inlet and discharge flow through the valves respectively, the specific heat ratio for air γ is 1.4, $c_{iL,H} = \sqrt{(\gamma R T_{iL,H})}$ is the speed of sound in the inlet plenum, and $c_{dL,H} = \sqrt{(\gamma R T_{dL,H})}$ is the speed of sound in the cylinder, R is the gas constant at $287 \text{ m}^2 \text{ s}^{-2} \text{ K}^{-1}$ for air. The absolute temperature of the gas in the cylinder is calculated using the following equation:

$$T_{cL,H} = T_{iL,H} \left(\frac{P_{cL,H}}{P_{iL,H}} \right)^{\frac{\gamma-1}{\gamma}} \quad (5.32)$$

$p_{cL,H}$ and $p_{iL,H}$ represents the internal cylinder pressure and the inlet pressure respectively, and $T_{iL,H}$ is the average absolute temperature of the inlet air (atmospheric temperature°C + 273K).

5.7 Mass Flow Models

Mass flow through the suction and discharge valves are represented by $\dot{m}_{viL,H}$ and $\dot{m}_{vdL,H}$ respectively. In order to avoid any confusions, the mass flow models are presented in two parts. First, the expression for suction mass flow model would be given in subsection 5.7.1, then the discharge mass flow model in subsection 5.7.2.

5.7.1 Suction Mass Flow Model

The mass flow rate ($\dot{m}_{viL,H}$) of air through the suction valve is mathematically expressed as:

$$\dot{m}_{viL,H} = \beta_{iL,H} c_{diL,H} (\chi) \cdot A_{fiL,H} \sqrt{\frac{2\rho_{cL,H}}{P_{iL,H}^e - P_{cL,H}}} \quad (5.33)$$

Where;

$\beta_{iL,H} = \text{sign}(P_{iL,H}^e - P_{cL,H})$, the sign would be +1 for normal flow and -1 for backflow, $P_{iL,H}^e$ is the pressure in the inlet plenum, $P_{cL,H}$ is the cylinder pressure while,

$$c_{diL,H}(\chi) = 0.42 \frac{\chi_{L,H}}{\chi_{\max L,H}} \quad .$$

$A_{fiL,H} = 2\pi r_{L,H} \cdot d_{iff}$ is the flow area around the valve plate and d_{iff} is the distance between the outer edge of the valve plate and the inner wall of the valve chamber. $\rho_{cL,H}$ is the density of air in both first and second stage cylinders for mass flow through the suction valve.

$$\rho_{iH} = \rho_{dL} \left(\frac{P_{iH}}{P_{dL}} \right)^{\frac{1}{\gamma}} \quad (5.34)$$

Where $\rho_{iL,H}$ is the density of air at intake of the two cylinders, ρ_{dL} is the density of air at discharge of first stage, and the air density $\rho_i = 1.177 \text{kg/m}^3$.

5.7.2 Discharge Mass Flow Model

The mass flow rate ($\dot{m}_{vdL,H}$) of air out of the discharge valve is mathematically expressed as:

$$\dot{m}_{vdL,H} = \beta_{dL,H} c_{ddL,H}(\chi) \cdot A_{fdL,H} \sqrt{\frac{2\rho_{cL,H}}{P_{cL,H} - P_{dL,H}^e}} \quad (5.35)$$

$c_{ddL,H}(\chi)$ is a variable discharge coefficient mathematically expressed as follows:

$$c_{ddL,H}(\chi) = 0.35 \frac{\chi_{dpL,H}}{\chi_{\max L,H}} \quad (5.36)$$

$\chi_{\max L,H}$ is the maximum valve plate displacement. The discharge valve for the first and second stage have the same maximum displacement and the two suction valves have the same displacement. $A_{fdL,H}$ is the maximum flow area of discharge valve. The flow coefficients are adopted from (Price & Botros, 1992), who took measurements on similar valves. To allow for the probability of backflow, the absolute value of the pressure differential across the valve is taken. The pressure in the discharge plenum is $P_{dL,H}^e$.

$\beta_{dL,H} = \text{sign}(P_{cL,H} - P_{dL,H}^e)$ is +1 for normal flow and -1 for backflow,

$$\rho_{cL,H} = \rho_{iL,H} \left(\frac{P_{cL,H}}{P_{iL,H}} \right)^{\frac{1}{\gamma}} \quad (5.37)$$

Here $\rho_{cL,H}$ is the density of air in the cylinders and $\rho_{iL,H}$ is the density of air in the plenum.

$$\rho_{dL,H} = \rho_{iL,H} \left(\frac{P_{dL,H}}{P_{iL,H}} \right)^{\frac{1}{\gamma}} \quad (5.38)$$

In Equation (5.38), $\rho_{dL,H}$ is the density of air in the discharge valves while $\rho_{iL,H}$ is the density of air in the suction valves.

5.8 Valve Dynamics

This section covers the equations for the dynamic behaviour of the suction and discharge valves of the Broom Wade TS9 reciprocating compressor used for this experimental study. Each valve is made up of a valve plate, spring and a pneumatic chamber. Figure (5.5) shows the motion of the valve plate as a single-degree-of-freedom, and is therefore modelled in this section as a simple mass, spring and damper system.

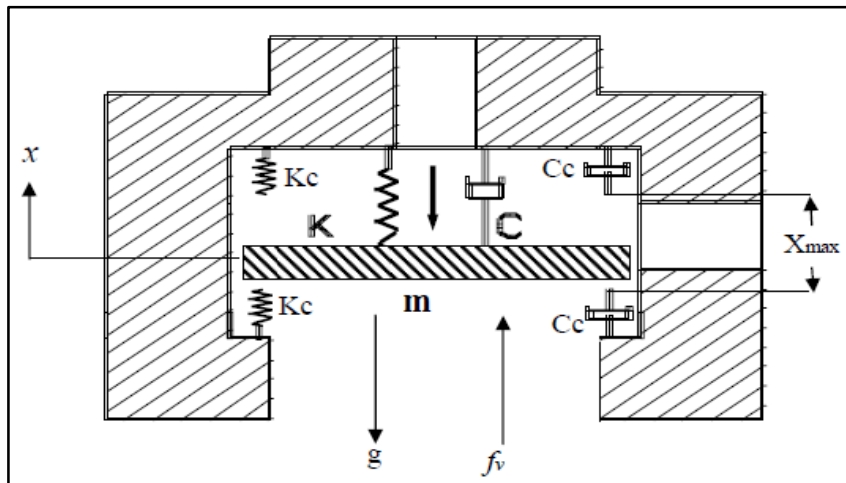


FIGURE 5.5: SINGLE DEGREE OF MOTION OF A RECIPROCATING COMPRESSOR VALVE (ELHAJ M. A., 2005)

The suction and discharge mass flow rates are functions of the distance between valve plate and seating (valve lift). Forces acting on the valve plate causes it to move up and down. These forces result from three contributing factors: The spring, the pressure difference across the valve, and resistance forces in the initial stages of valve opening. Due to the numerous equations for both suction and discharge valve motion equation, this section would be sectioned

in two; one to describe the equations and expressions for suction valve motion and the second for discharge valve motion to prevent any confusions.

5.8.1 Suction Valve Motion

The equation of motion of the suction valve is based on Newton's second law:

$$m_{vsL,H} \ddot{x}_{vsL,H} + c_{sL,H} \dot{x}_{vsL,H} + k_{vsL,H} x_{vsL,H} = \sum f_{vsL,H} \quad (5.39)$$

The equation of motion for suction valve changes slightly when the valve plate is in contact with the valve seats causing the valve to be completely open or closed. This is represented in equation (5.40) below as:

$$m_{vsL,H} \ddot{x}_{vsL,H} + c_{csL,H} \dot{x}_{vsL,H} + k_{csL,H} x_{vsL,H} = \sum f_{vsL,H} \quad (5.40)$$

Where;

- $m_{vsL,H}$ = valve plate mass (see equation 5.39),
- $c_{sL,H}$ = damping coefficient,
- $c_{csL,H}$ = damping coefficient when valve is fully open/closed,
- $k_{vsL,H}$ = non-linear spring stiffness,
- $k_{csL,H}$ = contact stiffness when valve is fully open/closed,

The valve acceleration, velocity and displacement are denoted as $\ddot{\chi}_{vsl,h}$, $\dot{\chi}_{vsl,h}$ and $\chi_{vsl,H}$ respectively; $\sum f_{vsl,H}$ is sum of all the forces acting on the valve plate. For simplicity, the subscripts L, H representing first, and second stages would be omitted from this point on ward. However, the equations that would be described are applicable to both stages.

$$m_{vs,d} = m_{plate} + \frac{1}{3} m_{spring} \quad (5.41)$$

$$c_{s,d} = 2\xi \sqrt{k_{v(s,d)} m_{v(s,d)}} \quad (5.42)$$

Where ξ is the damping ratio of the valve unit, and is calculated as follows:

$$\frac{\omega_v}{\omega_n} = \sqrt{1 - 2\xi^2} \quad (5.43)$$

$$\omega_n = \sqrt{\frac{k_{v(s,d)}}{m_{v(s,d)}}} \quad (5.44)$$

Here, ω_v is the valve unit frequency and ω_n is the natural frequency of the valve unit. The total forces acting on the valve plate is given by the following equation:

$$\sum f_{vsL,H} = fvs + fgs - fso \quad (5.45)$$

Bearing in mind, this equation covers both first and second pressure cylinders.

The weight of the suction valve plate for both cylinders is $fgs = (-mg)$, fso is the pre-set spring, and $fvs = cfs \cdot Sv (pi - pc)$.

Where,

cfs = force coefficient

Sv = slot area for a single channel

pi = pressure in the suction plenum for both cylinders

pc = the cylinder pressure

5.8.2 Discharge Valve Motion

The equations given and described for suction valve motion equation is the same for discharge valve motion. For this reason, the motion equation for the discharge valve would not be fully described. For full mathematical expressions and explanation, see suction valve motion section 5.8.1.

$$m_{vdL,H} \ddot{x}_{vdL,H} + c_{dL,H} \dot{x}_{vdL,H} + k_{vdL,H} x_{vdL,H} = \sum f_{vdL,H} \quad (5.46)$$

When the valve plate is completely open and closed, the equation of motion becomes:

$$m_{vdL,H} \ddot{x}_{vdL,H} + c_{dL,H} \dot{x}_{vdL,H} + k_{cdL,H} x_{vdL,H} = \sum f_{vdL,H} \quad (5.47)$$

5.9 Discharge Plenum Pressure

In this study, the discharge plenum pressure for only the second-stage cylinder is simulated and experimentally investigated. The discharge plenum is made up of two cavities as seen in Figure 5.6. The pressure in these cavities are given as:

$$\dot{p}_{cv1} = \frac{1}{v_{cv1}} \left[cc_{2H}^2 \dot{m}_{vdH} - cc_{cv1}^2 \dot{m}_{cv1} - \gamma p_{cv1} \left(\dot{x}_{vdH} (\pi cv1 r^2) \right) \right] \quad (5.48)$$

$$\dot{p}_{cv2} = \left(\frac{1}{v_{cv2}} - (A_{cv2} \dot{x}_{vdH}) \right) \left[cc_{1d}^2 \dot{m}_{cv1} + (A_{cv2} \dot{x}_{vdH}) - c_p \dot{m}_p \right] \quad (5.49)$$

Where,

$v_{cv1,2H}$ is the volume of cavity one and two chambers;

\dot{m}_{cv1} is the mass flow rate of cavity one;

A_{cv2} is the cross-sectional area of cavity two chamber;

$cc_{cv1,2}^2$ is the speed of sound in cavity one and two chambers;

$p_{cv1,2}$ is the initial pressure in cavity one and two;

$cv1r$ is the radius of cavity one;

c_p is the speed of sound in the pipeline;

\dot{m}_p is the mass flow in the pipeline.

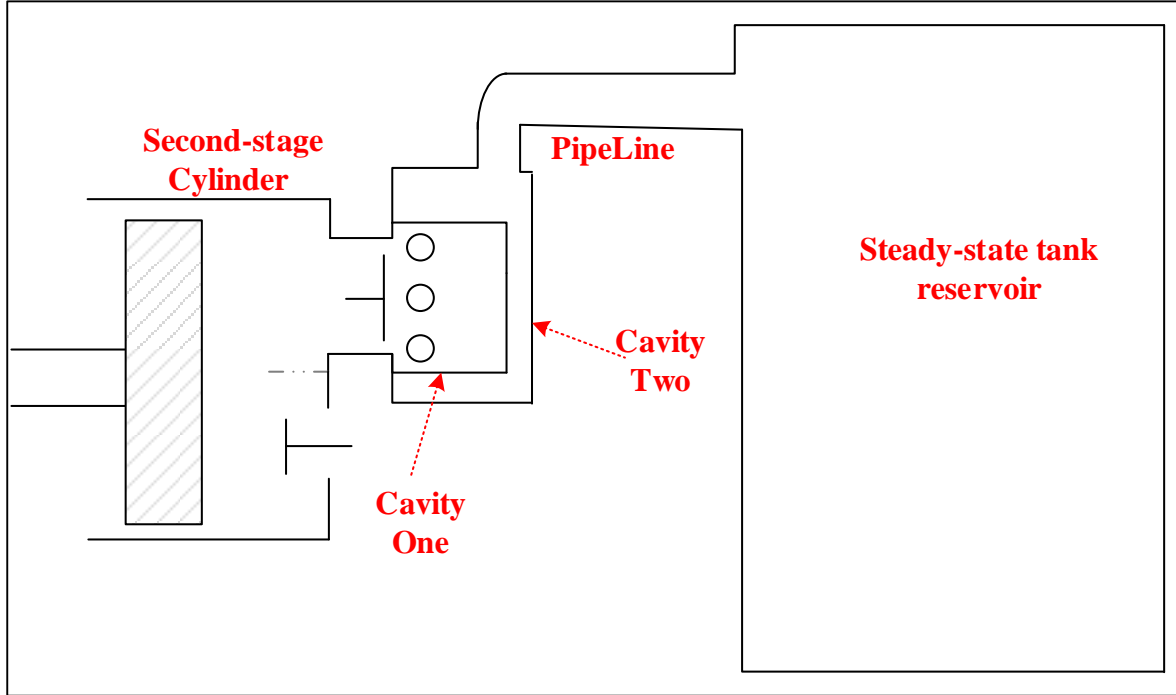


FIGURE 5.6: DISCHARGE PLENUM AND PIPING SYSTEM

5.10 Fault Simulation

Second-stage discharge valve leakage and intercooler leakage are the two main faults simulated in this study. The simulation if accurately done should predict the signatures for the above faults when examined experimentally.

5.10.1 Second Stage Discharge Valve Leakage

Leaking discharge valves are modelled as an added flow through an orifice in-line with the usual valve flow. The mass flow rate of the discharge leakage is $\dot{m}_{viL,H} > 0$ when the discharge plenum pressure (P_{dH}^e) is greater than the cylinder pressure (P_{cH}), That is during expansion, suction, and compression. Equation 5.50 was used to determine the mass flow rate for gas flow through the discharge valve orifice.

$$\dot{m}_{vdH} = \beta_{dH} c_{dH}(\chi) \cdot A_{lk} \sqrt{\frac{2\rho_{dH}}{P_{dH}^e - P_{cH}}} \quad (5.50)$$

Where; A_{lk} is the size of leakage on the discharge valve and $c_{dH}(\chi)$ is a variable discharge coefficient. P_{dH}^e is the pressure in the discharge plenum and $\beta_{iL,H} = \text{sign}(P_{iL,H}^e - P_{cL,H})$.

5.10.2 Intercooler leakage

For there to be a small leakage in the intercooler of the two-stage reciprocating compressor Equation 5.51 is used.

$$\dot{p}_{ic} = \frac{1}{V_{ic}} \left[c_{iL}^2 \dot{m}_{vdL} - c_{iH}^2 \dot{m}_{viH} - c_{ic}^2 \dot{m}_{ic} \right] \quad (5.51)$$

The faulted intercooler mass flow rate is given by Equation 5.52 below.

$$\dot{m}_{ic} = \beta_{ic} c_{ic}(\gamma) A_{ic} \sqrt{\frac{2\rho_{ic}}{P_{ic} - P_0}} \quad (5.52)$$

Where;

$A_{ic} = 2\pi r_{L,H} \chi$ is the leakage flow area allowing gas to escape from the intercooler,

γ is the specific heats of the process gas of sound in the 1.4 for air and $\beta_{ic} = \text{sign}(P_{ic} - P_0)$.

CHAPTER SIX

6 MODEL VALIDATION

This chapter verifies the accuracy of the models developed in chapter five using several parameters including in-cylinder pressure, valve motion, and discharge chamber pressure of a healthy two-stage reciprocating compressor. The mathematical equations are solved numerically in MATLAB programming environment and the predicted results are compared with the corresponding results from the experimental measurements. More so, the prediction trends of the two fault simulations, second-stage discharge valve leakage and intercooler leakage are also compared with corresponding experimental fault measurements. The prediction and measurement trends show good agreement, which means the model and fault simulations are accurate and can be used for further simulation studies.

6.1 Introduction

The fundamental purpose of condition monitoring of the reciprocating compressor is to determine the current and future working condition of a machine while in operation. In order to fulfil this purpose, vibration analysis is employed to obtain vital information about the internal condition of the compressor for fault detection. Vibration analysis is frequently used for condition monitoring of machines including reciprocating compressors because changes to the system can be detected immediately and it can indicate the actual cause of fault from signals with great noise.

Chapter Five presents the developed mathematical model of the two-stage reciprocating compressor to predict healthy and common fault signatures. The model is validated by comparing predicted results from the model with measured experimental results for all test cases starting with the compressor working under normal condition (Baseline), then comparing the two faults cases: second stage discharge valve leakage, and intercooler leakage. The comparative analysis is done for in-cylinder pressure, vibration signals, and the new developed discharge chamber pressure from the second-stage cylinder.

6.2 Model Analysis

6.2.1 Physical Parameters and Constants

The physical parameters used to model the dynamics of the reciprocating compressor are obtained mostly from the manufacturer or were measured in the laboratory. Table 6.1 presents the parameters used.

TABLE 6.1: PHYSICAL PARAMETERS OF THE TWO-STAGE RECIPROCATING COMPRESSOR (BROOM WADE, 1964; COMP AIR UK LTD, 2002)

Broom Wade TS9 Two-Stage Reciprocating Compressor System		
Components	Low Pressure Cylinder	High Pressure Cylinder
Piston mass (kg)	1.78	0.89
Piston head diameter (mm)	93.6	55.6
Cylinder bore (mm)	101.6	63.5

CHARACTERISING VIBRO-ACOUSTIC SIGNALS OF A RECIPROCATING
COMPRESSOR FOR CONDITION MONITORING

Suction pressure (kPa/psi)	100/14.7	220/32.2
Discharge pressure (kPa/psi)	270/39.7	816/120
Suction temperature (°C)	21	41
Discharge temperature (°C)	50	80
Mass of valve plate (g)	2.3	2.1
Mass of valve spring	1.0	2.0
Outer radius valve plate	21.0	14.0
Inner radius valve plate	12.5	10.5
Number of cylinders	2 (90° opposed)	
Compressor speed (rpm)	425	
Motor speed (rpm)	1450	
Motor power (KW)	2.2	
Flywheel ratio %	3	
Tank capacity (litres)	272	
Piston stroke (mm)	76.2	
Connection rod length (mm)	171.6	
Crank radius (mm)	38.1	
Maximum suction valve lift (mm)	1.5	
Maximum discharge valve lift (mm)	1.5	

6.3 Healthy Simulation Results

6.3.1 In-Cylinder Pressure Signal

Figure 6.1 shows the predicted in-cylinder pressure readings from the model at different tank pressures 0.138MPa, 0.276MPa, 0.552MPa, and 0.837MPa (20, 40, 80, and 120 Psi respectively) for first stage and second stage.

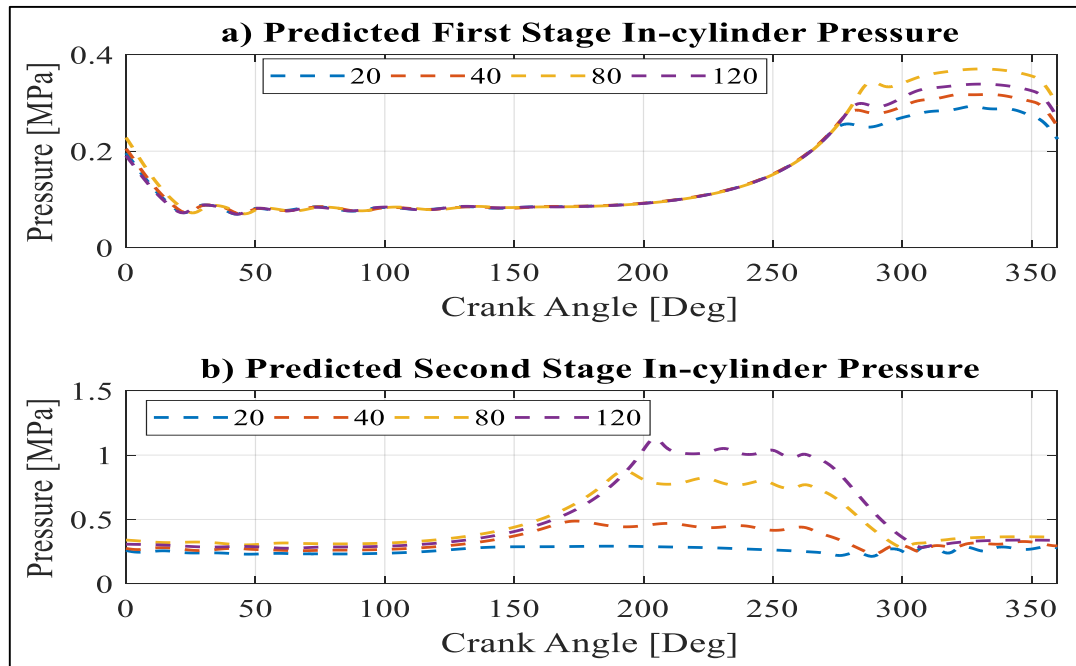


FIGURE 6.1: PREDICTED HEALTHY PRESSURE SIGNALS AT DIFFERENT TANK PRESSURES: A) FIRST STAGE B) SECOND STAGE

From Figure 6.1 above, the in-cylinder pressure increases as the load increases for both first stage and second stage. This is in accordance with the findings of experimentally measured healthy in-cylinder pressure signals for the same tank pressure levels in Figure 6.2 below.

A comparative representation of the predicted and measured healthy in-cylinder pressure waveforms of first and second stage tank pressure at 0.827 MPa (120 Psi) is given in Figure 6.3 for validation purposes. It can be seen that the degree of discrepancy between the predicted and measured results are minimal in both stages. The minor discrepancies can be attributed to the age of the compressor and inability to contact the (terminated) manufacturing company for verification of some of the compressor parameters used for modelling.

The close match between the predicted and measured waveforms is an indication that the model is reliable and accurately represents the compressor dynamics.

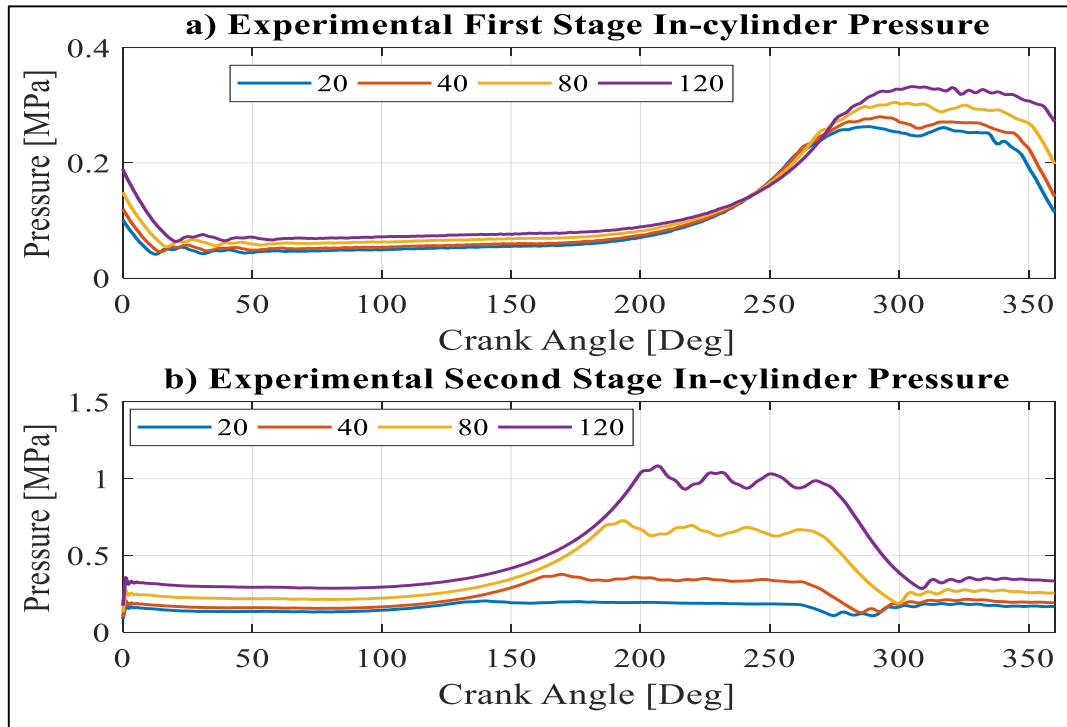


FIGURE 6.2: EXPERIMENTAL HEALTHY PRESSURE SIGNALS AT DIFFERENT TANK PRESSURES: A) FIRST STAGE B) SECOND STAGE

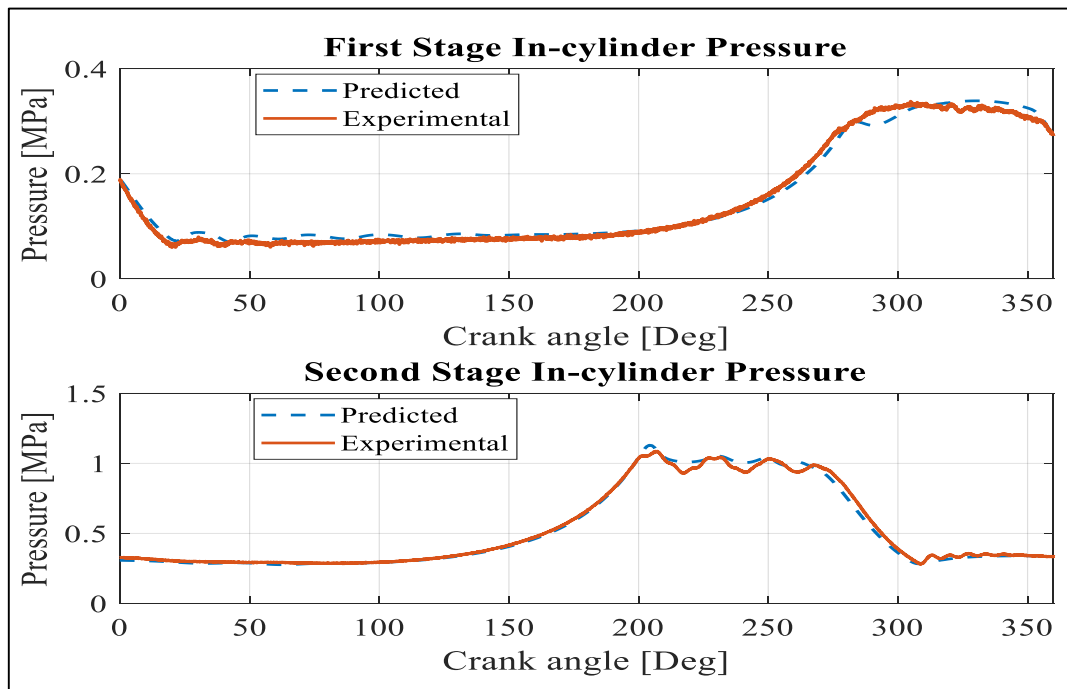


FIGURE 6.3: PREDICTED AND MEASURED IN-CYLINDER PRESSURE SIGNALS AT 0.827 MPa (120PSI) FIRST STAGE AND SECOND STAGE

6.3.2 Valve Displacement and Vibration Signals

Suction and discharge valve displacements for both cylinders have been modelled to predict the valve opening and closing times. Figures 6.4 and 6.5 shows the opening and closing times for first and second stage cylinders under healthy compressor working cycle. The opening and closing of the valves depend on the in-cylinder pressure, which is a function of piston position.

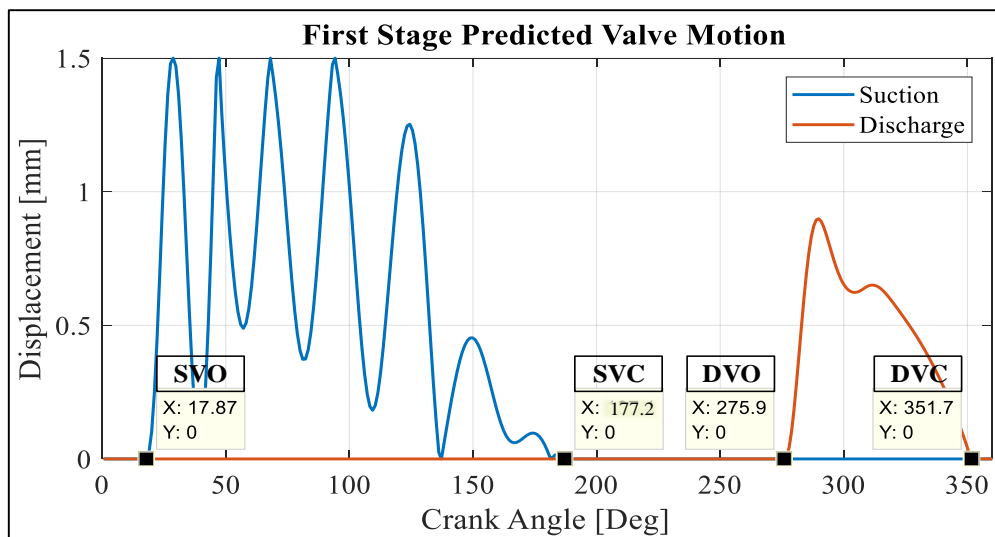


FIGURE 6.4: PREDICTED SUCTION AND DISCHARGE VALVE MOTIONS FOR FIRST STAGE CYLINDER AT 0.827 MPa (120 PSI)

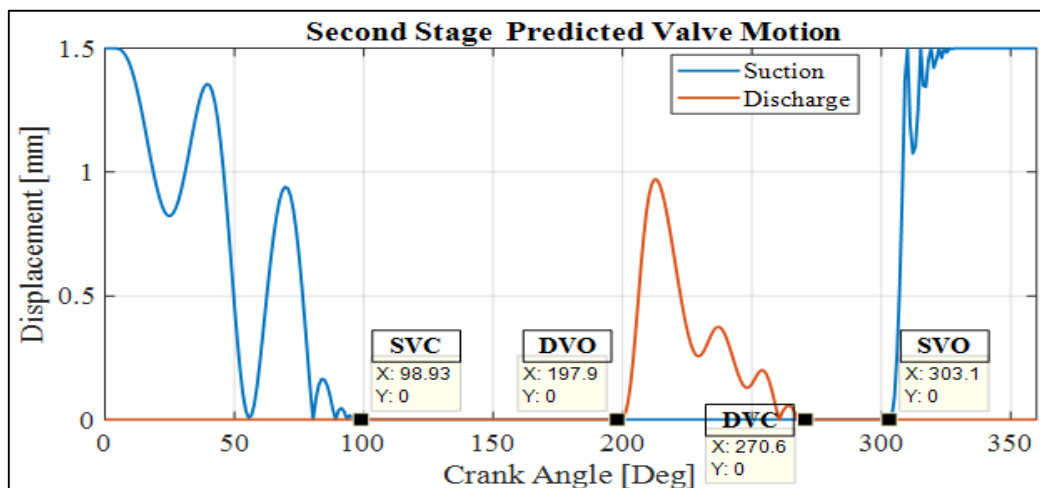


FIGURE 6.5: PREDICTED SUCTION AND DISCHARGE VALVE MOTIONS FOR SECOND STAGE CYLINDER AT 0.827 MPa (120 PSI)

Figure 6.6 presents the measured healthy vibration signals for the first and second stage cylinder heads for one compressor cycle. The vibration signals consists of noise and several transient events including valve and flow-induced impacts, which are difficult to identify without the dynamic modelling and a good understanding of the reciprocating compressor unit.

Four significant valve events including suction valve opening (SVO), suction valve closing (SVC), discharge valve opening (DVO), and discharge valve closing (DVC) have been identified in Figure 6.6 based on the opening and closing times of the predicted valve motions presented in Figures 6.4 and 6.5 for first and second stage cylinders respectively.

The valve opening and closing times predicted in this study are consistent with those from Elijahs research; a fellow scholar who used a similar compressor to reveal the valve operating times (Elhaj M. A., 2005). It can be seen that the predicted valve opening and closing times are in good agreement with the measured vibration signal from the first and second stage cylinders.

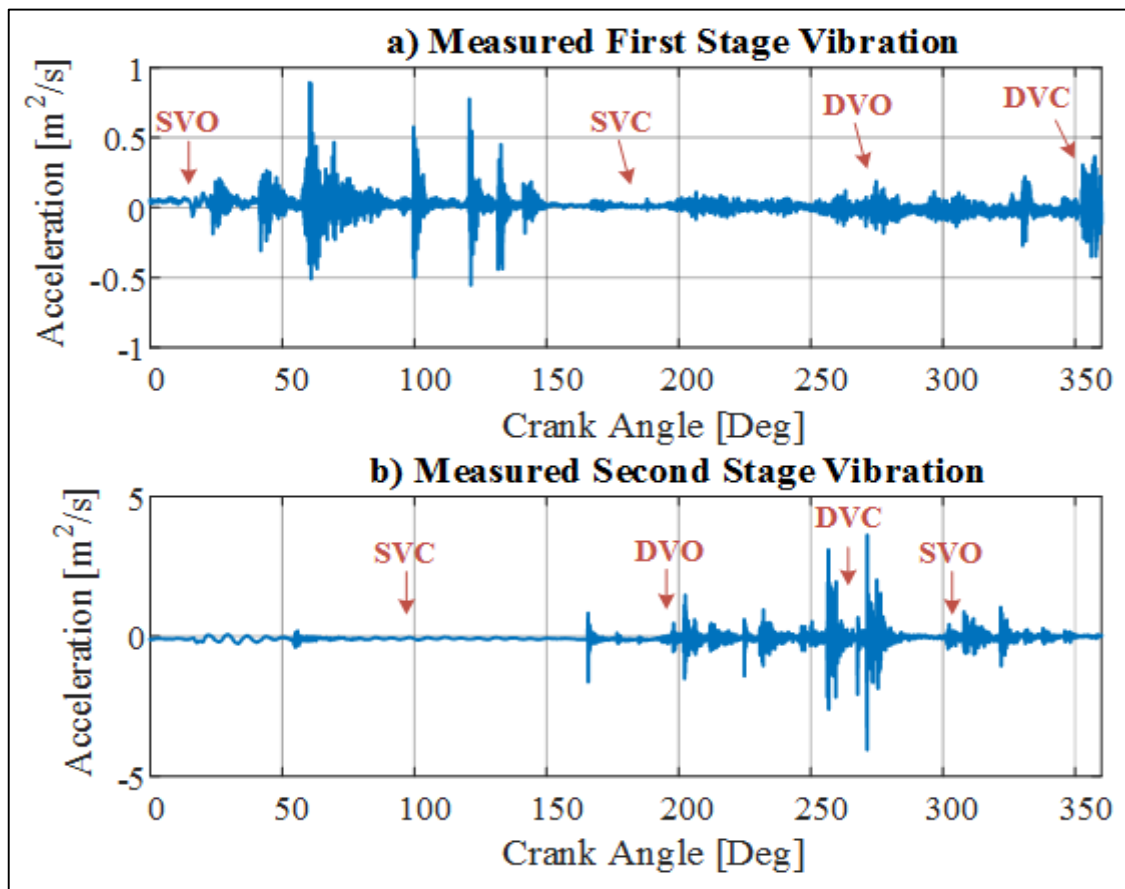


FIGURE 6.6: MEASURED VIBRATION SIGNALS AT 0.827 MPa (120PSI) FOR A) FIRST STAGE CYLINDER AND B) SECOND STAGE CYLINDER

6.3.3 Discharge Chamber Pressure

The discharge chamber pressure for the second cylinder is composed of two cavity chambers illustrated in Chapter Five (see Figure 5.6). Two equations for the discharge cavity pressures were described in the previous chapter. Figure 6.7 shows the plots of in-cylinder, cavity one and cavity two pressure predictions during discharge period at 0.827MPa. It can be seen that the two cavity waveforms accurately predicts the valve opening angle and shows the valve

flutter. Moreover, both cavity pressure predictions show the effects of delayed valve opening angle with increasing tank pressure in Figure 6.8.

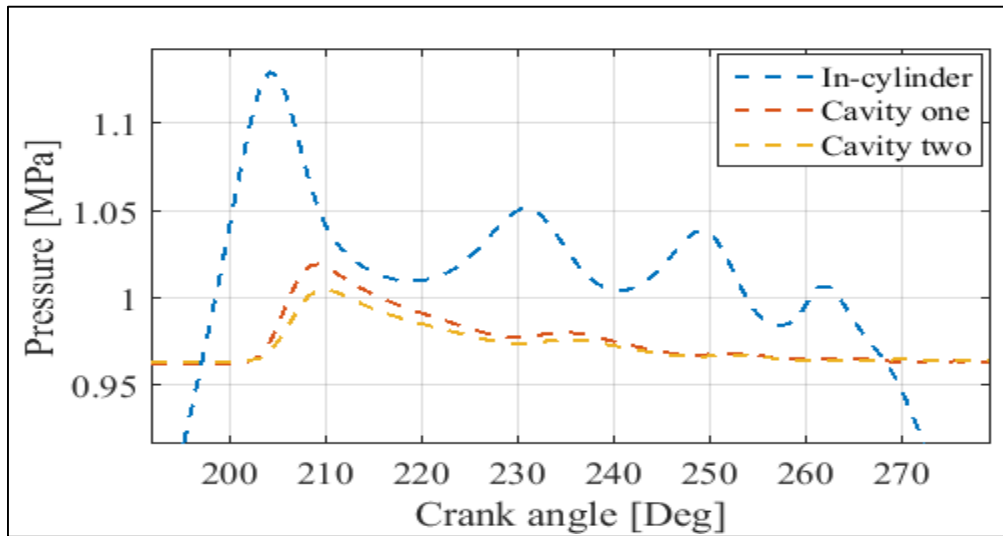


FIGURE 6.7: PREDICTED PLOT OF IN-CYLINDER, CAVITY ONE, AND CAVITY TWO PRESSURE AT DISCHARGE PERIOD

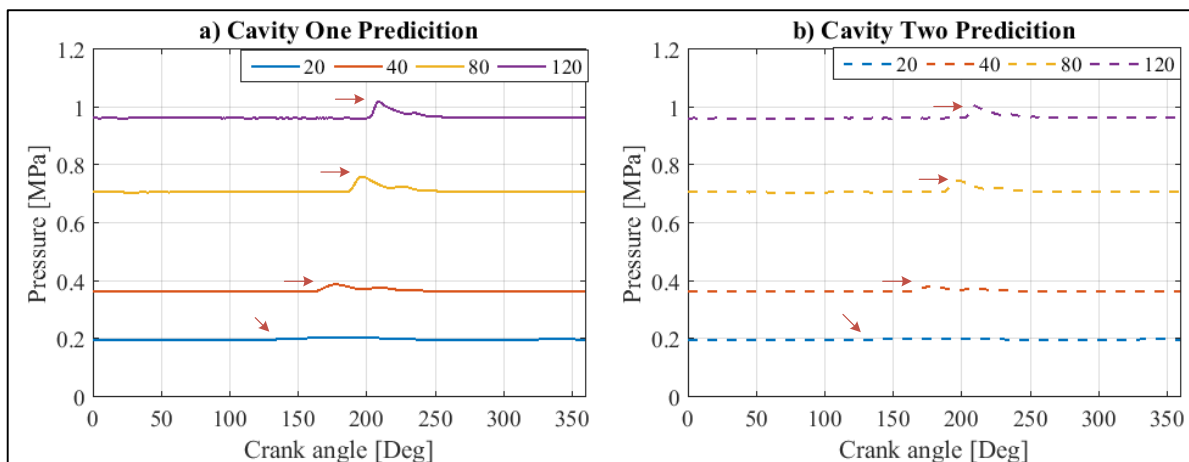


FIGURE 6.8: A) CAVITY ONE B) CAVITY TWO PRESSURE PREDICTIONS AT DIFFERENT TANK PRESSURES

6.4 Discharge Valve Fault Simulation Results

6.4.1 In-Cylinder Pressure Fault Signal

Predicted in-cylinder pressure and valve motion waveforms simulated under second-stage discharge-valve compressor fault condition is presented in this section. The discharge valve in-cylinder pressure prediction at 0.827 MPa (120psi) is compared with the experimental in-cylinder pressure waveform under the same fault condition. Figures 6.9 shows the first and

second stage results comparing the predicted in-cylinder fault signature with that of experimental, and from the plots, it can be seen that the predicted and experimental waveforms for discharge valve fault condition are in good agreement with some minor differences.

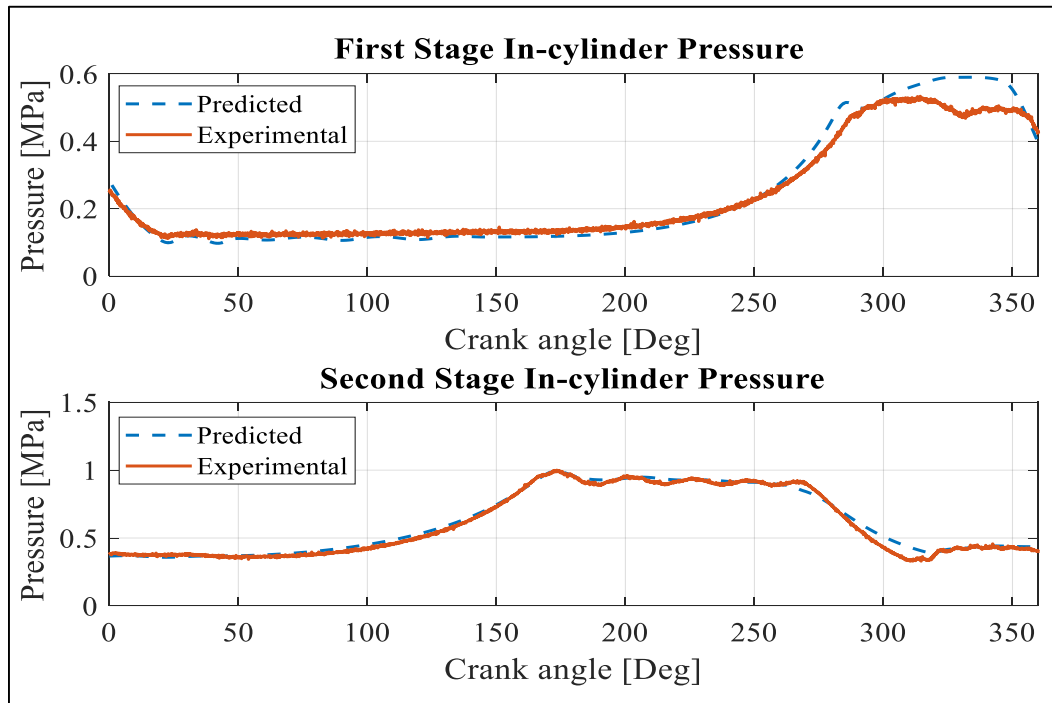


FIGURE 6.9: PREDICTED AND EXPERIMENTAL SECOND STAGE DISCHARGE VALVE FAULT WAVEFORMS FOR FIRST AND SECOND STAGE IN-CYLINDER PRESSURE AT 0.823 MPa

6.4.1.1 Baseline and Discharge Valve Leakage

The predicted waveform for the discharge valve leakage is labelled DVF-Fault and it is plotted with that of predicted healthy signal in Figure 6.10; furthermore, the same conditions (healthy and faulty) for the experimental measurement are also presented for comparison with the predicted results. The discharge valve leakage is carried out as explained in section (4.6.1)

From the subplots of Figure 6.10, it can be seen that the waveform patterns for the predicted first-stage in-cylinder pressure of healthy and faulty conditions are very similar to those from the experimental measurement.

Moreover, the waveform for the predicted second-stage in-cylinder pressure of healthy and faulty conditions are also very similar to those from the experimental measurements as seen in Figure 6.11. When there is a discharge valve leakage on the second-stage cylinder, the valve opens earlier as seen from the plot and the discharge process takes a longer time to complete. These resulting effects are due to high-pressure air from the pipeline leaking into the cylinder,

which causes an earlier pressure differential time across the valve and a longer discharge process.

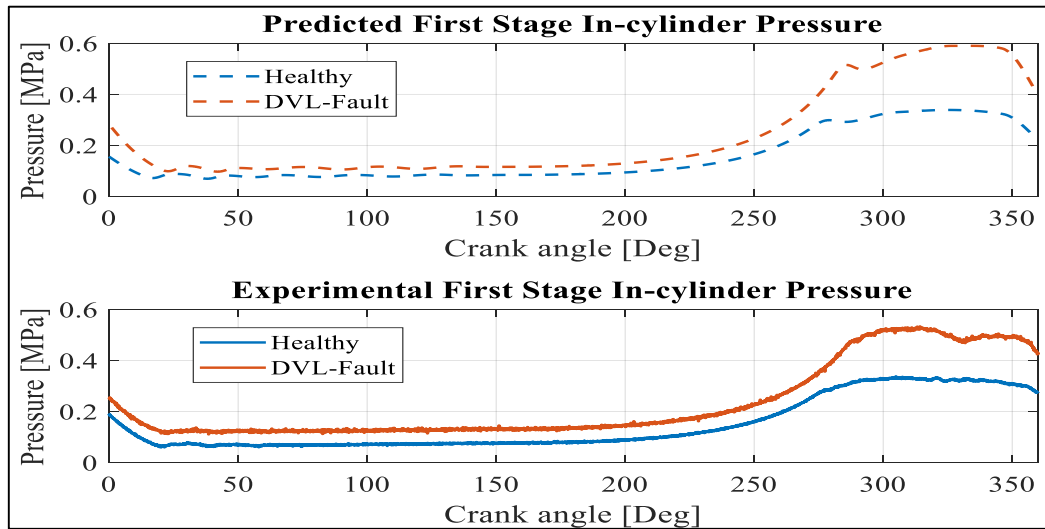


FIGURE 6.10: PREDICTED AND EXPERIMENTAL FIRST STAGE IN-CYLINDER PRESSURE WAVEFORMS FOR HEALTHY AND DVL-FAULT CONDITIONS

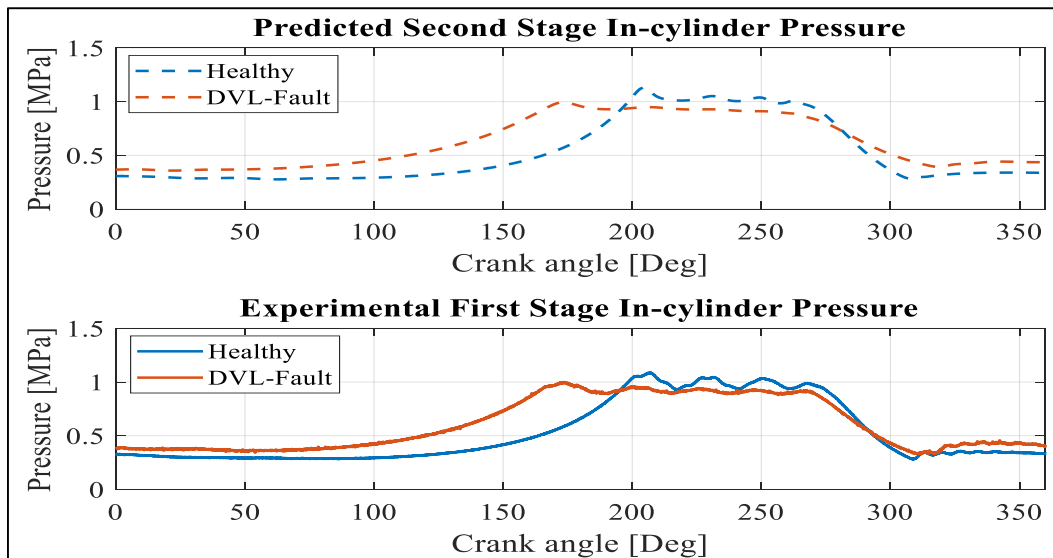


FIGURE 6.11: PREDICTED AND EXPERIMENTAL SECOND STAGE IN-CYLINDER PRESSURE WAVEFORMS FOR HEALTHY AND DVL-FAULT CONDITIONS

Therefore, because of these similar behavioural patterns between predicted results and experimental results, it can be concluded that the in-cylinder pressure from the reciprocating compressor can be used for leaking discharge valve fault detection and diagnosis.

6.4.2 Valve Displacement and Vibration Fault Signals

Figure 6.12 shows the effects of leaks on the second stage valve plate via the first stage valve displacement waveform. From the plot, it is observed that in the event of a leak, the suction and discharge valves open later than normal. This is because the leaks from the second stage delays the time at which pressure in the cylinder would be high enough to overcome the pressure in the intercooler. This effect is also seen in the predicted healthy and faulty in-cylinder traces presented in Figure 6.10.

Figure 6.13 shows the measured first stage vibration signature for healthy and discharge valve leakage conditions. There is a slight delay in the suction valve opening angle 20.72° for DVL (Faulty) vibration signature compared to healthy vibrations, which opens at 17.87° . The discharge valve for healthy vibration signal opens at 275.9° , while that of fault condition opens at 289.5° about 14° delay. Moreover, the introduction of leaks causes high levels of vibration amplitude.

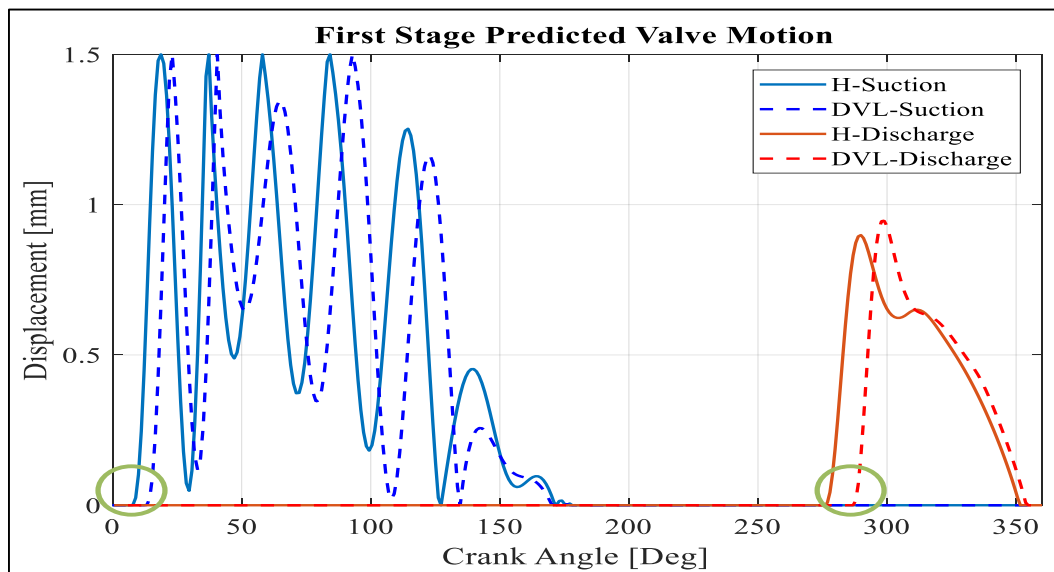


FIGURE 6.12: FIRST STAGE VALVE DISPLACEMENT COMPARISON OF HEALTHY AND VALVE LEAKAGE FAULT PREDICTIONS

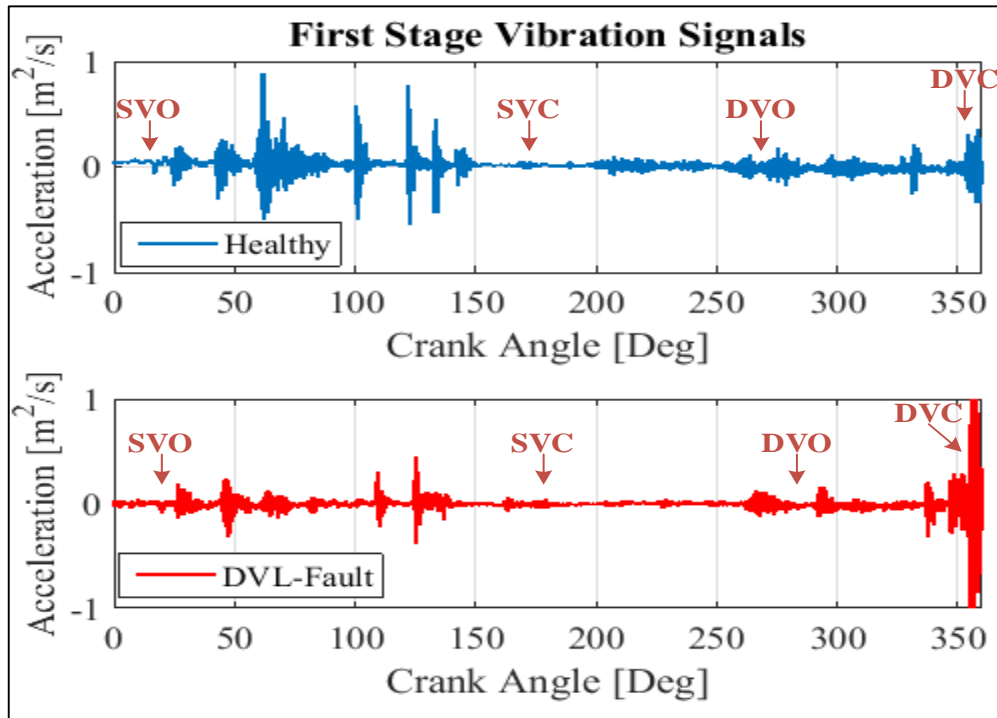


FIGURE 6.13: MEASURED FIRST STAGE VIBRATION SIGNALS FOR HEALTHY AND DISCHARGE VALVE FAULT CONDITIONS

The second stage suction and discharge valve displacements are presented in Figure 6.14 for both healthy and fault conditions. The healthy and faulty valve displacement comparison shows a significant difference in second stage suction valve closing, opening, and discharge valve opening times (crank angles). When there are leaks on the second stage discharge valve, the suction valve opens 38° earlier than normal and the valve displacement amplitude is significantly reduced. Moreover, the discharge valve for the faulty condition opens earlier (167.3°) than normal (198.9°) with a difference of 31.6° in crank angle. Furthermore, the suction valve opens later than normal when there is a discharge valve leakage on the second stage; with a delay of 17° . From Figure 6.15, it can be observed that, the introduction of leaks through the second stage discharge valve causes increased vibrations that make it difficult to determine the valve opening and closing times on the vibration signal.

From the above analysis, it can be concluded that careful analysis of the vibration signal can be used to determine the presence of discharge valve leaks on the second stage cylinder. The level of vibration increases particularly during discharge valve closing times (angles).

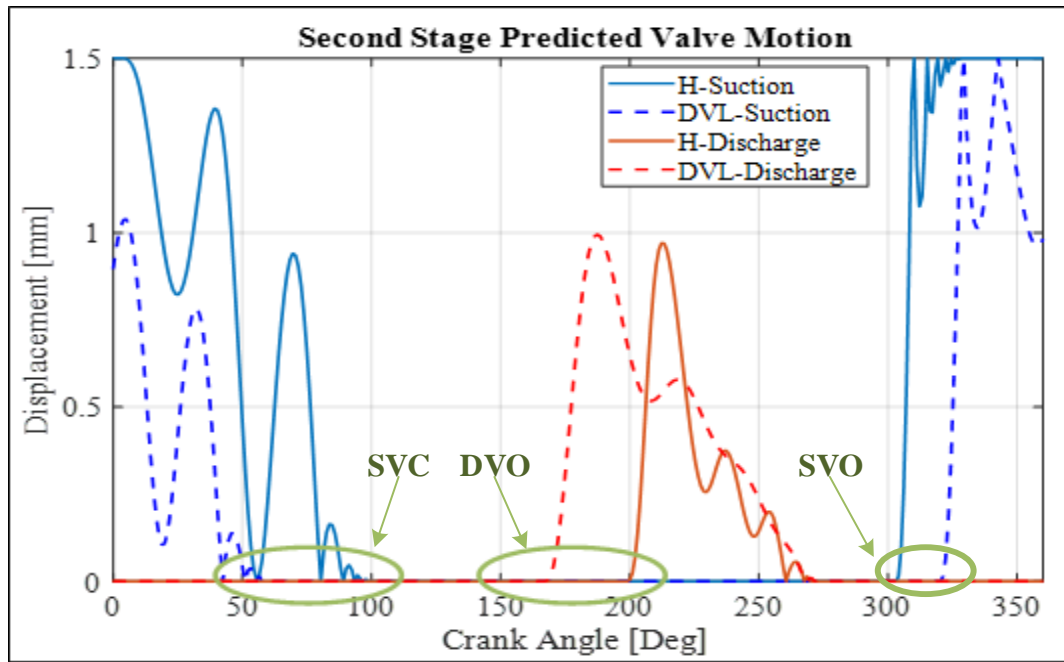


FIGURE 6.14: SECOND STAGE VALVE DISPLACEMENT COMPARISON OF HEALTHY AND VALVE LEAKAGE FAULT PREDICTIONS

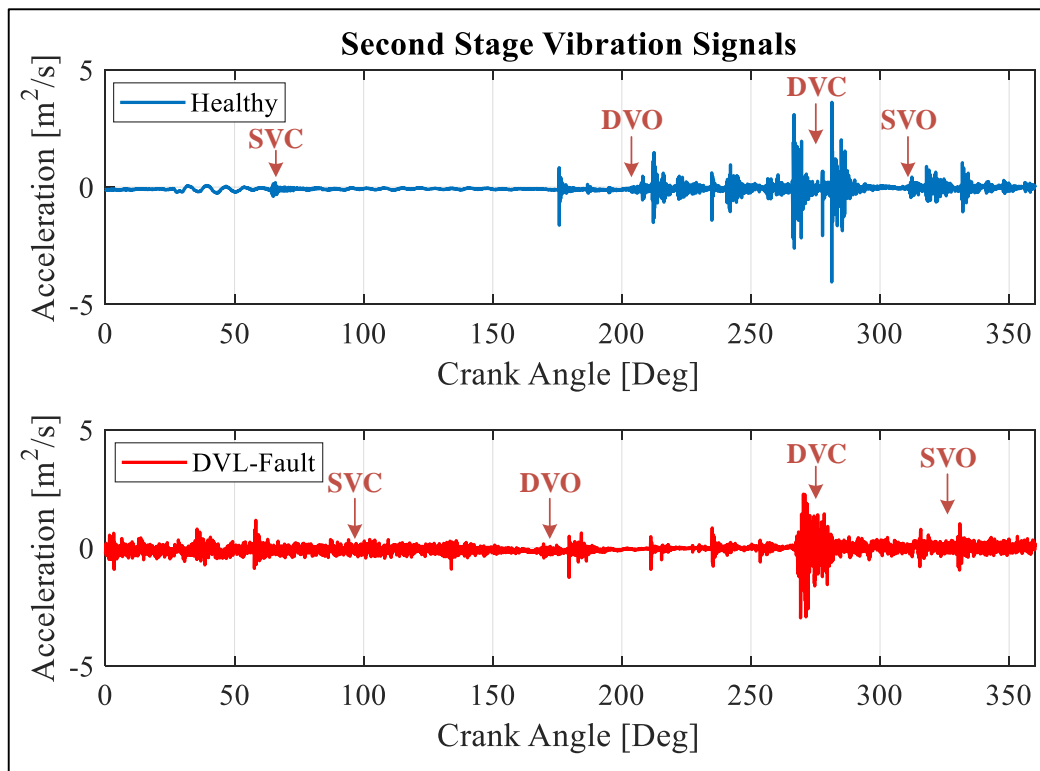


FIGURE 6.15: MEASURED SECOND STAGE VIBRATION SIGNALS FOR HEALTHY AND DISCHARGE VALVE FAULT CONDITIONS

6.5 Intercooler Fault Simulation Results

6.5.1 In-Cylinder Pressure Fault Signal

Predicted in-cylinder pressure and valve motion simulated under leaking intercooler fault are presented in this section. The predicted intercooler leakage result at 0.827 MPa (120psi) is compared with experimental measurement when the compressor is working under the same fault condition. Figures 6.16 shows the first and second stage results comparing the predicted in-cylinder waveform trends with that of experimental, and from the plots, it can be seen that the predicted and experimental waveforms for intercooler leakage are in good agreement with the exception of some minor differences at first stage pressure plot.

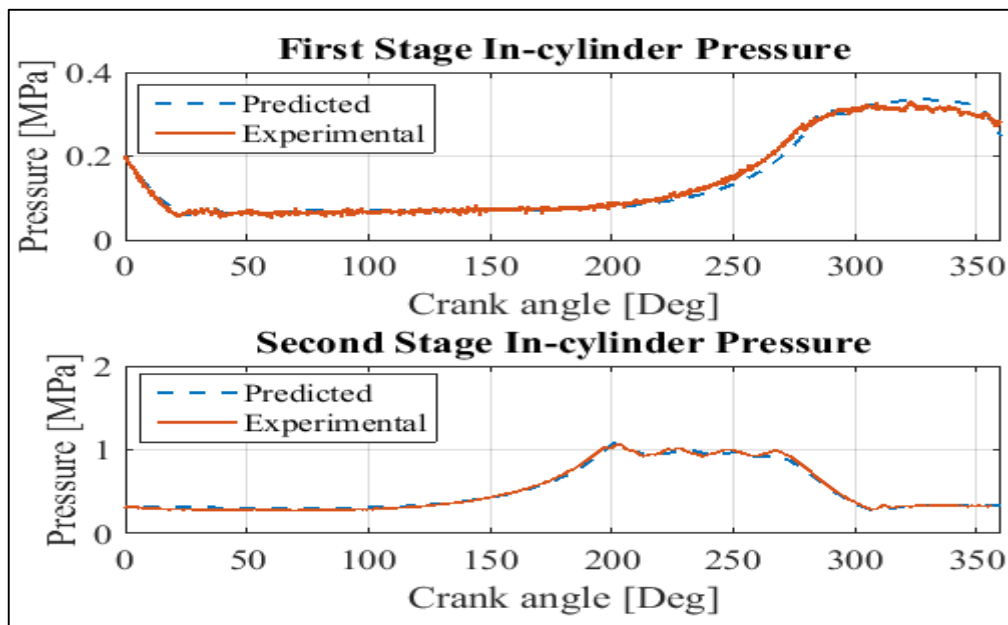


FIGURE 6.16: PREDICTED AND EXPERIMENTAL INTERCOOLER LEAKAGE TRENDS FOR FIRST AND SECOND STAGE IN-CYLINDER PRESSURE AT 0.823 MPa

Figures 6.17 shows the comparison graph of healthy and intercooler fault (ICL-Fault) for first stage predicted and measured in-cylinder pressure signals. The first stage discharge valve opens slightly early when there is a leakage on the intercooler coil, and the suction valve also opens slightly earlier when there are leaks on the intercooler pipeline. These effects are evident in the predicted plot as well as the measured results.

Also in the second stage healthy and faulty comparison graphs (Figure 6.18), the discharge valve opens slightly earlier under fault conditions for both predicted and experimental measurements. However, it is noted that this change is not significant enough due to the

quantity of leaks seeded on the intercooler pipeline and simulated mathematically. Moreover, the intercooler fault carried out in this study does not appear to have an adverse effect on the in-cylinder pressure signatures of the reciprocating compressor

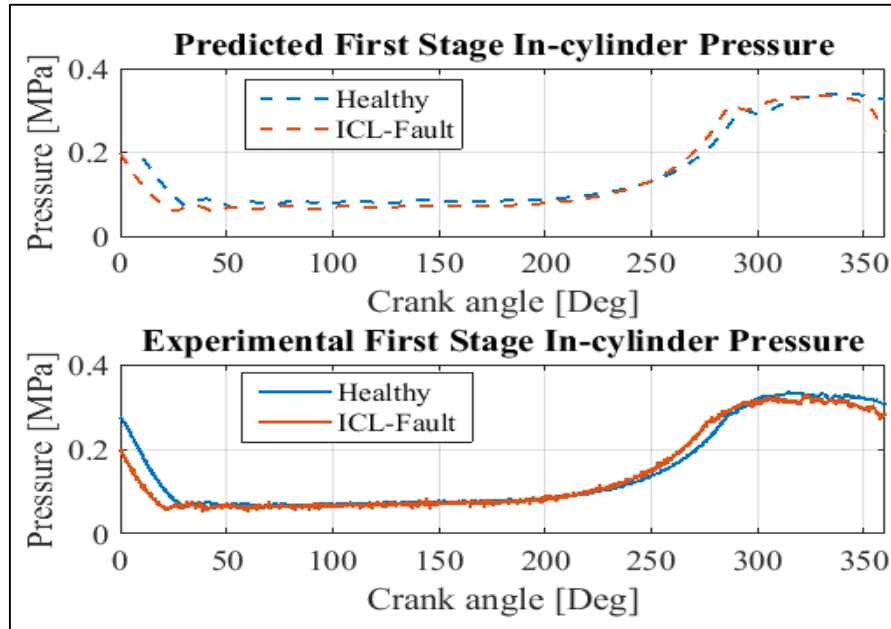


FIGURE 6.17: PREDICTED AND EXPERIMENTAL FIRST STAGE IN-CYLINDER PRESSURE WAVEFORMS FOR HEALTHY AND ICL-FAULT CONDITIONS

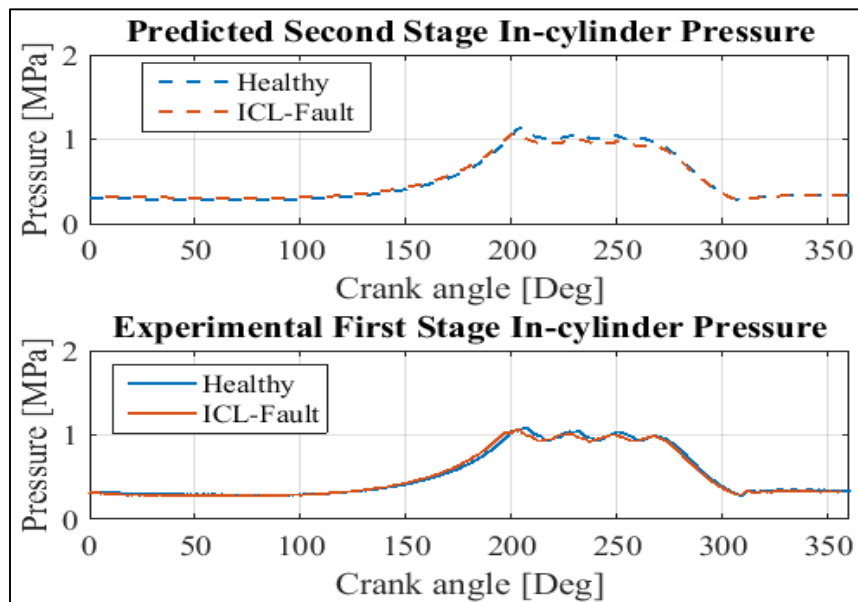


FIGURE 6.18: PREDICTED AND EXPERIMENTAL SECOND STAGE IN-CYLINDER PRESSURE WAVEFORMS FOR HEALTHY AND ICL-FAULT CONDITIONS

6.5.2 Valve Displacement and Vibration Fault Signals

Figure 6.19 shows the first stage valve displacement trends when there are leaks on the intercooler pipeline. From the graph, there are no significant changes between the healthy and faulty predicted trends for both suction and discharge valve motion.

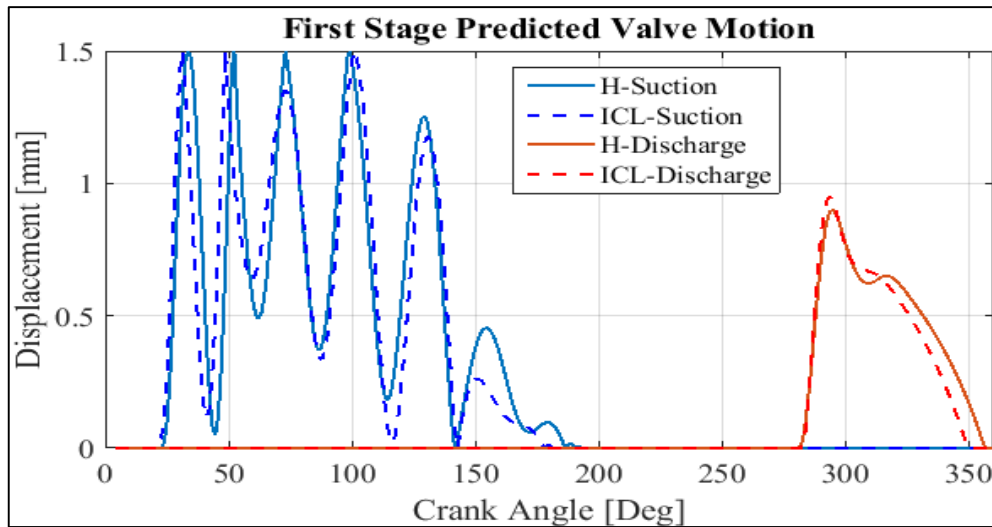


FIGURE 6.19: FIRST STAGE VALVE DISPLACEMENT COMPARISON OF HEALTHY AND INTERCOOLER FAULT PREDICTIONS

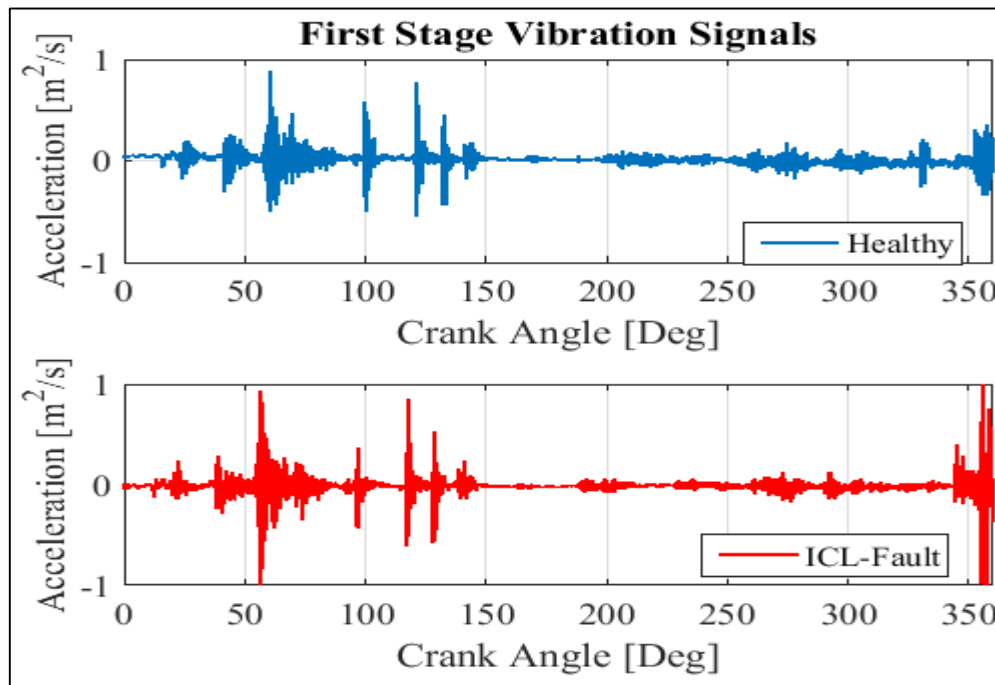


FIGURE 6.20: MEASURED FIRST STAGE VIBRATION SIGNALS FOR HEALTHY AND INTERCOOLER FAULT CONDITIONS

Figure 6.20 shows the measured first stage vibration signature for healthy and faulty intercooler. The delays in valve opening and closing times are not apparent from the graphs. However, it is observed that the introduction of leaks on the intercooler pipeline causes high levels of vibration amplitudes, particularly when the discharge valve closes about 352° .

The second stage suction and discharge valve displacements are presented in Figure 6.21 for healthy and faulty conditions. The healthy and faulty valve displacement comparison shows no significant difference in suction and discharge valve opening and closing times (crank angles). Also, from Figure 6.22, which presents the measured vibration trends when intercooler leaks are introduced to the system, it is difficult to point out the differences in valve event times (angles) between healthy and intercooler fault vibration signatures.

From the above analysis, it can be concluded that the degree of intercooler leakage seeded and mathematically simulated in this study does not show any notable trend differences compared with healthy trends. However, it is worth noting that, increased levels of leaks on the intercooler system do have adverse effects on the compressor efficiency (Zheng, 2005).

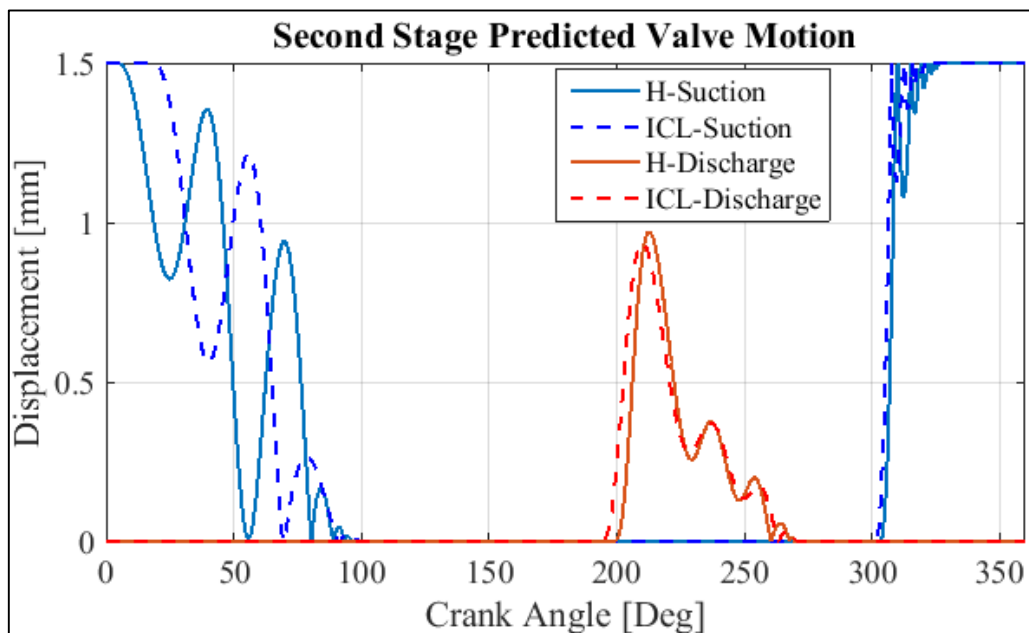


FIGURE 6.21: SECOND STAGE VALVE DISPLACEMENT COMPARISON OF HEALTHY AND INTERCOOLER FAULT PREDICTIONS

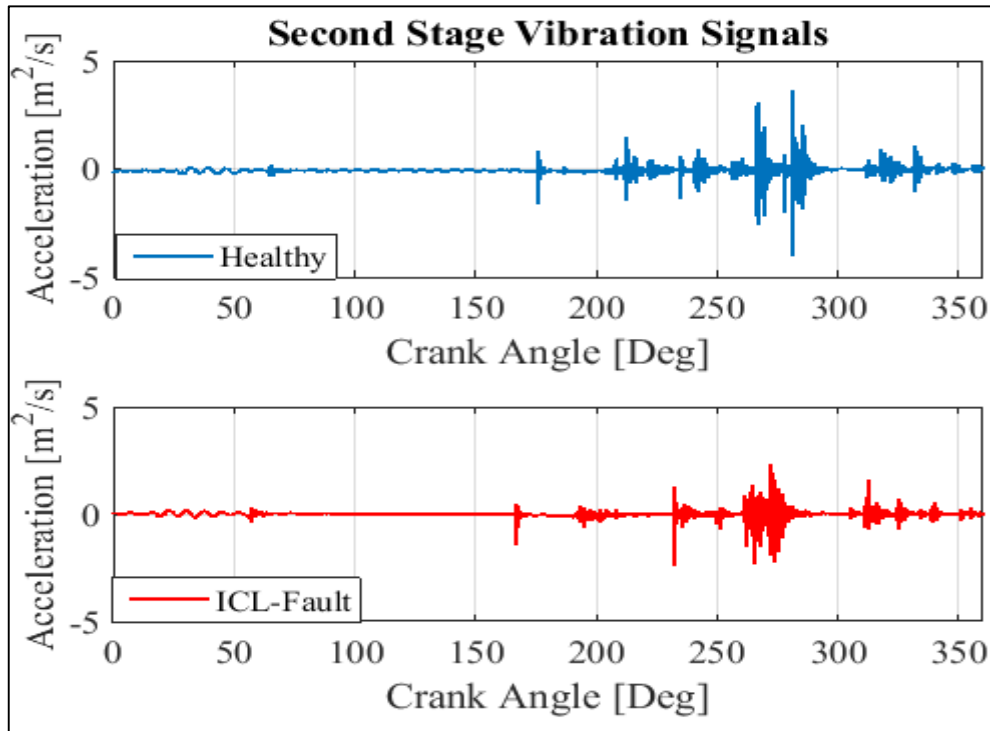


FIGURE 6.22: MEASURED SECOND STAGE VIBRATION SIGNALS FOR HEALTHY AND INTERCOOLER FAULT CONDITIONS

6.6 Discharge Chamber Fault Simulation Results

The effects of four fault conditions namely; second stage discharge fault (DVL), intercooler fault (ICL), reservoir pipeline fault (PPL), and combined fault of DVL and PLL on the discharge chamber have been simulated. The experimental results of all four fault conditions are compared with healthy signal at 0.82MPa as seen in Figure 6.23. The effects of the experimental results in Figure 6.23 are correlated with the fault predictions in Figure 6.24. From the experimental results it can be seen that the intercooler fault (ICL) cannot be detected from the gas pulsation signal and this effect is identical to the predicted intercooler fault simulation. Very little almost insignificant effect is observed from the experimental reservoir pipeline fault where the gas pulsation amplitude of the faulty signal is slightly higher than that of the healthy signal. Also, this effect can be seen in the corresponding fault simulation (PLL). The discharge valve fault and combined fault experimental signals had the greatest effect on the gas pulsation signal with a significantly reduced amplitude of fault signals and visible deformed waveform at the discharge opening times. Also, the discharge valve opens slightly earlier with the two fault conditions. All three effects described are present in the simulated results. From the results, it can be concluded that the model is reliable and accurately represents

the fault effects on the gas pulsation signal from the second-stage cylinder discharge chamber of a reciprocating compressor.

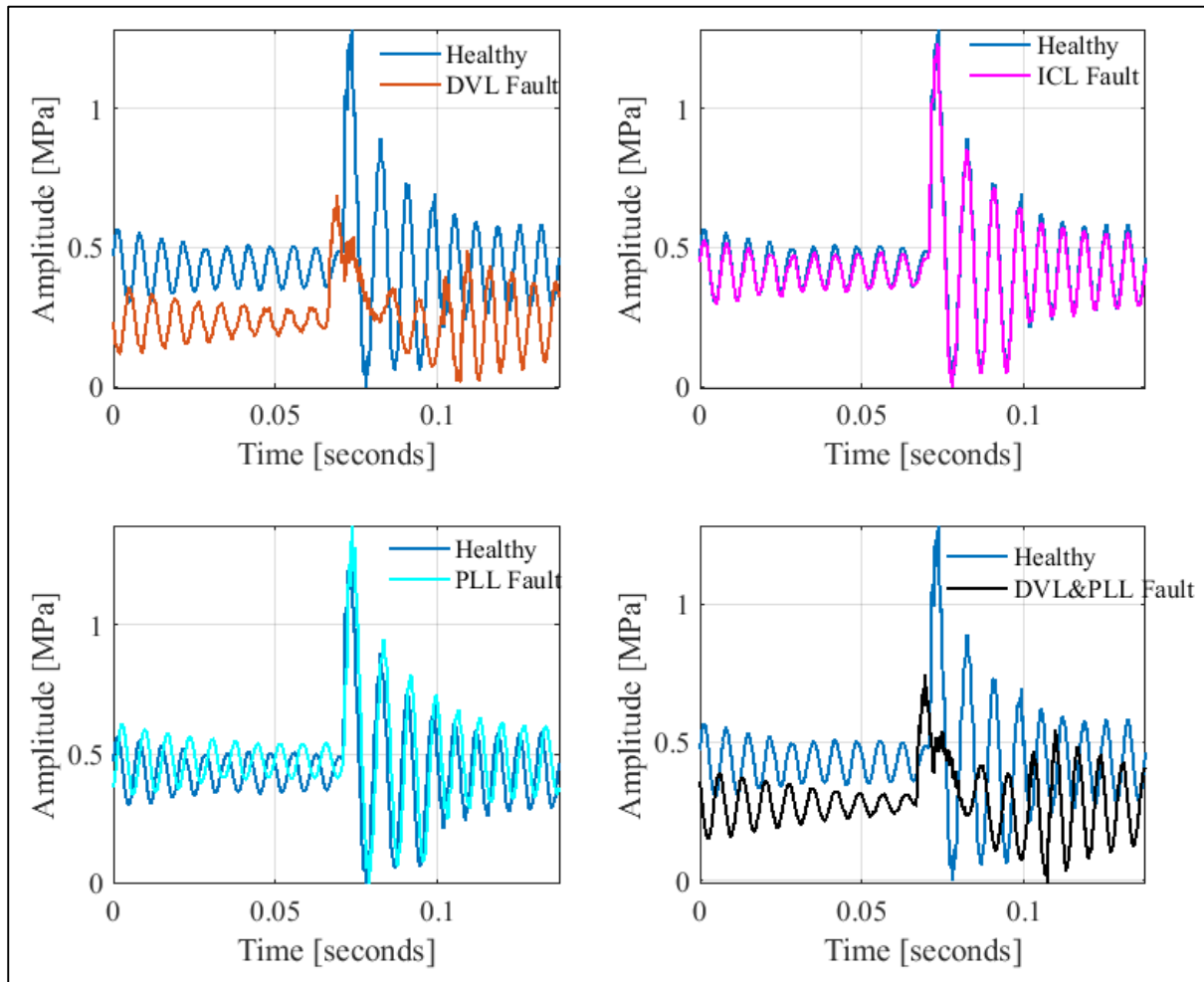


FIGURE 6.23: EXPERIMENTAL COMPARISON OF HEALTHY AND FOUR FAULT CONDITIONS OF DISCHARGE CHAMBER SIGNAL AT 0.83MPA

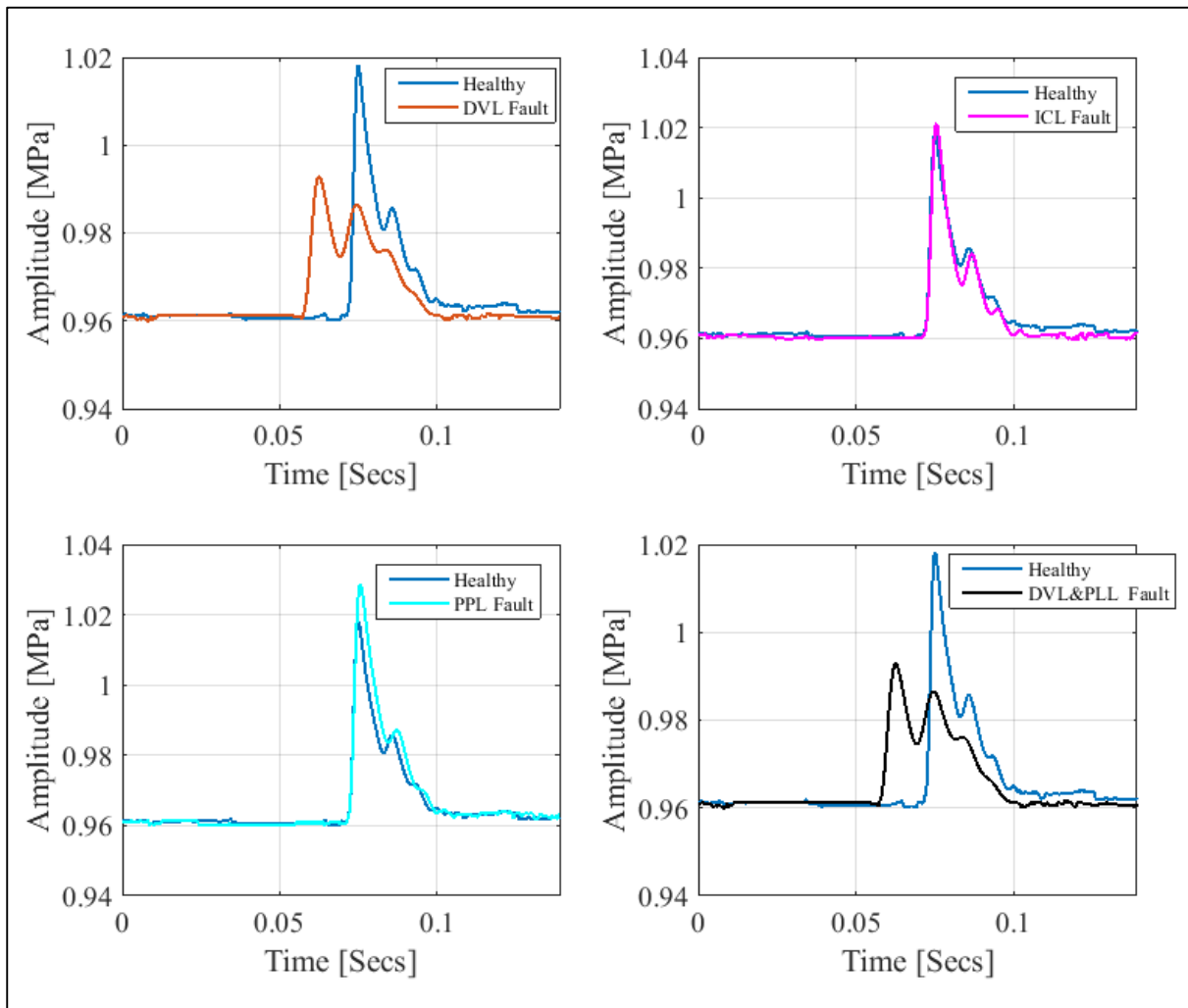


FIGURE 6.24: PREDICTED COMPARISON OF HEALTHY AND FOUR FAULT CONDITIONS OF DISCHARGE CHAMBER SIGNAL AT 0.83MPA

CHAPTER SEVEN

7 CHARACTERISTICS OF VIBRATION SIGNALS FROM A RECIPROCATING COMPRESSOR

This chapter describes the characteristics of vibro-acoustic signals from the reciprocating compressor based on vibration measurement. Time domain and frequency domain signal processing techniques are used to find features due to specific faults (valve and intercooler leaks) common to the reciprocating compressor. It was revealed that frequency domain analysis is better at detecting the investigated faults compared to using key time domain statistical features studied, however, an advance signal processing tool is needed for a more robust diagnostic.

7.1 Introduction

Vibration analysis is the most widely used signal processing technique for machine monitoring and early fault diagnosis of most mechanical systems including reciprocating compressors (RC). In this chapter, fundamental vibration techniques are used to detect common reciprocating compressor faults before the faults become catastrophic. The vibration signals are measured from the head of the two-stage (first and second) compressor cylinders (see section 4.2.1). Figure 7.1 shows typical one cycle vibration signals from the two RC cylinder heads.

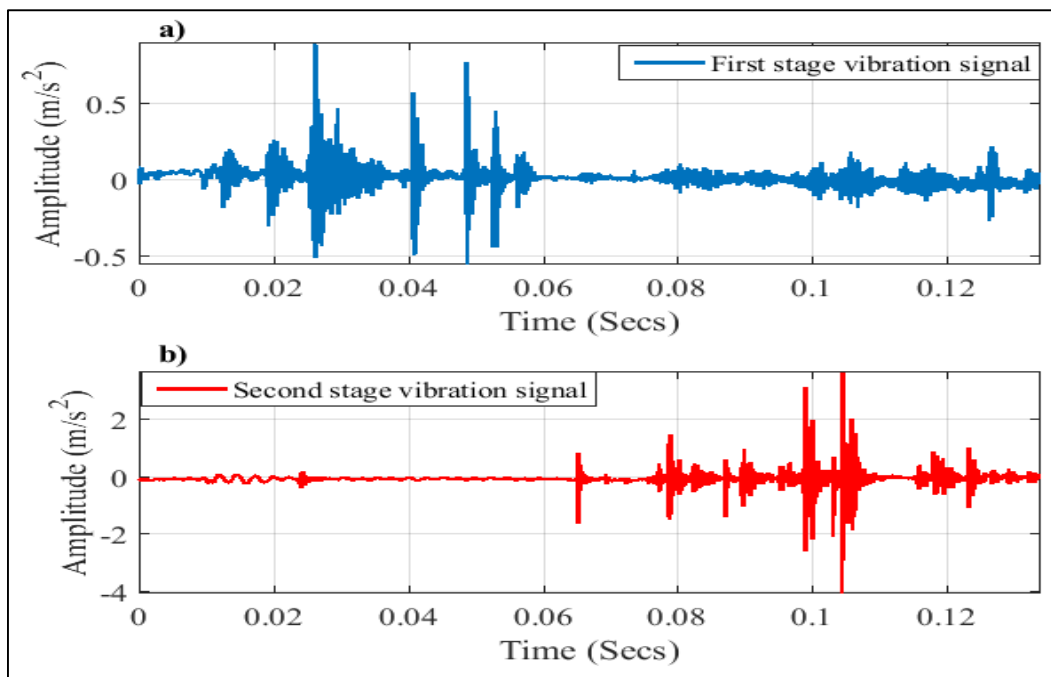


FIGURE 7.1: MEASURED VIBRATION SIGNAL AT 0.82 MPa A) FIRST CYLINDER, AND B) SECOND CYLINDER

The vibration signal from the compressor cylinder head is composed of flow-induced and impact induced excitations. The flow-induced excitations are caused by air interactions with valves resulting in periodic flow oscillations; while impact induced excitations are caused by the effects of the valve plate hitting the seat when opening and closing.

In vibration analysis, time domain and frequency domain analysis are fundamental techniques for interpreting data. Changes in machine condition can be detected by analysing time-domain statistical parameters such as root-mean-square, crest factor, peak level, kurtosis etc. The frequency domain analysis is used to show individual frequency components within the signal,

which can identify fundamental characteristics of the machine and detect sources of defects within the system.

In this chapter, time domain and frequency domain analysis are applied to the measured vibration signal from the reciprocating compressor cylinder-head to extract useful information, which will aid effective condition monitoring of the machine. A wide range of tank pressures (0.01MPa to 0.82MPa) are investigated and three common reciprocating compressor faults including second-stage discharge valve leakage, intercooler leakage, and a combination of the two faults are studied for fault detection purposes. Sources of vibration from the reciprocating compressor are discussed and the application of time-domain and frequency-domain methods are employed to determine the compressors' condition.

7.2 Time Domain Analysis of Vibration Signal

In this section, vibration signatures from the cylinder head of the two-stage reciprocating compressor are examined at all tank pressures. Three statistical parameters including Root Mean Square (RMS), and kurtosis are presented and results for healthy and faulty compressor conditions are analysed.

Figures 7.2 and 7.3 show the raw vibration signals from the first stage and second stage compressor cylinder heads at all tank pressures. The plots of vibration signals presented in Figure 7.2 shows the complexity and impulsive nature of the vibration signals from the compressor. There are some differences between waveforms at several tank pressures; for instance, at 0.13 seconds, high amplitudes can be observed for low to mid tank pressure range (0.01MPa to 0.55MPa) as a result of low resistance in the form of pressure build-up in the discharge plenum of the first-stage cylinder. However, other differences are not so obvious from the waterfall plot. In Figure 7.3, significant impacts at 0.1 seconds are observed from mid to higher tank pressure range (0.48MPa to 0.82MPa) and they occur at the discharge valve closing (DVC) time for the second-stage cylinder. These high amplitude impacts result from high pressure air acting as a resistant force in the discharge plenum of the cylinder causing the valve to close harshly. This shows that changes in tank pressure influences vibration signatures from the reciprocating compressor. Furthermore, the overall vibration amplitudes from the second-stage cylinder head are greater than those from the first-stage RC cylinder head, because the second-stage cylinder compresses gas at a higher pressure.

Figures 7.4 and 7.5 presents the healthy and faulty vibration signatures from the first-stage cylinder head at 0.82MPa (maximum tank pressure).

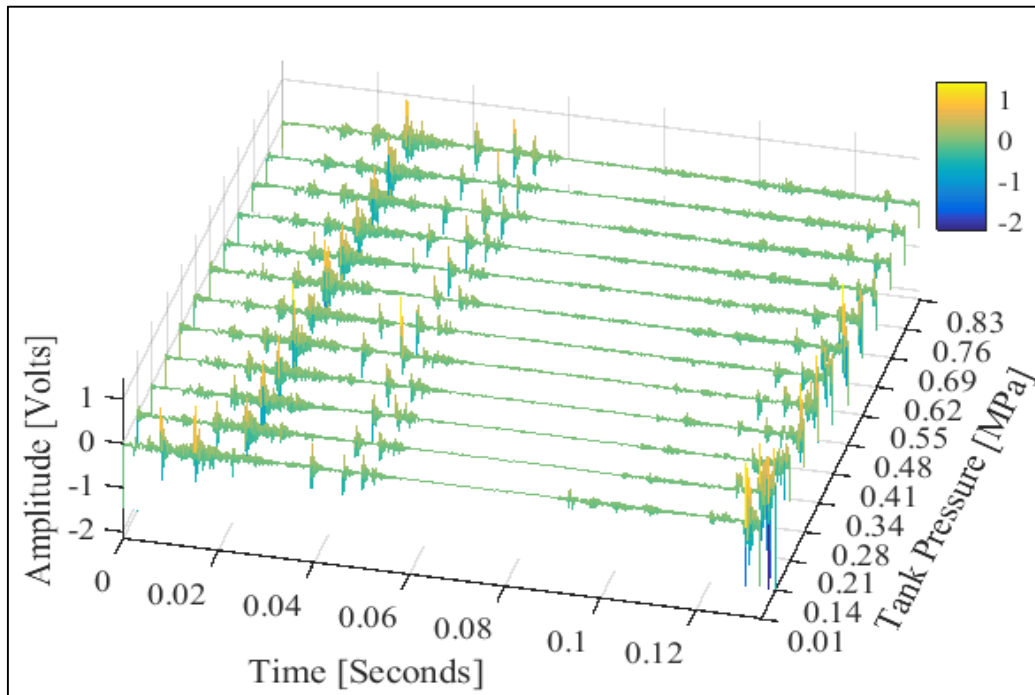


FIGURE 7.2: FIRST STAGE VIBRATION SIGNATURES OVER A WIDE PRESSURE RANGE UNDER NORMAL (HEALTHY) COMPRESSOR CONDITION

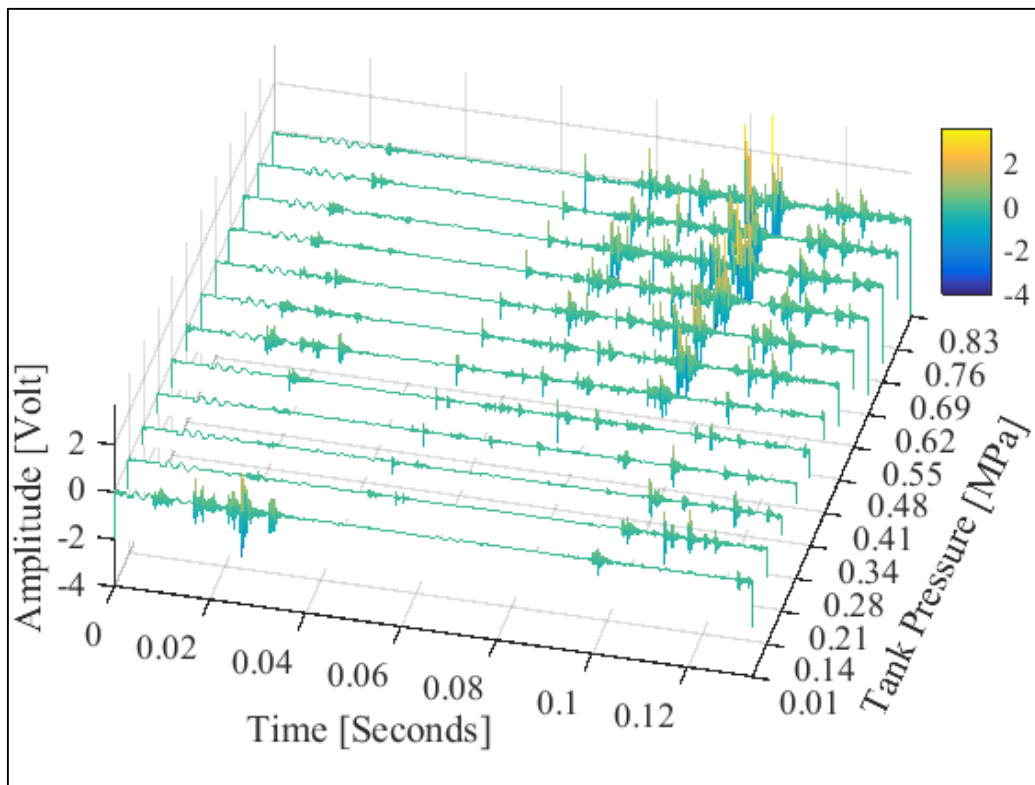


FIGURE 7.3: SECOND STAGE VIBRATION SIGNATURES OVER A WIDE PRESSURE RANGE UNDER NORMAL (HEALTHY) COMPRESSOR CONDITION

The differences in healthy and faulty signal amplitudes for the two stages are not very clear and can be quite misleading as the general amplitude of the healthy vibration signatures (BL) are high compared to discharge valve leakage (DVL) and combined fault (DVL+ICL) signatures in Figure 7.4. Furthermore, in Figure 7.5, the normal (BL) vibration amplitude is also higher than those of fault signatures at 0.82MPa maximum tank pressure.

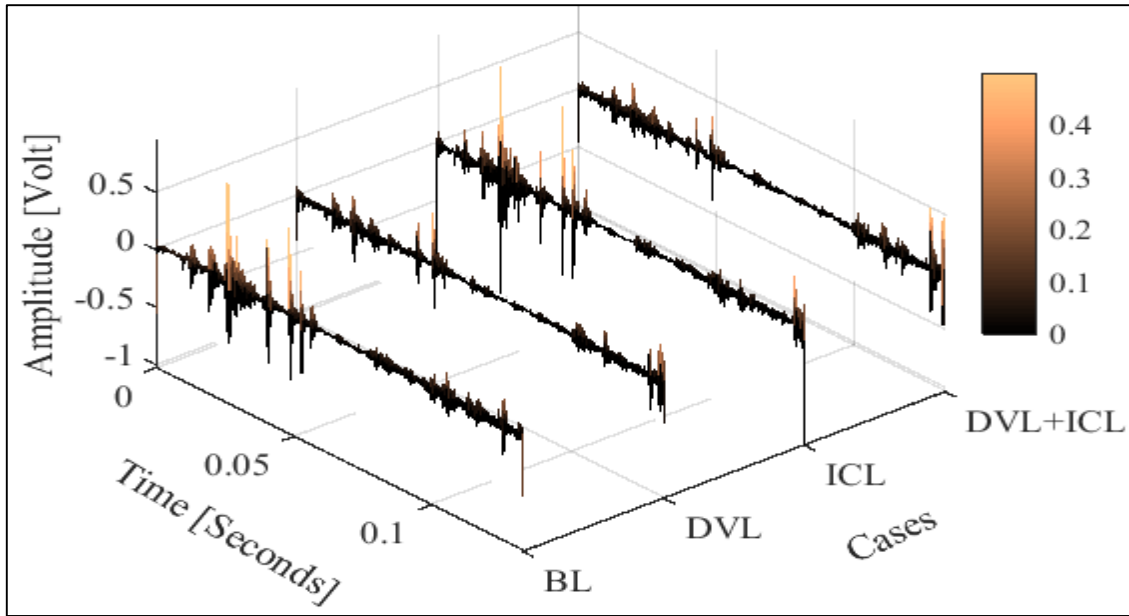


FIGURE 7.4: HEALTHY AND FAULTY VIBRATION SIGNATURES FROM FIRST STAGE CYLINDER HEAD AT 0.82MPa

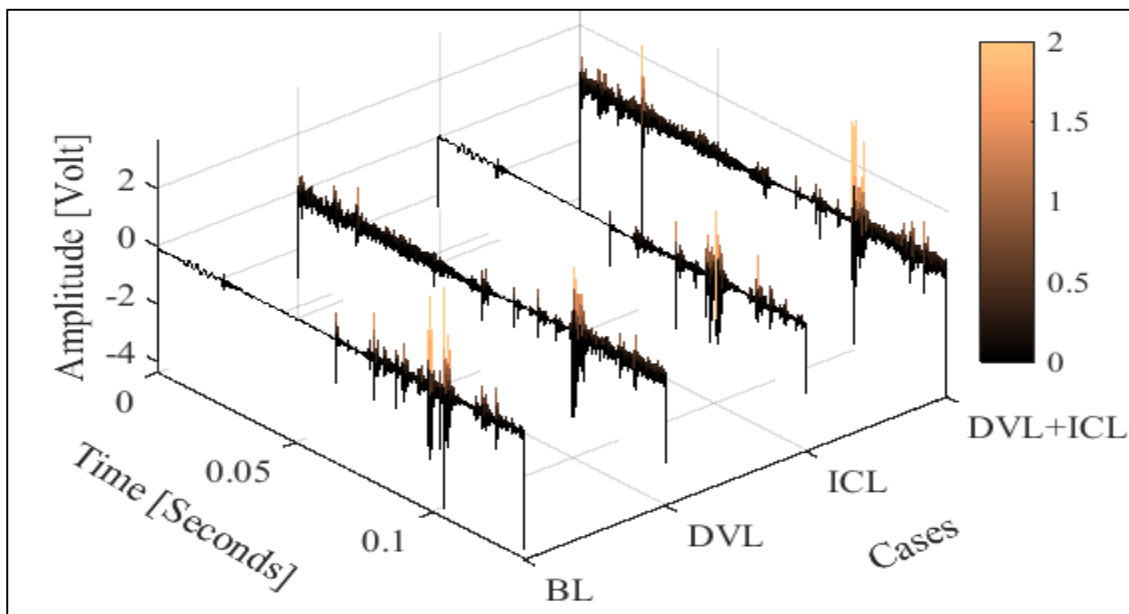


FIGURE 7.5: HEALTHY AND FAULTY VIBRATION SIGNATURES FROM SECOND STAGE CYLINDER HEAD AT 0.82MPa

7.2.1 RMS

Root Mean Square (RMS) measures the overall changes in the system; it is computed to understand the signals more accurately and to identify healthy and faulty signals clearly under a wide pressure range. The result in Figure 7.6 shows how the RMS values for first and second stage vibration signals vary with increasing tank pressure. It is observed that the RMS values for the first stage vibration measurement are generally lower than the RMS values for second stage vibration measurement from mid to high tank pressure range; also, the second stage RMS values show an increasing linear trend for mid to high tank pressure ranges.

Figure 7.7 presents a comparison of healthy and faulty RMS values for first stage vibration signals at several tank pressures. The random trends over the wide tank pressure range (0.01MPa - 0.82MPa) observed in all cases do not provide significant information concerning the condition of the RC, and therefore, cannot be used as a fault indicator.

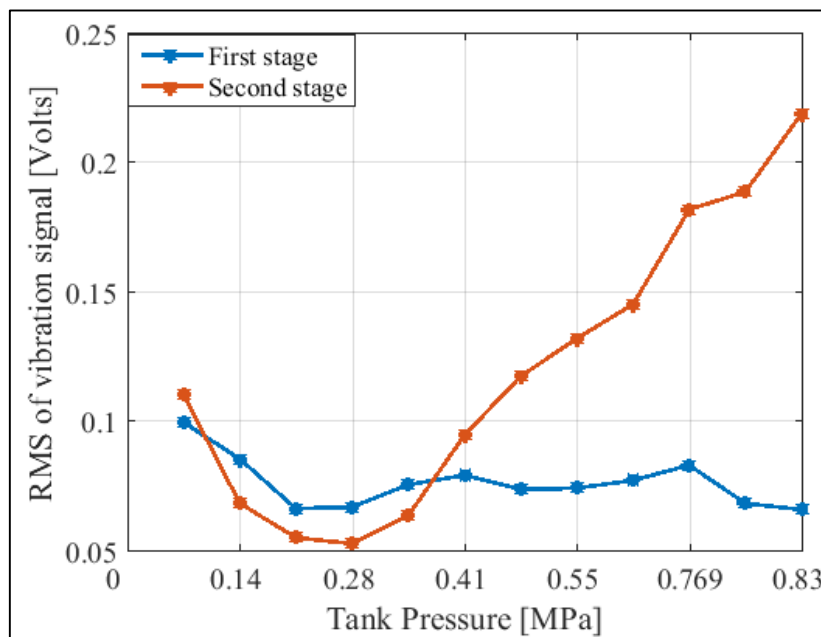


FIGURE 7.6: FIRST AND SECOND STAGE VIBRATION RMS VALUES FOR SEVERAL TANK PRESSURES

In Figure 7.8, the second-stage vibration measurement RMS under healthy and all fault cases are presented. Here, it is seen that the mid to high tank pressure RMS values increase linearly for all cases, however, there are very little variances between the healthy and faulty RMS values, which shows it is not a suitable fault indication means.

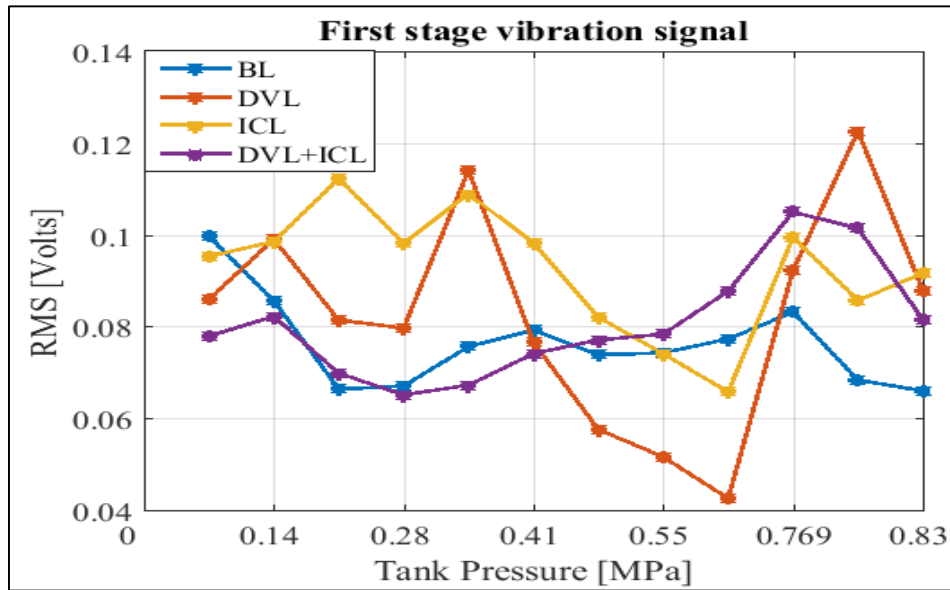


FIGURE 7.7: HEALTHY AND FAULTY FIRST STAGE VIBRATION RMS VALUES AT SEVERAL TANK PRESSURES

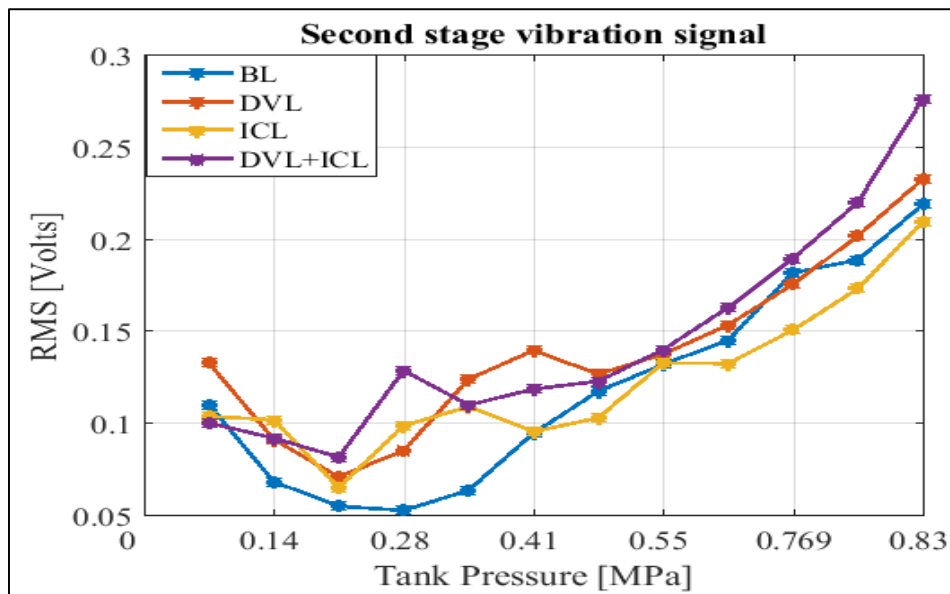


FIGURE 7.8: HEALTHY AND FAULTY SECOND STAGE VIBRATION RMS VALUES FOR SEVERAL TANK PRESSURES

7.2.2 Kurtosis

The fourth statistical moment popularly known as kurtosis is a widely used statistical feature in condition monitoring. Figure 7.9 shows the kurtosis for the first and second stage vibration signal across a wide tank pressure range. The results for both first and second stage kurtosis plots do not exhibit any reliable trends with increasing tank pressure. However, the kurtosis values for low to mid (0.01MPa to 0.41MPa) tank pressure range of first-stage vibration

measurements are higher than the corresponding tank pressure range of second-stage vibration measurements. This means that the first-stage vibration signals have more infrequent extreme deviations (or outliers) compared to those from the second-stage.

The kurtosis results for healthy and fault cases are compared for first stage vibration signals in Figure 7.10 and second stage vibration signals in Figure 7.11 across all tank pressure range. The results reveal no significant variance across the entire pressure range for healthy and faulty results but rather a very random trend with increasing tank pressures, which means that the time-domain kurtosis results cannot be used to give accurate diagnosis of the RCs' condition.

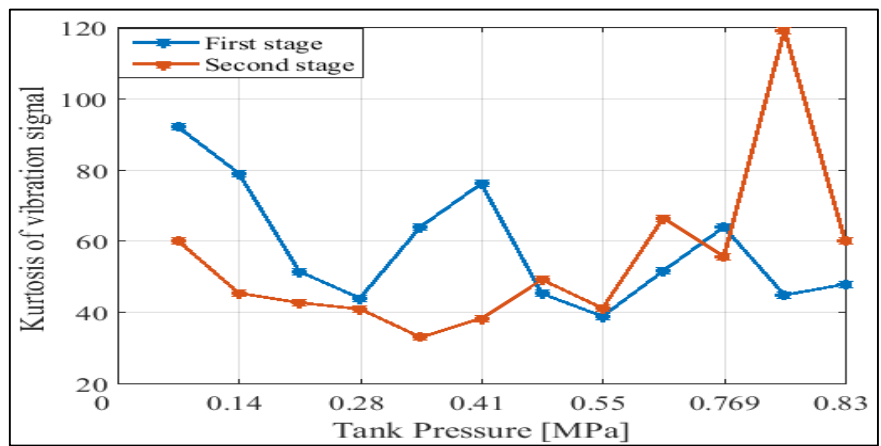


FIGURE 7.9: KURTOSIS VALUES FOR FIRST AND SECOND STAGE VIBRATION SIGNALS AT SEVERAL TANK PRESSURES

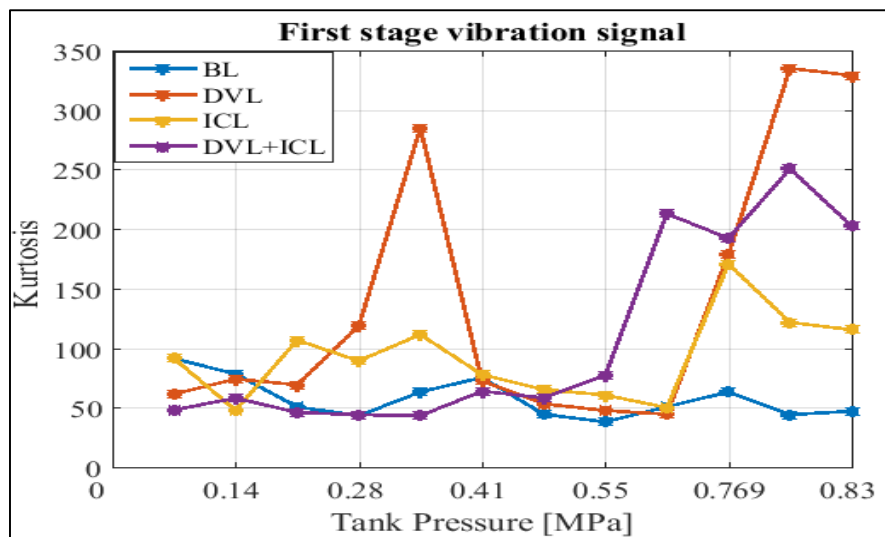


FIGURE 7.10: HEALTHY AND FAULTY KURTOSIS RESULTS FOR FIRST STAGE VIBRATION SIGNALS AT SEVERAL TANK PRESSURES

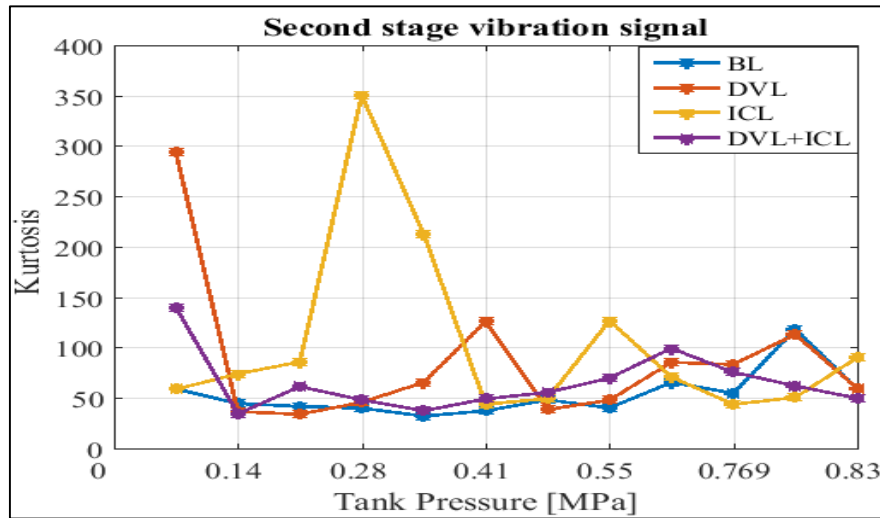


FIGURE 7.11: HEALTHY AND FAULTY KURTOSIS RESULTS FOR SECOND STAGE VIBRATION SIGNALS AT SEVERAL TANK PRESSURES

In summary, due to the randomness and non-linear nature of statistical features from the measured first and second stage vibration signals across a wide range of pressure, it is difficult to detect and monitor common faults developed on the reciprocating compressor using the investigated traditional time domain analytical methods.

7.3 Frequency Domain Analysis

The previous section revealed that the considered time-domain statistical parameters were not able to detect the presence of common reciprocating compressor faults for a wide tank pressure range. Therefore, frequency domain analysis is investigated in this section for condition monitoring of the machine.

The vibration spectra for healthy first-stage and second-stage vibration measurements from the reciprocating compressor are presented in Figure 7.12a and 7.12b respectively. From the plots, it can be observed that the low frequencies have the greatest amplitude in both spectra, and the magnitude of the second stage spectra is generally greater than that from the first-stage cylinder head.

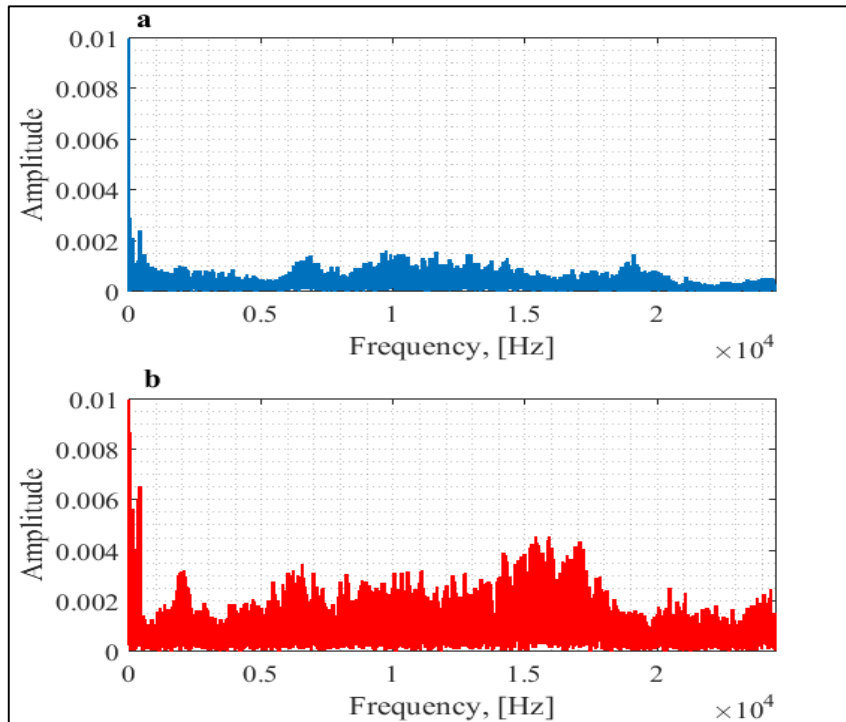


FIGURE 7.12: ONE SIDED VIBRATION SPECTRA FOR HEALTHY A) FIRST STAGE AND B) SECOND STAGE VIBRATION MEASUREMENTS AT 0.82MPA

Figures 7.13 and 7.14 shows the changes in vibration spectra with increasing tank pressure for first and second-stage vibration signals respectively. From the healthy first-stage vibration spectra plot, it can be observed that there are no significant changes in amplitudes with increasing tank pressure. However, for the healthy second-stage vibration spectra, at high frequency range between 12 kHz to 17 kHz particularly, high frequency amplitudes are present from mid to high tank pressure range. Figure 7.14 show that increasing tank pressure does have some significant effect on the spectrum amplitude of the second-stage vibration measurements.

Figure 7.15 shows the waterfall plots of first-stage vibration spectrum for all tank pressure range under healthy and fault conditions. At lower frequencies, high frequency amplitudes are seen in the plots of all three fault cases at certain tank pressures, while the healthy signal (BL) has relatively low amplitude. Introducing leaks (DVL and ICL) increases the amplitude of the vibration spectra.

The vibration spectra from the second-stage measurements have greater amplitudes than those from the first-stage cylinder for all cases studied including healthy signals. The increased amplitude is a result of the greater discharge pressure from the second-stage cylinder.

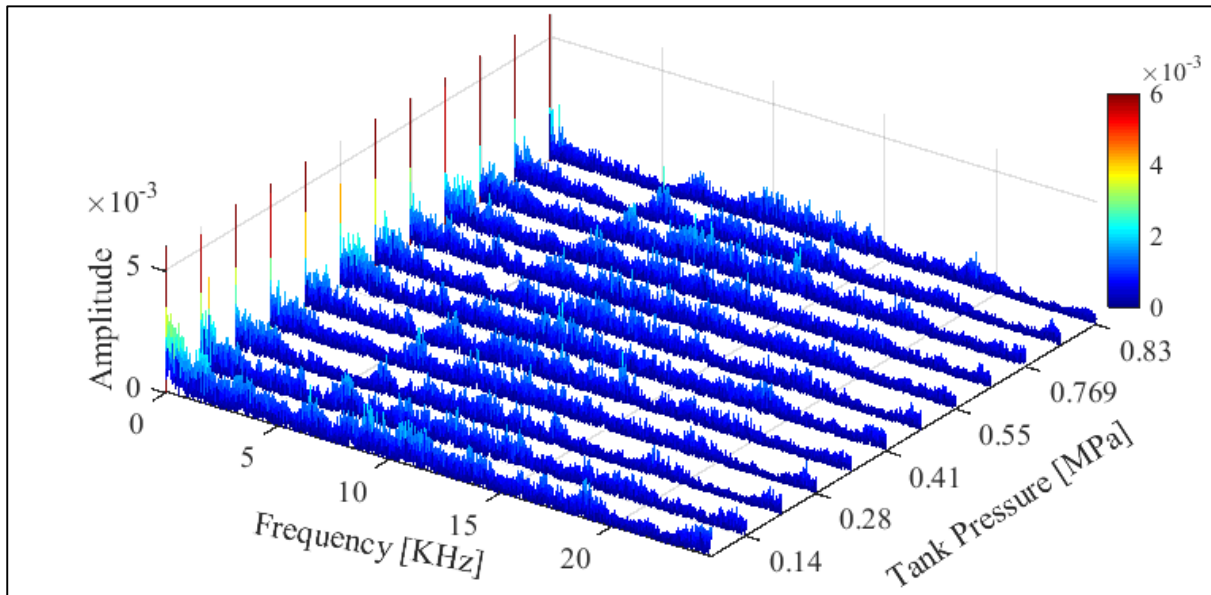


FIGURE 7.13 : HEALTHY FIRST STAG VIBRATION SPECTRA FOR SEVERAL TANK PRESSURES

Figure 7.16 presents the waterfall plots of second-stage vibration spectra for all tank pressures under healthy and the three fault conditions. In the combined fault (DVL+ICL) plot, increased amplitudes are observed in the 5 kHz to 13 kHz frequency range at high tank pressure levels compared to other fault conditions including healthy case. The greatest peak is seen at 5646 Hz. The intercooler fault spectral plot has the lowest overall amplitude compared to the other cases.

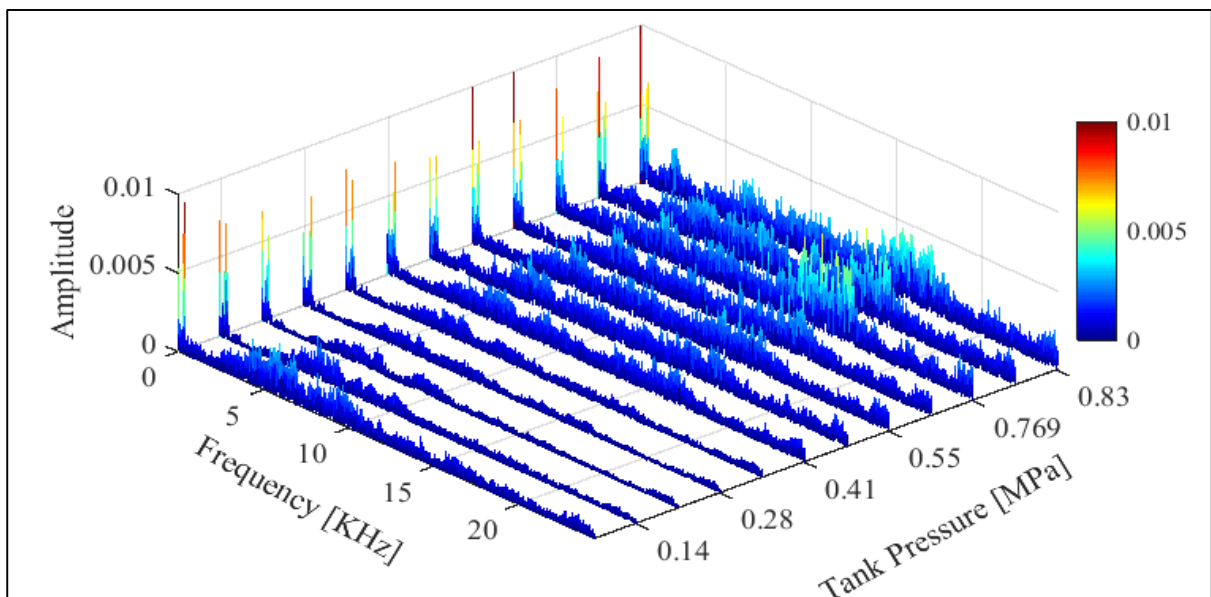


FIGURE 7.14: HEALTHY SECOND STAGE VIBRATION SPECTRA FOR SEVERAL TANK PRESSURES

CHARACTERISING VIBRO-ACOUSTIC SIGNALS OF A RECIPROCATING COMPRESSOR FOR CONDITION MONITORING

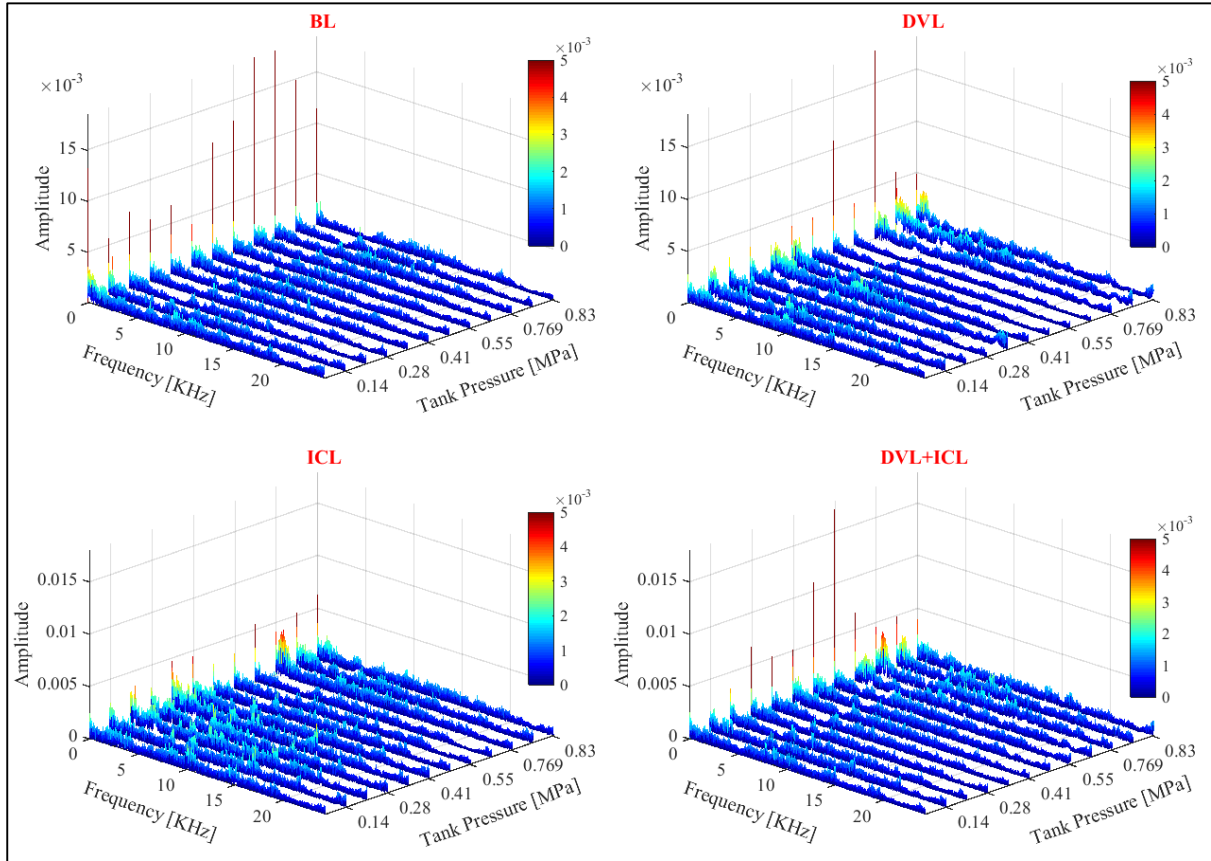


FIGURE 7.15: WATERFALL PLOTS OF FIRST STAGE VIBRATION SPECTRUM FOR HEALTHY AND ALL FAULT CASES

The spectrum analysis of the measured vibration signals for healthy and fault conditions show that the spectral amplitudes are important indicators for detecting common reciprocating compressor faults particularly, when there is a discharge valve leakage.

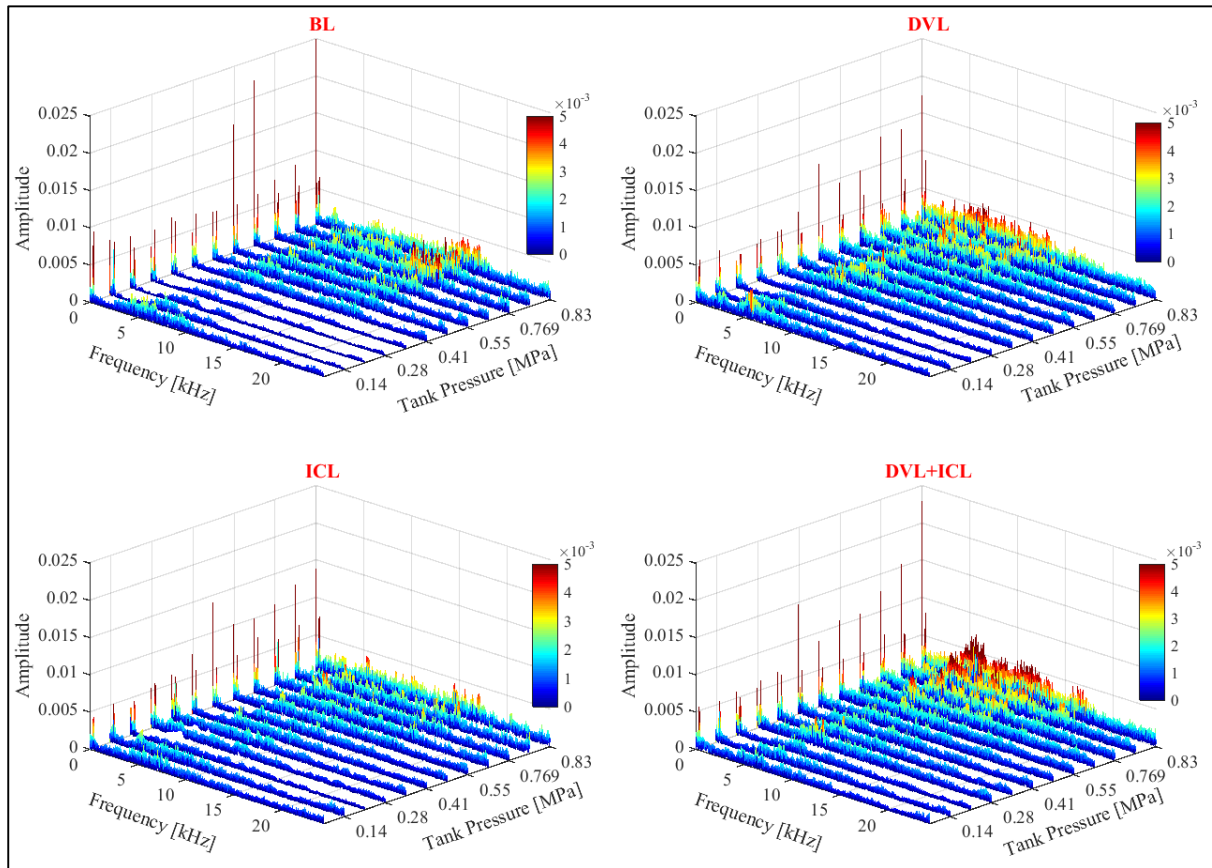


FIGURE 7.16: WATERFALL PLOTS OF SECOND STAGE VIBRATION SPECTRUM FOR HEALTHY AND ALL FAULT CASES

7.4 Summary

In this chapter, three common fault cases including second-stage discharge valve leakage, intercooler leakage and a combination of the two faults are investigated experimentally. Time domain and frequency domain analyses are used to determine vibration characteristics of the signals from the first-stage and second-stage cylinder heads. The time-domain signal waveform revealed several impacts and corresponding magnitudes caused by the valve and gas flow, two key time domain statistical parameters were unable to clearly differentiate fault features from that of healthy signal for a wide tank pressure range. Therefore, it can be concluded that time domain statistical features cannot be used as an effective fault detection tool for condition monitoring of the two-stage reciprocating compressor.

The frequency domain analysis revealed, that spectral amplitudes present significant variations at high tank pressure range, particularly, for second-stage vibration signals. Moreover, spectral amplitudes of fault cases increase, mostly at high tank pressure range over a certain frequencies (5 kHz to 14 kHz) for the second-stage vibration signals. Conventional signal processing (time-

domain and frequency-domain) methods are often used for early fault detection, however, the diagnostic features investigated in this chapter were ineffective as a diagnostic tool because of the wide variety of operating conditions (tank pressures) and the complex impulsive nature of the vibration signals.

CHAPTER EIGHT

8 CHARACTERISTICS OF DISCHARGE GAS PULSATION FROM A RECIPROCATING COMPRESSOR

This chapter presents a practical approach to condition monitoring of reciprocating compressors based on gas pulsation signals from the compressor valve discharge chamber (plenum) for the detection of common reciprocating compressor faults (second-stage discharge valve plate leakage, intercooler pipe leakage, and discharge-to-reservoir pipe leakage). The noise characteristics from the measured pulsation signals are investigated using conventional time domain and frequency domain methods.

It is concluded that the pulsation waves can provide accurate representation of the valve opening times and any delays that may occur with increasing discharge/tank pressure. However, statistical features of the time-domain analysis were insufficient for fault detection. Furthermore, several resonances were present in the gas pulsation spectrum, but challenges were encountered in accurately selecting the optimal resonance band, to effectively characterise the investigated faults across several discharge/tank pressure range. Finally, using the 1/3rd octave band analysis, band 22 and 23, which corresponds to centre frequency 500Hz and 630Hz gave the best fault separations from the baseline (healthy) signal.

8.1 Experimental Setup

The experimental setup of the reciprocating compressor is described in chapter four section 4.2.1. Figure 8.1 presents a schematic of the reciprocating compressor rig setup with specifications of supporting components listed in Table 6.1.

The gas pulsation signal is collected via a piezoelectric dynamic pressure transducer (CY-YD-212) installed on the head of the second-stage discharge system. The transducer has a frequency range of more than 100 kHz, operating range of 0 to 10MPa, a temperature range of - 40°C to +150°C, and sensitivity of 100pC/MPa. In addition to the acoustic measurement acquired by the dynamic pressure transducer, eight transducers were installed on the test rig to acquire additional data on vibration, in-cylinder pressure, temperature, instantaneous angular speed and current signals. These signals were collected using the following transducers:

- Accelerometers (two)
- Static pressure sensors (two)
- Thermocouples (two)
- An optical encoder
- A hall effect current transducer

8.1.1 Test Procedure

The data acquisition system was set to collect 40384 samples of data at a sampling frequency of 49019 Hz. The 40384 samples collected make up six cycles of data collected at several discharge pressure levels including 0.275 MPa, 0.413 MPa, 0.62, and 0.827 MPa. Five different cases were investigated: baseline (BL), second-stage discharge valve leakage (DVL), intercooler leakage (ICL), discharge to tank storage pipeline leakage (PLL), and a combined fault of the discharge valve and pipeline leakage (DVL&PLL) under the tank pressure levels specified above.

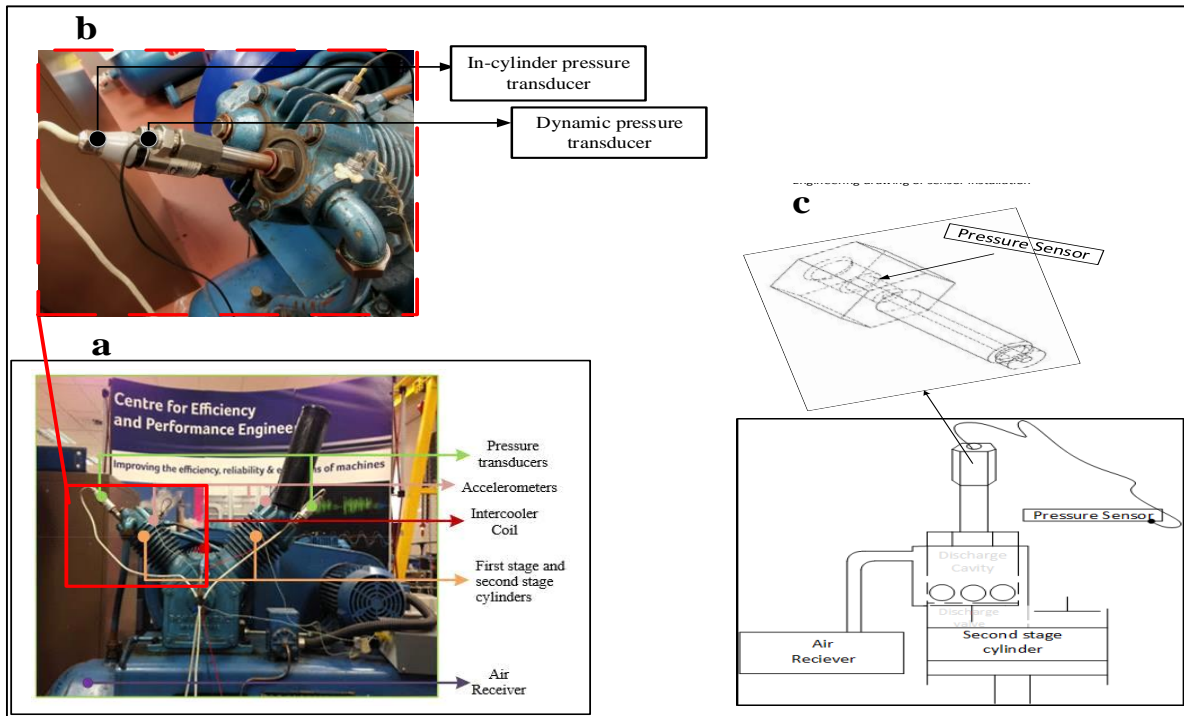


FIGURE 8.1: A) EXPERIMENTAL TEST RIG SETUP OF THE RECIPROCATING COMPRESSOR B) HIGH-PRESSURE CYLINDER WITH SENSOR INSTALLATIONS, C) SCHEMATIC OF ACOUSTIC SENSOR INSTALLATION

The DVL and ICL faults have been described in chapter four section 4.6. PLL is seeded by loosening the nut connecting the second-stage discharge chamber to the tank air receiver. While the combined fault (DVL+PLL) data is collected when the two faults are in effect.

8.2 Time Domain Analysis

A typical one-revolution time domain analysis of the gas pulsation signal from the second-stage discharge chamber of the reciprocating compressor used for this study is shown in Figure 8.2a). It is difficult to determine the four compression process (suction, compression, discharge, and expansion) from this plot; therefore, the gas pulsation signal is plot against the In-cylinder pressure signal in Figure 8.2b).

The four processes, which are triggered by valve events namely: suction valve opening (SVO) and closing (SVC), discharge valve opening (DVO) and closing (DVC) are not easily discernible from the airborne (gas) acoustic signal. The only clear process is the discharge process, which has significantly high amplitudes.

Figure 8.3 shows the time domain waveforms of raw pulsation signals from the reciprocating compressor operating under normal conditions at several tank pressures (0.275 MPa, 0.413 MPa, 0.620, and 0.827 MPa). This waterfall plot presents a clearer view of the pressure acoustic

signal for one cycle. The most apparent difference in this graph is the increases in peak amplitudes as the discharge pressure increases. Furthermore, delays in the discharge valve opening times for different discharge pressures are clearly shown in red. These delays in discharge valve opening times are due to increasing pressure difference across the valve as the storage tank pressure increases. Furthermore, it is observed that for lower tank pressures (0.275 MPa and 0.413 MPa), the second ring count has the highest amplitude while for the other two high tank pressures (0.62 MPa and 0.827 MPa); the first ring count has the highest amplitude.

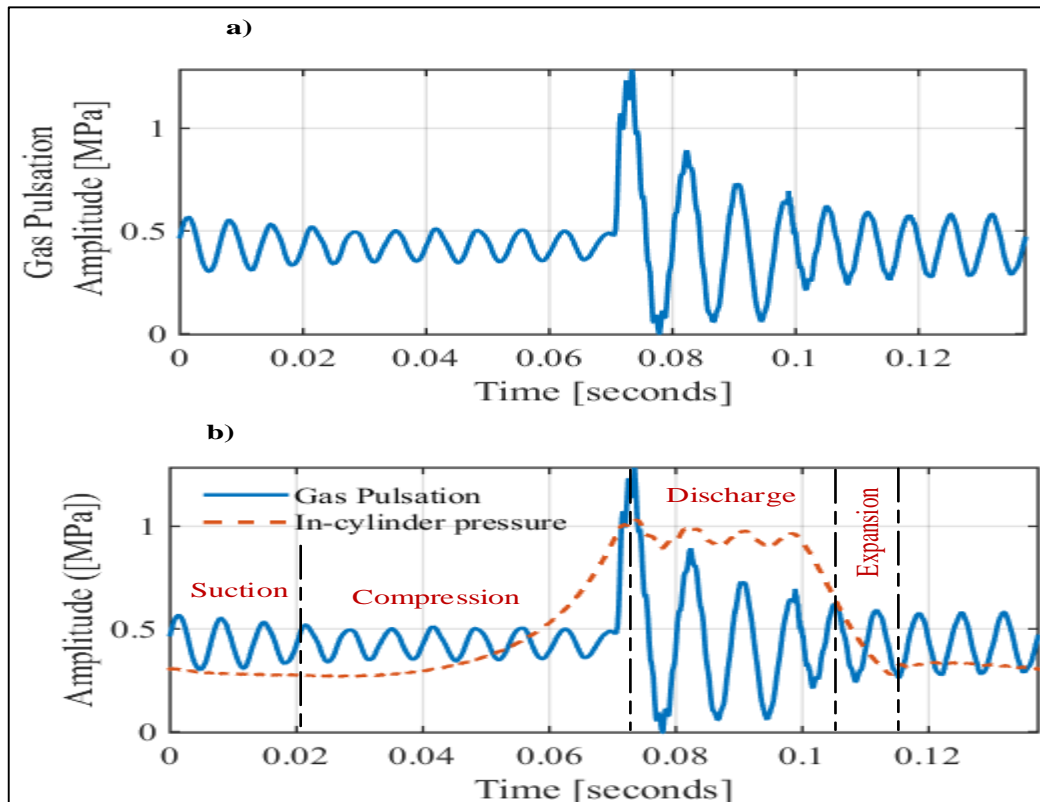


FIGURE 8.2: HEALTHY A) TIME DOMAIN OF GAS PULSATION SIGNAL, B) GAS PULSATION AND IN-CYLINDER WAVEFORMS, IDENTIFYING THE FOUR COMPRESSOR PROCESSES.

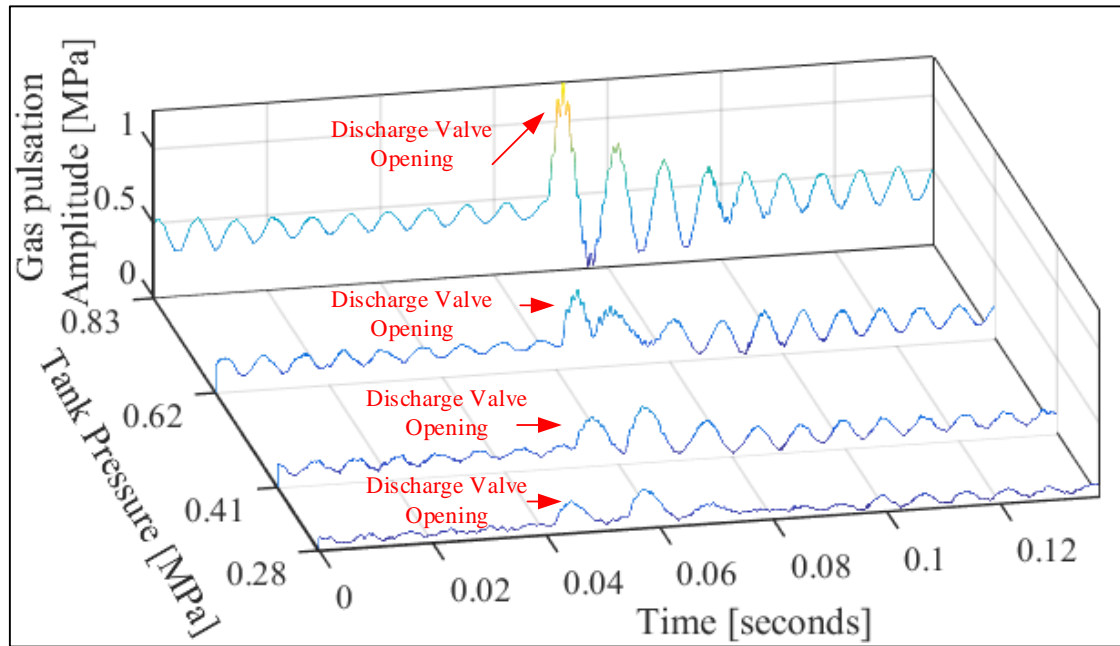


FIGURE 8.3: ONE CYCLE WAVEFORM OF GAS PULSATION SIGNALS AT SEVERAL TANK PRESSURES

8.2.1 Gas Pulsation Time Domain Waveform for Fault Cases

The waveform of the four fault cases and healthy case studied are compared in the waterfall plots for each discharge pressure range investigated. Table 8.1 summarises the observed differences between healthy condition and fault cases for all studied discharge pressure ranges. From the observations, it can be concluded that the differences between healthy and fault, although evident by comparing waveforms, are not sufficient and clear enough to confidently detect the common reciprocating compressor faults studied across the wide discharge pressure range.

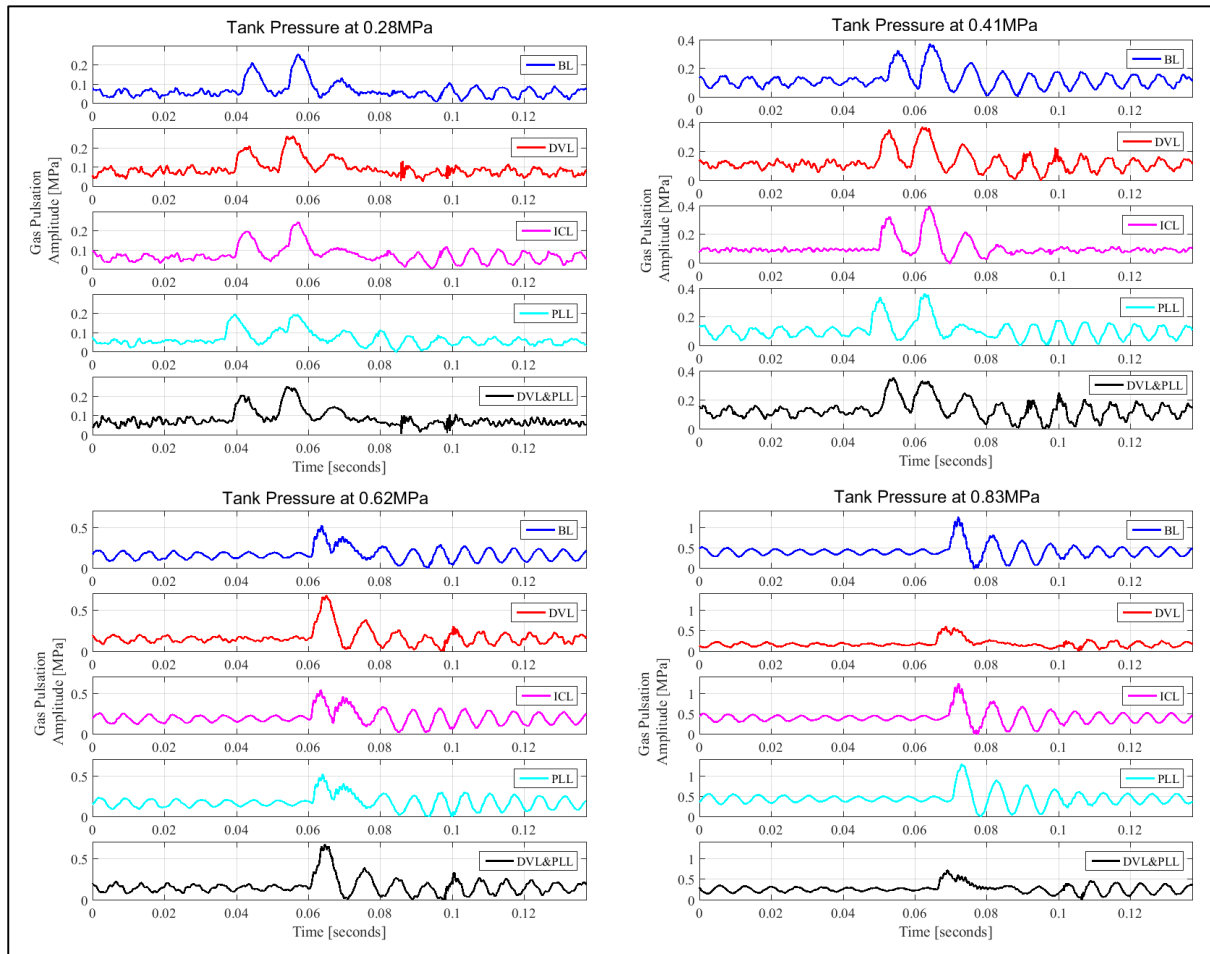


FIGURE 8.4: GAS PULSATION WAVE COMPARING NORMAL AND FAULT CONDITIONS AT SEVERAL DISCHARGE PRESSURES

TABLE 8.1: SUMMARY OF DIFFERENCES BETWEEN NORMAL AND FAULT CASES OF AIRBORNE ACOUSTIC WAVEFORM AT SEVERAL TANK PRESSURES

Cases	Discharge Pressure at 0.28MPa
BL	The second pulse from the discharge valve opening time has the greatest amplitude (0.252). The discharge valve opens at 0.044 seconds for BL case.
DVL	The amplitude of the second pulse from the discharge valve opening time is almost the same as BL (0.264). The discharge valve opens at 0.043 seconds. Two short impulsive events are seen just before the discharge valve closes at 0.1 seconds.
ICL	The second pulse from the discharge valve opening time has the greatest amplitude of 0.245. The discharge valve opens at 0.043 seconds.
PLL	The waveform of PLL is significantly different from the other cases at the second count (pulse) from the discharge valve opening time. In addition, the amplitude of the second count is lower (0.196) compared to other cases. The discharge valve opens at 0.039 seconds.

CHARACTERISING VIBRO-ACOUSTIC SIGNALS OF A RECIPROCATING
COMPRESSOR FOR CONDITION MONITORING

DVL&PLL	The second pulse from the discharge valve opening time also has the greatest amplitude of 0.254. The discharge valve opens at 0.041 seconds, and two small impulsive events are evident at the end of discharge process.
	Discharge Pressure at 0.41MPa
BL	The second pulse from the DVO time has the greatest amplitude (0.374). The waveform seems to have less noise and appears smoother compared to fault cases. The DVO time for BL is at 0.055 seconds
DVL	The amplitude of the second pulse from the DVO time is the same as that of BL at 0.374. However, two short impulsive events are present just before the discharge valve closes. These events are caused by the discharge valve impact on the valve seat as the process comes to an end. The DVO time for DVL is at 0.052 seconds slightly earlier than BL
ICL	The amplitude of the second pulse from the DVO time has the greatest overall amplitude at 0.392 compared to other cases. Like the DVL fault case, two short impulsive events can be seen during discharge valve closing times but of a smaller magnitude. The DVO time for ICL is at 0.053 seconds again slightly earlier than BL
PLL	The amplitude of the second pulse from the DVO time decreased somewhat for PLL fault case (0.3575) compared to normal (BL). The DVO time for PLL is at 0.050 seconds noticeably earlier than BL
DVL&PLL	The amplitude of the first pulse from the DVO time has the greatest peak rather than the second count, which has been observed for other cases. The DVO time is at 0.054 seconds
	Discharge Pressure at 0.62MPa
BL	The first pulse from the DVO time has the greatest peak value at 0.525.
DVL	The DVO time amplitude is 0.682, slightly higher than the healthy case. A short impulsive event can be observed on the waveform during the discharge valve closing time.
ICL	The DVO time amplitude of 0.536 is almost the same level as BL case.
PLL	The DVO time amplitude at 0.516 reduced slightly for PLL fault case.
DVL&PLL	The peak DVO time for the combined fault is at 0.673, slightly higher than BL. In addition, a short burst of impulse can be observed on the waveform during the discharge valve closing time.
	Discharge Pressure at 0.83MPa

BL	The peak DVO amplitude at 1.25MPa occurs at 0.07 seconds during normal condition (BL)
DVL	The highest DVO amplitude reduces to 0.61MPa and occurs 0.01 seconds earlier at 0.06 seconds than BL. Furthermore, the pressure levels decrease significantly after the peak count. Moreover, two short impulsive events are present during valve closing time.
ICL	The highest DVO amplitude at 1.23MPa occurs at 0.07 seconds.
PLL	The maximum DVO amplitude of 1.27MPa is slightly higher than BL case and opens at 0.07 seconds.
DVL&PLL	The maximum DVO amplitude reduces to 0.7MPa and occurs 0.01 seconds earlier at 0.06 seconds than BL. The waveform is very similar to that of DVL.

8.3 Conventional Statistical Measures from Time Domain Signal

8.3.1 Probability Density Function

Figure 8.5 shows the Probability Density Function (PDF) of the gas pulsation signal for several discharge pressures under normal (BL) condition. It is clear from the plot that the PDF amplitudes reduces and broadens as the pressure increases following a linear trend. However, in Figure 8.6 where the PDF curves of each discharge pressure (DP) range is plotted for all fault cases and healthy case (BL), the peaks for signals measured at maximum DP (0.82MPa) had the most visible significant variance compared to other DP levels.

Figures 8.7 shows the comparison of healthy and all fault PDF peak values at several discharge pressures. From the plot, it can be concluded that PDF peak is not a suitable fault indication tool for the reciprocating compressor faults examined, as there is no apparent trend in PDF peak values across the discharge pressure range for all faults studied.

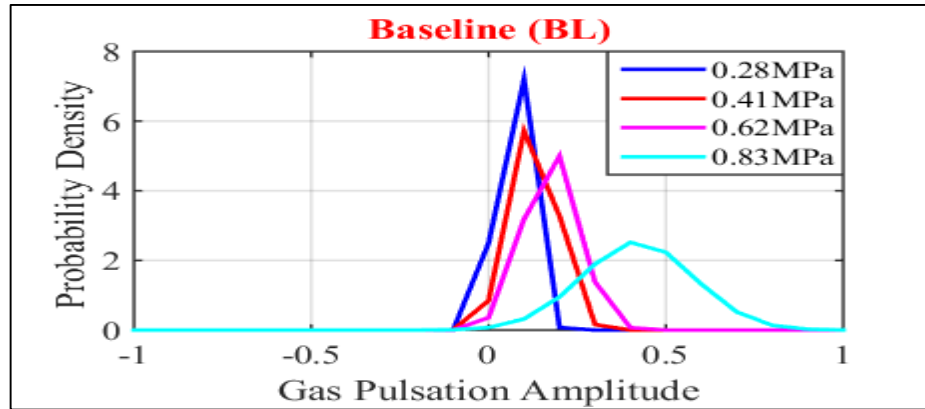


FIGURE 8.5: PDF CURVE OF NORMAL (BL) GAS PULSATION SIGNAL FOR DIFFERENT DPs

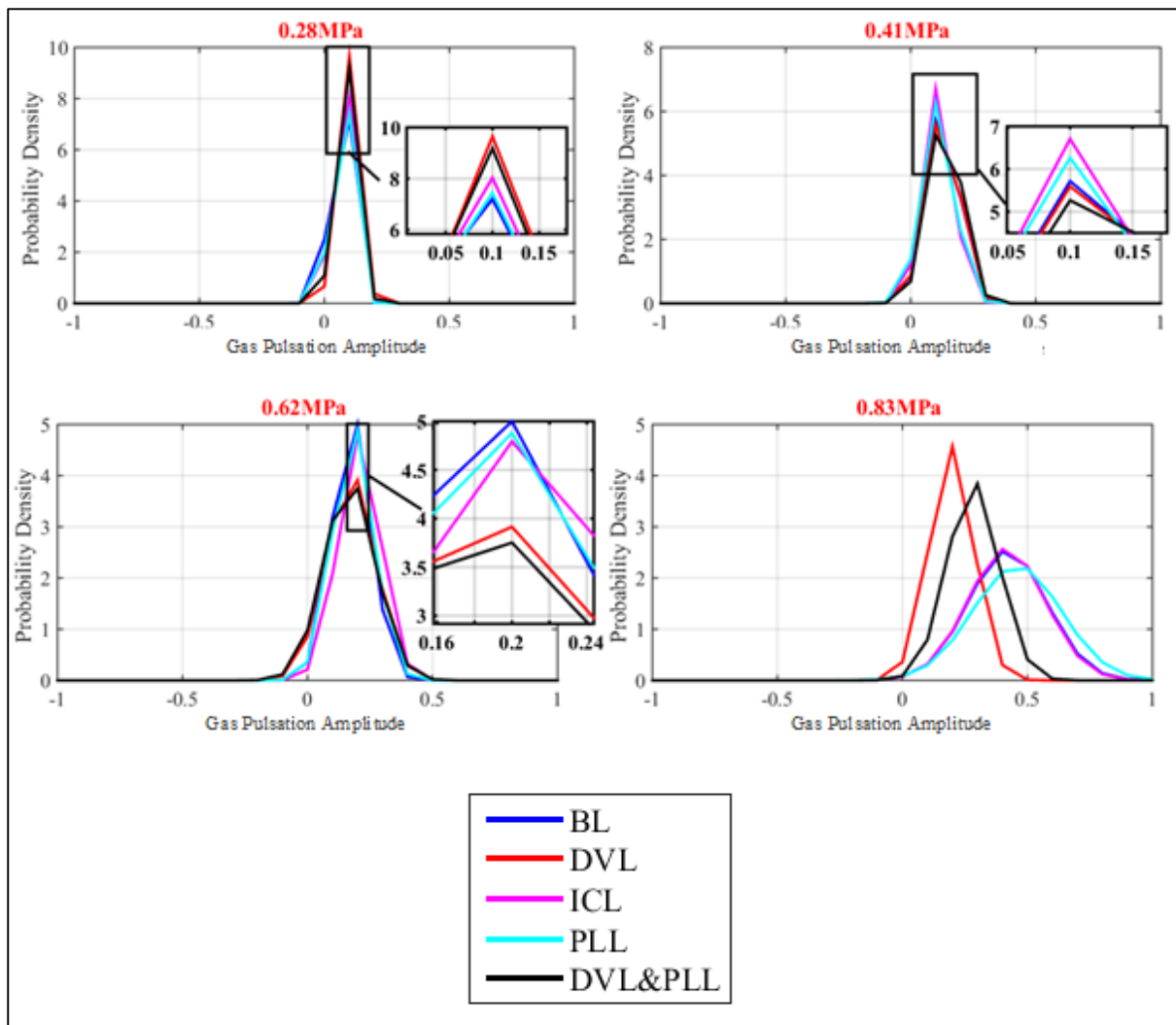


FIGURE 8.6: PDF FAULT COMPARISON CURVES FOR GAS PULSATION SIGNALS AT SEVERAL DPs

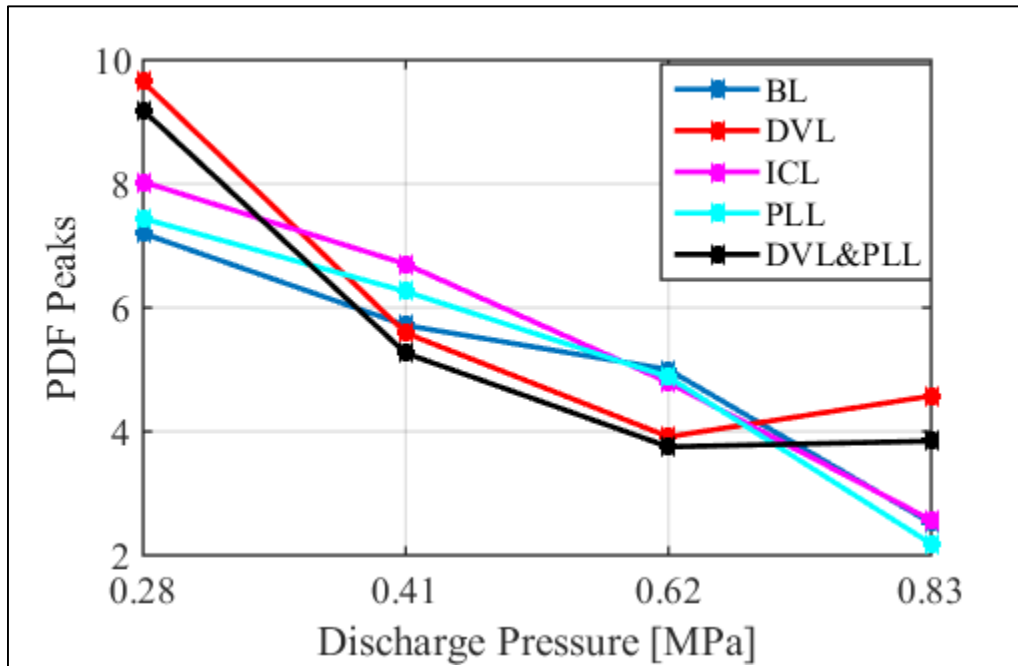


FIGURE 8.7: COMPARISON OF HEALTHY AND FAULT PDF PEAKS FOR SEVERAL DISCHARGE PRESSURES

8.3.2 Root Mean Square and Kurtosis

Figures 8.8 and 8.9 show the RMS and kurtosis plots respectively, for the different discharge pressures; comparing results of all fault cases including healthy (BL) signal. It is observed from Figure 8.8 that the RMS values increase gradually with increasing discharge pressure at 0.28MPa, 0.41MPa, and 0.62MPa for all cases. However, at 0.83MPa, there is a slight fall in the RMS values for DVL and DVL&PLL. Moreover, there are no clear variances in the RMS values of healthy and faulty cases across all discharge pressures.

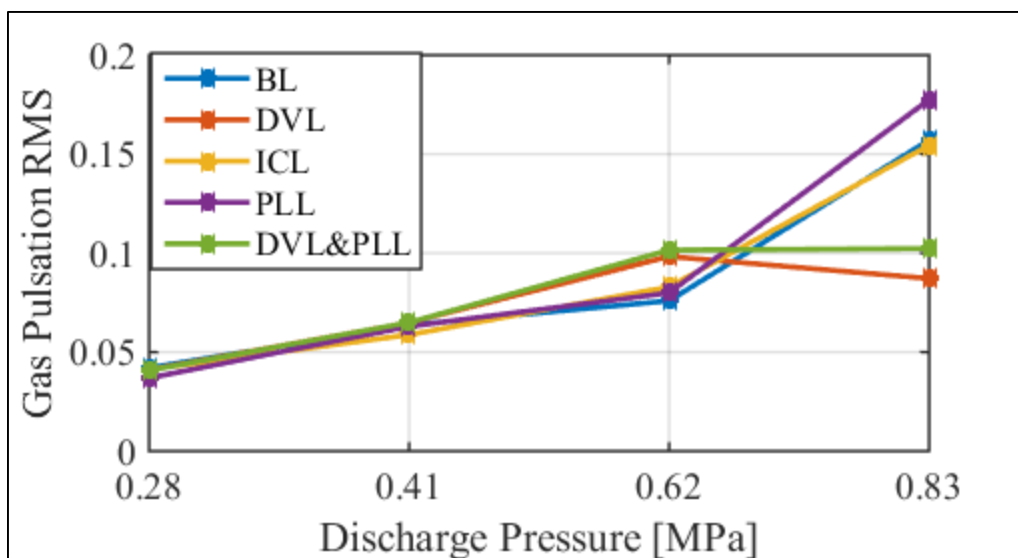


FIGURE 8.8: RMS OF GAS PULSATION SIGNAL AGAINST FAULT CASES AT SEVERAL DISCHARGE PRESSURES

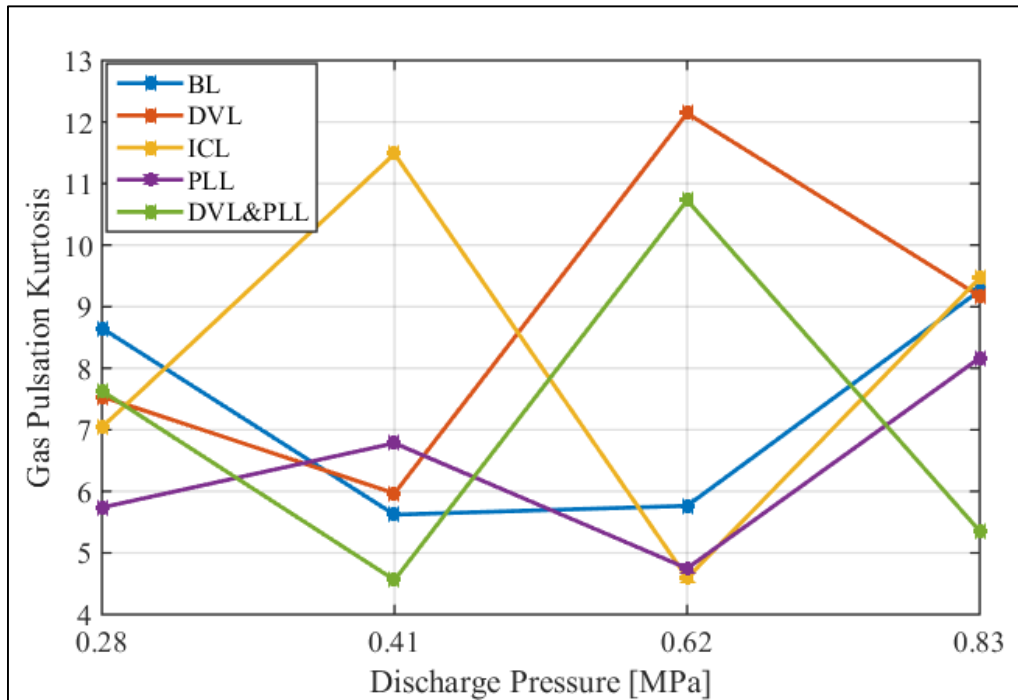


FIGURE 8.9: KURTOSIS OF GAS PULSATION SIGNAL AGAINST SEVERAL DISCHARGE PRESSURES FOR ALL CASES

Observing Figure 8.9, the kurtosis of the signals for all cases are greater than the normal Gaussian distribution, which is 3 (Kwok, 2018), and are therefore classed as heavily tailed. The kurtosis values are randomly distributed and do not show any trend distinguishing the healthy case from fault cases.

8.4 Frequency Domain Analysis

Figure 8.10 shows the differences between frequency components from the acoustic pressure pulsations of the reciprocating compressor under several Discharge Pressures (DP). The spectrum is characterised by discrete components and broadband noise. For the reciprocating compressor, the fundamental frequency usually corresponds to the rotational speed of the compressor at 7.28Hz, and its harmonics make up the discrete components in the spectrum. The acoustic wave energy is concentrated in the low-frequency regions seen in Figure 8.10. Therefore, the frequency analysis is tailored to low frequency region (0 to 2500Hz).

The waterfall plots of healthy and fault frequency spectra of each DP are presented in Figures 8.11. The differences in sound pressure levels are not very obvious from these waterfall plots. However, several resonant modes can be seen. The most obvious is at the maximum discharge pressure (0.82MPa). In order to analyse the source of sound waves generated at the compressor head, a scale of one-third octave bands are developed to split the spectrum into specific range of frequencies giving a more detailed view of the sound spectrum compared to the 1/1 octave

band splitting. The root mean square powers of each centre frequency is computed and presented in Figure 8.12 for all discharge pressures. The sound pressure level (SPL) is determined by the following equation:

$$SPL = 20\log(P/P_0) \text{ dB} \quad (8.1)$$

Where P is the sound pressure in Pascal and P_0 is the reference sound pressure of 0.00002 Pascal which is equivalent to 0dB.

The RMS power of each band is defined as the sum of the absolute square of the centre frequency band signals divided by the signal length.

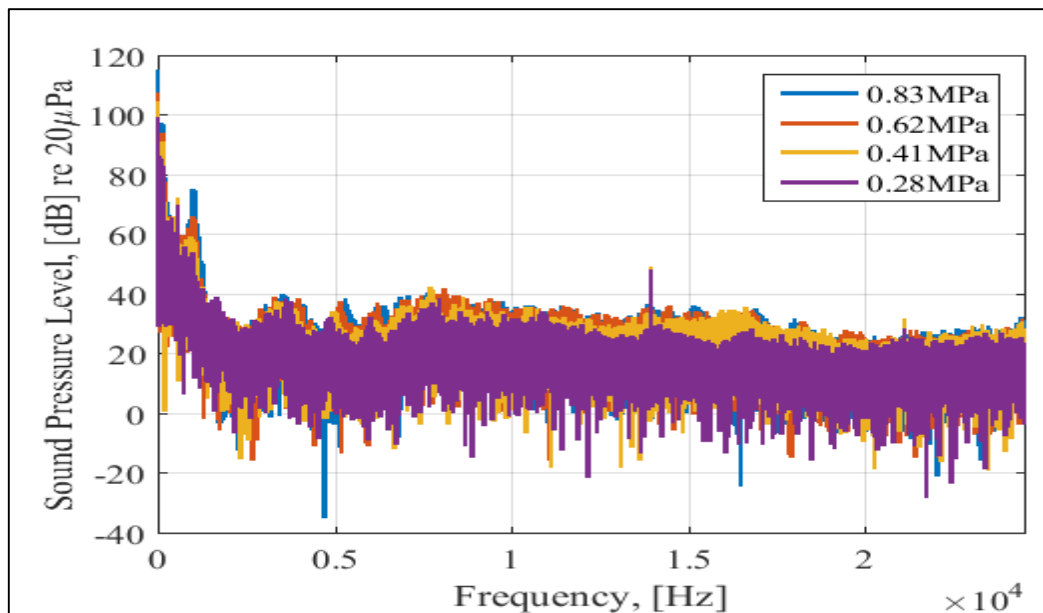


FIGURE 8.10: SOUND PRESSURE LEVEL OF GAS PULSATION SIGNALS UNDER NORMAL CONDITION (BL) FOR SEVERAL DISCHARGE PRESSURES

Table 8.2 presents the full 1/3rd octave bands with lower, centre and upper frequency values. The comparison of healthy and all fault RMS power level values at several discharge pressures are presented in Figure 8.13. In Figure 8.13, it can be seen that band 22 and 23 (corresponding to frequency 500 Hz and 630 Hz) gives the best separation, where the RMS power level of DVL and DVL&PLL fault cases are well above that of healthy case as seen in Figure 8.14. The RMS power levels for ICL and PLL fault cases do not vary significantly from healthy (BL) case. The one-third octave band analysis can be used as a possible fault indication tool, however, a more robust technique is needed for better understanding and efficient fault classification of the gas pulsation spectrum.

CHARACTERISING VIBRO-ACOUSTIC SIGNALS OF A RECIPROCATING COMPRESSOR FOR CONDITION MONITORING

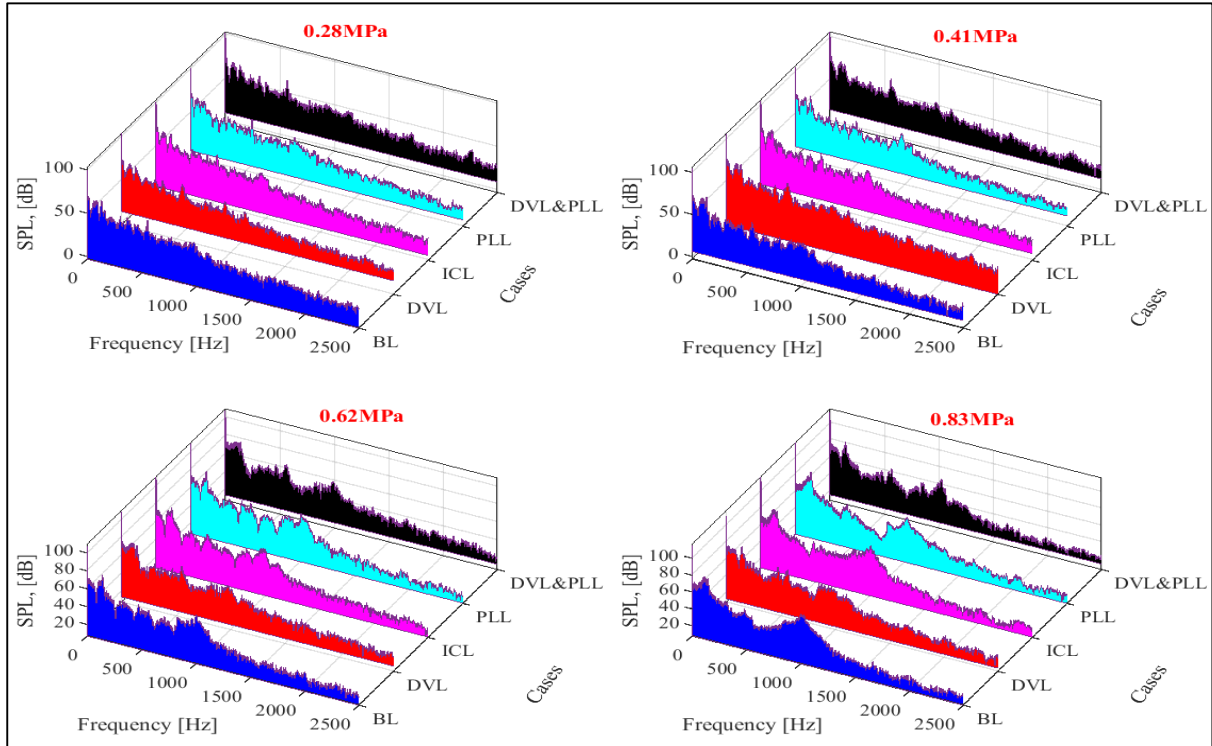


FIGURE 8.11: WATERFALL PLOT OF HEALTHY AND FAULT FREQUENCY SPECTRUM AT SEVERAL DISCHARGE PRESSURES

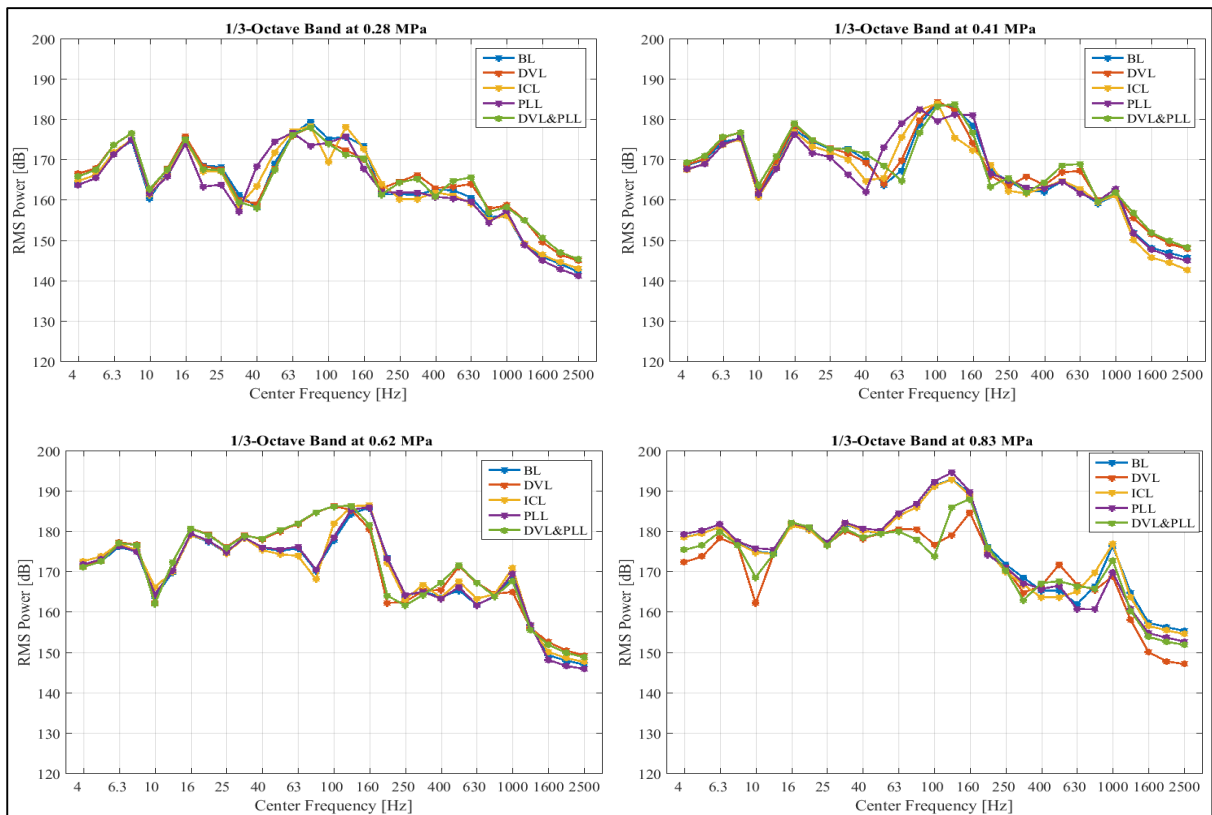


FIGURE 8.12: 1/3 OCTAVE BAND SPECTRA OF HEALTHY AND ALL FAULT CASES AT SEVERAL DISCHARGE PRESSURES

CHARACTERISING VIBRO-ACOUSTIC SIGNALS OF A RECIPROCATING
COMPRESSOR FOR CONDITION MONITORING

TABLE 8.2: 1/3RD OCTAVE BAND FREQUENCIES

Band No.	Low Frequency	Centre Frequency	High Frequency	Band No.	Low Frequency	Centre Frequency	High Frequency
1	3.55	4	4.45	16	110	125	140
2	4.45	5	5.6	17	140	160	180
3	5.6	6.3	7.1	18	180	200	225
4	7.1	8	8.9	19	225	250	280
5	8.9	10	11	20	280	315	355
6	11	12.5	14	21	355	400	445
7	14	16	18	22	445	500	560
8	18	20	22.5	23	560	630	710
9	22.5	25	28	24	710	800	890
10	28	31.5	35.5	25	890	1000	1100
11	35.5	40	44.5	26	1100	1250	1400
12	44.5	50	56	27	1400	1600	1800
13	56	63	71	28	1800	2000	2250
14	71	80	89	29	2250	2500	2800
15	89	100	110				

CHARACTERISING VIBRO-ACOUSTIC SIGNALS OF A RECIPROCATING COMPRESSOR FOR CONDITION MONITORING

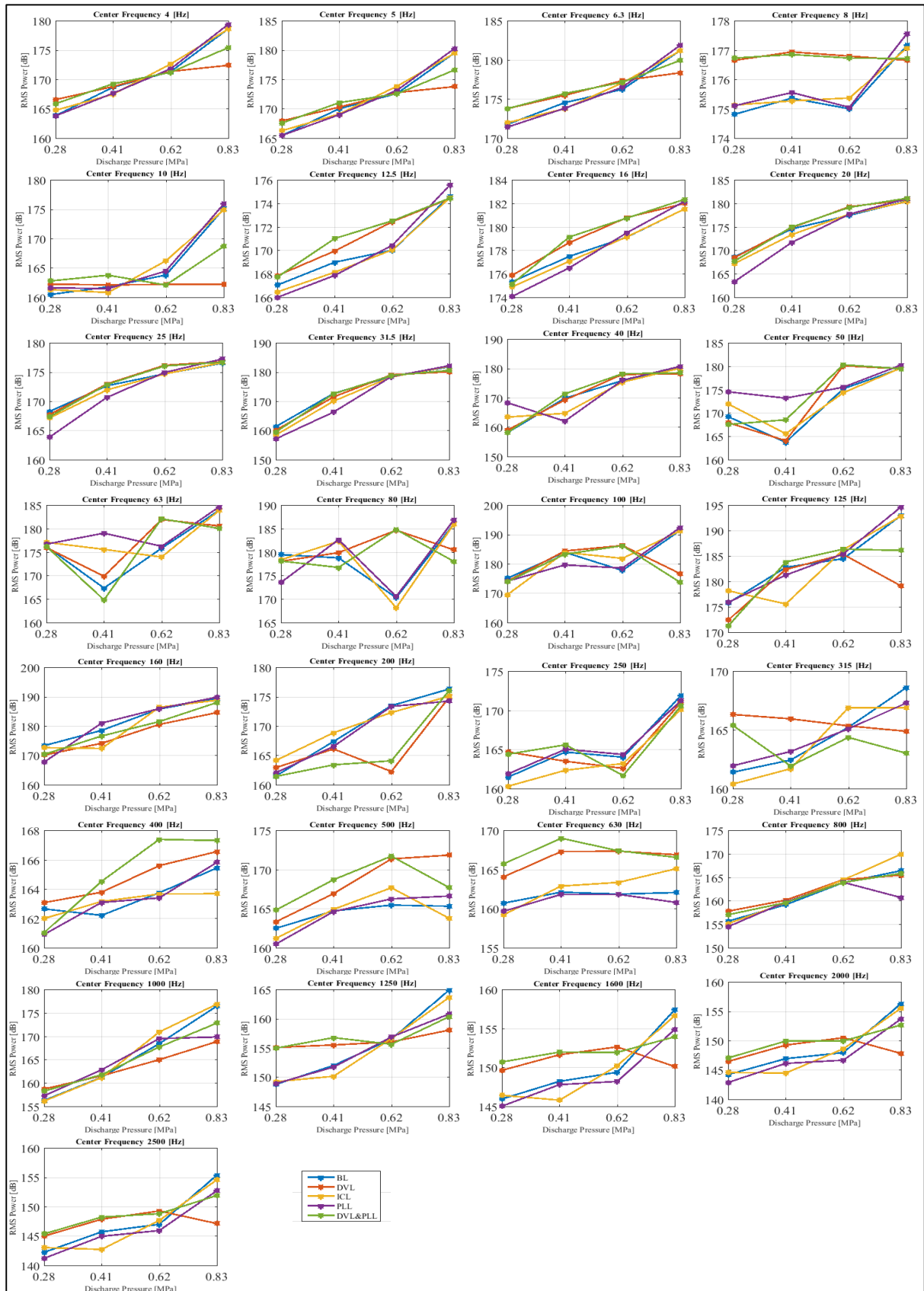


FIGURE 8.13: HEALTHY AND FAULT COMPARISON OF 1/3RD OCTAVE BAND RMS POWER AT SEVERAL TANK PRESSURES

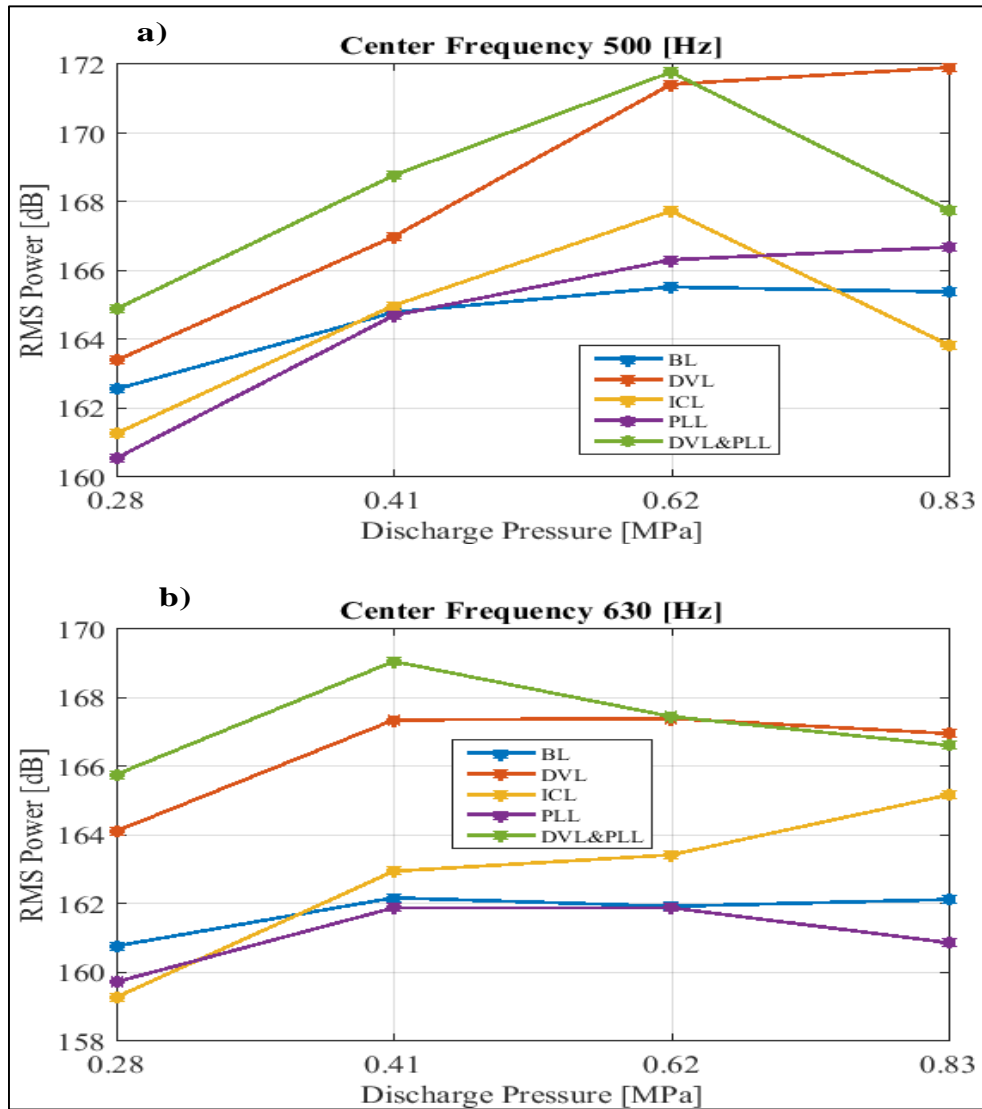


FIGURE 8.14: OCTAVE BANDS WITH BEST FAULT SEPARATION

CHAPTER NINE

9 ANALYSIS OF VIBRATION SIGNAL USING WAVELET PACKET TRANSFORM WITH ENVELOPE ANALYSIS

This chapter presents the analysis of vibration signal from a two-stage reciprocating compressor using wavelet packet transform and envelope analysis. Vibration signal from a reciprocating compressor are non-stationary and consists of impulsive events, which are mostly from high turbulent flow excitations, and mechanical valve impacts. This is why conventional signal processing techniques are unsuitable for condition monitoring of vibration signals from a reciprocating compressor. Therefore, wavelet packet transform is used to extract the time-frequency information of the signal and envelope analysis of the reconstructed signal is computed for fault classification of three common reciprocating compressor fault cases (second-stage discharge valve leakage, intercooler leakage, and a combination of the two faults) using the fundamental frequency and the its third harmonic frequency.

9.1 Theoretical Background of Wavelet Transform

Wavelet transform is the stretching and compressing of a short wavy function over a given signal to obtain its frequency and time information in one domain for monitoring purposes wavelet packet transform (WPT). The wavelet transform has an adaptive and multi-resolution capability, which makes it a powerful mathematical and signal processing tool for determining the operating conditions of several machines. Wavelet transform is applicable to areas such as image processing, pattern recognition, computer graphics, submarine detection, medical image technology and many more.

9.1.1 Continuous Wavelet Transform (CWT)

Continuous wavelet transform (CWT) was developed to correct the noted failures of the Fourier analysis as described in the introduction section (9.1). However, because the wavelet coefficients at every scale is calculated, a lot of repetitive information is generated causing a longer computational time (Al-Badour, Sunar, & Cheded, 2011). The term scale is used instead of frequency and translation instead of time. Continuous wavelet transform of a given signal $s(t)$ is given as (Peng & Chu, 2004):

$$CWT(a, b; \psi) = a^{-1/2} \int s(t) \psi^* \left(\frac{t-b}{a} \right) dt \quad (9.1)$$

a represents the scaling parameter, b is the translation parameter, $\psi(t)$ is the mother wavelet, and $*$ is the complex conjugate of the mother wavelet.

9.1.2 Discrete Wavelet Transform (DWT)

Mallat used the conjugate quadratic filters (CQF) to create the algorithm for DWT. The application of DWT is faster than CWT and has fewer parameters. DWT has a better time-frequency resolution, and the frequencies are localised accurately in time. DWT is achieved by the discretisation of CWT; the given signal $s(t)$ is decomposed into low-pass approximation coefficients and high-pass detail coefficients, and then on next levels only the approximation coefficients are decomposed into low-pass approximation and the high-pass details keeping the high-pass coefficients on subsequent levels as presented in Figure 9.1. The discretisation of the scale a and translation b parameters are as follows:

$$a = a_0^n, \quad b = m_{d_0}^n b_0 \quad (9.2)$$

Where n and m are integers, therefore the continuous wavelet function in equation (9.1) becomes the discrete wavelets and the discretisation of the scale and time parameter gives the DWT in equation (9.2) below

$$DWT(m, n; \psi) = a_0^{-m/2} \int s(t) \psi * (a_0^{-m} t - nb_0) dt \quad (9.3)$$

The disadvantage of DWT is that the high-frequency information which might contain fault features is lost because subsequent detail coefficients are not decomposed.

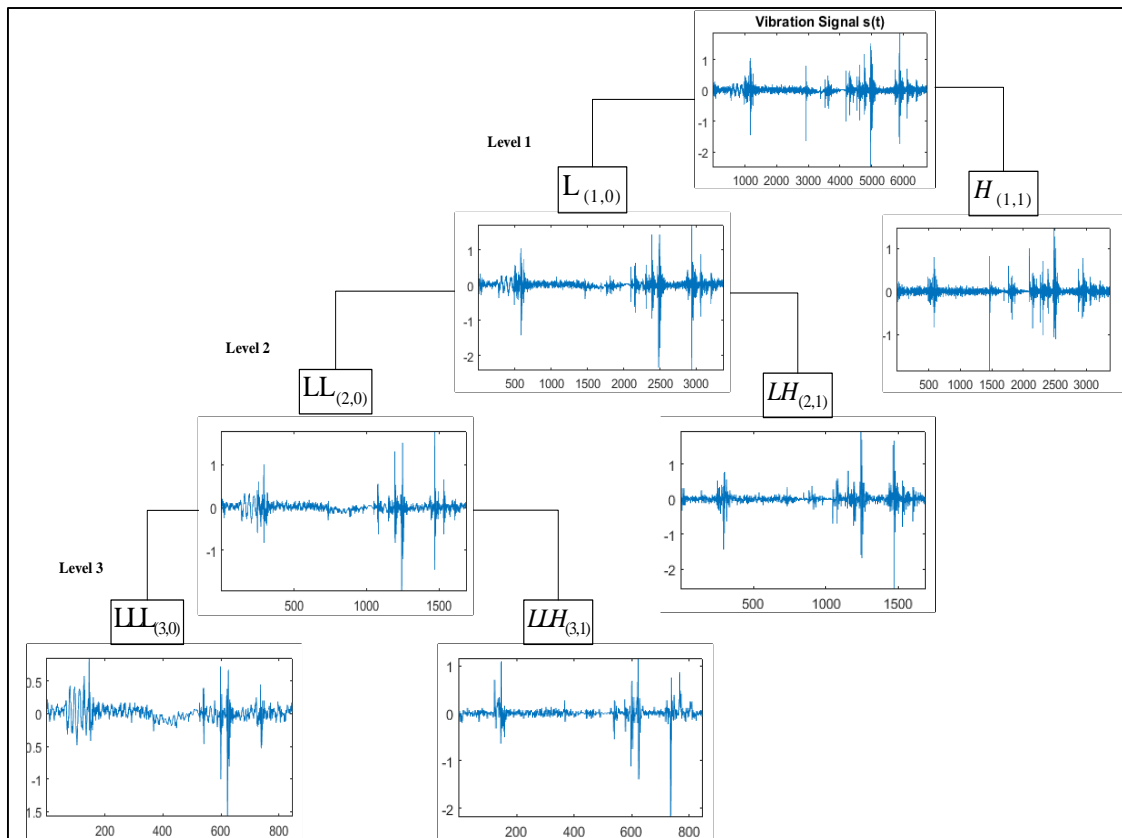


FIGURE 9.1: THREE LEVELS DISCRETE WAVELET DECOMPOSITION TREE

9.1.3 Wavelet Packet Transform (WPT)

Coifman, Meyer, and Wickerhauser extended the DWT to Wavelet packet transform in 1992. WPT has been found to be a more efficient tool because both low and high frequency components are decomposed on every level of the decomposition tree (Bendjama, Bouhouche, & Boucherit, 2012). Figure 9.2 illustrates a 3-level WPT decomposition tree with L representing the low-frequency approximation coefficients and H high-frequency detail coefficients. The original signal $s(t)$ is convoluted with both low and high pass filters and down-sampled by two to give approximate coefficients $L_{(1,0)}$, and detail coefficients $H_{(1,1)}$ with

length half the size of the original signal. The low pass and high pass filters are applied again to the decomposed signal in level two to give four sub-bands ($LL_{(2,0)}, LH_{(2,1)}, HL_{(2,2)}, HH_{(2,3)}$) of decomposed signals with one-fourth the signal length (Saleh & Rahman, 2005). The process is repeated until all levels are decomposed. The wavelet packet has three integers i, n , and m , which represent the modulation, scale and translation parameters respectively. The wavelet functions are determined from the recursive equations given below (Rafiee, Tse, Harifi, & Sadeghi, 2009)

$$\psi^{2n}(t) = \sqrt{2} \sum_{-\infty}^{\infty} h(m) \psi^i(2t - m) \quad (9.4)$$

$$\psi^{2n+1}(t) = \sqrt{2} \sum_{-\infty}^{\infty} g(m) \psi^i(2t - m) \quad (9.5)$$

The original signal $s(t)$ after n level of decomposition is defined as:

$$s(t) = \sum_{i=1}^{2n} s_n^i(t) \quad (9.6)$$

While the wavelet packet signal is given as follows:

$$s_n^i(t) = \sum_{m=-\infty}^{\infty} c_{n,m}^i(t) \psi_{n,m}^i(t) \quad (9.7)$$

Where the wavelet packet coefficients $c_{n,m}^i(t)$ are calculated by (Rafiee, Tse, Harifi, & Sadeghi, 2009):

$$c_n^i(t) = \int_{-\infty}^{\infty} s(t) \psi_{n,m}^i(t) dt \quad (9.8)$$

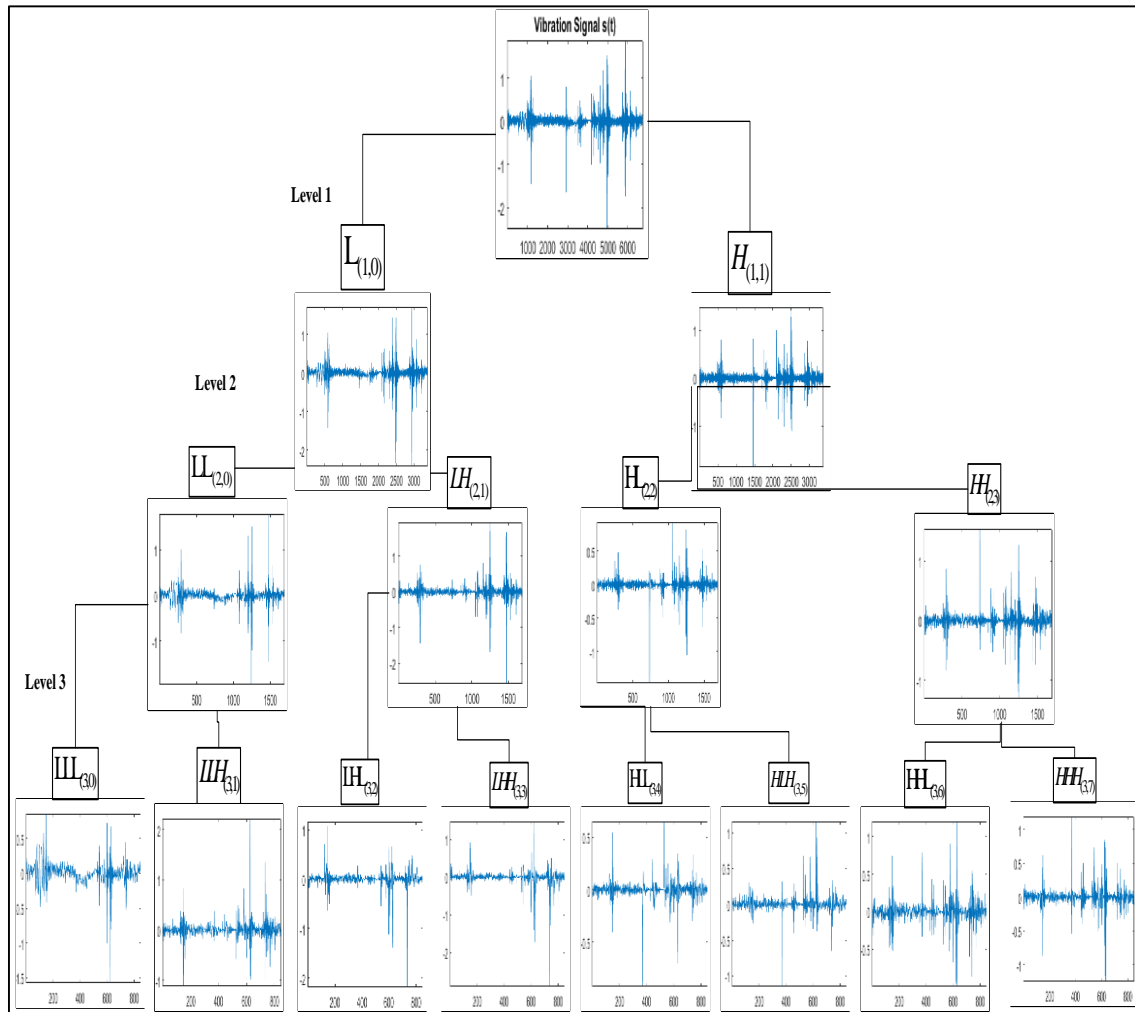


FIGURE 9.2: ILLUSTRATION OF THREE LEVEL WAVELET PACKET TRANSFORM DECOMPOSITION TREE

9.2 Selecting Mother Wavelet

There are several types of mother wavelets used for signal transformation and they are classified as either orthogonal, biorthogonal, or nonorthogonal (chui, 1997). The orthogonal wavelet families include Daubechies, Coiflet, and Symlet, while B-Spline is classed as biorthogonal wavelet. Morlet and Mexican Hat fall under the non-orthogonal wavelet class (chui, 1997); (Zaman, 2003). Until date, there are no standardised guidelines for selecting the best mother wavelet or scale level for any particular application (Chrfi, ALHaddad, & Francois , 2004). Charfi et al. used Daubechies (db4) to investigate the characteristics of an incipient fault in a three-phase induction motor drive after analysing several mother wavelets (Chrfi, ALHaddad, & Francois , 2004). Bendjama et al. found Daubechies₄ (Db4) to be more effective for diagnosing faults from vibration signals (Bendjama, Bouhouche, & Boucherit,

2012); also, findings by Al-Badour et al., found that Daubechies and Meyer to be the best mother wavelets for transient vibration signals (Al-Badour, Sunar, & Cheded, 2011).

It is important to choose the optimal mother wavelet for any particular application because studies have found that the choice of mother wavelet will affect results obtained by the wavelet packet transform (Chrfi, ALHaddad, & Franqois , 2004). Kumar and Sriram mentioned in their study on selecting optimal mother wavelet that scholars' (Yan R. , 2007), and (Gao & Yan, 2011) employed two approaches when selecting the best wavelet basis (Kankar, Satish, & Harsha, 2011). A qualitative approach, which is based on the properties of the mother wavelet (such as orthogonality, compact support, symmetry, and vanishing moment) and the signal shape similarity to the chosen mother wavelet. The second approach is based on quantitative means, which is much easier to implement compared to visual matching of signal shape to mother wavelet (Kumar, Srinivasa, Sriram, & Vijay, 2014). In recent years, several researchers have studied quantitative means greatly. For instance, Ruqiang used energy to entropy ratio and mini-max information criterion to choose an optimal wavelet basis for bearing vibration signal. Kumar and his colleagues used minimum Shannon entropy criteria with maximum energy to Shannon entropy ratio criterion to determine the optimal mother wavelet for bearing vibration signal (Kumar, Srinivasa, Sriram, & Vijay, 2014).

For this study, Daubechies, Coiflet, Symlet, B-Spline and discrete Meyer wavelets were studied intensively based on trial and error. The Coiflet wavelet function with one vanishing moment (Coif1) was chosen because it gave the best fault separation result. Four levels of decomposition were implemented on the reciprocating compressor vibration signal using Coiflet wavelet. Level 4 decomposition was appropriate because higher levels did not give good time localisation and lower levels gave poor frequency resolutions. Care was taken in choosing the best wavelet packet node (frequency band); after several investigations the percentage energy was used to choose the best wavelet packet node, which offered maximum feature separation (Yen & Lin, 2000).

9.3 Envelope Analysis

Envelope analysis is a useful signal processing tool for monitoring machine condition. It is based on Hilbert transform $\hat{s}(t)$, which creates a special analytical signal of a complex function. Envelope analysis is achieved by first band pass filtering of the signal, then envelope extraction of the filtered signal using Hilbert transform is performed, and finally spectrum extraction of

the enveloped signal using Fast Fourier Transform (FFT) (Tse, Peng, & Yam, 2001); (Yaqub, Gondal, & Kamruzzaman, 2011). Hilbert transform equation of a given signal $s(t)$ can be defined as follows (Wang X. , 2006):

$$\hat{s}(t) = \left(s(t) * \frac{1}{\pi t} \right) = \frac{1}{\pi} \int_{-\infty}^{\infty} \frac{s(\tau)}{t - \tau} d\tau \quad (9.9)$$

It can be seen from equation (9.9) above that, the Hilbert function is a convolution with an impulse function $1/\pi(t)$. Envelope analysis is applied to the selected wavelet packet node to extract the characteristic features for fault classification of the vibration signal.

9.4 Experimental Setup

The experimental setup of the reciprocating compressor is described in chapter four section 4.2.1. Figure 8.1 presents a schematic of the reciprocating compressor rig setup with specifications of supporting components listed in Table 6.1.

Seven main sensors including two pressure transducers, two accelerometers, two thermocouples and an encoder are used for collecting vital data from this machine. One pressure transducer is seeded into each cylinder, one accelerometer mounted on each cylinder head, one thermocouple on each cylinder body and an encoder on the flywheel.

9.5 Test Procedure

The reciprocating compressor piston in the first cylinder travels from top-dead centre (TDC) to bottom-dead centre (BDC), atmospheric air is collected and filtered into the cylinder, as the piston moves back up to TDC the filtered air is compressed and eventually discharged into the intercooler when the pressure of the compressed air exceeds that in the intercooler. The high-pressured air released into the intercooler is cooled before entering the suction chamber of the second-stage cylinder, and as the piston of this cylinder travels back up to TDC, compressed air is discharged into the tank receiver once its pressure exceeds that in the receiver. The tank receiver stores the compressed air until the maximum pressure capacity is reached then the system shutdowns automatically if not stopped manually.

The sampling frequency is set at 49,019 Hz, and 32768 data samples are collected for five discharge pressures (0.55MPa, 0.83MPa). Vibration signal is only collected from the second-stage (high-pressure) cylinder because previous findings have found that the fault effects are more prominent from the high pressure cylinder. The cases investigated are: baseline (BL),

second-stage discharge valve leakage (DVL), intercooler leakage (ICL), and a combined fault of the second-stage discharge valve and intercooler leakages (DVL+ICL).

9.6 Results and Discussion

9.6.1 Traditional Time Domain and Frequency Domain Analysis

The RMS value is a popular statistical tool for identifying changes in machine condition. However, in cases where the signal contains information from multiple components, RMS computation might not be very efficient in detecting faults in certain cases as can be seen in Figure 7.7. Amplitude trends for investigated cases and tank pressures are random and therefore unsuitable for effective condition monitoring.

The vibration spectrum in Figure 9.3b and 9.4b, presents a broad picture of the frequency content of each signal. Individual frequency components and noise levels of the signal can be identified and tracked. Although, a simple spectrum analysis is not a very suitable technique for effectively analysing faults on a reciprocating compressor because of its non-stationary signal characteristics and high noise levels. However, useful information about the compressor dynamics can be obtained by examining the signal frequency content.

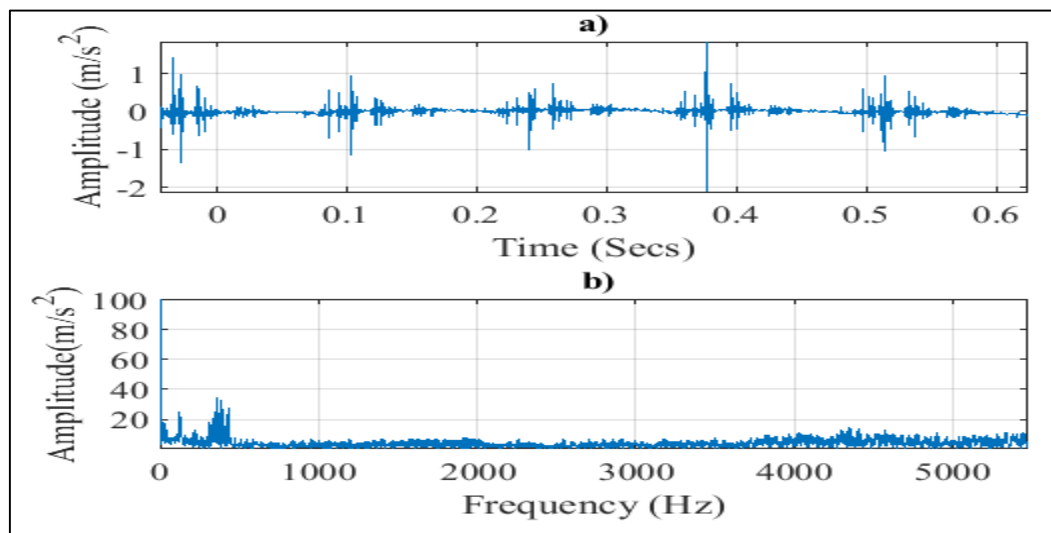


FIGURE 9.3: TIME WAVEFORM AND B) FREQUENCY SPECTRUM OF NORMAL (BL) VIBRATION SIGNAL AT 0.83MPa TANK PRESSURE

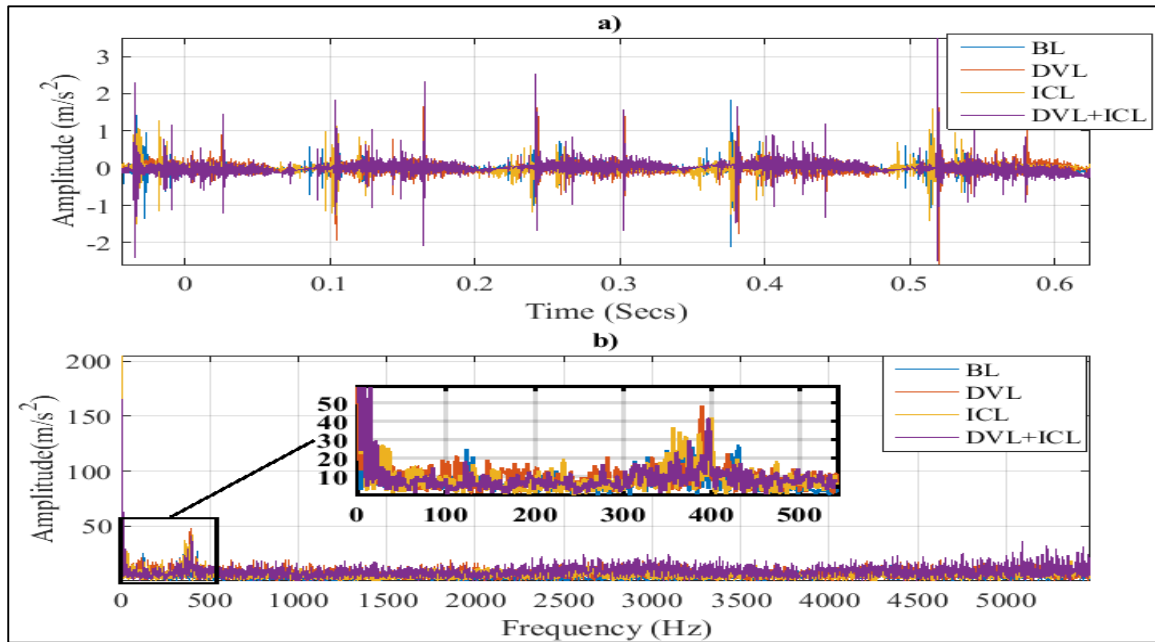


FIGURE 9.4: TIME WAVEFORM AND B) FREQUENCY SPECTRUM OF ALL CASES AT 0.83MPa TANK PRESSURE

9.6.2 Wavelet Packet Transform and Wavelet Packet Energy

As a pre-processing phase to wavelet packet application, the original vibration signal is resampled to reduce the decomposition levels required. Therefore, 10953 data points were collected for five cycles of vibration signal at a reduced sampling rate of 16384Hz. The resampled signal is decomposed as explained in section 9.2.3 using Coiflet 1 mother wavelet up to four levels. Level 4 gave the best result as higher levels required more computational time and gave poor time resolution as seen in Figure 9.5.

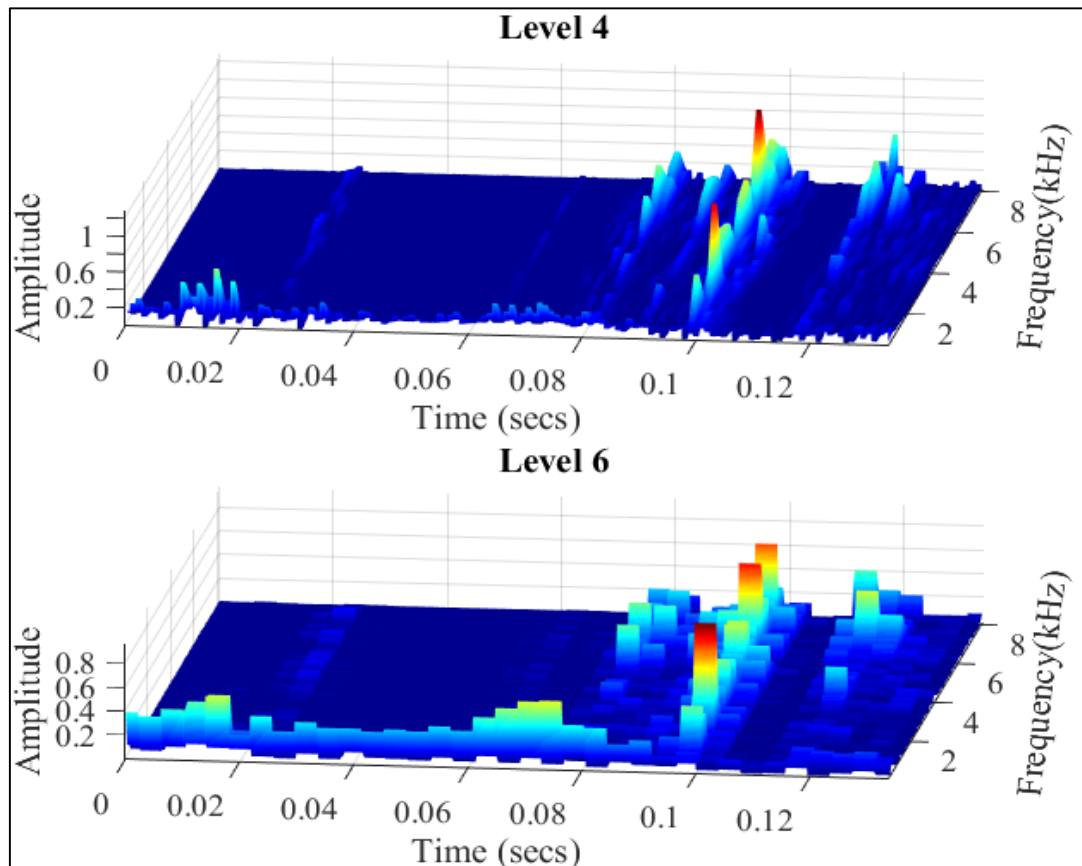


FIGURE 9.5: DECOMPOSED VIBRATION SIGNAL AT LEVEL 4 AND LEVEL 6

Sixteen terminal (last) nodes are obtained from the four-level decomposition and the frequency range of each terminal node is presented in Table 9.1.

Figure 9.6 presents the time-frequency plots, which shows information about changes in the spectral content of the signals with time. It can be observed that high energy is present mostly when the valve closes at about 0.1 seconds. From the plots of all four cases presented, it can be observed that, the amplitudes of DVL and DVL+ICL are greater than those of BL and ICL.

TABLE 9.1: TERMINAL NODE FREQUENCY RANGE

Terminal Nodes	Nodes	Frequency Range (Hz)	Terminal Nodes	Node	Frequency Range (Hz)
1	(4, 0)	0-512	9	(4, 8)	4096-4608
2	(4, 1)	512-1024	10	(4, 9)	4608-5120
3	(4, 2)	1024-1536	11	(4, 10)	5120-5632
4	(4, 3)	1536-2048	12	(4, 11)	5632-6144
5	(4, 4)	2048-2560	13	(4, 12)	6144-6656
6	(4, 5)	2560-3072	14	(4, 13)	6656-7168
7	(4, 6)	3072-3584	15	(4, 14)	7168-7680
8	(4, 7)	3584-4096	16	(4, 15)	7680-8192

The percentage energy of coefficients for terminal nodes are computed using Equation (9.10)

$$E(T) = 100 \times \left(\frac{\sum c_T^2}{\sum s^2} \right) \quad (9.10)$$

Where $\sum c_T^2$ is the energy of each terminal node and $\sum s^2$ is the energy of the original signal. Figure 9.7 shows the percentage energy of all terminal nodes for all cases and tank pressure ranges studied. The first node (4.0), which has the highest overall energy is reconstructed and used for envelope analysis. Envelope analysis of the vibration signal is computed as stated in section 9.4.

CHARACTERISING VIBRO-ACOUSTIC SIGNALS OF A RECIPROCATING COMPRESSOR FOR CONDITION MONITORING

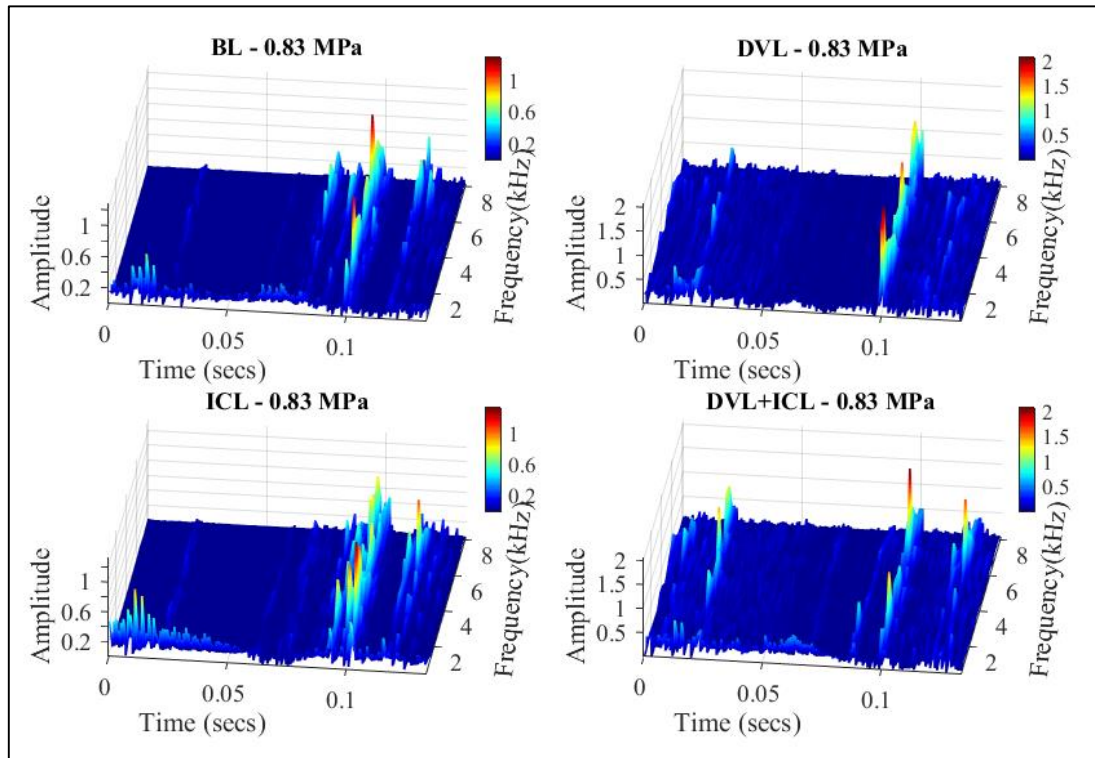


FIGURE 9.6: SPECTROGRAM OF ALL CASES AT 0.83 MPa

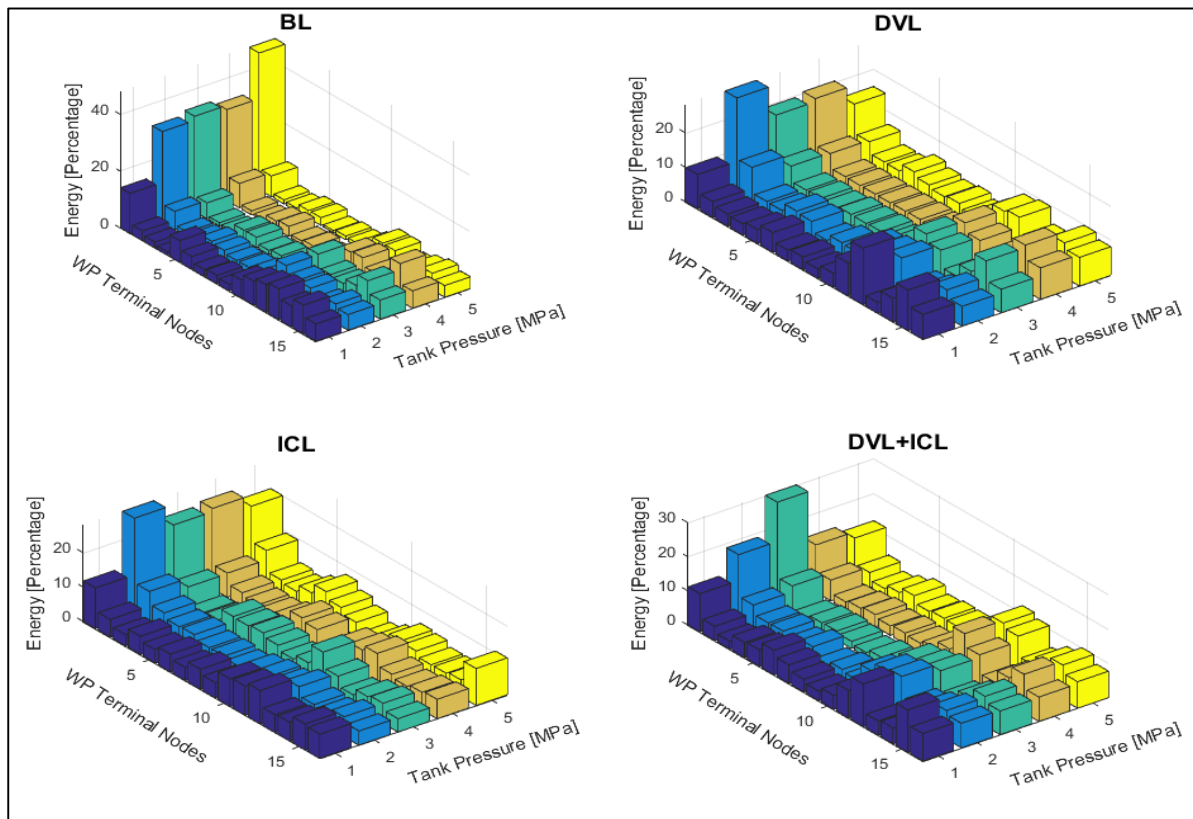


FIGURE 9.7: PERCENTAGE ENERGY OF WAVELET PACKET TERMINAL NODES FOR ALL CASES AND TANK PRESSURE RANGES

9.6.3 Fault Classification Using Harmonic Changes

The fundamental frequency and its harmonics are used for fault classification of the vibration signal. Figure 9.8 shows how the frequency amplitudes vary with increasing tank pressure (0.55 to 0.83MPa) for all cases investigated. From the fundamental frequency plot, it can be seen that the amplitude increases when a fault is present, and the discharge valve leakage fault had the highest amplitude. The amplitude of the fundamental frequency at 0.55MPa does not give very good fault separation as seen from the first plot in Figure 9.8, therefore it was not used for further classification.

Furthermore, the fundamental frequency and each of its harmonics for the remaining four tank pressures (0.62MPa, 0.69MPa, 0.76MPa, and 0.83MPa) are used for further classification. The classification using the fundamental frequency values and the third harmonic frequency gave the best results as seen in Figure 9.9.

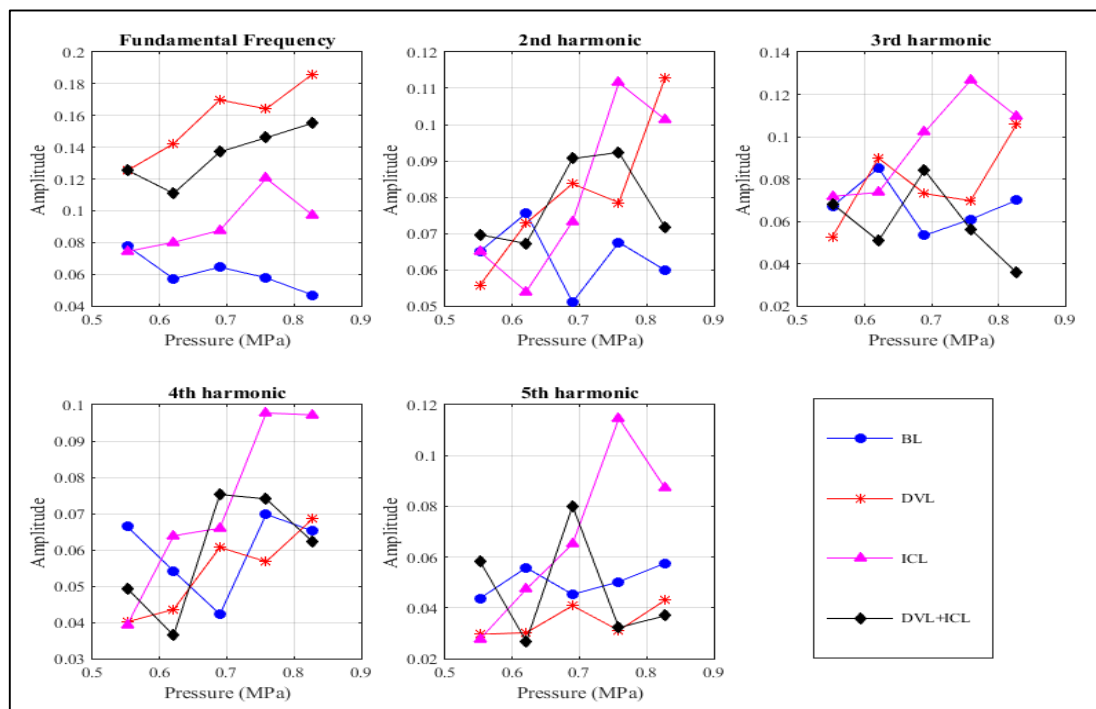


FIGURE 9.8: FUNDAMENTAL FREQUENCY AND ITS HARMONICS PLOTS OF THE SIGNAL FOR ALL CASES AT ALL TANK PRESSURE RANGE INVESTIGATED

9.7 Conclusions

Vibration signal from a reciprocating compressor are non-stationary and transient in nature, which makes processing using traditional signal processing techniques very difficult. Therefore, this chapter investigated the application of time-frequency signal processing

technique (wavelet packet transform) together with envelope analysis of the vibration signal for fault detection and diagnosis. The results showed that the decomposition of the signal using Coiflet mother wavelet with one vanishing moment up to four levels revealed significant amplitude variations of all fault cases studied. From the spectrogram, it was observed that the amplitudes of fault signals were greater than that of normal (BL) signal, particularly, the discharge valve leakage fault signal, which had the greatest overall frequency amplitude at the valve closing times.

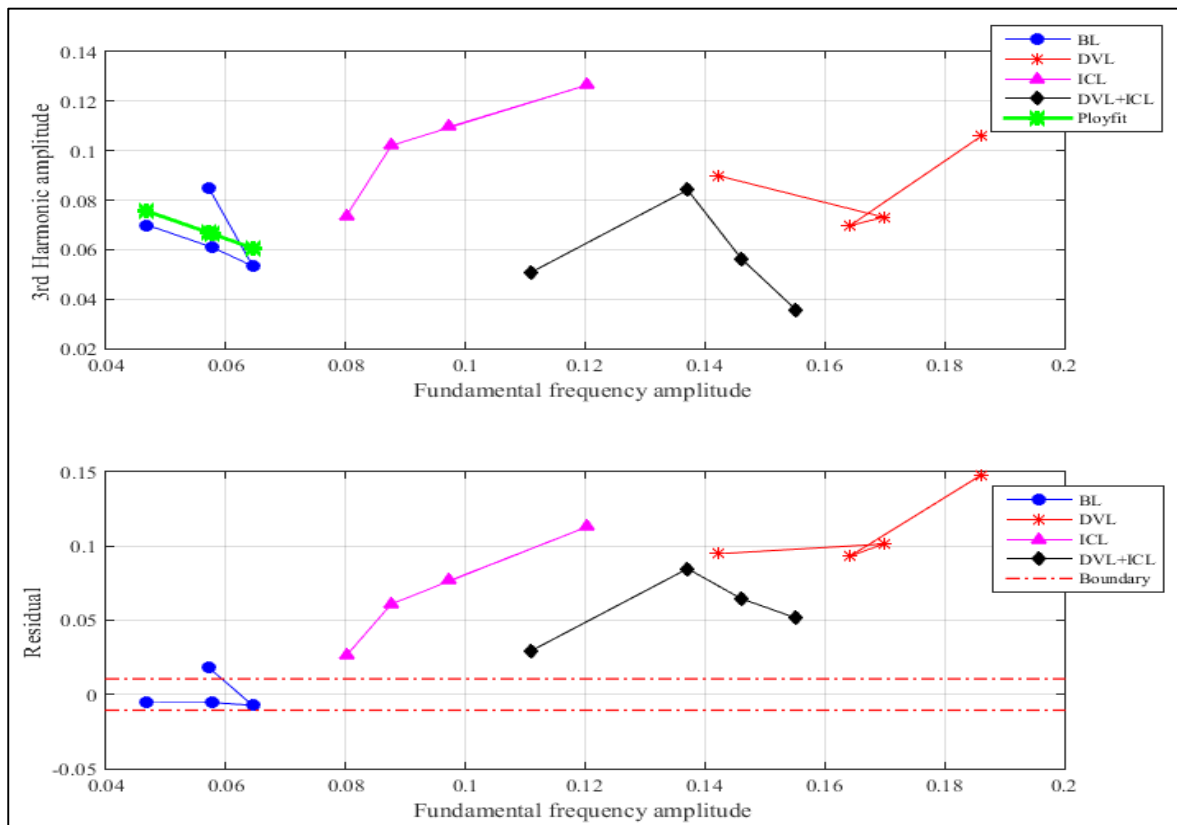


FIGURE 9.10: FAULT CLASSIFICATION RESULTS (A) 3RD HARMONIC AND FUNDAMENTAL FREQUENCY (B) RESIDUAL AND FUNDAMENTAL FREQUENCY

Furthermore, reconstruction of the signal using coefficients from the first terminal node (4, 0), which had the highest percentage energy and employing envelope analysis of the signal could effectively detect the three common reciprocating compressor faults seeded for the purpose of this research study. Classification using the fundamental frequency and its third harmonic gave good separation results between normal (BL) signals and the three fault signals.

CHAPTER TEN

+

10 ANALYSIS OF DISCHARGE GAS PULSATIONS USING WAVELET PACKET TRANSFORM WITH ENVELOPE ANALYSIS

This chapter presents the analysis of gas pulsation signal from a two-stage reciprocating compressor using wavelet packet transform and envelope analysis. Gas pulsation signals from a reciprocating compressor are non-stationary in nature and consists of resonance frequencies, which can be detrimental to the system if significantly high in amplitude. Wavelet packet decomposition is used to divide the signal into bands before de-noising individual bands using an adaptive hard threshold based on standard deviation. Furthermore, envelope analysis of the reconstructed signal is computed for each band and the band with the best root mean square fault variation is used for classification by means of statistical features (kurtosis and entropy plot).

The results show wavelet packet decomposition allows for easy band-pass filtering for further analysis on the chosen band of interest aiding fault detection and condition monitoring of reciprocating compressors. I also shows that gas pulsation signals can be used to identify the systems resonance but the main difficulty is in identifying the source of resonance.

10.1 Gas Pulsation Source and Resonance Assessment

The flow of gas through the discharge chamber and piping system of the reciprocating compressor are unsteady and contains time varying pulses superimposed on the steady (average) flow. Figure 10.1 shows a typical flow pulsation signal through the valves of the reciprocating compressor cylinder head indicating the compressor process within a cycle and the valve opening and closing times. These pulses are made-up of the geometrical, physical and mechanical characteristics of the compressor (Shejal & Desai, 2014). The frequencies of the signal are functions of the mechanical features of the compressor, while the acoustical response in the discharge chamber and piping systems are functions of the mechanical and fluid characteristics of the compressor, also it is hugely a function of the acoustical network by the adjoining discharge chamber, piping systems and, storage units/or dampeners.

Figure 10.2 lists the sources of gas pulsation from a reciprocating compressor.

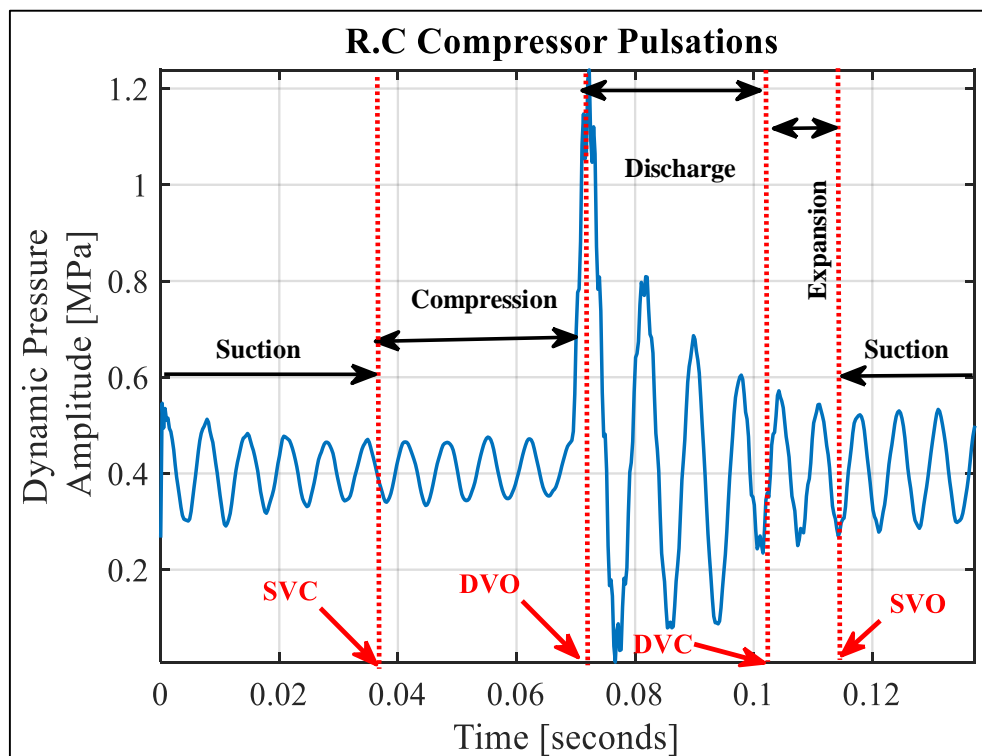


FIGURE 10.1: GAS PULSATIONS WAVES FROM THE DISCHARGE CHAMBER OF A HEALTHY R.C AT 0.827MPA

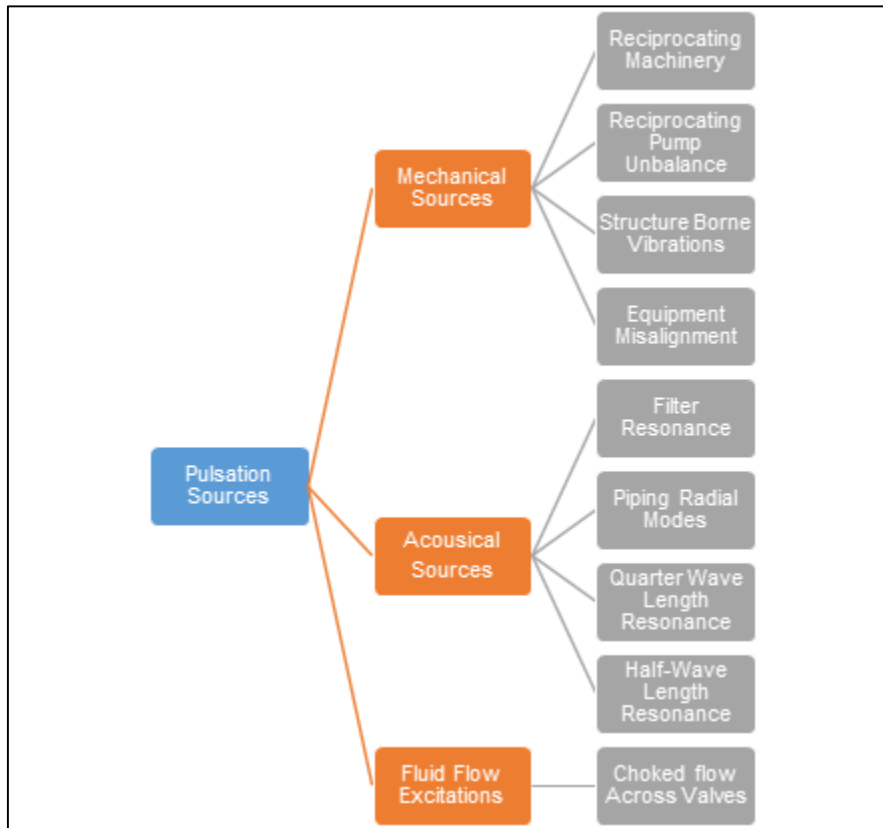


FIGURE 10.2: SOURCES OF RECIPROCATING COMPRESSOR GAS PULSATIONS

10.1.1 Simplified Resonance Assessment of the System

Resonances (dynamic pressure amplification) occur when a harmonic of the compressor running speed matches or is close to the acoustical natural frequency of the dampener. These resonances are either simple organ-pipe resonances or of complex modes involving the discharge chamber and the piping system. Resonances are detrimental to the system because they create unbalanced forces that amplify vibrations causing high levels of noise and shortening compressor valve life if not avoided or controlled (Shejal & Desai, 2014); (Enzo, Marco, Matteo , & Stefano , 2006).

10.1.1.1 Quarter-Wavelength Resonance

The pipe lengths determine the acoustic natural frequencies depending on the boundary conditions (open and/ or closed ends) illustrated in Figure 10.3. If the natural frequency of the compressor occur at integer multiple of half or a quarter of the wavelength of the piping system, an acoustical resonance can be excited (Greenfield, & Luis de la Roche, 2018).

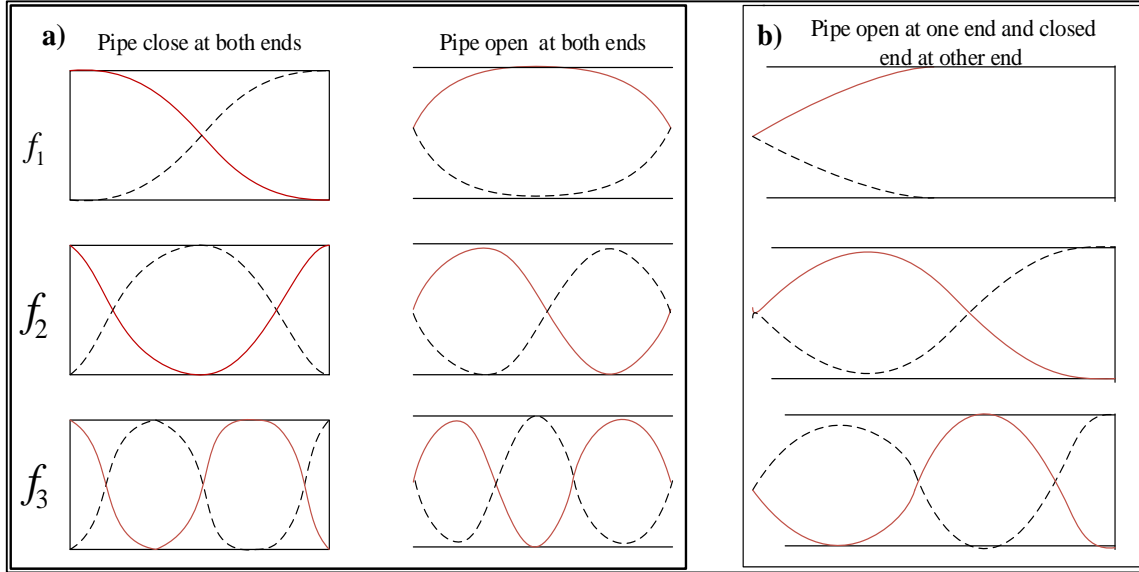


FIGURE 10.3: A) MODE SHAPE OF HALF WAVE RESPONSE B) MODE SHAPE OF QUARTER WAVE RESPONSE

The formulas for half wave resonance (f_{hw}) and quarter wave resonance (f_{qw}) are given by the following respective equations (Schwartz & Nelson, 1984) :

$$f_{hw} = n \frac{a}{2L_p} \quad (10.1)$$

$$f_{qw} = (2n - 1) \frac{a}{2L_p} \quad (10.2)$$

Where a is the speed of sound in air, L_p is the pipe length, and $n = harmonic(1, 2, 3, \dots)$. The discharge chamber-pipe configuration of the reciprocating compressor is analysed as an open-closed end system and therefore Equation 10.2 is used to calculate its quarter wave resonance frequency and eight harmonics of the simplified system presented in Figure 10.4. The speed of sound a in the discharge plenum of the reciprocating compressor (RC) is calculated using equation 10.3 for several discharge pressures are presented in Figure 10.5. For this study, four discharge pressure ranges are investigated (0.28MPa, 0.42MPa, 0.62MPa and, 0.83MPa) and their acoustic natural frequencies based on the quarter-wave length Equation 10.2 are presented in Table 10.1. These values presented in Table 10.1 constitute the excitation frequencies where resonances are expected for the respective discharge pressures.

$$a = \sqrt{(\gamma RT)} \quad (10.3)$$

Where γ is the specific heat ratio for air at 1.4, R is the gas constant at $287\text{m}^2\text{s}^{-2}\text{K}^{-1}$ for air and T the absolute temperature of the gas in the cylinder is calculated using equation 5.30 in chapter five.

When analysing the effects of pulsations in a reciprocating compressor system, it is important to determine the maximum pulsation. This is obtained using the wavelength, speed of sound and, frequency relations described below (Greenfield, & Luis de la Roche, 2018):

$$\lambda = \frac{a}{f_{qv}} \quad (10.4)$$

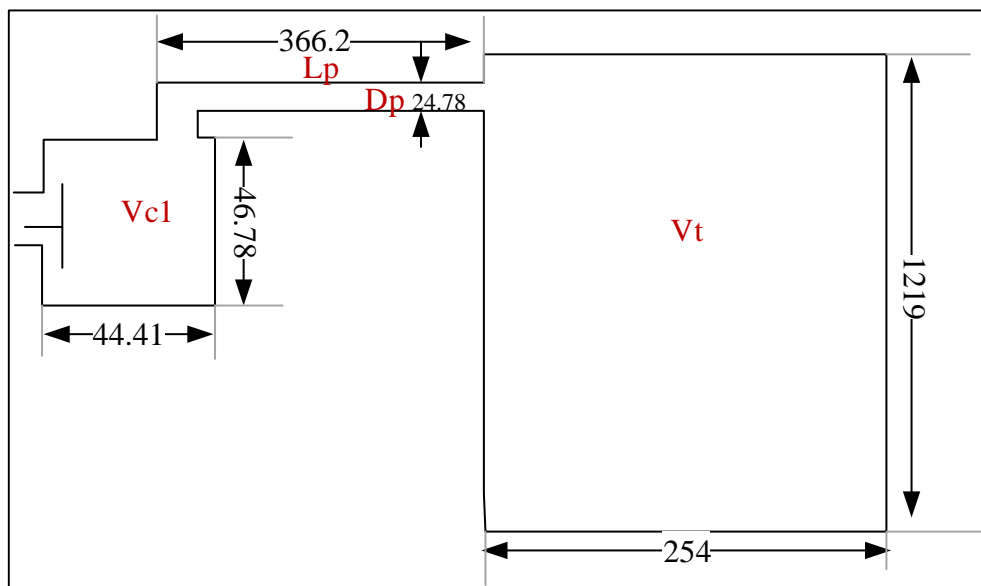


FIGURE 10.4: SIMPLIFIED MODEL OF THE DISCHARGE CHAMBER AND STORAGE TANK PIPE CONFIGURATION WITH DIMENSIONS IN [MM]

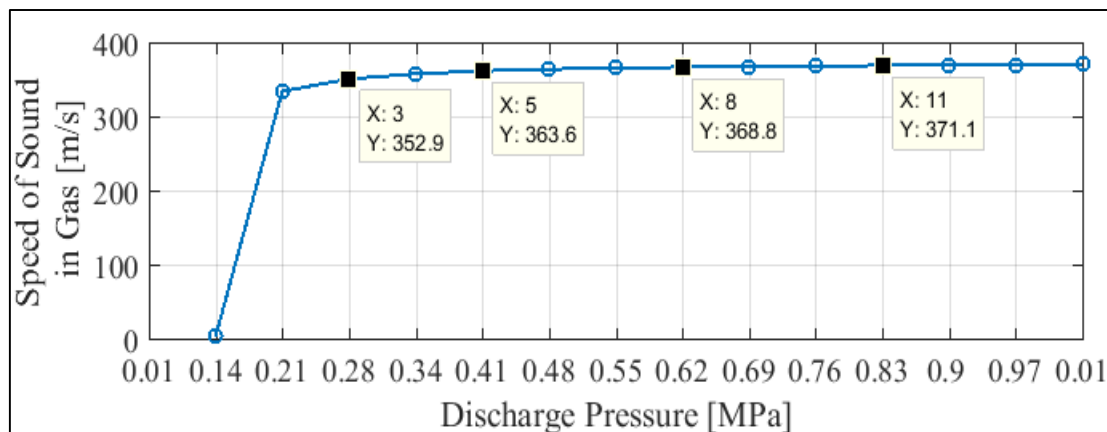


FIGURE 10.5: SPEED OF SOUND IN GAS FOR SEVERAL DISCHARGE PRESSURES OF THE RC

The quarter wave frequency, which gives a wavelength equal to the maximum pipeline length of the compressor (0.3662m), is the fourth harmonic frequency (4X). For the reciprocating compressor used in this research, the compressor speed is within the range 420–460 RPM (7-7.6 Hz), therefore, based on the wavelength calculation, the maximum quarter wave resonance will occur at the hundred and fortieth harmonic (140X) of the compressor running speed.

TABLE 10.1: ACOUSTIC NATURAL FREQUENCY AND HARMONICS OF THE DISCHARGE PIPE

Discharge Pressures [MPa]	Speed of Sound in Gas [m/s]	Quarter-Wave Acoustical Frequencies [Hz]							
		1X	2X	3X	4X	5X	6X	7X	8X
0.28	353	241	482	723	964	1205	1446	1686	1927
0.42	364	248	496	745	993	1241	1489	1737	1986
0.62	369	252	504	755	1007	1259	1511	1763	2014
0.83	371	253	507	760	1013	1227	1520	1773	2027

10.1.1.2 Filter Resonance

The system presented in Figure10.4 could also act as an acoustic filter, and the lowest resonant frequency of an acoustic filter (Helmholtz frequency) is given by (API STANDARD 618, 2007):

$$f_H = \frac{c}{2\pi} \left(\frac{\mu}{Vc1} + \frac{\mu}{Vt} \right)^{1/2} \quad (10.5)$$

Where

c is the speed of sound of gas (meters per second);

$Vc1$ is the volume of gas in the chamber (cubic meters);

Vt is the volume of gas in the storage tank (cubic meters);

μ is the acoustic conductivity (meters).

The acoustic conductivity is described as:

$$\mu = \frac{A}{L_p + 0.6D_p} = \frac{A}{L} \quad (10.6)$$

Where

A is the internal cross-sectional area of the chamber (square meters);

L_p is the actual length of the pipe (meters);

L is the acoustic length of the pipe (meters);

D_p is the diameter of the pipe (meters).

The calculated Helmholtz frequencies of the simplified model of the discharge chamber pipeline at several discharge pressures are presented in Table 10.2. Since the Helmholtz frequencies are very close to the calculated quarter wave frequencies, it can be assumed that the system in Figure 10.4 acts also as a Helmholtz resonator.

TABLE 10.2: HELMHOLTZ RESONANT FREQUENCIES OF THE RC AT SEVERAL TANK PRESSURES

Discharge Pressures [MPa]	Speed of Sound in Gas [m/s]	Helmholtz Frequencies [Hz]							
		1X	2X	3X	4X	5X	6X	7X	8X
0.28	353	235	450	705	939	1174	1409	1644	1879
0.42	364	242	484	726	968	1210	1452	1694	1936
0.62	369	246	491	736	982	1227	1473	1718	1964
0.83	371	247	494	741	988	1235	1482	1729	1976

10.1.2 Gas Pulsation Propagation Simulation

Pressure and flow waves caused by a reciprocating compressor are modelled as one-dimensional waves. The computer programs used in simulating pressure pulsations can be classified into two groups, namely; frequency domain programs and time domain programs (Ghanbariannaeni & Ghazanfarihashemi, 2014).

The simpler frequency domain programs are based on acoustic plane wave theory and do not include nonlinearities unlike the time domain programs which also account for time-varying boundary conditions at the valves (Ghanbariannaeni & Ghazanfarihashemi, 2014). Several studies have shown that the time domain models are more accurate than the older frequency

domain models although, the program requires longer solution time (Ghanbariannaeni & Ghazanfarihashemi, 2014), (Brejaud, Higelin, Charlet, & Chamailard, 2011). Characteristics method and finite difference method are two of the most popular time-domain model programs used to predict piping acoustics.

The continuity equation, momentum and energy equations are the three conservation laws that govern gas pulsation propagation through a medium. Gas pulsation propagation simulation is beyond the scope of this research and therefore would not be investigated. For more detailed on gas pulsation propagation simulation refer to Brejaud, Higelin, Charlet, & Chamailard, 2011, Benson, 1982, and Winterbone, Pearson, & Horlock, 2000.

10.2 Application of Wavelet Packet Transform

Several signal processing techniques including wavelet transform (Ogbulafor, Guojin, Mones, Gu, & Ball, 2017), empirical mode decomposition (Muo, Madamedon, Gu, & Ball, 2017), (Lei, Lin, He, & Zuo, 2013), Wigner-Ville distribution (Baydar & Ball, 2001), and singular value decomposition (Yang & Tse, 2003) have been explored for feature extraction, signal denoising, enhancing weak feature extraction, signal decomposition and many more. Among these signal-processing methods, wavelet transform is most commonly used for analysing non-stationary signals. Wavelet transform provides a platform whereby the signal can be represented in both time and frequency domain. The principle of wavelet transform and the three common wavelet transform categories are discussed in chapter nine.

The wavelet packet transform is employed in this study to decompose the gas pulsation signal from the compressor into low and high frequency bands because of its excellent high-frequency resolution property. The gas pulsation analysis in time-frequency domain gives robust information about the signal compared to time domain and frequency domain analysis separately. By employing wavelet transform, it is possible to understand the effects of several frequency bands of the gas pulsation signal.

The combination of wavelet packet transform and envelope analysis is proposed for detection of common reciprocating compressor faults in several frequency bands. The flow chart in Figure 10.6 shows the diagnostic approach to faults on a reciprocating compressor through the gas pulsation signals from the discharge chamber.

10.2.1 Selection of Base Wavelet

An appropriate base wavelet can be chosen by visually matching the shape of the gas pulsation signal from the reciprocating compressor to the base or mother wavelet. An alternative and more efficient way of selecting the best base wavelet is by employing quantitative measures such as energy and Shannon entropy measures, similarity measures (correlation coefficient), and information theoretic measures (such as joint entropy, conditional entropy and mutual information) (Yan R. , 2007). In this study, the maximum energy to Shannon entropy ratio criterion, maximum correlation coefficient, and minimum Shannon entropy criterion have been employed for selecting the optimum base wavelet for the reciprocating compressor gas pulsation analysis.

10.2.1.1 Minimum Shannon Entropy Criterion

The Shannon entropy of the wavelet coefficients is given by (Yan R. , 2007):

$$E_{entropy}(s) = -\sum_{i=1}^N p_i \cdot \log_2 p_i \quad (10.7)$$

Where

$N = \text{length of signal}$

$p_i = \text{energy probability distribution of the wavelet coefficients}$

$$p_i = \frac{|wt(s,i)|^2}{E_{energy}(s)} \quad (10.8)$$

The mother wavelet, which minimises the computed entropy of the wavelet coefficients, represents the best wavelet for analysing the signal.

10.2.1.2 Maximum Energy to Shannon Entropy Ratio Criterion

The maximum energy to Shannon entropy ratio is a combination of two qualitative measures. The criterion involves extracting the maximum energy content and minimum Shannon entropy of the corresponding wavelet coefficients is described as (Yan R. , 2007):

$$R(s) = \frac{E_{energy}(s)}{E_{entropy}(s)} \quad (10.9)$$

The amount of energy content in wavelet coefficients of a given signal is expressed as:

$$E_{energy} = \iint |wt(s,t)|^2 dsd\tau \quad (10.10)$$

The base wavelet with the greatest energy to Shannon entropy ratio is chosen as the best wavelet for analysing the gas pulsation signals from the reciprocating compressor.

10.2.1.3 Maximum Correlation Coefficient

The signal similarity is described by the correlation coefficient of the original signal and the reconstructed wavelet signal. The degree of similarity between two signals X and Y for instance is described as (Yan R. , 2007):

$$C(X,Y) = \frac{C_{XY}}{\sigma_X \sigma_Y} \quad (10.11)$$

Where σ_X and σ_Y are the standard deviation of the data sequences X and Y , respectively. The symbol C_{XY} represents the covariance.

Thirty base wavelets are pre-selected from six wavelet families. The maximum energy to entropy ratio, maximum correlation measure, and the minimum Shannon entropy values for the pre-selected base wavelets applied to the original gas pulsation signal are listed in Table 10.3. The reverse bi-orthogonal mother wavelet has the highest maximum energy to entropy ratio, maximum correlation measure, and the minimum Shannon entropy values, and is therefore, considered as the optimal wavelet for the signal.

TABLE 10.3: REAL-VALUED QUANTITATIVE MEASURES FOR OPTIMAL BASE WAVELET SELECTION

Mother Wavelet	Maximum Energy-to-Entropy Ratio	Maximum Correlation Measure	Minimum Shannon Entropy	Mother Wavelet	Maximum Energy-to-Entropy Ratio	Maximum Correlation Measure	Minimum Shannon Entropy
Sym2	0.2255	0.0240	440.389	Coif4	0.2246	0.0246	444.360
Sym3	0.2263	0.0243	440.266	Coif5	0.2241	0.0246	445.325
Sym4	0.2258	0.0245	441.648	Haar	0.2222	0.0228	441.768
Sym6	0.2256	0.0245	442.330	Bior1.3	0.2227	0.0253	442.475
Sym8	0.2253	0.0246	443.025	Bior2.4	0.2270	0.0243	444.607
Sym10	0.2249	0.0246	443.718	Bior2.6	0.2266	0.0245	445.315
Db2	0.2255	0.0240	440.389	Bior4.4	0.2248	0.0244	439.805
Db4	0.2264	0.0245	440.638	Bior5.5	0.2231	0.0245	435.348
Db6	0.2258	0.0245	442.162	Bior6.8	0.2257	0.0246	444.215
Db8	0.2254	0.0246	442.844	rBio1.3	0.2252	0.0237	442.475
Db10	0.2255	0.0246	442.715	rBio2.4	0.2238	0.0245	444.607
Db20	0.2236	0.0246	446.475	rBio2.6	0.2238	0.0244	445.315
Coif1	0.2251	0.0240	441.256	rBio4.4	0.2264	0.0246	439.805
Coif2	0.2255	0.0245	442.227	rBio5.5	0.2288	0.0246	435.348
Coif3	0.2251	0.0245	443.300	rBio6.8	0.2246	0.0246	435.348

10.3 Proposed Methodology

The experimental test rig of the reciprocating compressor used for the gas pulsation analysis is presented and described in chapter eight (section 8.3). Dynamic (acoustic) pressure transducers are used for the acquisition of gas pulsation measurement data. The raw gas pulsation signal is pre-processed by resampling the signal from 49019Hz to 4092 Hz. In chapter eight, it was discovered that lower frequency range (< 2000Hz) of the pulsation signal had resonances with higher amplitudes (greater than 40dB) compared to high frequency range (>2000Hz). For this reason, the signal pre-processing stage is necessary to exclude high frequencies, which would require more decomposition levels if included in the wavelet packet decomposition process. Figure 10.6 illustrates the flow chat process of the proposed method employed for fault detection of the gas pulsation signals.

A new reduced data length of 3375 samples for six cycles is obtained as a result of signal resampling and several tank pressures are investigated including 0.275 MPa, 0.413 MPa, 0.62, and 0.827 MPa. Baseline (BL), second-stage discharge valve leakage (DVL), intercooler leakage (ICL), discharge to tank storage pipeline leakage (PLL), and a combined fault of the discharge valve and pipeline leakage (DVL&PLL) are the five cases investigated under the tank pressure range specified above. The pipeline fault (PLL) is seeded by untightening the

connection between the second-stage discharge chamber and the air receiver storage tank. While the combined fault (DVL+PLL) is implemented by running the compressor when the two faults are in effect.

Based on the optimal base wavelet criterion presented earlier, the reverse bi-orthogonal mother wavelet is used to decompose the signal into three levels (corresponding to $2^3 = 8$ terminal nodes). The wavelet packet transform acts as a band-pass filter and Table 10.4 presents the respective frequency range covered by each terminal node for the entire sampling frequency (4092 Hz). It should be noted that, the frequency ordering of wavelet packet coefficients is in Gray code order rather than successive order. This is because the output of every level is the result of both low/high pass filtering followed by down sampling as seen in the previous chapter (Figure 9.9.2). Thereby switching the order of low and high pass components in subsequent decompositions.

A hard threshold based on the standard deviation of each terminal node is applied to the coefficients before reconstructing the de-noised signal. Then, envelope analysis (see Section 9.4) of the eight reconstructed wavelet packet coefficients are computed. The results present a new time domain signal of each of the eight reconstructed coefficients consisting of their respective frequency bands. The RMS values of all bands are compared and used to eliminate bands with insufficient faults variations. Subsequently, two key statistical features, kurtosis and entropy values of the enveloped signals are computed and used for fault classification.

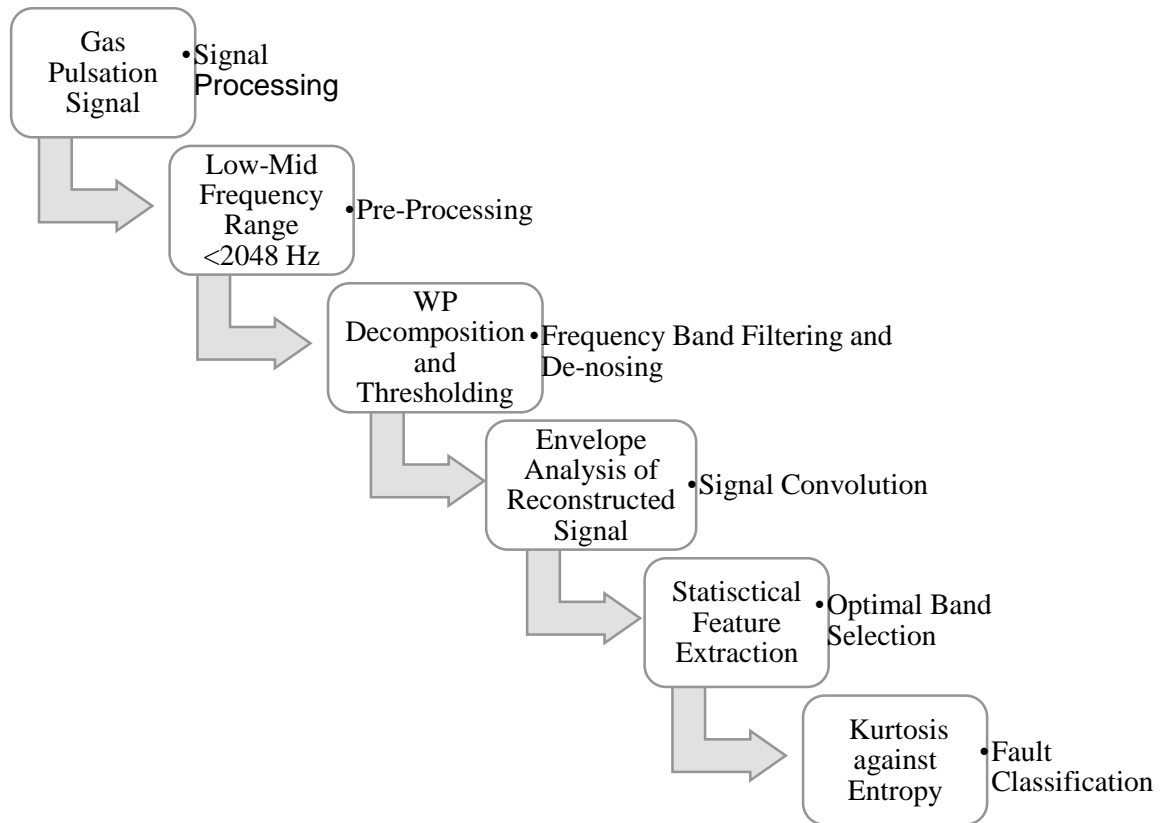


FIGURE 10.6: FLOW CHART FOR FAULT DIAGNOSIS USING GAS PULSATION SIGNAL

TABLE 10.4: FREQUENCY RANGE FOR EACH TERMINAL NODE UNDER 4092 HZ SAMPLING FREQUENCY IN GRAY CODE SEQUENCE

Terminal Nodes	Frequency Range (Hz)	Terminal Nodes	Frequency Range (Hz)
1	0-256	5	1792-2048
2	256-512	6	1536-1792
3	768-1024	7	1024-1280
4	512-768	8	1280-1536

10.4 Experimental Results and Discussion

The reciprocating compressor runs at speed of 420-460 RPM, which means the fundamental order of excitation occurs between 7-7.6 Hz. From Table 10.1, which shows the quarter wave resonant frequency and its harmonic for the simplified plenum system, the fourth harmonic (4X) resonance frequency at 1013 Hz is very close to the 141st harmonic (1019 Hz) of the average compressor shaft frequency 7.282Hz. Also, from the spectrum, it can be seen that the broadest resonance occurs at this frequency (1019Hz). Resonance is greatly affected

by the operating condition of the gas pulsation signal; therefore, for the different discharge pressure range investigated, the resonant frequencies would vary.

Resonance frequencies of the pulsation signal at several tank pressures studied are presented in Figure 10.8. Several low frequency acoustic resonances are excited at different tank pressures. The pulsation frequencies at 1X, 2X, 3X, and 4X resulting from equation (10.2) for several tank pressures are nearly coincident with standing resonances in Figure 10.8. Pulsations and hence unbalanced forces are generated at the resonance frequencies causing vibration problems at several harmonics.

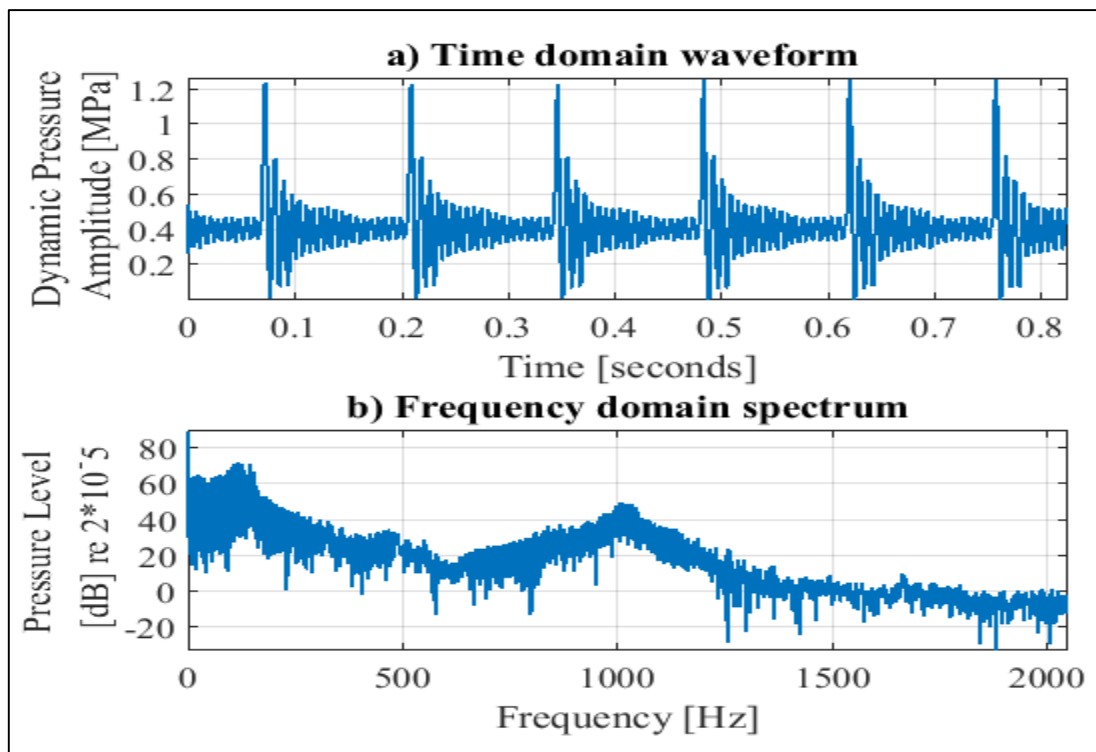


FIGURE 10.7 A) TIME DOMAIN AND B) FREQUENCY DOMAIN ANALYSIS OF GAS PULSATION SIGNAL AT 0.827MPA

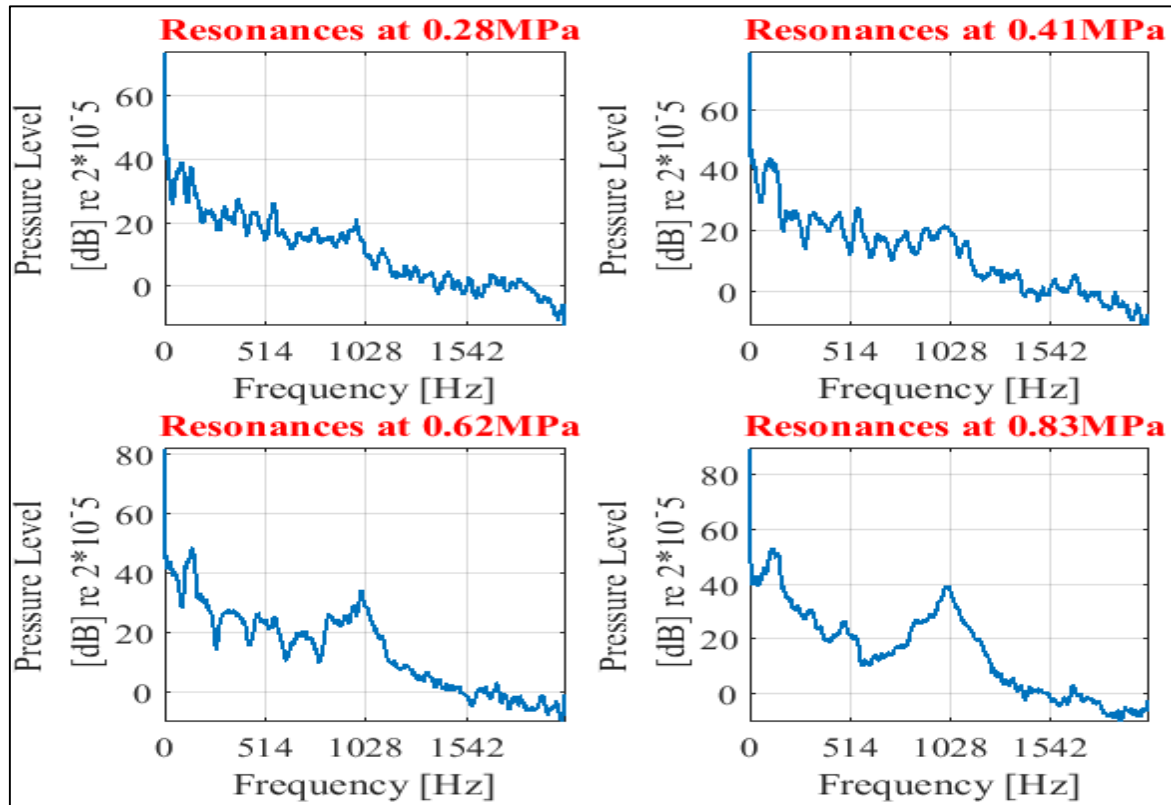


FIGURE 10.8: ACOUSTIC RESONANCES FOR SEVERAL TANK PRESSURES UNDER NORMAL CONDITIONS

10.4.1 WPT Analysis of the Discharge Chamber Gas Pulsations

Wavelet packet transform is used as a powerful tool to decompose the gas pulsation signal in the entire frequency domain. The wavelet packet transform is implemented on the gas pulsation signal for all conditions (healthy and faulty) and several tank pressures. Figure 10.9 shows the time-frequency representation of healthy and all fault conditions at the highest tank pressure (0.83MPa). Key differences between the healthy (BL) spectrogram and the spectrogram of each fault condition investigated are outlined in Table 10.5.

The wavelet decomposition for three levels gives eight terminal nodes of several frequency bands (see Table 10.4). Each terminal node is de-noised using an adaptive hard threshold based on the standard deviation of individual terminal node coefficients. Figure 10.10 shows the reconstructed signals for each band after de-noising with its corresponding frequency spectrum.

CHARACTERISING VIBRO-ACOUSTIC SIGNALS OF A RECIPROCATING COMPRESSOR FOR CONDITION MONITORING

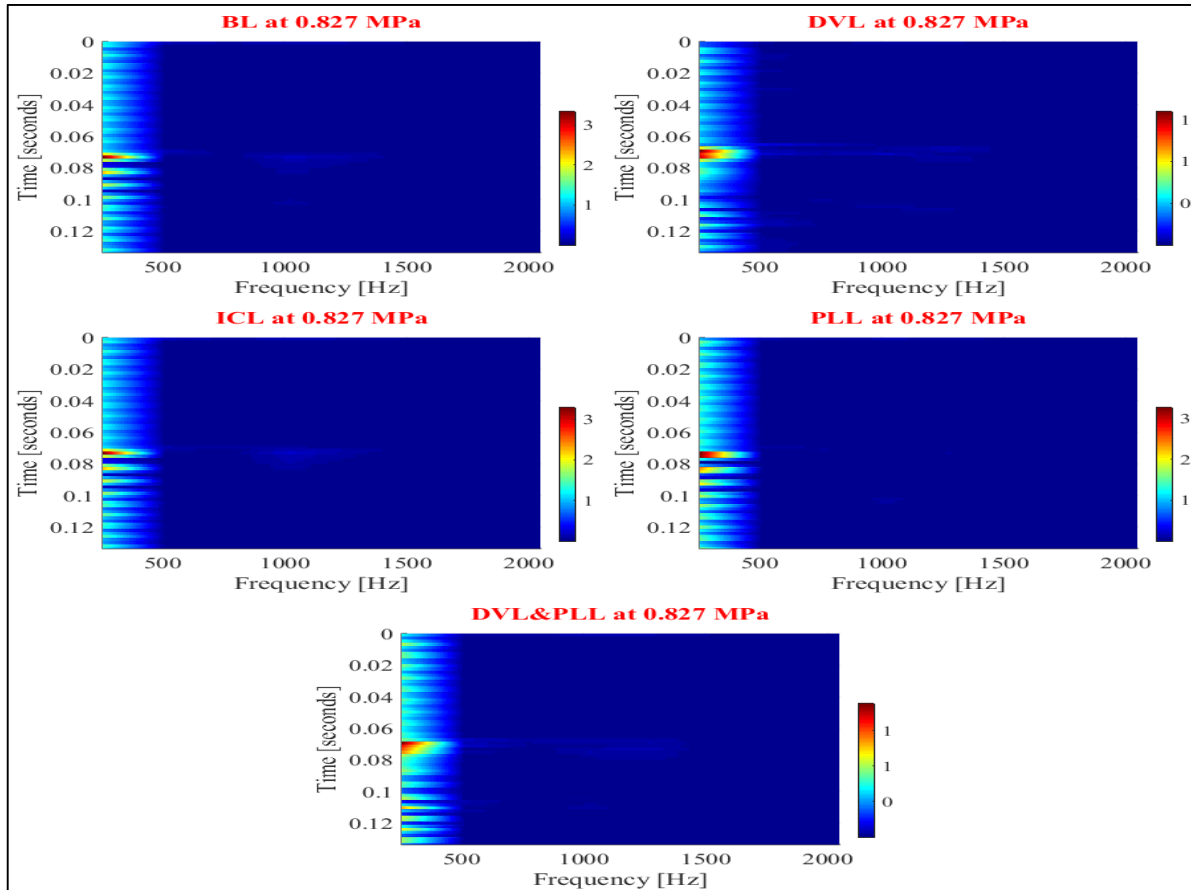


FIGURE 10.9: SPECTROGRAM OF HEALTHY AND FAULTY GAS PULSATION SIGNALS AT 0.827MPa

TABLE 10.5: SUMMARISED DIFFERENCES BETWEEN HEALTHY AND ALL FAULTY SPECTROGRAMS

FAULT CONDITIONS	OBSERVATIONS
<p>Discharge Valve Leakage (DVL)</p>	<p>Decreased peak pressure energy during DVO time compared to baseline (BL) spectrogram within the lower frequency range (0-256Hz).</p> <p>High-energy present at all four pulses during discharge period (0.07 to 0.075 seconds) compared to baseline, which has most of the energy concentrated at the first discharge opening pulse (0.07) again within lower frequency range.</p> <p>At mid frequency range (768-1500Hz), it is difficult to differentiate between the low energy seen at healthy and on the faulty spectrum.</p>
<p>Intercooler Leakage (ICL)</p>	<p>The spectrogram for ICL shows little to no difference from that of baseline (BL), this is because pulsations do not travel through cylinders.</p>

CHARACTERISING VIBRO-ACOUSTIC SIGNALS OF A RECIPROCATING
COMPRESSOR FOR CONDITION MONITORING

<p>Discharge Line Pipe Leakage (PPL)</p>	<p>Increased peak pressure energy during DVO time compared to the baseline (BL) spectrogram within the lower frequency range (0-256Hz).</p> <p>Low energy within the mid frequency range (768-1500Hz) seen in baseline (BL) spectrogram are not present in the PLL spectrogram.</p>
<p>Combined Leakage (DVL&PLL)</p>	<p>Decreased peak pressure energy during DVO time compared to baseline (BL) spectrogram within the lower frequency range (0-256Hz).</p> <p>High-energy concentration spread across the discharge period; also, within the lower frequency range.</p> <p>At mid frequency range (768-1500Hz), it is difficult to differentiate between the low energy seen at healthy and on the faulty spectrum</p>

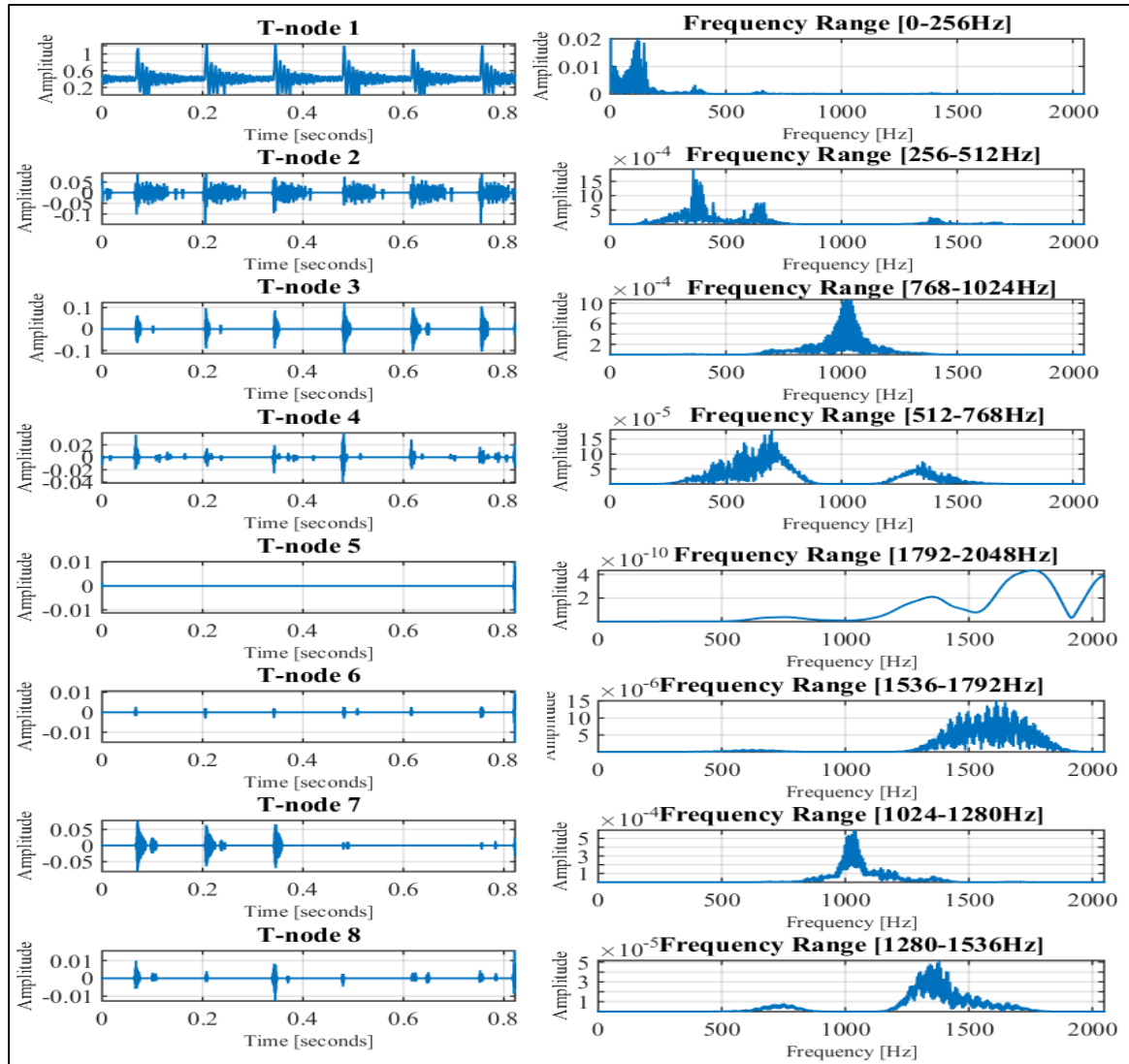


FIGURE 10.10: RECONSTRUCTED TERMINAL NODE WAVEFORMS AND CORRESPONDING SPECTRUM FOR GAS PULSATION SIGNAL AT 0.827MPA

10.4.2 Envelope Analysis and Feature Extraction of Discharge Chamber Gas Pulsations

The envelope of gas pulsation signals in different frequency-bands is calculated using Hilbert-transform (Cizek , 1970). Chapter Nine (section 9.4) of this thesis already presents a brief description of envelope analysis; however, a thorough review of the technique may be found in (Wang X. , 2006).

The root-mean-square (RMS) of the enveloped signal for each frequency band is calculated to detect the best band-pass filter, which gives the optimal fault separation seen in Figure 10.11 as terminal node 4 (512-768Hz) and terminal node 6 (1536-1792Hz) respectively. The envelope and envelope spectrum of terminal nodes 4 and 6 seen in Figure 10.12 and Figure

10.13 are used for fault classification. The envelope of terminal nodes 4 and 6 can be used to detect the investigated faults, as there are clear differences between healthy and faulty plots

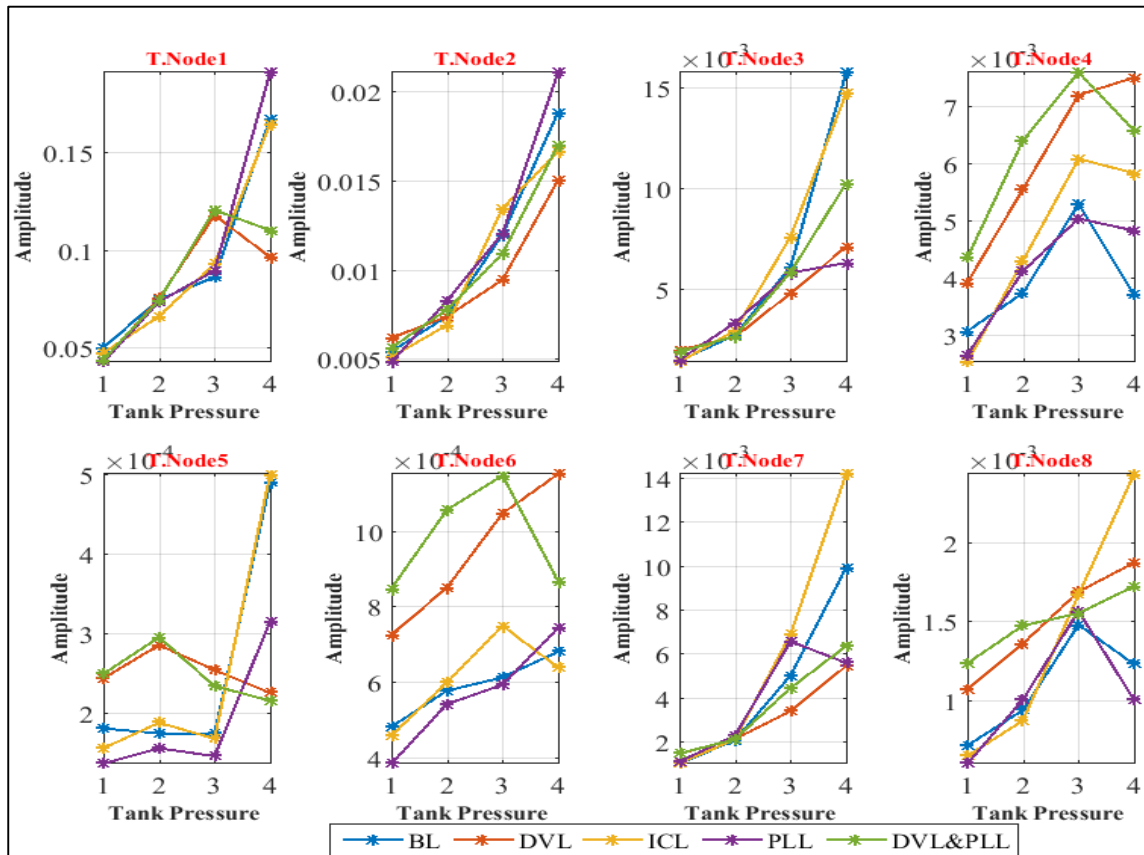


FIGURE 10.11: RMS OF ALL TERMINAL NODES FOR ALL CONDITIONS AND TANK PRESSURES

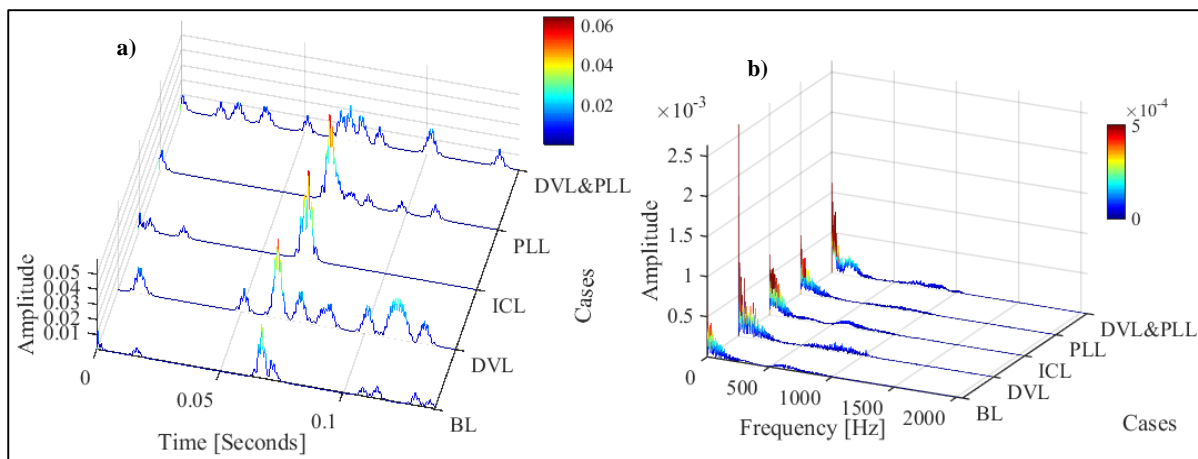


FIGURE 10.12: ENVELOPE AND B) ENVELOPE SPECTRUM OF TERMINAL NODE 4 FOR ALL CONDITIONS AT 0.827MPA

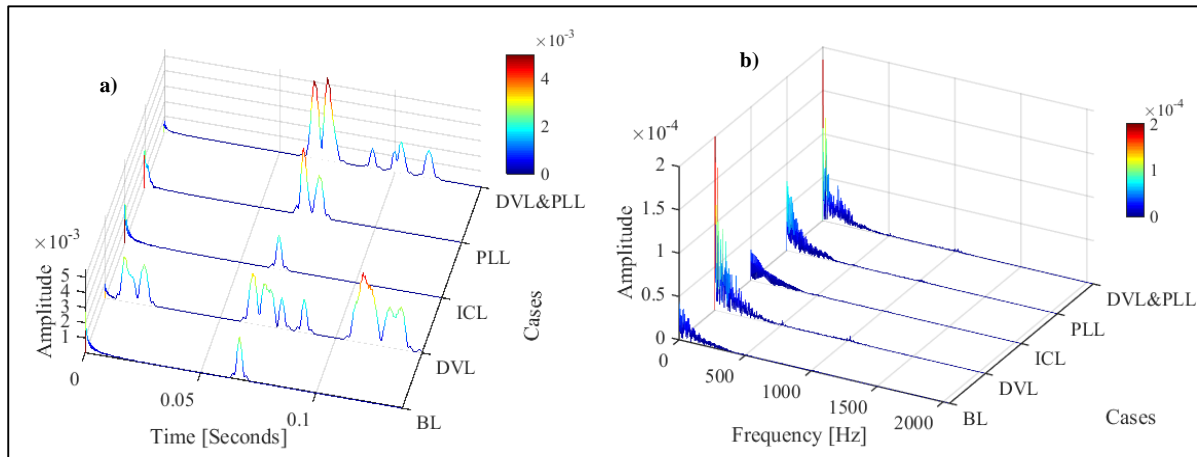


FIGURE 10.13: ENVELOPE AND B) ENVELOPE SPECTRUM OF TERMINAL NODE 6 FOR ALL CONDITIONS AT 0.827MPA

10.4.3 Fault Classification using Statistical Features

The kurtosis and entropy values of the enveloped gas pulsation signals are used for fault classification. As mentioned in chapter 7 the kurtosis characterises the relative peakedness or flatness of the signal (Dyer & Stewart, 1978). A high kurtosis value means the signal is sharply peaked and has a longer tail while a low kurtosis value indicates that the signal has smoothed peaks and thinner tail. Shannon entropy measures the amount of randomness and sparseness of a signal. Therefore, a signal with minimum entropy has the greatest signal-to-noise ratio.

In this study, a combination plot of kurtosis and entropy values of the enveloped signal is used as a tool for classification of common faults through gas pulsation signals from the discharge chamber of a reciprocating compressor. Figure 10.14 presents the result for classification using the aforementioned tool for terminal node 4 and Figure 10.15 presents that for terminal node 6.

For terminal node 4 band, it can be seen that pipe leakage faults (intercooler (ICL) and discharge line (PLL)) do not show good separation from the baseline values, whereas, the valve faults (DVL and DVL&PLL) are clearly separated from the baseline and are above boundary line. Particularly, the intercooler fault (ICL) because pulsations do not travel through the cylinders as the intercooler pipe connects first-stage cylinder to second-stage cylinder and the suction and discharge valves do not open at the same time for the transducer located at the discharge chamber of the second cylinder to detect the intercooler fault. Therefore, the intercooler-fault signal results are in line with expectations.

Results from Figure 10.15, although slightly similar to that of Figure 10.14 gives a better result, in that, values for the valve faults (DVL and DVL&PLL) are well above the boundary line. From the plot, it can be observed that the valve faults have high entropy values compared to other cases, which means that the noise level for these fault are significantly high. Based on the results from the classification, it is concluded that terminal node 6 is best at classifying the investigated faults on a reciprocating compressor using gas pulsation signals from the discharge chamber.

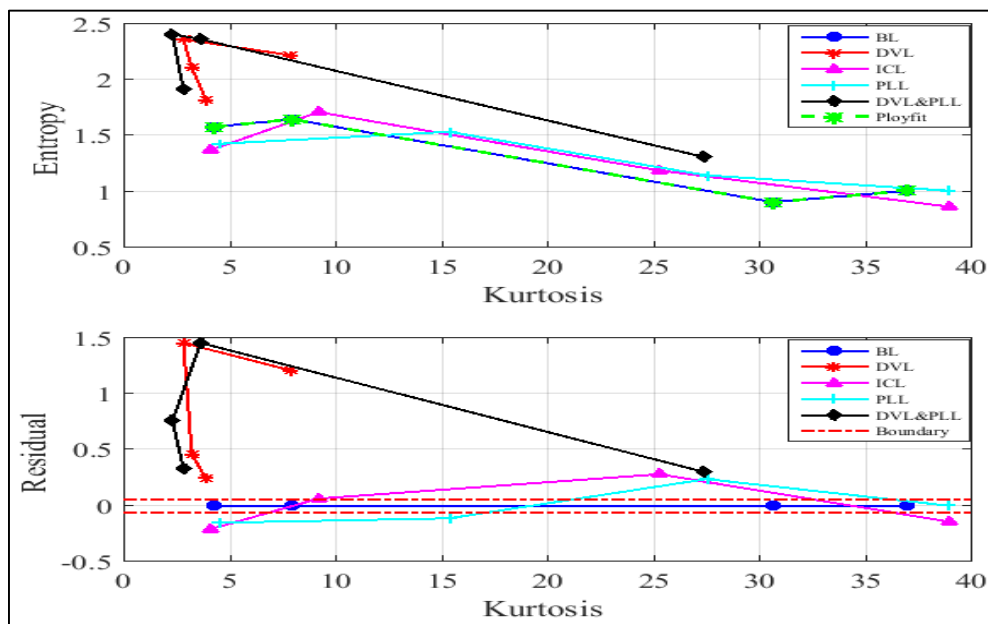


FIGURE 10.14: FAULT CLASSIFICATION USING ENTROPY AGAINST KURTOSIS PLOT OF TERMINAL NODE 4 ENVELOPED SIGNAL

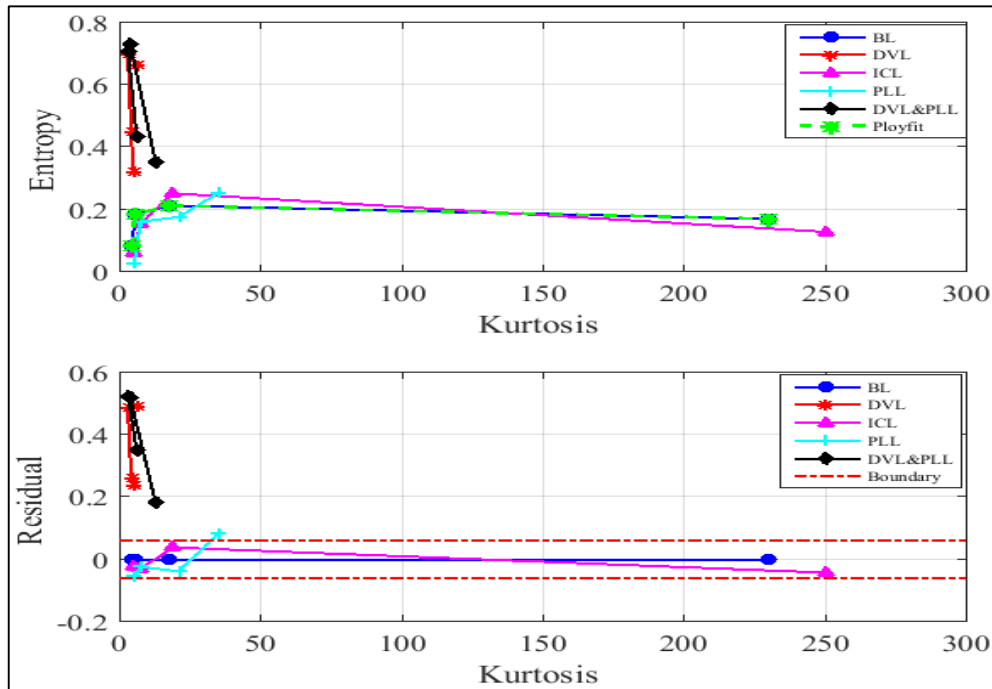


FIGURE 10.15: FAULT CLASSIFICATION USING ENTROPY AGAINST KURTOSIS PLOT OF TERMINAL NODE 6 ENVELOPED SIGNAL

10.5 Conclusion

Gas pulsations from the discharge chamber of a reciprocating compressor can be problematic if the chamber or piping frequencies correspond to multiples of the compressor running frequency or its harmonics. Moreover, these gas pulsation signals are non-stationary in nature making it challenging to use time domain and frequency domain analysis for fault detection and diagnosis. Therefore, in this chapter, wavelet packet transform and envelope analysis are adopted for condition monitoring of gas pulsation signals from the reciprocating compressor. The optimal wavelet basis is selected based on Shannon to entropy ratio criteria and cross correlation and three levels of the wavelet packet decompositions are performed to give eight band-pass filters (terminal nodes). An adaptive hard threshold using standard deviation of each band coefficients is applied and the coefficients of each band is reconstructed. Furthermore, envelope analysis of each band (reconstructed terminal node coefficients) is computed and the root mean square values are used to select the optimal band that gives the best fault separation. Finally, the optimal terminal nodes (4 and 6) were used for classification by plotting their kurtosis values against entropy values. Terminal node 6 (1536-1792Hz) gave a more superior valve fault separation when used for classification compared to terminal node 4 (512-768Hz).

CHAPTER ELEVEN

11 CONCLUSIONS AND RECOMMENDATIONS FOR FURTHER WORK

This chapter summarises the achievement of the research described in this thesis and relates them to the objectives defined in Section 1.5. Conclusions are drawn from key findings on the study of condition monitoring of a two-stage single-acting reciprocating compressor with common faults seeded for research purposes at the university of Huddersfield diagnostics laboratory. Furthermore, five relevant contributions to study have been outlined and suggestions for future work are presented.

11.1 Review of Thesis Objectives and Achievement

The major achievements and new contributions made by this research are discussed. This study focused on determining the characteristics of vibro-acoustic signals from a reciprocating compressor for condition monitoring purposes.

Theoretical analysis and experimental works were carried out, and several signal processing methods and techniques were employed to study the characteristics of vibration and gas pulsation signals measured under normal and common RC fault conditions.

The set out thesis objectives are carefully correlated to the key achievements of this research study.

- **Objective 1:** To set up a comprehensive reciprocating compressor test rig, and to develop experimental procedures for condition monitoring of the two-stage reciprocating compressor. This will allow condition monitoring using gas pulsation and vibration sensors, and will also allow specific compressor faults to be seeded onto the compressor: valve leakage, intercooler leakage, and discharge pipeline leakage.
 - **Achievement 1:** A suitable reciprocating compressor test rig facility was developed and data acquisition system, relevant measurement sensors were purchased and used to aid condition monitoring as presented in Chapter four of this thesis. The Broom Wade TS9 reciprocating compressor is a V-shaped, two-cylinder, single acting machine with a horizontal air receiver tank used for this research. The research environment in which measurements were conducted was similar to an industrial environment with real applications. The rig was used to determine compressor performance under normal and faulty conditions and the results were used to validate the developed mathematical model of the two-stage reciprocating compressor.
 - **Objective 2:** To review various condition-based monitoring techniques presently adopted in industry and to assess the performance of crucial monitoring techniques suitable for early fault detection.
 - **Achievement 2:** Of the many condition-monitoring techniques reviewed and investigated in chapter three of this thesis, it was discovered that with reciprocating compressors, most works were concerned with detection of valve faults using vibration and in-cylinder pressure signals whilst adopting conventional signal processing techniques and a few on advanced signal processing techniques such as continuous wavelet transform. To the best of this researcher's knowledge, no work has been done
-

on the use of advanced signal processing techniques (wavelet packet transform and envelope analysis) for diagnosing faults using gas pulsation signals from the discharge chamber of the reciprocating compressor. Most studies are rather focused on the modelling and effectiveness of installed dampeners on the reciprocating compressor.

- **Objective 3 and Objective 4:** To develop a mathematical model of the two-stage reciprocating compressor, which includes the gas pulsation behaviour to aid in understanding the physical properties of the reciprocating compressor; to validate the mathematical model developed by correlating measured and simulated results.
- **Achievement 3 and Achievement 4:** In chapter five, a thermodynamic model was developed using the design parameters of the Broom Wade TS9 reciprocating compressor. The model consists of a crankshaft equation, two in-cylinder pressure equations, four equations to represent the valve motion, and an equation for second-stage discharge gas pulsation. In particular, the introduction of second-stage discharge gas pulsations simulations into the model required substantial adjustments of the mass flow equations and subsequent changes to the in-cylinder pressure equations for second stage (see section 5.9). Furthermore, valve and pipeline fault simulations are also included in the model. The model predications show good agreement with measured results.
- **Objective 5:** To determine the characteristics of gas pulsation and vibration measurements from the reciprocating compressor using traditional signal processing methods.
- **Achievement 5:** Several signal-processing methods were applied to the collected data from gas pulsation and vibration transducers. Data was examined using time domain and frequency domain analysis. The effectiveness of these methods in detecting common reciprocating compressor faults were investigated for the two condition monitoring techniques (vibration and gas pulsation). The results from the two techniques are presented in Chapters seven and eight.
- **Objective 6:** To analyse and examine the nonstationary vibration and gas pulsation signatures by the application of advanced signal processing techniques, such as Hilbert transform (envelope analysis) based convolution and wavelet packet transform.
- **Achievement 6:** It was discovered that conventional signal processing methods (time domain and frequency domain) on vibration signals from the reciprocating compressor were unsuitable for effectively detecting the common faults investigated. Therefore,

advanced means for signal processing using wavelet packet transform together with Hilbert transform was used to give a more robust fault classification in Chapter nine. Time-domain and frequency-domain analysis of the gas pulsation signals were useful in detecting faults and identifying resonance frequencies of the piping system. However, Chapter ten, which presents the application of wavelet packet transform and Hilbert transform on gas pulsation signals proved to be a more superior and effective means for band pass filtering of acoustical resonances and fault detection of valve faults on the reciprocating compressor.

- **Objective 7:** To provide guidelines for future research in this field based on the investigations conducted.
- **Achievement 7:** Some suggestions are provided for future work on condition monitoring of multi-stage reciprocating compressors using different faults in Section 11.4 below.

11.2 Conclusion on Condition Monitoring of Vibro-acoustic Signals from a Reciprocating Compressor

Early detection of failure is of prime importance and the use of vibration and gas pulsation based monitoring techniques are suitable for condition monitoring of reciprocating compressors. Based on the theoretical and experimental analysis of vibro-acoustic signals from the RC, the following conclusions are drawn:

- **Conclusion 1:** Based on the repeatability experiments carried out in section 4.7, it is concluded that the overall repeatability of the measurements is acceptable, although there were slight differences particularly for repeated vibration measurements; the one-way ANOVA null hypothesis of the repeated vibration measurement is accepted because the computed P-value was less than the 5 percent significance level set. Hence, validating the repeatability of the vibration signal.
- **Conclusion 2:** There were some positive correlations between the discharge pressure and the RMS and Kurtosis of the vibration signals, however, the influence of studied faults on both statistical features did not follow any particular pattern and were highly inseparable for second-stage vibration measurements across a wide pressure range.
- **Conclusion 3:** Pulsation waves could provide an accurate representation of the discharge valve opening (DVO) times and any delays that may occur with increasing discharge pressure. However, there were no positive correlation between the discharge

pressure and the RMS and Kurtosis of pulsation waves. The influence of studied faults on both statistical features and PDF values were very close together and showed a random pattern across a wide pressure range.

- **Conclusion 4:** The frequency domain analysis revealed, that spectral amplitudes show significant variations at high tank pressures especially for second stage vibration signals; also spectral amplitudes of fault cases increase mostly at high tank pressure ranges over a particular frequency range (5kHz to 14kHz) for second-stage vibration signals
- **Conclusion 5:** The spectrum of the acoustic (gas) pulsations revealed several resonances, which varied with discharge pressure. However, challenges were encountered in accurately selecting the optimal resonance band that would effectively characterise the investigated faults across several discharge pressures. Finally, using the 1/3rd octave band analysis, band 22 and 23 with centre frequencies 500Hz and 630Hz respectively gave the best valve leakage and combined fault separations from the baseline signals.
- **Conclusion 6:** The application of WPT and envelope analysis on the vibration signal showed that WPT decomposition using Coiflet mother (base) wavelet with one vanishing moment for four levels gave the best separation for fault detection results across a wide discharge pressure range. From the spectrogram, it was observed that the amplitudes of fault signals were greater than those of normal (BL) signal, particularly, the discharge valve leakage fault signal, which had the greatest overall frequency amplitude at the discharge valve closing (DVC) times. Furthermore, reconstruction of the signal using coefficients from the first terminal node (4, 0), which had the highest percentage energy and application of envelope analysis could effectively detect the three common reciprocating compressor faults seeded. Finally, classification using the fundamental frequency and its third harmonic gave good separation results between normal (BL) signals and the three fault signals.
- **Conclusion 7:** The application of WPT and envelope analysis on the gas pulsation signals from the reciprocating compressor provides accurate monitoring information for the RC. The optimal wavelet basis is selected based on maximum Shannon to entropy ratio criteria, maximum cross correlation, and minimum Shannon entropy. Three levels of the wavelet packet decompositions are performed to give eight band-pass filters (terminal nodes). An adaptive hard threshold using standard deviation of

each band coefficients is applied and the coefficients of each bands are reconstructed to reveal the de-noised signal. Then envelope analysis of each band (reconstructed terminal node coefficients) is computed and the root mean square values are used to select the optimal band that gives the best fault separation. Finally, the optimal terminal nodes (4 and 6) were used for classification by plotting its kurtosis values against entropy values. Terminal node 6 (1536-1792Hz) gave a more superior valve fault separation when used for classification compared to terminal node 4.

- **Conclusion 8:** Condition monitoring using vibration measurement still remains a more superior technique compared to other signal processing types and indeed gas pulsation measurement. From this study, using proposed methods, vibration measurements could classify all faults investigated (valve and pipeline related faults); however, the gas pulsation measurement was more effective at identifying valve related faults compared to pipeline leakages. Nevertheless, the author highly recommends the use of both vibration and gas pulsation measurement to better characterise the vibro-acoustic signals from a reciprocating compressor. The key characteristics of a reciprocating compressor have been summarised in Figure 11.1 below.

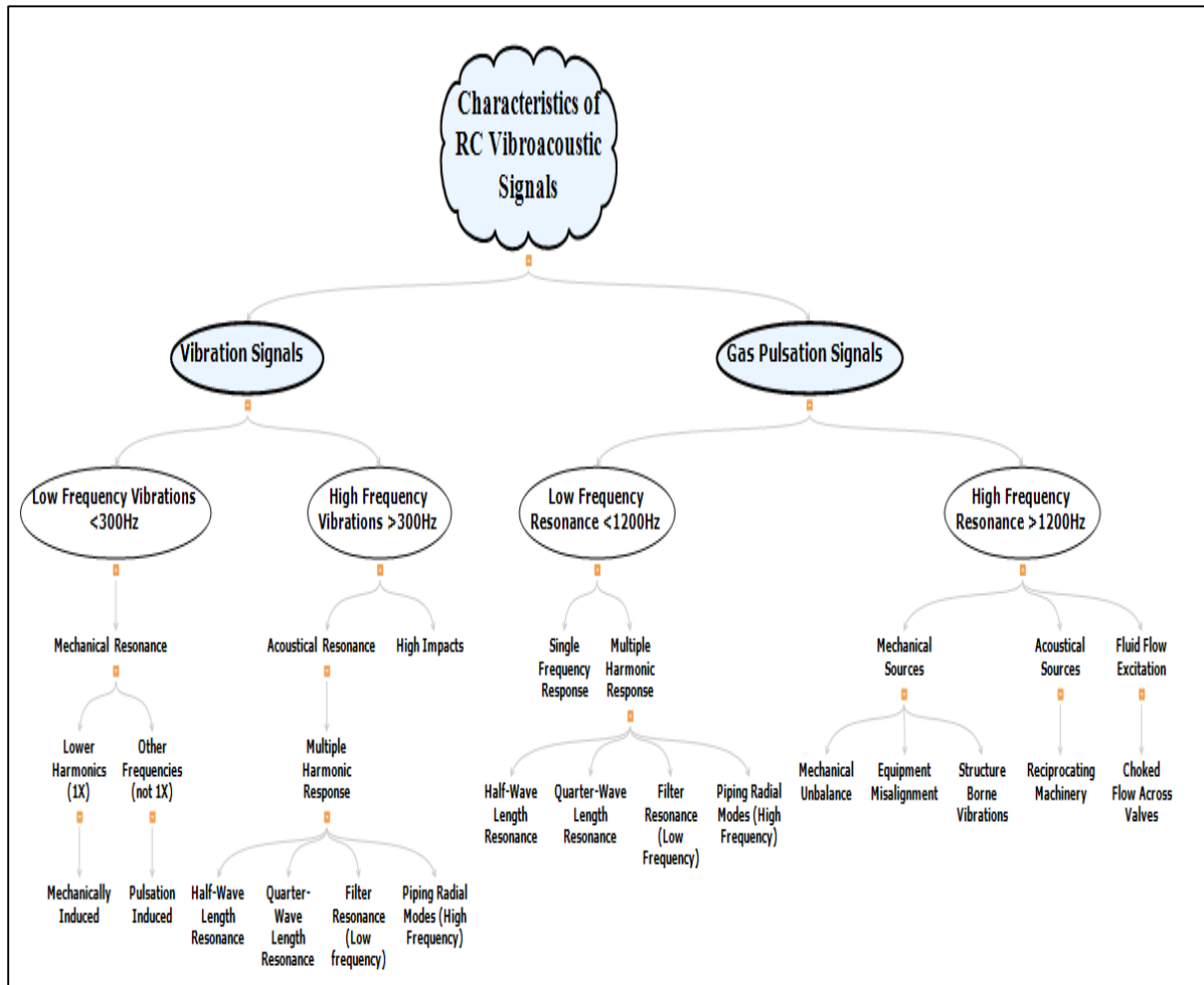


FIGURE 11.1: CHARACTERISTICS OF VIBRO-ACOUSTIC SIGNALS FROM A RECIPROCATING COMPRESSOR

11.3 Contribution to Knowledge

The main contributions to knowledge made by this research are:

- **Contribution 1:** The author of this thesis believes that the processing of gas pulsation signals for detection and diagnosis of reciprocating compressor faults such as discharge valve leakage, intercooler leakage, and discharge pipeline leakage is novel (Chapter 8 and 9). Prior to this study, no work has been found in literature that describes the characteristics of gas pulsation signals using time-domain, frequency-domain and time-frequency domain analysis for condition monitoring of a double-stage RC.
- **Contribution 2:** The model predictions of the pressure in the discharge chamber of a two-stage reciprocating compressor has not been simulated numerically (Section 5.9).
- **Contribution 3:** The author believes that the application of WPT for analysis of vibration and gas pulsation signals for condition monitoring of a reciprocating

compressor is novel as no reports in literature uses the combination of the two methods applied in this thesis for fault detection and diagnosis of RCs.

- **Contribution 4:** It shows that vibro-acoustic signal analysis by the wavelet packet transform and envelope methods are able to diagnose changes in reciprocating compressor behaviours. The classification tool using the fundamental frequency and third harmonic of the transformed envelope vibration signal showed changes between healthy and all fault conditions monitored across a wide pressure range.
- **Contribution 5:** Finally, the achievements have provided sufficient experimental supports to show that vibration and gas pulsation signals along with the proposed advanced signal processing methods can be an effective technique for on-line monitoring of reciprocating compressors.

11.4 Recommendation for Future Work

1. It is recommended that further research be conducted on the gas pulsation signals in the first-stage discharge chamber to investigate possible resonances from the intercooler pipeline, and the effects of common faults on the system.
2. It is recommended that further academic research be conducted on other valve related faults such as faulty valve spring to determine their effects on gas pulsation signals from the reciprocating compressor.
3. To develop faster algorithm to achieve optimal mother (base) wavelet selection so that vibration and gas pulsation-based analysis can be implemented more efficiently online.
4. To directly extend this study by using intelligent algorithms (neural networks, fuzzy logics, genetic algorithms, etc.) to examine the combination of features such as entropy, kurtosis, crest factor, PDF values etc. from all terminal nodes of the transformed vibration and gas pulsation signals to optimise recognition of common reciprocating compressor faults
5. To carry out complex mode analysis of the discharge pipeline system to verify sources of low frequency resonance present in the gas pulsation signals. Also, this would require coupling of the one-dimensional flow model of the pipe to the already existing compressor model to give a complete representation of the reciprocating compressor system.

12 APPENDIX 1

TABLE 12.1: FAILURE MODES OF POSITIVE DISPLACEMENT ROTARY COMPRESSORS

CAUSES	PROBLEMS									
	No Air/Gas Delivery	Insufficient Discharge Pressure	Insufficient Capacity	Excessive Wear	Excessive Heat	Excessive Vibration and Noise	Excessive Power Demand	Motor Trips	Elevated Motor Temperature	Elevated Air/Gas Temperature
Air Leakage into Suction Piping or Shaft Seal		√	√			√				
Coupling Misalignment				√	√	√	√		√	
Excessive Discharge Pressure			√	√		√	√	√		√
Excessive Inlet Temperature/Moisture			√							
Insufficient Suction Air/Gas Supply		√	√	√		√		√		
Internal Component Wear	√	√	√							
Motor Failure	√									
Pipe Strain on Compressor Casing				√	√	√	√	√	√	
Rotating Element Bending				√	√	√	√	√	√	
Solid or Dirt in Inlet Air/Gas Supply				√						
Speed Too Low		√	√					√		
Suction Filter or Strainer Clogged	√	√	√			√			√	
Wrong Direction of Rotation	√	√							√	

CHARACTERISING VIBRO-ACOUSTIC SIGNALS OF A RECIPROCATING
COMPRESSOR FOR CONDITION MONITORING

TABLE 12.2: FAILURE MODES OF RECIPROCATING POSITIVE DISPLACEMENT COMPRESSORS

CAUSES	PROBLEMS													
	Air discharge temperature above normal	Compressor Fails to Start	Compressor Fails to Unload	Compressor Noisy and Knocks	Compressor Parts Overheats	Delivery Less than rated Capacity	Discharge pressure below Normal	Excessive Compressor Vibration	Motor Overheating	Operating Cycle Abnormally Long	Piston Ring, rod, piston, Cylinder, Wear Excessive	Receiver Pressure Above Normal	Starts too Often	Valve wear
Air filter Defective											√			√
Ambient Temperature too High	√				√			√						
Incorrect Assembly														√
Belts Slipping				√		√	√							
Belt too Tight		√			√			√						
Defected Check or Discharge Valve					√									
Clogged Strainer			√											
Clogged Control Air Line											√			
Dirty Cylinder, Head, and cooler	√													
Worn cylinder or piston	√			√	√	√	√	√	√	√				
Dirt, Rust entering the cylinder										√				√
Discharge Pressure above rating	√			√	√	√		√	√	√	√	√	√	
Electrical Conditions Wrong		√						√						
Blown Fuse		√												
Intake filter clogged	√			√	√	√	√	√						
Liquid Carry-over				√						√				√

REFERENCES

- Al-Badour, F., Sunar, M., & Cheded, L. (2011). Vibration analysis of rotating machinery using time-frequency analysis and wavelet techniques. *Mechanical Systems and Signal Processing*, 25, 2083-2101.
- Albarbar, A., Elhaji, M., Gu, F., & Ball, A. (2004). Independent Component Analysis for Enhancing Diesel Engine Air-Borne Acoustics Signal to Noise Ratio. *Proc. 9th Int. Conference on Mechtronics*, (pp. 345-355). Turkey.
- Albarbar, A., Gu, F., Ball, A. D., & Starr, A. (2010). Acoustic Monitoring of Engine Fuel Injection Based on Adaptive Filtering Techniques. *Applied Acoustics*, 71(12), 1132-1141.
- Al-Qattan, M. J. (2007). *Industrial Application of Speed and Power for fault Detection and Diagnosis of Large Compressor*. University of manchester, School of Mechanical, Aerospace and Civil Engineering. Manchester: University of Manchester.
- Al-Qattan, M., Al-Juwayhel, F., Elhaj, M., Ball, A., & Gu, F. (2009). Instantaneous angular speed and power for the diagnosis of single-stage, double-acting reciprocating compressor. *Journal of engineering tribology*, 223(part J).
- API STANDARD 618. (2007, December). Reciprocating Compressors for Petroleum, Chemical, and Gas Industry Services.
- Arnold, K., & Stewart, M. (1999). *Surface Production Operations* (2nd ed., Vol. I). Houston: Butterworth-Heinemann.
- Ball, A. D. (2000). *Reciprocating Engines and Compressors. Maintenance Engineering M12, section 11*. Manchester England: University of Manchester.
- Ball, A., Gu, F., & Li, W. (2000). Ball, A. D., Gu, F., & Li, W. (2000). The condition monitoring of diesel engines using acoustic measurements part 2: fault detection and diagnosis. *SAE technical paper*.
- Barber, A. (1992). *Handbook of Noise and Vibration Control* (6th ed.). Oxford: Elsevier Science Publishers.

- Baydar, N., & Ball, A. (2001). A comparative study of acoustic and vibration signals in detection of gear failures using Wigner-Ville distribution. *Mechanical Systems and Signal Processing*, 15(6), 1091–1107.
- Bendjama, H., Bouhouche, S., & Boucherit, M. S. (2012). Application of Wavelet transform for fault Diagnosis in Rotating Machinery. *International Journal of Machine Learning and Computing*, 2(1), 82-87.
- Benson, R. S. (1982). *The thermodynamics and gas dynamics of internal combustion engines* (Vol. 1). Oxford,UK: Clarendon Press.
- Bentley, J. P. (1993). *An introduction to reliability and quality engineering* . Harlow: Longman Scientific & Technical .
- Boulahbal, D., Golnaraghi, F. M., & Ismail, F. (1999). AMPLITUDE AND PHASE WAVELET MAPS FOR THE DETECTION OF CRACKS IN GEARED SYSTEMS. *Mechanical Systems and Signal Processing*, 13(3), 423-436.
- Boyce, M. P. (2009). *Centrifugal Compressors: A Basic Guide*. Oklahoma: PennWell.
- Brablik, J. (1969). The Influence of Gas Pulsations on the Operation of Automatic Compressor Valves. *Commission 3, IIR Conference*, (pp. 121-126). Prague.
- Brablik, J. (1972). Gas Pulsations affecting Operation of Automatic valves in reciprocating Compressors. *1st Purdue Compressor Technology Conference*, (pp. 188-195).
- Brablik, J. (1972). Gas Pulsations as a Factor Affecting Operation of Automatic Valves in reciprocating Compressors. *Purdue Compressor Technical Conference*, (pp. 188-195). Purdue.
- Bradley, P., Ball, A., & Gu, F. (2000). A Head-to-head Assessment of the Relative Fault Detection and Diagnosis Capabilities of Conventional Vibration and Airborne Acoustic Monitoring. *Proc. 13th Int. Congress on Condition Monitoring and Diagnoses Engineering Management (COMADEM)*, (pp. 233-242). Texas.
- Braun, S. (1986). *Mechanical Signature Analysis*. London: Academic Press.

- Brejaud, P., Higelin, P., Charlet, A., & Chamailard, Y. (2011, April 15). Development and experimental validation of a new one-dimensional valve boundary condition based on the method of characteristics. *Journal of Automobile Engineering*, 225(Part D).
- Brown, R. N. (2005). *Compressors: Selection and Sizing* (3rd ed.). Oxford: Elsevier Inc.
- Caie, A., & Bickmann, T. (2017, September). *Advanced Online Condition Monitoring and Diagnostics support Operational and Maintenance Decisions in an Offshore Gas Compression and Export System Unit*. Retrieved from Baker Hughes aGE company: https://www.gemeasurement.com/sites/gemc.dev/files/gea33192_chevron_europe_cas_e_study_r3.pdf
- Cambridge Electronic Design Limited. (1991). *The CED 1401 Plus. Intelligent Interface Programmer's Handbook*. Cambridge, UK: Cambridge Electronic Design.
- castro, B., Kogan, D., & Geva, A. B. (2000). ECG Feature Extraction using Optimal Mother Wavelet. *IEEE convention of Electrical and Electronic Engineers in Israel*, 346-350.
- Chen, J., Li, Z., Pan, J., Chen, G., Zi, Y., Yuan, J., . . . He, Z. (2016). Wavelet transform based on inner product in fault diagnosis of rotating machinery: A review. *Mechanical Systems and Signal Processing*, 1-35.
- Chrfi, F., ALHaddad, K., & Franqois , B. (2004). Power System Fault Monitoring Using Wavelet Transform. *Annul IEEE Power Electronics Specialists Conference*.
- chui, C. K. (1997). *Wavelets: A Mathematical Tool for Signal Analysis*. Philadelphia: SIAM.
- Cipollone, R. (2016). Sliding vane rotary compressor technology and energy saving. *Journal of Process mechanical Engineering*, 230(3), 208-234.
- Cizek , V. (1970). Discrete Hilbert transform . *IEEE Transactions on Audio and Electroacoustics*, 18(4), 340 - 343.
- Collacott, R. (1977). *Mechanical Fault Diagnosis and Condition Monitoring*. London: Chapman and Hall Ltd.
- Costagliola, M. (1950). The Theory of Spring-Loaded Valves for Reciprocating Compressors'. *ASME Journal of Applied Mechanics*, 17(4), 415-420.

- Daniel, G. (2014, June). *Reciprocating Compressor Suction and Discharge Valve Monitoring: Evaluating the strengths and weaknesses of the most common online monitoring technologies*. Retrieved from prognost: https://www.prognost.com/wp-content/uploads/2018/03/ct2-06-14_compressor-valve-monitoring.pdf
- Danielson, D. (2003). *Vectors And Tensors In Engineering And Physics*. Boca Raton: CRC Press.
- Dong, Z. (2012). *A study of non-stationar signal processing for machinery condition monitoring*. huddersfield: Univeristy of huddersfield.
- Duan, L., Wang, Y., Wang, J., Zhang, L., & Chen, J. (2016). Undecimated Lifting Wavelet Packet Transform with Boundary Treatment for Machinery Incipient Fault Diagnosis. *Shock and Vibration*, 1-9.
- Dyer, D., & Stewart, R. M. (1978). Detection of Rolling Element Bearing Damage by Statistical Vibration Analysis. *Journal of Mechanical Design*, 100(2), 229-235.
- Elhaj, M. A. (2005). *CONDITION MONITORING OF RECIPROCATING COMPRESSOR VALVES*. manchester: University of Manchester.
- Elhaj, M. A. (2005). *CONDITION MONITORING OF RECIPROCATING COMPRESSOR VALVES*. Huddersfield: University of Huddersfield.
- Elhaj, M., Gu, F., Ball, A. D., Albarbar, A., Al-Qattan, M., & Naid, A. (2008). Numerical simulation and experimental study of a two-stage reciprocating compressor for condition monitoring. *Mechanical Systems and Signal Processing*, 22, 374-389.
- Elhaji, M., Gu, F., Shi, J., & Ball, A. (2001). Comparison of the Condition Monitoring of Reciprocating Compressor Valves Using Vibration, Acoustic, Temperature and Pressure Measurements. *Electronic Proc. 6th Annual Maintenance and Reliability Conference (MARCON)*,. Gatlinburg, Tennessee.
- Elson, J. P., & Soedel, W. (1972). A Review of Discharge and Suction Line Oscillation Research. *International Compressor Engineering Conference*, 49, 311-315.
- Enzo, G., Marco, P., Matteo , R., & Stefano , G. (2006). FORCED RESPONSE OF CYLINDER MANIFOLD FORCED RESPONSE OF CYLINDER MANIFOLD. *8th*

CHARACTERISING VIBRO-ACOUSTIC SIGNALS OF A RECIPROCATING
COMPRESSOR FOR CONDITION MONITORING

Biennial ASME Conference on Engineering Systems Design and Analysis (pp. 1-10).
Torino, Italy: ASME.

Forsthoffer, M. S. (2017). *More Best practices for Rotating Equipment*. Oxford: Butterworth-Heinemann.

Gao, R. X., & Yan, R. (2011). *Wavelets: Theory and applications for manufacturing*. US: Springer US.

Gaspar, P. D., & Da Silva, P. D. (2015). *Handbook of Research on Advances and Applications in Refrigeration Systems and Technologies*. Pennsylvania: Engineering Science Reference (an imprint of IGI Global).

Geng, Z., Jin, C., & Hull, B. J. (2003). Analysis of engine vibration and design of an applicable diagnosing approach. *International Journal of Mechanical Sciences*, 45, 1391-1410.

Ghanbariannaeni, A., & Ghazanfarihashemi, G. (2014). Gas pulsation study for reciprocating compressors in chemical plants. *Journal of Process Mechanical Engineering*, 230(1), 65-75.

Giampaolo, T. J. (2010). *Compressor handbook: Principles and practice*. Lilburn, GA, USA: The Fairmont press. Retrieved from <http://www.ebrary.com>

Glen, P., & Eugene, E. (1989). Computer Simulation and Acoustic Tuning of Rolling Piston Vapor Compressors. *Computer Modeling and Simulation in Engineering & Sciences*, 4(2), 117-123.

Goldman, S. (1984). Periodic Machinery Monitoring: Do It Right. *Hydrocarbon Process*, 51-56.

Goyal, D., & Pabla, B. S. (2016). The vibration monitoring methods and signal processing techniques for structural health monitoring: A review. *Archives of Computational Methods in Engineering*, 23(4), 585-594.

Greenfield,, S. D., & Luis de la Roche, L. (2018, september 22). *Introduction to Vibration & Pulsation in Reciprocating Compressors*. Retrieved from Vibration, dynamics and noise: www.woodgroup.com/VDN

- Grib, V. V., & Zhukov, R. V. (2001, January). ANALYSIS OF VIBROACOUSTIC CHARACTERISTICS OF PISTON COMPRESSORS. *Chemical and Petroleum Engineering*, 37(1), 40-42.
- Gu, F., & Ball, A. (1995). Use of the smoothed pseudo-Wigner–Ville distribution in the interpretation of monitored vibration data maintenance. *10*, 16-23.
- Gu, F., Li, W., Ball, A., & Leung, A. Y. (2000). The condition monitoring of diesel engines using acoustic measurements Part1: Acoustic characteristics of the engine and representation of the acoustic signals. *SAE world congress*, 1-9.
- Gursoy, I. M., Yilmaz, S. A., & Ustun, V. S. (2018). A PRACTICAL REAL-TIME POWER QUALITY EVENT MONITORING APPLICATIONS USING DISCRETE WAVELET TRANSFORM AND ARTIFICIAL NEURAL NETWORK. *Journal of Engineering Science and Technology*, 13(6), 1764-1781.
- Hamilton, J. (1974). *Extension of Mathematical Modelling of Positive Displacement. Type Compressor; Ray W Herrick Laboratories*. Purdue : Purdue University, USA.
- Hanlon, P. C. (2001). *Compressor Handbook*. New York: McGraw-Hill.
- Heinz, B., & John, J. (1996). *Reciprocating Compressors, Operation & Maintenance*. Houston: Butterworth-Heinemann.
- Jardine, A. K., Lin, D., & Banjevic, D. (2005). A review on machinery diagnostics and prognostics implementing condition-based maintenance. *Mechanical Systems and Signal Processing*, 20, 1483–1510.
- Jiang, J., Gu, F., Gennish, R., Moore, D. J., Harris, G., & Ball, A. (2008). Monitoring of diesel engine combustions based on the acoustic source characterisation of the exhaust system. *Mechanical Systems and Signal Processing*, 22(6), 1465-1480.
- Jiangming, J., & Weirong, H. (2012). Valve Dynamic and Thermal Cycle Model in Stepless Capacity Regulation for Reciprocating Compressor. *CHINESE JOURNAL OF MECHANICAL ENGINEERING*, 25(6), 151-160. doi:10.3901/CJME.2012.06.1151, available online at www.springerlink.com; www.cjmenet.com; www.cjmenet.com.cn

- Kankar, P. K., Satish, S. C., & Harsha, S. P. (2011). Rolling element bearing fault diagnosis using wavelet transform. *Neurocomputing*, 74, 1638-1645.
- Khan, N. (2018). *Improved image compression with comparative analysis of progressive coding techniques*. MCS.
- Komonen, K. (1998). *The Structure and Effectiveness of industrial maintenance*. Finnish Academy of Technology.
- Komonen, K. (2002, September). The structure and effectiveness of industrial maintenance for profitability analysis and benchmarking. *International Journal of production economics*, 79(1), 15-31.
- Kulkarni, P. G., & Sahasrabudhe, A. D. (2013). Application Of Wavelet Transform For Fault Diagnosis of Rolling Element Bearings. *INTERNATIONAL JOURNAL OF SCIENTIFIC & TECHNOLOGY RESEARCH*, 2(4), 138-148.
- Kumar, H. S., Srinivasa, P. P., Sriram, N. S., & Vijay, G. S. (2014). Selection of Mother Wavelet for Effective Wavelet Transform of Bearing. *Advanced Materials Research*. 1039, pp. 169-176. Switzerland: Trans Tech Publications.
- Kwok, T. F. (2018, January). An Automated Energy Detection Algorithm Based on Kurtosis-Histogram Excision. *US Army Research Laboratory*, pp. 1-38.
- Lei, Y., Lin, J., He, Z., & Zuo, M. J. (2013). A review on empirical mode decomposition in fault diagnosis of rotating machinery. *Mechanical Systems and Signal Processing*, 35(1-2), 108-126.
- Leonard, S. M. (1996, January). *Increasing the Reliability of Reciprocating Compressors on Hydrogen Services*. New York: Dresser-Rand.
- Li, Y., Gu, F., Harris, G., Ball, A., Bennett, N., & Travis, K. (2005). The measurement of instantaneous angular speed. *Mechanical Systems and Signal Processing*, 19, 786-805.
- Liang, B., Gu, F., & Ball, A. (1996). A Preliminary Investigation of Valve Fault Diagnosis in Reciprocating Compressors. *Journal of MAINTENANCE*, 11(2), 3-8.
- Liebetau, J., & Grollnisch, S. (2017, September 11). *Predictive Maintenance with Airborne Sound Analysis*. Retrieved from Processing Solutions for the Process Industries:

CHARACTERISING VIBRO-ACOUSTIC SIGNALS OF A RECIPROCATING
COMPRESSOR FOR CONDITION MONITORING

Prevent machinery breakdown with acoustic condition monitoring:
<https://www.processingmagazine.com/2017/09/11/predictive-maintenance-airborne-sound-analysis/>

- Loutas, T. H., & Kostopoulos, V. (2017). *Utilising the Wavelet Transform in Condition-Based Maintenance: A Review with Applications*.
- Maclaren , J. F., Kerr, S. V., Tramschek, A. B., & Sanjines, O. A. (1974). A Model of a Single Stage Reciprocating Gas Compressor Accounting for Flow Pulsations . *International Compressor Engineering Conference* (pp. 144-150). Purdue: University' of Strathclyde, Glasgow, U.K. .
- Malago, M., Mucchi, E., & Dalpiaz, G. (2016). Fault detection in heavy duty wheels by advanced vibration processing techniques and lumped parameter modeling. *Mechanical Systems and Signal Processing*, 70-71, 141-160.
- Manea, D., Mihaela, A. C., & Mutihac, R. (2018). Applications of fractional wavelet-based denoising method in biomedical hyperspectral imaging. *PROCEEDINGS OF SPIE* (pp. 1-8). Strasbourg, France: SPIEDigitalLibrary.
- Manepatil, S., Yadava, G., & Nakra, B. (2000, October). Modelling and Computer Simulation of Reciprocating Compressor with Faults. *Journal of the Institution of Engineers* , 81(3), 108 - 116.
- Maurice, G., Kendall, M. A., & Alan, S. (1961). *The advanced theory od statistics* (Vol. II). New York: Hafner publishing company.
- McLaren, J., & Kerr, J. (1968). Valve Behaviour in a Small Refrigeration Compressor Using Digital Computer. *Journal of Refrigeration*, 11(6), 78 - 89.
- Mobley, K. R. (1999). *Root Cause Failure Analysis: Plant Engineering Maintenance Series*. Massachusetts : Butterworth-Heinemann.
- Mobley, K. R. (2004). *Maintenance Fundamentals* (2nd ed.). Oxford: Elsevier Butterworth–Heinemann.
- Mohanty, A. R. (2015). *Machinery Condition Monitoring: Principles and Practices*. Florida: taylor and Francis Group, LLC.

- Muo, U. E., Madamedon, M., Gu, F., & Ball, A. (2017). Wavelet Packet Analysis and Empirical Mode Decomposition for the Fault Diagnosis of Reciprocating Compressors. *23rd International Conference on Automation & Computing* (pp. 1-7). Huddersfield: University of Huddersfield.
- Naid, A., Gu, F., & Ball, A. (2007). Fault Detection and Diagnosis of Reciprocating Compressors Using Motor Current Signature Analysis. *2nd World Cong. on WCEAM and 4th CM2007*. Harrogate.
- Namdeo, R., Manepatil, S., & Saraswat, S. (2008). Detection of Valve leakage in reciprocating Compressor using Artificial Neural Network (ANN). *International Compressor Engineering Conference* (pp. 14-17). Purdue.
- National Instrument Company. (2003). *LabWindows/CVI User Manual, Version 5.5*. London, UK: National Instrument Company.
- Newland, D. E. (1994). Wavelet analysis of vibration, Part I: theory. *Journal of Vibration and Acoustics*, 116, 409-419.
- Norton, M., & Karczub, D. (2003). *Fundamentals of Noise and Vibration Analysis For Engineers*. UK: CUP.
- Ogbulafor, U. E., Guojin, F., Mones, Z., Gu, F., & Ball, A. (2017). Application of Wavelet Packet Transform and Envelope Analysis to Non-stationary Vibration Signals for Fault Diagnosis of a Reciprocating Compressor. *First World Congress on Condition Monitoring*. London: University of Huddersfield.
- Ormer, H. V. (2002, November 30). *Compressors drive the system*. Retrieved from Hydraulics and Pneumatics: <http://www.hydraulicspneumatics.com/other-technologies/compressors-drive-system>
- Ozturk, C., Deblauwe, F., & Kopgeroolu, Y. (1996). Acoustic Features of the Reciprocating Refrigeration Compressors. *International Compressor Engineering Conference* (pp. 729-734). Purdue University.
- Padilla, E. (1971). *Computer Simulation of a Two-cylinder Refrigeration Compressor with Special Attention to the Cylinder and Cavity Interactions*. Purdue: Purdue University.

- Pan, F., & Jones, D. J. (1999). Gas Path Sound Transmission in Spherically-Shaped Reciprocating Compressors: Theory and Experiment. *J. Vib. Acoust*, 121(1), 8-17.
- Pascual, R., Meruane, V., & Rey, P. A. (2008). On the effect of downtime costs and budget constraint on preventive and replacement policies. *Reliability Engineering and System Safety*, 93(1), 144-151.
- Peng, Z. K., & Chu, F. L. (2004). Application of the wavelet transform in machine condition monitoring and fault diagnostics: a review with bibliography. *Mechanical Systems and Signal Processing*, 18, 199-221.
- Pichler, K., Lughofer, E., Pichler-Scheder, M., Buchegger, T., Klement, E. P., & Huschenbett, M. (2013). Detecting cracks in reciprocating compressor valves using pattern recognition in the pV diagram. *EE/ASME International Conference on Advanced Intelligent Mechatronics*. 18, pp. 461-472. Australia: IEEE.
- Price, G. R., & Botros, K. (1992). Numerical and Experimental Analysis of the Flow Characteristics through a Channel Valve. *Purdue Compressor Technology Conference*, 1215- 1225.
- Rafiee, J., & Tse, P. W. (2009). Use of autocorrelation of wavelet coefficients for fault diagnosis. *Mechanical Systems and Signal Processing*, 23, 1554-1572.
- Rafiee, J., Tse, P. W., Harifi, A., & Sadeghi, M. H. (2009). A novel technique for selecting mother wavelet function using an intelligent fault diagnosis system. *Expert Systems with Applications*, 36, 4862-4875.
- Raharjo, P. (2013). *An Investigation of Surface Vibration, Airbourne Sound and Acoustic Emission Characteristics of a Journal Bearing for Early Fault Detection and Diagnosis*. Huddersfield: University of Huddersfield.
- Rao, B. K. (1998). *Handbook of Conditon Monitoring: Techniques and Methodology*. (A. Davies, Ed.) Cardiff: Springer Science and Business Media Dordrecht.
- Rao, S. S. (2004). *mechanical Vibration* (5th ed.). Miami: Pearson.
- Robinson, J. D. (1990). *Submarine-installed Machinery Monitoring and Diagnostics: A State-of-the-art Review*. Monterey: Calhoun: The NPS Institutional Archive.

- Robison, D. H., & Beaty, P. J. (N.d). Compressor types, classification, and applications. *Proceeding od the twenty-first turbomachinery symposium*, (pp. 183-188).
- Ross, S. M. (2004). *Introduction to Probability and Statistics for Engineers* (3rd ed.). London;Amsterdam: Elsevier Academic.
- Salah, A. M., Hui, K. H., Hee, L. M., & Salman, L. (2018). Automated valve fault detection based on acoustic emission parameters and support vector machine. *Alexandria engineering journal*, 57, 491-498.
- Saleh, S. A., & Rahman, M. A. (2005). Modeling and Protection of a Three-Phase power Transformer Using Wavelet Packet Transfrom. *IEEE transactions on Power delivery*, 20(2), 1273 - 1282.
- Scheideman, F., Schary, M., & Singh, R. (1978). Thermodynamic and Acoustic Simulation of Positive Displacement Refrigeration Compressors. *International Compressor Engineering Conference*, 290-299.
- Schultheis, S. M., Lickteig, C. A., & Parchewsky, R. (2007). Reciprocating compressor condition monitoring. *36th Turbomachinery symposium*, (pp. 10-13). Texas: College station.
- Schwartz, R., & Nelson, R. (1984). *Acoustic Resonance Phenomena In High Energy Variable Speed Centrifugal Pumps*. Texas: Turbomachinery Laboratories, Department of Mechanical Engineering, Texas A&M University. Retrieved from [http : / /hdl .handle .net /1969 .1 /164375](http://hdl.handle.net/1969.1/164375)
- Schwerzler, D. (1971). *Mathematical Modelling of a Multicylinder Refrigeration Compressor*. Purdue: Purdue University.
- Scruby, C. B. (1987). An introduction to acoustic emission. *Journal of physics E: Scientific Instruments*, 945-953.
- Sharma, V., & Parey, A. (2016). Gearbox fault diagnosis using RMS based probability density function and entropy measures for fluctuating speed conditions. *Structural Health Monitoring*, 16(6), 682–695.

- Shejal, P. P., & Desai, A. D. (2014). Pulsation and Vibration Study Of Reciprocating Compressor According to API 618 5th Edition. *International journal of Modern Engineering Research*, 4(7).
- Sikorska, J. Z., & Mba, D. (2008). Challenges and obstacles in the application of acoustic emission to process machinery. *Journal of Process Mechanical Engineering*, 222, 1-19.
- Sim, H., Ramli, R., Saifizul, A. A., & Abdullah, M. (2014). Empirical investigation of acoustic emission signals for valve failure identification by using statistical method. *Measurement*, 165–174.
- Singh, R. (1975). *Modeling of Multicylinder Compressor Discharge Systems*. Purdue: Purdue University.
- Smith, S. W. (1999). *Digital Signal Processing* (2nd ed.). San Diego: California Technical Publishing.
- Soedel, W. (2007). *Sound and Vibrations of Positive Displacement Compressors*. New York: CRC Press.
- Srinivas, M. N., & Padmanabhanb, C. (2002). Computationally efficient model for refrigeration compressor gas dynamics. *International Journal of Refrigeration*, 25, 1083–1092.
- Staszewski, W. (1994). *The Application of Time-Variant Analysis to Gearbox Fault Detection*. Manchester: University of Manchester.
- Staszewski, W. J., & Worden, K. (1997). Classification of faults in gearboxes — pre-processing algorithms and neural networks. *Neural Computing & Applications*, 5(3), 160-183.
- Stiaccini, I., Galoppi, G., Ferrari, L., & Ferrara, G. (2016). A reciprocating compressor hybrid model with acoustic FEM characterization. *international journal of refrigeration*, 63, 171-183.
- Thobiani, F. W. (2011). *The Non-intrusive Detection of Incipient Cavitation in Centrifugal Pumps*. Huddersfield: University of Huddersfield.

- Toyota, T., Niho, T., Chen, P., & Komura, H. (2001). CONDITION DIAGNOSIS OF RECIPROCATING MACHINERY USING INFORMATION THEORY. *Condition Monitoring and Diagnostic Engineering Management*, 657-662.
- Tse, P. W., Peng, Y. H., & Yam, R. (2001). Wavelet analysis and envelope detection for rolling element bearing fault diagnosis—their effectiveness and flexibilities. *Journal of Vibration and Acoustics*, 303-310.
- US Department of Energy. (2003). *Improving Compressed Air System Performance*. Retrieved October 6, 2014, from Energy Efficiency and Renewable Energy: www.oit.doe.gov/bestpractices/compressed_air
- Wachel, J. C. (N.D). *Turbine and Compressor Vibrations*. San Antonio: Engineering Dynamics, Inc.
- Wang, F., Song, L., Zhang, L., & Li, H. (2010). , Fault diagnosis for reciprocating air compressor valve using p-V indicator diagram and SVM. *3rd International Symposium on Information Science and Engineering*,, (pp. 255-258). Shanghai, China.
- Wang, W. J. (1996). Wavelet transform in vibration analysis for mechanical fault diagnosis. *Shock and Vibration*, 3(1), 17-26.
- Wang, W. J., & McFadden, P. D. (1996). APPLICATION OF WAVELETS TO GEARBOX VIBRATION SIGNALS FOR FAULT DETECTION. *Journal of Sound and Vibration*, 192(5), 927-939.
- Wang, X. (2006). *NUMERICAL IMPLEMENTATION OF THE HILBERT TRANSFORM*. Saskatoon,: University of Saskatchewan.
- Wang, Y., Gao, A., Zheng, S., & Peng, X. (2015). Experimental investigation of the fault diagnosis of typical faults in reciprocating compressor valves. *Journal of Mechanical Engineering Science*, 230(13), 2285 - 2299.
- Wang, Y., Xue, C., Jia, X., & Peng, X. (2015). Fault diagnosis of reciprocating compressor valve with the method integrating acoustic emission signal and simulated valve motion. *Mechanical Systems and Signal Processing*, 56-57, 197-212.

- Wasmbasganss, M. (1966). *Mathematical Modelling and Design Evaluation of High-Speed Reciprocating Compressors*. Purdue: Purdue University, USA.
- Wickerhauser, M. V. (1994). *Adapted wavelet analysis from theory to software*. Natick: Wilesley.
- Williams, J. H., Davies, A., & Drake, P. R. (1994). *Condition-Based Maintenance and Machine Diagnostics*. London: Chapman & Hall.
- Winterbone , D. E., Pearson, R. J., & Horlock, J. (2000). *Theory of engine manifold design: Wave Action Methods for IC Engines*. Wiley-Blackwell.
- Wu, J.-D., & Chiang, P.-H. (2009). Application of Wigner–Ville distribution and probability neural network for scooter engine fault diagnosis. *Expert Systems with Applications*, 36(2), 2187-2199.
- Wu, J.-D., & Lui, C.-H. (2009). An expert system for fault diagnosis in internal combustion engines using wavelet packet transform and neural network. *Expert Systems with Applications*, 36(3,Part 1), 4278-4286.
- Xiao, H., Wang, Z., & Ren, X. (2005). Classification of surface EMG signal using relative wavelet packet energy. *Computer Methods and Programs in Biomedicine*, 79(3), 189-195.
- Yan, J., Heng-hu, Y., Yang , H., Feng, Z., Zhen, L., Ping, W., & Yan, Y. (2015). Nondestructive Detection of Valves Using Acoustic Emission Technique. *Advances in Materials Science and Engineering*, 1-9.
- Yan, R. (2007). *Base wavelet selection criteria for non-stationary vibration analysis in bearing health diagnosis*. UMass Amherst.
- Yang , W. X., & Tse, P. W. (2003). Development of an advanced noise reduction method for vibration analysis based on singular value decomposition. *NDT & E International*, 36(6), 419-432.
- Yang, B.-S., Hwang, W.-W., Kim, D.-J., & Chit Tan, A. (2005). Condition classification of small reciprocating compressor for refrigerators using artificial neural networks and support vector machines. *Mechanical Systems and Signal Processing*, 371-390.

- Yaqub, M. F., Gondal, I., & Kamruzzaman, J. (2011). Envelope-Wavelet Packet Transform for Machine Condition Monitoring. *International Journal of Mechanical, Aerospace, Industrial, Mechatronic and Manufacturing Engineering*, 5(11), 2477-2482.
- Yen, G. G., & Lin, K. C. (2000). Wavelet packet feature extraction for vibration monitoring. *IEEE Transaction on Industrial Electronics*, 650-667.
- Yen, G. G., & Lin, K. C. (2000). Wavelet packet feature extraction for vibration monitoring. *IEEE transactions on industrial electronics*, 47, pp. 650-667.
- Yesilyurt, I. (1997). *Gearbox Fault Detection and Severity Assessment Using Vibration Analysis*. University of Manchester.
- Yongbo, L., Xu, M., Wei, Y., & Huang, W. (2014). Diagnostics of reciprocating compressor fault based on a new envelope algorithm of empirical mode decomposition. *Journal of Vibroengineering*, 16(5), 2269-2286.
- Zaman, M. R. (2003). *Artificial Neural Network Based Protection of Power Transformers*. Canada: Memorial University of Newfoundland.
- Zhan, L., Cheng, J., & Quanke, F. (2015). Effect of a cross-flow perforated tube on pressure pulsation and pressure loss in a reciprocating compressor piping system. *Proceedings of the Institution of Mechanical Engineers, Part C: Journal of mechanical Engineering Science*, 231(3), 473-484.
- Zhen, D., Alibarbar, A., Zhou, X., Gu, F., & Ball, A. (2011). Electrical Motor Current Signal Analysis using a Dynamic Time Warping Method for Fault Diagnosis. *9th International Conference on Damage Assessment of Structures*, (pp. 1-8).
- Zheng, Y. (2005). *Numerical Simulation of a Multi-Cylinder Reciprocating Compressor for Condition Monitoring*. Manchester: University of Manchester, Faculty of Engineering and Physical Sciences.
- Zhou, W., Kim, J., & Soedel, W. (2001). New iterative scheme in computer simulation of positive displacement compressors considering the effects of gas pulsations. *Transactions of the ASME*, 123, 282-288.

CHARACTERISING VIBRO-ACOUSTIC SIGNALS OF A RECIPROCATING
COMPRESSOR FOR CONDITION MONITORING

Zhu, J., Nostrand, T., Spiegel, C., & Morton, B. (2014). Survey of Condition Indicators for Condition Monitoring Systems. *Annual Conference of the Prognostics and Health Management Society*, (pp. 1-13). Vermont.

Zhuanga, Z., Li, F., & Wei, C. (2012). A Probability Density Estimation for Fault Detection. *Advanced Materials Research*, 562-564, 1113-1116.